FRICTION WEAR LUBRICATION ③

Tribology Handbook

ТРЕНИЕ, ИЗНАШИВАНИЕ И СМАЗКА

Под редакцией И. В. КРАГЕЛЬСКОГО и В. В. АЛИСИНА

FRICTION
WEAR
LUBRICATION

Vol 3

Tribology
Handbook

Edited by Prof. I. V. KRAGELSKY
D. Sc. (Eng.)
V. V. ALISIN
Cand. Sc. (Eng.)
Institute for Machine Sciences, Moscow

Translated from
the Russian
by
Felix Palkin
and Valerian Palkin

The Russian Alphabet and Transliteration

Аа	a	Кк	k	Хх	kh
Бб	b	Лл	l	Цц	ts
Вв	v	Мм	m	Чч	ch
Гг	g	Нн	n	Шш	sh
Дд	d	Оо	o	Щщ	shch
Ее	e	Пп	p	ъ	"
Ёё	ё	Рр	r	ы	y
Жж	zh	Сс	s	ь	'
Зз	z	Тт	t	Ээ	e
Ии	i	Уу	u	Юю	yı
Йй	y	Фф	f	Яя	ya

The Greek Alphabet

Αα	Alpha	Ιι	Iota	Ρρ	Rho
Ββ	Beta	Κϰ	Kappa	Σσ	Sigma
Γγ	Gamma	Λλ	Lambda	Ττ	Tau
Δδ	Delta	Μμ	Mu	Υυ	Upsilon
Εε	Epsilon	Νν	Nu	Φφ	Phi
Ζζ	Zeta	Ξξ	Xi	Χχ	Chi
Ηη	Eta	Οο	Omicron	Ψψ	Psi
Θθϑ	Theta	Ππ	Pi	Ωω	Omega

CONTENTS

MACHINE GUIDE WAYS

Guide ways are bearing surfaces that provide for the required relative position and the possibility of motion of machine components. Guide ways are classed as sliding guides and rolling guides.

Guide ways are widely used machine elements. The most common types are [19]:

(1) Sliding and rolling guides in metalcutting machine tools, which feature long travels, wide speed ranges (from fine feed rates to considerable main-motion speeds) and high accuracy requirements placed on them.

(2) Sliding guides in metalforming machines, which are subjected to great axial loads (in the direction of motion) and, in some machines, high temperatures.

(3) Sliding guides for cross-heads (sliders) in piston-type engines, with typically high speeds, elevated temperatures, and loads acting in a single plane.

(4) Sliding and rolling guides in instruments, where loads are insignificant, and accuracy requirements are very strict.

The main field of application for sliding and rolling guides is machine tools. The accuracy and life of guide ways are vital to machine-tool performance. Guide ways of machine tools have been thoroughly studied. Operating conditions for the main- and feed-motion guide ways in various machine tools are so diverse that it is always possible to liken them to the conditions found in other kinds of machines. For this reason, guide ways will be discussed here as applicable mainly to machine tools.

Guide ways are classified:

by the kind of friction, into sliding, rolling, and combination types;

by the kind of motion, into the main-motion (in the direction of cutting, operating at high speeds), the feed-motion (relatively low speeds), and the auxiliary-motion (for positioning the units stationary in the process of machining);

by the path of motion, into straight, circular, or curvilinear;

by the location of the path of motion in space, into horizontal, vertical and inclined;

by the design features, into ways made integral with machine frames, housings, or other components; attached ways (fastened, adhesive-bonded, etc.) in the form of plates, strips, etc.;

by the ability to withstand tilting moments and dislocating loads, into the closed type with special planks and gibs taking up these loads, and the open type, where the unit is held in contact with the ways by its gravity or by an external load acting in a definite direction.

22.1. SLIDING GUIDES

Sliding guides are by far the most common type of guide ways. As compared with rolling guides, sliding guides are less costly in manufacture and have a high damping capacity.

22.1.1. Design Features

Classification. By the kind of friction the sliding guides are classified into *fluid-friction, mixed-friction,* and *boundary-friction*
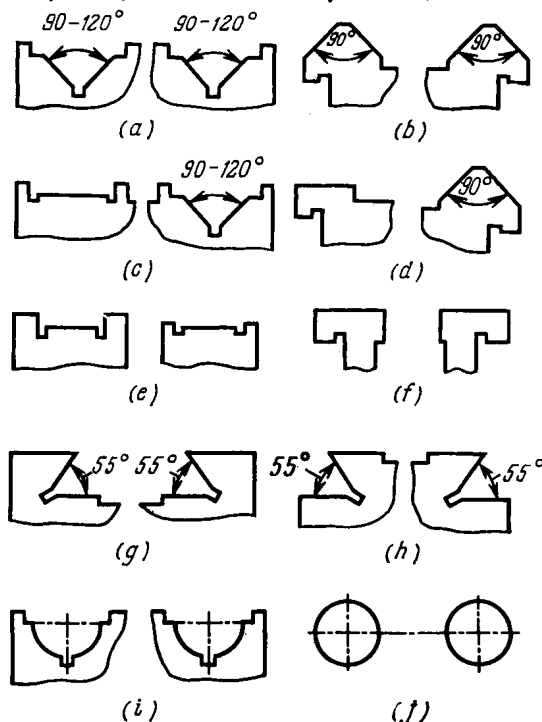
Fig. 22.1. Main types of straight-motion guide ways (cross-section shape of bed ways)

(a), (b) triangular [(a) Vee ways]; (c), (d) combination ways; (e), (f) rectangular; (g), (h) dovetail; (i), (j) round. Left—female ways, right—male ways

slideways. Fluid-friction slideways are subdivided into hydrodynamic ways, where a lift that arises during the sliding of the surfaces

10

in contact separates them completely (main-motion slideways in machine tools), and hydrostatic ways, where the rubbing surfaces are fully separated by oil delivered under pressure from a special control system (slideways in high-precision and heavy machine tools).
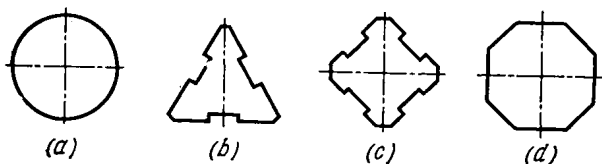
Fig. 22.2. Cross-sections of closed-contour guide ways

Mixed friction is found in most feed-motion slideways, and boundary friction, in feed-motion ways functioning at very low sliding speeds.

By their geometrical form, the slideways are classed into (a) prismatic ways—the most common type for straight motion—which are rectangular and triangular (including Vee ways and dovetail ways) in cross-section (Fig. 22.1); (b) flat ways (used in combination with other types); (c) cylindrical (bar-type) ways, used mainly for straight motion; and (d) cone-type ways for circular motion.

General characteristics. *Straight-motion ways.* Machine frames or stationary housing-type parts have female or male ways. When safely protected from dirt, the former are most suitable for a horizontal arrangement because they provide better lubricating conditions. The male way is employed in the case of low sliding speeds (feed motions). In most cases, a set of two ways is used for the motion of various machine units (Fig. 22.1). Where the space is limited, a single way is used, which has a closed-contour cross-section: round (Fig. 22.2a), which is the least costly in manufacture, or prismatic (Fig. 22.2b through d), which provides locking against angular displacement under the action of high torques.

Fig. 22.3. Main types of circular-motion guide ways
(a) flat; (b) bevelled; (c), (d) Vee ways

Restriction of lateral displacement on one way of the set is preferable to that on both ways, since that simplifies the manufacture and reduces the effects of temperature strains on accuracy.

Circular-motion guide ways are used for work tables and faceplates with a vertical axis of rotation, usually in combination with a spindle (Fig. 22.3). Work tables over 7 to 8 m in diameter are made

with two slideways. The major dimensions of slideways in metalcutting and woodworking machine tools, and those of the gibs are specified by Machine Tool Industry Standards.

Attached ways are used to increase wear resistance, to obtain favourable frictional characteristics, and to ensure the uniformity of slow movements of machine units along the ways. Attached ways on the machine frame (the longer member of a sliding pair) are usually
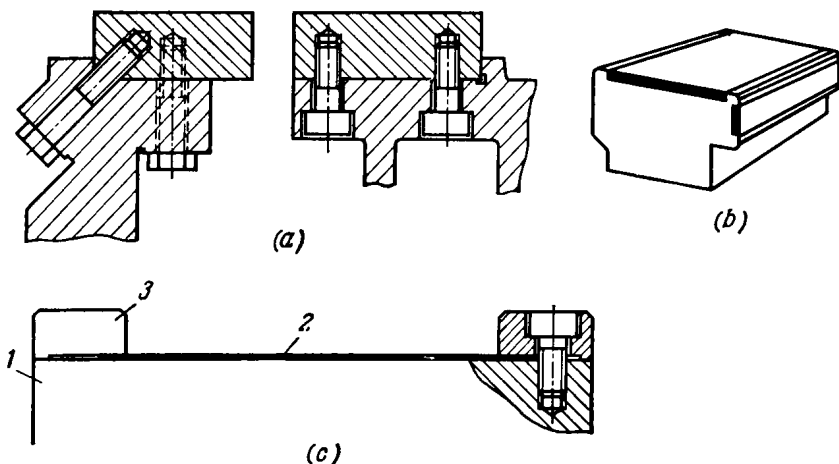
Fig. 22.4. Attached steel ways

(a) solid strips; (b) thin plates; (c) bands; *1*—bed way (cast iron); *2*—elastic hardened steel band; *3*—clamping strips

made of steel hardened to high numbers to increase wear resistance, particularly in abrasive wear. They are made mainly in the form of solid strips (Fig. 22.4a); for heavy machines, use is made of 4- to 5-mm thick plates set flush and adhesive bonded (Fig. 22.4b); and, sometimes, accurate bands 0.2 to 0.3 mm thick, clamped in place in stretched condition on the finish-ground ways (Fig. 22.4c).

Attached ways on work tables (the shorter member of a sliding pair) are made of plastics and non-ferrous alloys to achieve improved frictional characteristics and to eliminate stick-slip and scoring. Plastic ways are used in the form of strips 800 to 1 000 mm long and 1.5 to 3 mm thick (Fig. 22.5a), and bands 1.5 to 2 mm thick placed into special recesses and adhesive-bonded to the base. Strips of non-ferrous alloys 4 to 10 mm in thickness are bonded with adhesives based on epoxy resins with additional fastening by screws (Fig. 22.5b) or without (Fig. 22.5a).

Slideway working conditions. The maximum permissible pressures (with regard to tilting moments) on feed-motion ways with the most commonly used cast iron-on-cast iron* sliding pair amount

---

* Here and in what follows, the materials of the sliding pair elements are arranged in the following order: the material of shorter-member ways (usually in a movable unit, e.g. a work table, carriage, etc.)—the material of longer-member ways (in a stationary unit, e.g. a machine bed, column, etc.).

to 25 to 30 kgf/cm² in medium-size general-purpose machine tools, 100 kgf/cm² on gibs in some cases, 10 to 15 kgf/cm² in heavy machine tools, and 100 to 130 kgf/cm² in the slides of heavy machines with a bronze-on-cast iron sliding pair.

Sliding speeds v are up to 1.5 m/s in the main-motion slideways of planing and shaping machines, up to 10 m/s in vertical boring
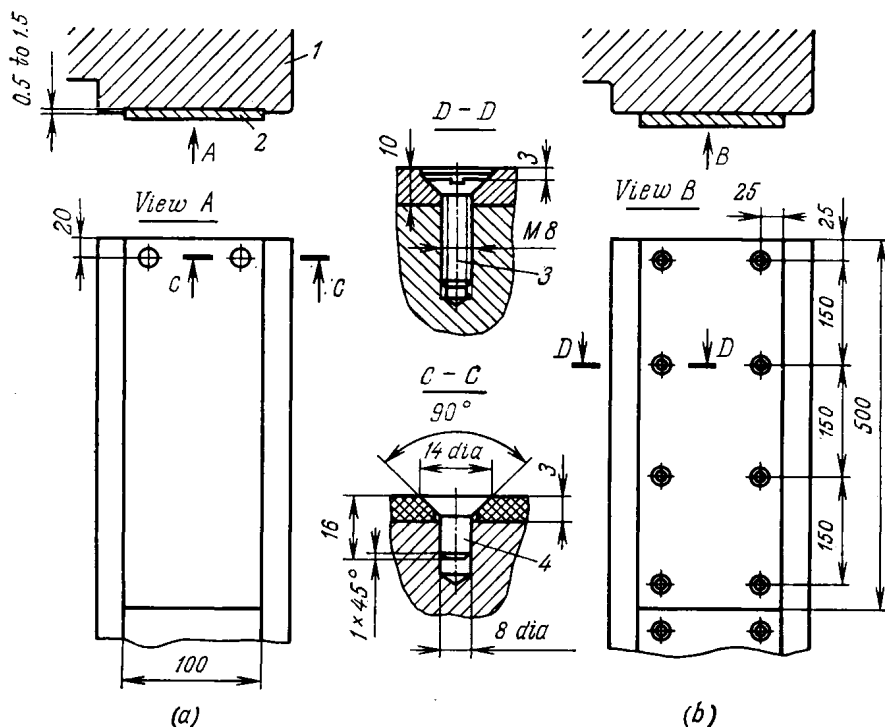
Fig. 22.5. Screw fastening of adhesive-bonded way strips

1—work table (saddle); *2*—attached way; *3*—screw (bronze grades БрАМц 9-2, БрАЖ 9-4 or steel); *4*—pin at strip ends (capron or textolite ПТ)

mills, and from hundredths of a millimetre per minute to 3-12 m/min in feed-motion slideways, the most typical being $v = 0.1$-0.3 m/min.

Swarf, abrasive grits, scales and other machining waste drastically increase the wear rate and friction losses in slideways. Feed-motion ways in many machine tools are oiled by stream lubrication, which is often meagre, the working temperature of the oil is normally close to the room temperature.

22.1.2. Materials

The following requirements are placed on slideway materials, that is, materials of the sliding pairs: wear resistance, including resistance to abrasive wear and scuffing; good frictional properties,

including low coefficients of sliding friction f and static friction f_t and their little dependence on the sliding speed and on the duration of static contact within the low feed-rate region, which greatly reduces stick-slip (see pp. 23, 24) and deformations under load and with time; and stability to working media.

In straight-motion guide ways, the longer member of a sliding pair is usually made of a harder and more wear-resistant material.

Materials used for slideways are described below. The frictional characteristics and wear resistance are given for the materials on unhardened cast iron (exceptions being indicated).

Unhardened cast irons. Specifications for the strength, hardness and microstructure of grey iron castings with slideway features are stipulated by Machine Tool Industry Standard. The hardness of slideways on beds must be no lower than HB 180; for heavy castings over 4 000 kg in mass, this figure may be reduced to HB 170. The ways on work tables, carriages and other components, which are shorter than the mating bed ways, must have a hardness not lower than HB 170.

The cast iron-on-cast iron sliding pair is advisable to use in light-duty machine tools with the slideways well protected from dirt and oiled automatically; also for infrequently functioning and less critical ways, whose wear has no effect on machining accuracy.

Hardened steel, cast iron and other hard materials. Heat treatment to high hardness allows a substantial increase in slideway life. The wear resistance of hardened feed-motion guide ways which are subject to predominantly abrasive wear can be increased from two (for inoculated cast iron) to 2.5 times (for alloy steels), and resistance to seizure can be raised many times. Wear resistance is also improved in an unhardened member of a sliding pair, and its increase proves to be even greater than in the hardened member of the pair. Hardened slideways on beds, uprights, etc. are recommended for heavy use, for applications where it is difficult to shield the ways completely from swarf and dirt and impossible to provide fluid friction, which is often the case with feed-motion guide ways.

With both mating ways hardened, it is possible to obtain a sharp increase (from three to five times) in overall wear resistance as against a cast iron-on-cast iron sliding pair.

Grey iron ways [1]: the initial hardness of castings up to 4 000 kg in mass should be no lower than HB 170; surface hardening is effected by induction or flame hardening methods; the structure obtained is martensite, HRC 48-53, the hardened layer depth is no less than 2.5 mm.

Attached steel ways in the form of solid strips (see Fig. 22.4) are made of the following steels:

—through-hardened high-carbon alloy steels ШХ15 (*HRC* 59-62), ШХ15СГ (*HRC* 59-62) and 7ХГ2ВМ (*HRC* 58-60); the choice of the grades depends on the strip thickness S: ШХ15 for strips up to 25 mm thick, ШХ15СГ for strips up to 50 mm thick, and 7ХГ2ВМ

for strips up to 70 mm thick; steel 7ХГ2ВМ whose resistance to abrasive wear is lower at a common hardness of HRC 58, is advisable for strips with substantially unsymmetrical cross-section;

—case-hardened (carburized) alloy steels 18ХГТ and 12ХН3А (HRC 59-62); the depth of the case after finish grinding should be no less than 1.2 mm; with $S \leqslant 40$ mm, use should be made of steel 18ХГТ; with $20 < S \leqslant 60$ mm, steel 12ХН3А. Carburized steels are employed for strips which are fastened with screws from the side opposite to the way's rubbing surface; greater hardness values (within the given limits) for both through-hardened and case-hardened steels result in higher wear resistance; the use of through-hardened steels is preferable;

—case-hardened (nitrided) alloy steel 20Х3МВФ (HRC 61-64); the depth of the nitrided layer is 0.5 mm; after finish grinding, no less than 0.3 mm. Steel 20Х3МВФ which exhibits the greatest wear resistance among the above-mentioned materials, is recommended for strips with symmetrical cross-section in applications where minimal wear is allowed (precision machine tools).

Attached steel ways in the form of thin strips (Fig. 22.4b) are made of steel ШХ15 (HRC 59-62). Heat treatment of thick and thin strips is described in [1].

Frame and column slideways can also be coated with wear resistant materials: a uniformly deposited hard chromium plating 25-50 μm thick, HRC 68-72; sprayed molybdenum coating, HRC 65; etc.

Non-ferrous alloys and plastics. Attached ways of bronze, zinc alloys, and plastics (Fig. 22.5) are used for work tables, slides, and other shorter ways in heavy and numerically controlled (NC) machine tools. The aim is to reduce friction, improve the uniformity and accuracy of feed and positioning motions, and to prevent scoring. The recommended materials are wrought bronze БрАМц9-2 and zinc alloy ЦАМ10-5. By wear resistance and friction properties bronze БрАМц9-2 is roughly similar to cast tin bronzes БрОЦС5-5-5 and БрОЦС6-6-3. Compared with alloy ЦАМ10-5, bronze БрАМц9-2 exhibits higher resistance to abrasive wear, lower resistance to wear in dry friction, and somewhat less favourable frictional characteristics (Fig. 22.6).

New polymeric materials based on fluoroplastic-4 (filled with bronze, coke, molybdenum disulphide, etc.) feature exceptionally low friction losses at low sliding speeds, that is, lower than those in cast iron-on-cast iron sliding pairs by a factor of 5 to 6 when lubricated with a base oil and by a factor of 2 when lubricated with a special slideway (antistick-slip) oil (Fig. 22.6). These polymeric materials have excellent antistick-slip properties similar to those of fluoroplastic-4 (see pp. 23, 24); their wear resistance, however, is much higher than that of fluoroplastic-4, particularly in dry friction. They are harder and less deformable under load than fluoroplastic-4. These materials, e.g. grade Ф4К15М5 made in the USSR and Turcite "B" made by V. F. Shamban and Co. in USA in the form

of a band 1.5 to 2 mm thick ready for adhesive bonding, find ever growing use in heavy, precision, and NC machine tools.

Use is also made of new quick-setting compositions based on epoxy resins (SKC-3 produced by Gleitbelag-Technik G.m.B.H. of FRG and some others). These are deposited in paste form on the ways of work tables (slides); the latter are placed on the finished mating ways of the bed. After the material has solidified, the table ways
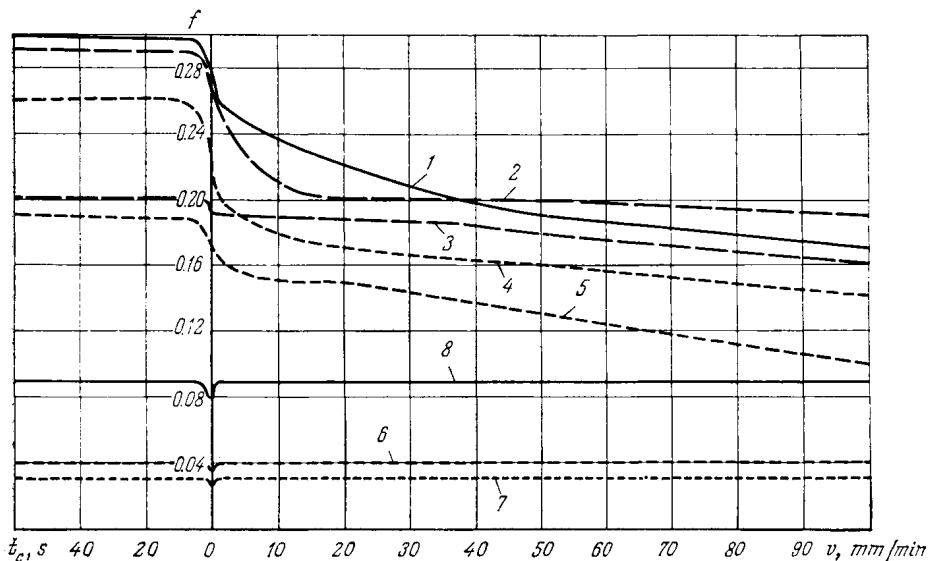
Fig. 22.6. Coefficient of friction as a function of time t_c of static contact and of sliding speed v. Testing on the ENIMS-LON-23N test rig [5]; rubbing against cast iron СЧ21-40, HB 180; specimens scraped (25 spots per unit area of 25 × × 25 mm², depth of scraping 2 to 5 μm) and run in, contact pressure 2 kgf/cm². Lubrication with oil И-40А
1—cast iron СЧ21-40; 2—textolite ПТ; 3—bronze БрОЦС 6-6-3; bronze БрАМц 9-2, chromium-plated cast iron; 4—capron Б; 5—zinc alloy ЦАМ 10-5; bronze БрОФ 10-1; 6—filled fluoroplastic-4; (Ф4К15М5, Turcite "В"); 7—fluoroplastic-4. Lubrication with slideway oil ПНСп-40; 8—cast iron СЧ21-40

are ready for service, usually without any additional processing. Although these materials are less advantageous in frictional characteristics, antistick-slip properties, and wear resistance than the filled fluoroplastics, they give substantial labour savings in the manufacture of guide ways, particularly in heavy machines.

Attached ways made of plastics such as textolite (cloth laminate) ПТ and moulded strips of capron resin Б have long been used in heavy machines to prevent scoring peculiar to cast iron-on-cast iron sliding pairs. Capron ways, which have better resistance to abrasive wear than textolite ways, are used only for feed-motion applications. To reduce the friction force in these ways use should be made of slideway oils.

16

Where slideways are exposed to dirt and swarf, non-ferrous alloy-(or plastic)-on-cast iron pairs exhibit a greater total wear than cast iron-on-cast iron pairs, mainly because the non-ferrous alloys (plastics) wear much heavier than the mating cast iron. Therefore the essential condition for the use of non-ferrous alloys and especially of plastics is reliable protection of the ways from mechanical impurities.

When high wear resistance and the uniformity of feed motion are required, combinations of plastic (based on fluoroplastic-4) and hardened steel (or cast iron) are recommended for use.

22.1.3. Selection of Oils

The grade and viscosity of oils are selected depending on the operating conditions: sliding speed, pressure, slideway protection against dirt, motion uniformity and positioning accuracy requirements, spatial arrangement of the ways, etc. (Table 22.1).

For slideways substantially free from dirt and swarf and with scant lubrication, industrial oils of higher viscosity should be selected from the grades given in Table 22.1. Greater loads and lower sliding speeds also call for oils of higher viscosity. Where exposure to dirt is considerable and lubrication is meagre, the lower-viscosity industrial oils (Table 22.1) are a better choice, because they will wash out particles of dirt and so prolong the wear life of the ways. With ample lubrication by a closed-circuit system, variation of oil viscosity within the range of the oils given in Table. 22.1 hardly has any effect on wear. Special slideway (antistick-slip) oils [17] are the most efficient for slideway application. The series ИНСп slideway oils (see Table 22.1) are used for slideways in NC machine tools, high-precision and heavy machines, instruments, metalforming machine tools and other machinery where strict requirements are placed on the uniformity of low-rate feed motions, the accuracy of positioning, and the frictional characteristics at low sliding speeds. The ИНСп oils have the following properties. They eliminate stick-slip in slideways with different combinations of materials at slow sliding speeds v, including extremely low speeds $v_m < 1$ mm/min (see p. 24). The oils provide low forces of both static friction and sliding friction at low sliding speeds. For instance, the coefficients of static friction and sliding friction ($v_m \leqslant 1$ mm/min) in guide ways with cast iron-on-cast iron and cast iron-on-hardened steel sliding pairs at pressures of 1 to 10 kgf/cm² amount to $f = 0.07$ to 0.10, which is lower by a factor of about 2.5 to 3 than the values obtained in lubrication with base oils (Fig. 22.6). The oils have good antiscuff properties, which makes it possible to use them for heavy-duty gear transmissions; antiwear qualities; tackiness, which retains them in place; etc.

The use of the slideway oils in machine tools provides a number of advantages.

Table 22.1

Oils recommended for lubrication of slideways

Slideways	Operating conditions	Oil grade	Kinematic viscosity at 50°C, cSt
Horizontal	—	И-30А*[1]	28-33
		И-40А	35-45
		ИНСп-40*[2]	35-45
	Increased pressures. Slideways in heavy machine tools. Horizontal slideways with vertical surfaces of large area	И-40А*[3]	35-45
		ИНСп-65*[2]	60-70
		ИНСп-110*[2]	100-120
	Limiting of table lift	ИНСп-20*[2]	18-25
Vertical	—	И-40А*[1]	35-45
		ИНСп-110*[2]	100-120
	Increased pressures. Slideways in heavy machine tools	ИНСп-110*[2]	100-120
	Lubrication with oil from hydraulic system	ИГП-18	16.5-20.5
		ИГП-30	28-31
		ИНСп-20*[2]	18-25
Horizontal and vertical	A single oiling system for horizontal and vertical ways. Limited variety of oils	И-40А*[1]	35-45
		ИНСп-65*[2]	60-70

*[1] Also used where slideways are exposed to dirt and lubrication is meagre.
*[2] Special slideway (antistick-slip) oils; for properties and application see p. 112.
*[3] Used only for stream lubrication on ways exposed to external impurities.

The machining accuracy and surface finish on various types of NC machines and finishing machine tools are improved owing to a greater uniformity of feed motions, higher accuracy of positioning, and reduced lifting of slides on the lubricant film through the use of lower-viscosity oils. The stiffness of machine tools is increased since smaller clearances in closed-contour slideways, quills and other movable joints are possible owing to reduced friction forces. The production rates are increased through reduced positioning time and more reliable operation of cutting tools. The amount of scrap is brought down; the power consumption of feed drives and the physical effort required for manual positioning of machine units is reduced.

Where slideways are relatively free of dirt, the slideway oils which give a stronger and more lasting film, reduce wear and scoring due to irregular lubrication. With considerable exposure to dirt and with scant lubrication, the slideway oils cause greater wear than plain industrial oils of the same viscosity. Increase in oil delivery tangibly reduces the wearing action of the slideway oils [12]. Therefore, the use of these oils requires the absence of, or adequate protection from, external impurities; when this is impossible, increased delivery of oil must be resorted to. When a slideway oil is introduced into the system, the ways should be run in over the whole length for no less than 30 min to form a boundary lubricant film. The full effect of the oil (the absence of stick-slip, etc.) is achieved after the running-in.

22.1.4. Friction in Slideways

Depending on slideway design and working conditions, the operation of the slideways may involve boundary friction, fluid friction, or mixed (simultaneously boundary and fluid) friction. Friction in slideways is treated in detail in [12].

Modes of friction

Boundary friction in slideways arises at particularly low sliding speeds (from fractions to a few millimetres and, sometimes, even tens of millimetres per minute). A very effective way of reducing friction is the use of fluoroplastics in the ways and also of additive-type slideway oils.

Mixed friction is characteristic of most feed-motion slideways in a wide range of working conditions. Typical relationships between the coefficient of static friction f_t and the duration of static contact t_c and also between the coefficient of sliding friction f and sliding speed v for a number of slideway materials are given in Fig. 22.6.

With plain industrial oils, the value of f_t which is determined at a very slow speed of the load applied, is stable for a given sliding pair and duration t_c of static contact; f_t somewhat grows with t_c, slightly decreases with an increase in oil viscosity, and drops with a rise in contact pressure. The coefficient of friction f for sliding pairs cast iron-on-cast iron or cast iron-on-hardened steel sharply drops on transition from static to sliding friction; as sliding speed increases, this decrease tends to slow down (see Fig. 22.6). The f-v relationship is given for low values of v, because in this speed range the level of f is not so much dependent on the design and size of the test stand and the specimens (i.e. on the hydrodynamic factor). For fluoroplastic-4 and its modifications, f_t is very low, and f exhibits a certain rise on transition from static to sliding friction ($t_c = 0$).

Relation between f and $\lambda = \dfrac{\eta v}{p}$ (which defines the working regime) at given values of oil dynamic viscosity η and pressure p,

and between f and λ/λ_{cr} (which is the relative characteristic of the working regime) corresponds to the f-v relation (Fig. 22.7). Here, $\lambda_{cr} = \frac{\eta v_{cr}}{p}$ is the critical characteristic of the working regime involving the critical speed v_{cr}, at which mixed friction changes to fluid friction and f drops to its minimum $(f = f_{fl})$. The magnitude of v_{cr} varies, depending on the design and material of slideways, the accuracy and finish of rubbing surfaces, the form and dimensions of oil grooves, the viscosity and grade of the oil, pressure, etc. Rationally designed slideways and their oiling systems are chara-
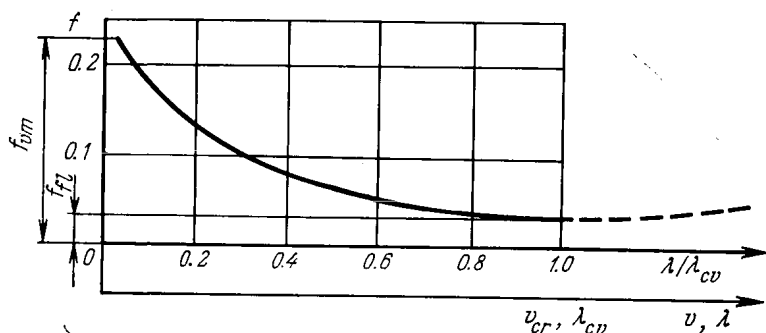
Fig. 22.7 Typical relationship between friction coefficient and sliding speed

cterized by small values of λ_{cr}. The λ/λ_{cr} ratio indicates how close a given regime is to the critical one corresponding to fluid friction conditions [12]. The decrease of f with increased λ (or v) is associated with a rise in the hydrodynamic lift. The hydrodynamic pressure in rectilinear-motion slideways is caused by a small, but rising with sliding speed, inclination of the moving work table (tool carriage), which creates an oil wedge between the rubbing surfaces [10]. The rounded or chamfered edges and increased wear of the slide ends are conducive to the emergence of the hydrodynamic pressure.

The influence of various factors on the friction in slideways is as follows [12].

Pressure p at very low speeds $(v < 30$ mm/min) has little effect on f; however, at higher speeds f rises with p since increased pressure impedes the development of the hydrodynamic pressure.

The viscosity of oil, η, at very low speeds hardly affects f; at higher speeds, the increase of viscosity results in significantly reduced f and in lower values of v_{cr}.

Increase in ratio L_p/B (where L_p is the length and B is the width of the ways) leads to greater side leakages of the oil, and that reduces the hydrodynamic pressure. The result is higher v_{cr} and λ_{cr}.

Longitudinal oil grooves sharply lower the hydrodynamic load carrying capacity of the ways (by raising L_p/B). Transverse grooves should be preferred; the required number of the grooves is calculated by the method described in [12]. The types and dimensions of

oil grooves on machine-tool slideways are recommended by Machine-Tool Industry Standards.

Any recesses that interrupt the slideway surface reduce the hydrodynamic pressure; al low speeds this effect is negligible, but at higher speeds it becomes significant.

The surface roughness and running-in of slideways at very low speeds ($v < 30$ to 50 mm/min) hardly affect the coefficient of friction, but the influence of these factors grows with the speed.

The frictional characteristics are substantially improved with the use of the hydraulic relief method whereby oil pressure takes up part of the external load. The coefficient of friction is reduced through a change in contact deformations, and this effect is not accompanied with the lifting of the slide. The coefficients of static and sliding friction in uniformly loaded hydraulically relieved slideways at $v < 50$ mm/min are approximately determined from the expression

$$f_{hr} \approx f\left(1 - \frac{N_{hr}}{N}\right)$$

where f is the coefficient of friction under the same conditions without hydraulic relief; N_{hr} is a hydraulic relief force, kgf; N is an external load, kgf.

Another method to reduce the friction coefficient is mechanical relief, where part of the load is taken up by rollers actuated by springs, hydraulic cylinders, etc. The coefficient of friction is found from the same expression, in which the force of hydraulic relief N_{hr} is replaced by the mechanical relief force $N_{mr} = ip_r$, where i is the number of the rollers, and p_r is the force of a spring (hydraulic cylinder) acting on one roller.

Fluid friction. *Hydrodynamic friction* occurs in main-motion slideways working at maximum speeds of about 1.5 to 10 m/s (planers and vertical boring mills). Conditions for fluid friction are substantially improved by providing oil grooves and wedge-forming bevels on the ways in accordance with Machine Tool Industry Standards. The fluid friction coefficient is a function of the working regime

$$f_{fl} = c\sqrt{\frac{\eta v}{p}}$$

where c is a coefficient determined by the geometry of the hydrodynamic ways.

Hydrostatic friction takes place where a special lubricating system provides separation of the slideway mating surfaces by an oil film of high rigidity. This regime is maintained over the whole range of working conditions by controlling the forced feed of oil.

The coefficient of friction [12]

$$f = \frac{T_{fl}}{N} = \frac{T_{fl}}{Ap} = \frac{1}{10^6 60 h_{\min}}\left(1 - \frac{A_p}{A}\right)\frac{\eta v}{p}$$

where T_{fl} is the force of fluid friction for one bearing zone (a section of the ways that has an oil pocket), kgf; N is the load on one bearing zone, kgf; A is the surface area of the bearing zone, cm²; p is pressure, kgf/cm²; A_p is the area of the grooves that form the pocket or the area of the pocket made as a single recess, cm²; v is the speed
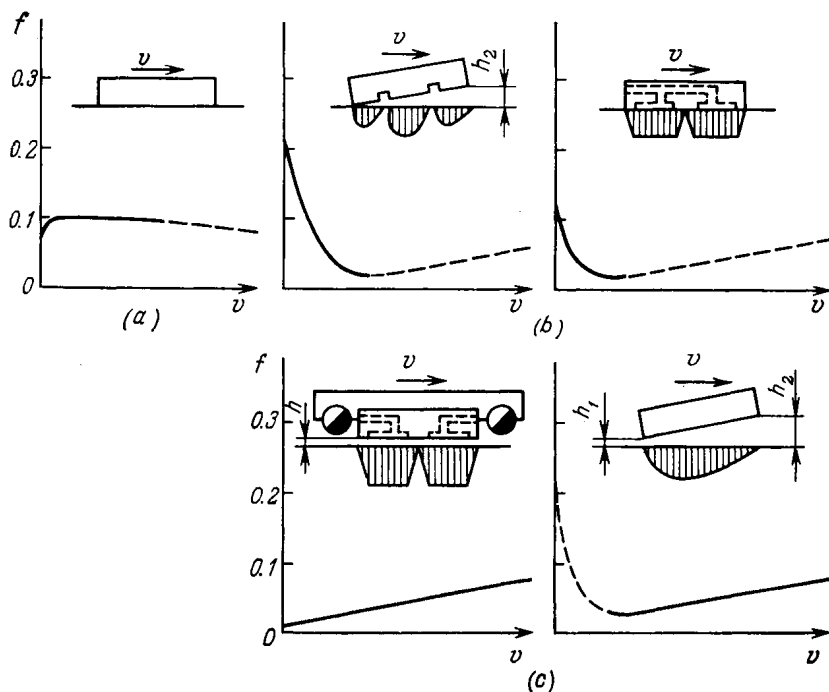
Fig. 22.8. The coefficient of friction as a function of sliding speed in slideways [12]

(a) boundary friction, lubrication with a slideway oil; (b) mixed friction (right—with hydraulic relief, left—without); (c) fluid friction (left—hydrostatic ways, right—hydrodynamic ways). Solid line defines the region corresponding to a given mode of friction

of the table (slide) movement, m/min; h_{min} is the minimum design thickness of the oil film, cm; and η is oil dynamic viscosity, cP.

Low and practically equal coefficients of static and sliding friction at low speeds ensure, along with a direct relationship between f and v, an exceptionally favourable frictional behaviour of hydrostatic ways. Typical frictional characteristics and pressure diagrams for various types of slideways are given in Fig. 22.8.

The uniformity of motion and the accuracy of positioning

During low-speed or fine-adjustment movement of slides in machine tools, instruments or other machines (with guide ways in the form of cast iron-on-cast iron or cast iron-on-hardened steel sliding pairs), a phenomenon is often observed that is known as

22

stick-slip. It manifests itself as an erratic feed motion and brings about the loss of machine response and positioning accuracy. The result is the impaired machining accuracy and surface finish, lower productivity, additional dynamic loading of drive systems, shorter life and breakdowns of cutting tools, and increased slideway wear rate. These effects are especially detrimental to the performance of precision, numerically controlled, and heavy machine tools.

The accuracy of small displacements depends on the drive stiffness and the mode of friction in the slideways. An oscillogram of
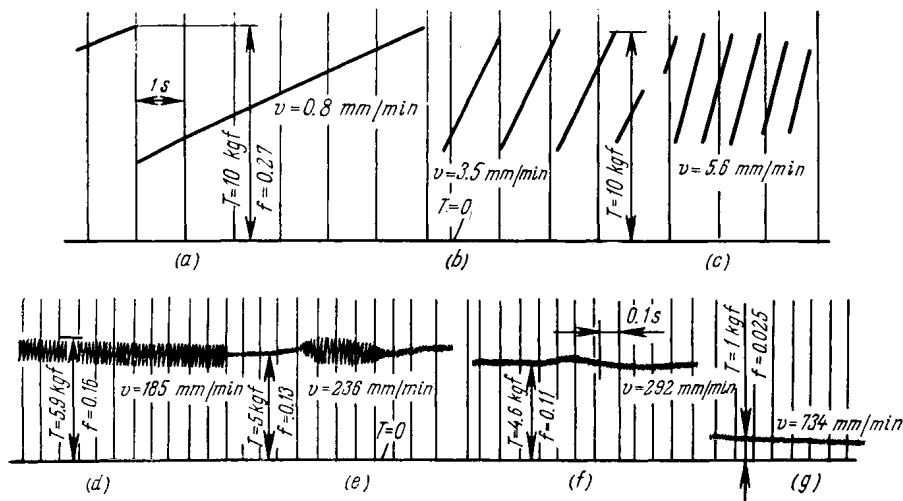
Fig. 22.9. Oscillograms of friction force variations in testing cast iron rubbing against cast iron

(a), (b), (c) relaxation oscillations; (d), (e) oscillations without halts; (f) uniform sliding; (g) fluid friction
Scraped rubbing surfaces; lubrication with oil И-40A; pressure $p = 2$ kgf/cm², drive stiffness $j = 167$ kgf/mm, $v =$ sliding speed

friction force variations on stepping up the sliding speed in tests on the ENIMS-LON23N test rig [5] which simulates friction in slideways, is presented in Fig. 22.9 [17].

Movement at very low speeds (cast iron-on-cast iron pairing, lubrication with a straight oil) gives rise to relaxation oscillations with halts (Fig. 22.9a through c); as the speed is increased, these change to oscillations without halts (Fig. 22.9d, e), and then, still within the region of mixed friction, the oscillations die out (Fig. 22.9f). The error of positioning of a machine unit moving at low speed can be roughly estimated by the formulas [16]

$$\delta = (1 \text{ to } 2) \frac{\Delta T}{j} \text{ μm}, \quad \Delta T = (f_t - f) N$$

where ΔT is the difference between the static and the sliding friction force, kgf; $f_t - f$ is the difference between the static and the

23

sliding friction coefficient (in sliding on cast iron and lubrication with straight oil, f is taken to be 0.1 for cast iron and cloth laminate, 0.06 for bronze, and zero for fluoroplastic-4 and the Ф4К15М5 composition); N is the normal force in the ways, kgf; and j is the stiffness of the drive, kgf/μm (in machine tools commonly $j = 5$ to 15 kgf/μm).

Reducing the coefficient of static friction in slideways is crucial to the prevention of relaxation self-oscillations. The factors that contribute to the rise of the hydrodynamic pressure (improved design of the slideways, better surface finish, higher viscosity of oil, etc.) only reduce that part of the mixed-friction region in which relaxation self-oscillations take place. This, however, has no tangible effect on the frictional characteristics and the uniformity of motion at very low speeds. A really significant reduction in the static friction coefficient is attained by using slideways made of fluoroplastic-4 based compositions and slideway oils. In rubbing against cast iron (steel) with the use of straight oil, fluoroplastic-4 and its modifications exhibit an extremely low coefficient of static friction f_0 at a zero contact time, even lower than that in very slow movement $(f_0 < f_{v_m})$, which is seen in Fig. 22.6, curves 6 and 7. This provides an exceptionally high stability of motion in slideways made of these materials. By contrast, the widely used materials, such as cast iron, bronze or laminated plastic ПТ, in rubbing against cast iron with straight-oil lubrication show a high coefficient of static friction f_t, and a sharp drop in the friction coefficient in sliding (Fig. 22.6, curves 1-5). These conventional materials often fail to provide stable slow motion.

The slideway oils make it possible to ensure highly uniform motion for practically any combination of materials used for slideways (see Fig. 22.6, curve 8). Although the magnitude of f_0 for various sliding pairs is greater than for the fluoroplastic-4-on-cast iron combination, the relationship $f_0 < f_{v_m}$ also holds here.

Figure 22.10 illustrates the results of testing a cast iron-on-cast iron sliding pair lubricated with a straight oil and slideway oils [17]. When comparing the curves in Fig. 22.10a and b, it is seen that the slideway oil ensures uniform motion at a very low speed; upon stopping the drive, the friction coefficient gradually decreases to f_0. The curves in Fig. 22.10c and d show different patterns of variation of the friction force with increased speed. With the straight oil, a considerable dropping section of the curve is observed; the stick-slip zone is defined by a bottom line (Fig. 22.10c), which corresponds to the minimum value of the friction coefficient (see the value of f at the end of a slip in Fig. 22.10a). With the slideway oil, a small ascending portion of the curve can be seen (Fig. 22.10d).

As well as the absence of stick-slip at very slow sliding movement, the ratio $k_f = \dfrac{f_0}{f_{v_m}}$ at a given pressure and drive stiffness can be used as a criterion for assessing the properties of sliding pairs

and oils. In tests on the LON23N test rig (with sliding speed $v_m = 0.8$ mm/min, pressure $p = 5$ kgf/cm^2, stiffness of the drive $j = 40$ kgf/mm), the following values of k_f have been obtained that define the frictional properties of oils: $k_f = 1$ — poor, $k_f = 0.96$ to 0.98 — moderate, $k_f \leqslant 0.95$ — good.

At present, the following means are resorted to for improving the uniformity of motion and the accuracy of positioning [12, 16]:
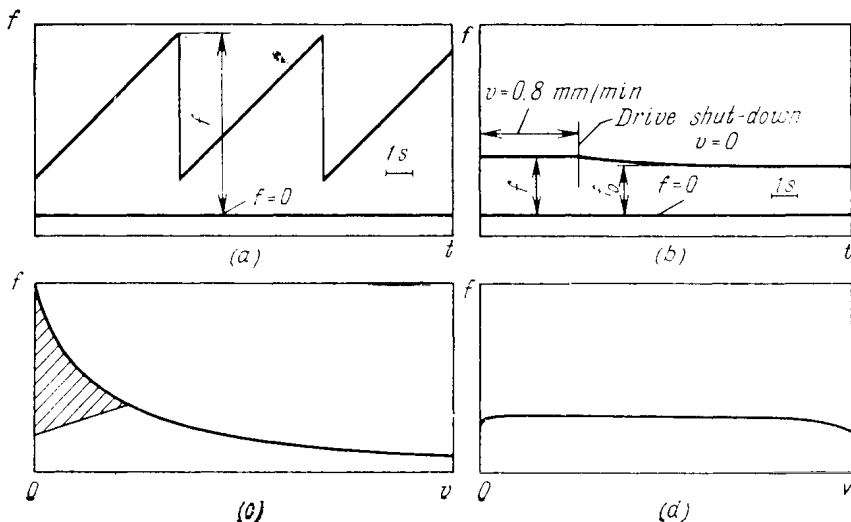
Fig. 22.10. Friction of cast iron on cast iron lubricated with straight oils (a), (c) and slideway oils (b), (d)
(a), (b) variation of friction coefficient f in time in slow movement (v_m) with drive stiffness being constant; (c), (d) variation of friction coefficient with sliding speed, the stick-slip region is shaded

(1) use of rolling guides;
(2) change-over to fluid-friction (hydrostatic) ways;
(3) use of slideway materials based on fluoroplastic-4;
(4) lubrication with special (slideway) oils;
(5) application of slideways relieved of pressure (hydraulically, mechanically, pneumatically, etc.);
(6) raising of the stiffness of drives and gear trains;
(7) use of special high-stiffness drive systems (thermodynamic, magnetostriction, and some other types);
(8) use of damping devices in feed drives;
(9) provision of small-amplitude transverse oscillations imparted to movable units in the plane of sliding;
(10) improvement of the quality of manufacture of slideways and feed drive mechanisms, proper installation of the machine tool to reduce friction in the ways and to increase the torsional stiffness of the drive.

25

22.1.5. Wear of Slideways

A relatively high rate of wear often observed in straight-motion slideways is caused by many factors. The principal are the use of the uncovered slideways which are impossible to protect securely against swarf and dirt, poor lubrication, operating conditions that exclude formation of oil wedges with adequate bearing capacity during slow motion, frequent stops and reversals of work tables or tool slides; and non-uniform use of slideways along the length.

Abrasive wear, the most common* in slideways, is characterized by high rates; it occurs when the slideways are exposed to machining waste. The wear rate grows with the size of foreign bodies (within limits which are smaller than clearances in the ways), their hardness, strength, and edge sharpness. Inadequate accuracy of contact between the mating surfaces of the ways also leads to increased wear rate. The machining waste includes (in order of increasing abrasive action) steel and cast-iron chips, scale, sand, and electrocorundum (aluminium oxide).

With respect to abrasive wear the plastic-on-cast iron sliding pairs have the following distinguishing features:

wear of the soft plastic by the rough hard metal way (microcutting);

the cross-sectional wear is non-uniform; individual portions of the plastic are charged with hard particles, and, wearing slower, they become convex and press into the cast iron surface, cutting a groove.

The life of slideways subject to abrasive wear is prolonged by introducing reliable protective devices, including seals [12], by arranging slideways in a zone where their exposure to abrasive particles is minimal, by hardening the ways to the hardness exceeding that of the abrasive particles (see pp 14,15).

Scuffing is particularly severe in slideways where cast iron rubs against cast iron (both unhardened), with little oil or none at all, and particularly in the presence of mechanical impurities and at high local pressures. The impurities initiate and intensify the development of seizure. Seizure on a considerable surface area is accompanied by scoring and other kinds of surface failures (through increased abrasive wear, etc.). The resulting severe wear often necessitates repairs of the slideways.

Scoring is caused by the following factors (in the cast iron-on-cast iron pairing)** [4]:

— in main-motion slideways — the loss of oil lubricity at a high temperature developing under conditions involving both high sliding speeds and high pressures, which is typical of the circular

---

* The mechanism of wear is not necessarily abrasive, especially considering the latest advances in protection techniques and improved maintenance of machinery (*Ed.*).

** The oiling system is presumed to be in working order.

ways in vertical boring mills*; in that case a steep rise in pressure results from temperature strains in the work table and the base [12];

— in feed-motion slideways (low sliding speeds) — the action of machining waste with inadequate lubrication at a high local pressure.

The hard mechanical particles retain the lubricant on their surface and so promote a change to dry friction conditions; they also scrape and deform the surface layers protected by oxide films and thereby give rise to scoring. High local pressures are particularly specific of heavy machine tools because of deformation of the frames, work tables and other units; among these deformations are temperature strains, elastic deformations, deformations due to residual stresses including those caused by strain hardening of the work-table top surfaces developed during service [3], etc. That, and also the difficulty of ensuring a high quality of metal in large iron castings account for scuffing as a major form of wear in the slideways of heavy machine tools. Scoring can also be attributed to steel chips getting under a moving unit and scratching the mating slideway surface, or to chips of non-ferrous metals, such as aluminium, which readily weld to cast iron, and also to vibrations at the sliding interface whereby the oil is squeezed out and scoring results.

The useful life of slideways is prolonged by a number of measures, including the provision of fluid friction [12]; the use of materials that either have no tendency to scoring (plastic or non-ferrous alloys rubbing on cast iron) or are less liable to scoring (cast iron on hardened cast iron or steel) than cast iron on cast iron (see pp 14 to 17). Some other measures are the use of high-reliability oiling systems; the improvement of lubrication methods and oil properties, specifically, the use of slideway oils; the introduction of dependable slideway protection devices; the elimination of high local pressures in the ways due to deformation of frames, work tables, and other units.

Normal wear under conditions, where the lubricant is clean of mechanical impurities and no scuffing takes place, involves a group of wear phenomena (including fatigue, corrosion and mechanical wear) that affect the thin surface layers of the slideways. The wear rate here is relatively low.

The average values of wear characteristics of the machine bed ways, namely, wear rate i_u and specific wear I for machines of different types operating in single-piece and small-lot production are given in Table 22.2. Values of i_u and I are found by the formulas

$$i_u = \frac{U}{t_{ef}} \ \mu\text{m/year}, \quad I = \frac{U}{pL} \ \mu\text{m cm}^2/(\text{kgf km})$$

where U is the maximum linear wear along the length of the most worn surface of the ways, μm; t_{ef} is the effective life of the machine,

---

* The main reason for scoring of the circular ways in these machines is failures of the oiling devices.

Table 22.2

Average values of yearly wear rate and specific wear for machine bed ways working in mixed-friction conditions

Machine-tool type. Slideway surfaces[1]	Bed-way material and hardness[2]	Slideway surface contamination	Sliding interface condition	I, μm cm²/ (kgf km)	i_u μm/year
Lathe[3] Frontal prismatic way	Cast iron СЧ 21-40 HB 180	Considerable	Joint faces closed	2.6-3.8	50
Lathe[3]. Rear flat way		Moderate	Joint faces parted	50-70	15
Single-column jig borer[4]	Cast iron СЧ 32-52 HB 200	Insignificant	Joint faces closed	1.1-1.6[5]	0.7[5]
Lathe[3] Frontal prismatic way	Cast iron СЧ 28-48 HRC 50	Considerable		1.4	30
Lathe[3]. Rear flat way		Moderate	Joint faces parted	25-35	10

[1] Combination male ways, see Fig. 22.1.
[2] Saddle (table) material — unhardened cast iron, grades СЧ 15-32 and СЧ 21-40.
[3] Swing over bed 400 mm; tool-carriage sliding distance per year about 17.3 km in work on a two-shift basis (70% on auxiliary motions).
[4] Table size 280×560 mm, sliding distance per year 1.1 km in two-shift operation.
[5] Steady-state wear.

i.e. the nominal working time after subtracting the longest periods of downtime in two-shift service, years; p is the nominal mean pressure, kgf/cm²; L is the length of the sliding path of the work table or carriage, km.

The ways of the bed and the work table (or tool slide) wear unevenly along the length. In plain and turret lathes, the most worn section of the bed ways is in the middle, somewhat nearer the spindle nose; the saddle ways have the ends worn harder than the middle, especially the end facing the spindle, where the amount of wear is 2-2.5 times the maximum wear of the bed ways. The lathes in large-lot and mass production show a wear of the bed ways that is 2 to 3 times the values given in Table 22.2. The rate of wear is associated with the clearances in the ways, because large abrading particles get into the contact zone and sharply intensify wear (see Table 22.2). In jig borers, the low values of i_u as compared with those for other types of machine tools are attributed primarily to a short sliding path of the work table.

Wear calculation. The following method of engineering calculation is based on the values of specific wear of the ways that have

been observed in operation under conditions of mixed friction and predominant abrasive action [13].

The main formula for approximate estimation of the ways wear is

$$U \approx I \sum_{i=1}^{n} k_i \frac{f_i}{f} L_i p_i$$

where U is the average linear wear at the most worn place of the ways, μm; i is the sequence number of an operating regime, i.e. cutting movement, auxiliary movement, etc.; n is the number of different regimes; L_i is the length of the sliding path of the work table (or carriage) in the i-th regime, km; p_i is the nominal mean pressure in the i-th regime, kgf/cm^2 (found by the method described in [18]); I is the specific wear in the basic regime, μm cm^2/kgf km; k_i is the ratio between the actual maximum wear along the slideway length and the wear that would occur at a uniformly distributed pressure and an invariable sliding path equal to the length of the table ways. Generally, k_i can be determined by the method given in [13, 15].

The factor f_i/f, which is the ratio between the friction coefficients in the i-th regime (f_i) and some regime used for reference (basic regime), takes into account the effect of a friction regime on wear. If, for instance, the basic regime defines motion at a very slow speed (under 10 mm/min) in which no lifting of the movable unit on the lubricant film takes place, this ratio will be $f_i/f = 0.1$ to 1. By introducing this ratio, allowance can be made for a decrease in the load due to the hydrodynamic lift, whose magnitude depends on the sliding speed, pressure, oil viscosity, etc.

Let us consider operation in two regimes: the cutting movement $(i = 1)$ and the auxiliary movement $(i = 2)$.

The cutting movement will be the basic regime; the formula will assume the form

$$U \approx k_1 I_1 L (\gamma_1 p_1 + \gamma_2 \gamma_3 p_2)$$

where L is the total length of the sliding path, km,

$$\gamma_1 = L_1/L, \quad \gamma_2 = L_2/L, \quad \gamma_3 = k_2 f_2/k_1 f_1$$

I, L, γ_1, γ_2, are determined from field observations, conducted by the procedure outlined in [11]; some values are given in Table 22.2. An example of the wear calculation is presented in [13].

22.1.6. Methods for Improving Slideways

1. Providing favourable frictional conditions:
(a) the use of hydrostatic ways (particularly in heavy machine tools) with a high-rigidity oil film, the use of aerostatic ways; (b)

for precision applications, the use of automatically controlled hydrostatic ways that ensure an extremely high rigidity of the film in the specified load range; (c) the use of slideways with lubricating systems utilizing both the hydrostatic and the hydrodynamic lift; (d) the use of hydraulically relieved slideways; (e) the use of combined sliding and rolling guides; (f) the optimal selection of oil grades; (g) the development of highly reliable oiling systems.

2. Improving protection, enhancing the accuracy of slideways: (a) complete insulation of slideways from external impurities by introducing reliable protective devices; (b) increasing the accuracy of manufacture and reducing deformations of slideways.

3. Improving slideways with mixed friction: (a) the use of hard materials for machine frames and columns, which have high wear resistance in operation with an impure lubricant and high resistance to scuffing; (b) the use of fluoroplastic-4 based materials and similar plastics for table and saddle ways ensuring low friction, the uniformity of feed motions, high accuracy of positioning, and high wear resistance; (c) the choice of the optimal cross-section of slideways for minimum wear effects on machining accuracy [14]; (d) the use of optimal surface finishes and coatings for improved running-in of the ways. All these measures along with simple construction, cost effectiveness, high contact rigidity and vibration damping typical of mixed friction, will make it possible to improve considerably the service properties of slideways.

22.2. ROLLING GUIDES

Rolling guides are finding ever increasing application in modern machinery and instruments. The engineering design and construction of rolling guides in machine tools are discussed in detail in [7].

Rolling guides offer significant advantages. The first is a low friction force which is by an order of magnitude smaller than in cast iron sliding guides with mixed friction and which practically does not depend on the speed of motion. The result is small drive forces, uniform slow movements, high accuracy of positioning and high response of machine units, the possibility of functioning with clearances fully taken up (preloaded assemblies). Other advantages are good positioning repeatability on reversals, accuracy maintained over time, and moderate lubrication requirements.

The drawbacks are high cost, comparatively large dimensions, and greater sensitivity to vibrations and to mechanical impurities.

Combination-type guide ways, which make it possible to use the best features of rolling guides (low friction, assembly without clearances) and sliding guides (high vibration damping, lower manufacturing costs) are being used more and more in metal-working machinery.

22.2.1. Construction

Classification of rolling guides. These are classified by the shape and construction of rolling elements as guides with balls (Fig. 22.11*b*, *k*, *l*), guides with rollers (Fig. 22.11*a*, *c*, *d*, *f*, *h*, *i*, *j*), guides with needle rollers (Fig. 22.11*g*) and guides with rollers mounted on fixed pivot pins (Fig. 22.12*a*, *b*).

By geometrical form, rolling guides are divided into prismatic (Fig. 22.11*a* through *k*) and cylindrical (Fig. 22.11*n*).

By the method of loading, rolling guides can be without preloading (Fig. 22.11*a* to *c*), partly preloaded (preload adjusted in a horizontal direction) and loaded by the weight of the unit in a vertical direction (Fig. 22.11*d* to *e*), and fully preloaded (Fig. 22.11*f* to *n*).

Rolling guides without preloading are much simpler and cheaper in manufacture, since often they can be made of cast iron, with lower accuracy requirements.

Preloaded rolling guides are hardened; these are designed for high stiffness and high tilting moments. With an increase of preload the stiffness of the guides initially rises steeply and then levels off; conversely, the friction force first varies little and then sharply rises. The optimum amount of preload deflection (normal to the way faces) in carefully machined ways comes to 5 to 6 μm, with the minimum being 2 to 3 μm. The maximum permissible preload deflection with regard to the surface layer strength (HRC 60) is 10 to 25 μm, depending on the diameter of the rolling elements.

Rolling guides can be arranged in three different modes according to the ratio between the lengths L_1 and L_2 of the ways of the mating units (Fig. 22.13).

(1) $L_1 > L_2$, $L_2 = L_p$, $l_c = L_p + 0.5s$ where L_p is the effective way length; l_c is the cage length, and s is the length of travel. This arrangement is used for medium lengths of travel (Fig. 22.13*a*).

(2) $L_1 = L_2 = L_p + 0.5s$. This is used for short-travel applications (Fig. 22.13*b*).

(3) $L_1 \gg L_2$, $L_2 = L_p$; the rolling elements recirculate along a closed path through return channels made in one of the mating units (usually the short one). The length of travel is not limited (Fig. 22.13*c*).

The main types. *Rolling guides with balls.* The ways are flat (Fig. 22.11*b*), prismatic (Fig. 22.11*b*, *k*) or cylindrical (Fig. 22.11*n*) in cross section. The prismatic shape can also be embodied by round bars (Fig. 22.11*l*). The cylindrical guide consists of a shaft, bushing, and balls. Rolling guides with balls are used for small loads; they have limited load carrying capacity and relatively low rigidity. The materials employed are hardened steels.

Rolling guides with rollers have a load carrying capacity which is 20 to 30 times greater than that of the ball-type rolling guides (on flat ways) of the same dimensions; their stiffness is 2.5 to 3.5 times the stiffness of rolling guides with balls. The length-to-diameter ra-
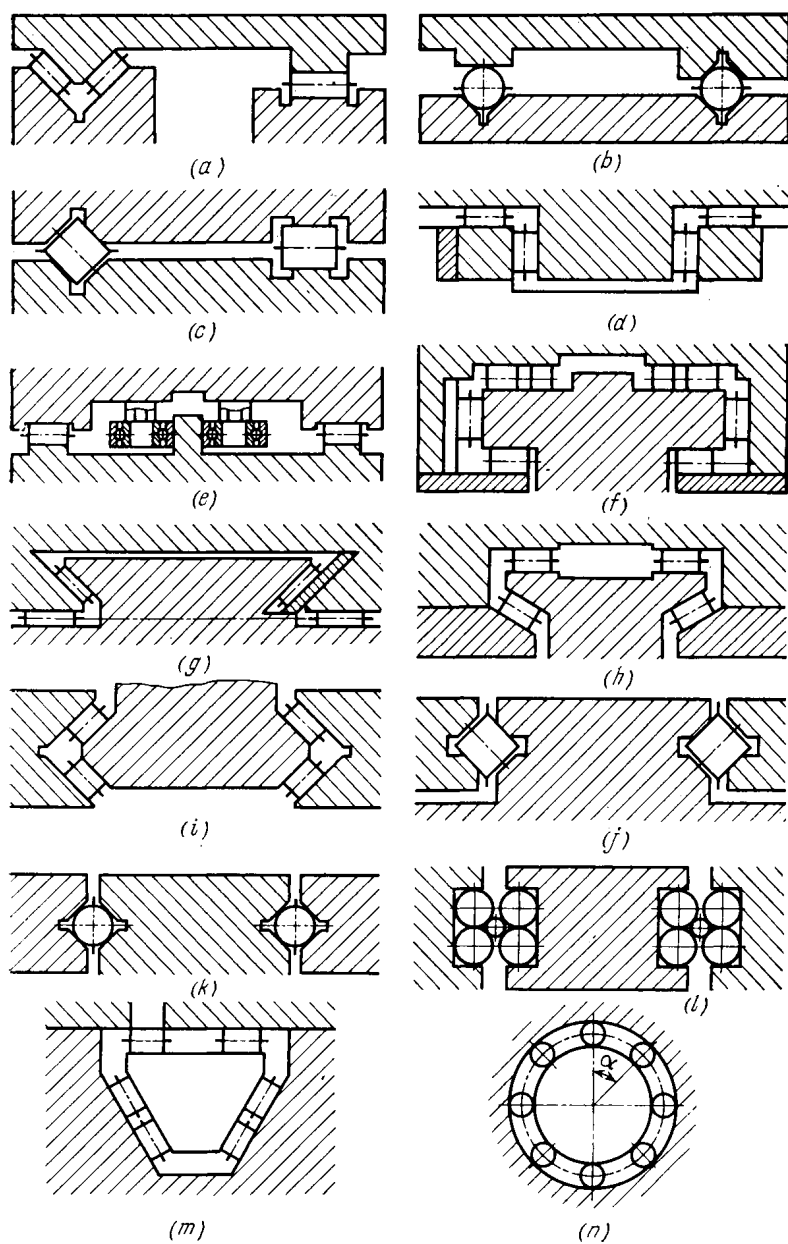
Fig. 22.11. Main forms of rolling guides [7]

tio of rollers for hardened steel ways is usually 1.5 to 2. Depending on the cross-sectional shape, guide ways with rollers fall into the following categories:
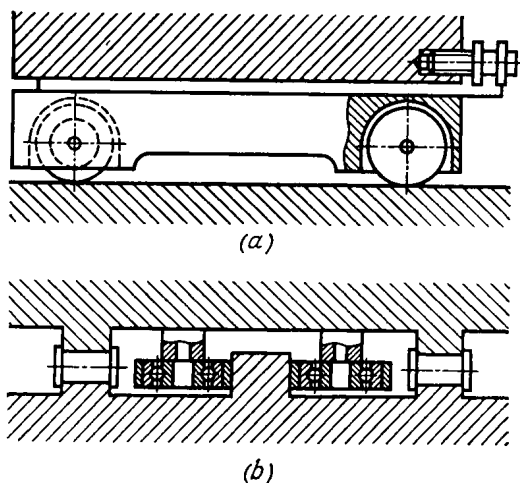
Fig. 22.12. Rolling guides with rollers on fixed pivot pins

— triangular and flat in combination, the most widely used design, featuring a low cost and reduced stiffness (Fig. 22.11a);
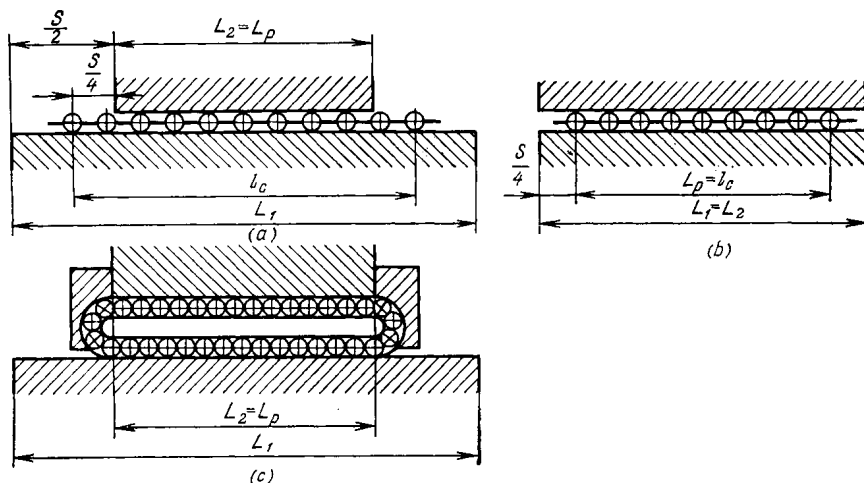
Fig. 22.13. Main design arrangements of rolling guides [7]

— rectangular, which are simple in manufacture and very stiff in the ways plane; preloading is done in a horizontal direction (Fig. 22.11d) or in both a horizontal and vertical directions (Fig. 22.11f);

— trapezoidal (dovetail), which are very costly to manufacture, but highly stiff and convenient in preload adjustment (Fig. 22.11*g*); with a 30° angle (instead of 55°), as shown in Fig. 22.11*h*, the ways are simpler to make but less stiff in the plane of motion;

— closed triangular, used with parallel-axes rollers (Fig. 22.11*i*), intersecting-axes rollers (Fig. 22.11*j*), and with staggered rollers in chain separators, known as crossed roller chains (Fig. 22.14); with
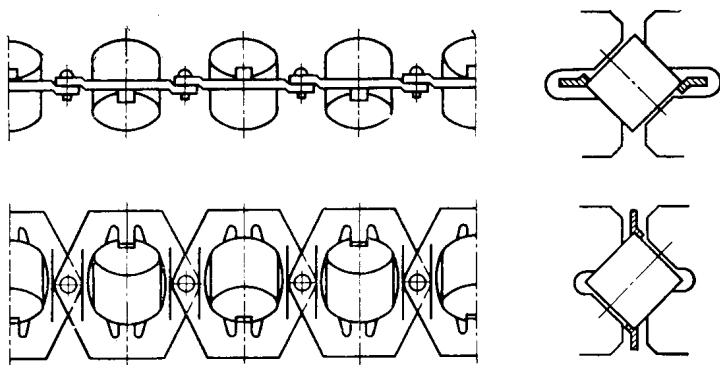
Fig. 22.14. Crossed roller chain

the same overall dimensions the first type has rollers much smaller in diameter than those in the second type, which leads to increased friction and skidding of the rollers; in the crossed roller chain the axes of adjacent rollers are arranged at 90°, the roller diameter is slightly larger than the length, and the assembly is compact.

Rolling guides with needle rollers are used where there are medium loads and dimensional limitations in a vertical direction. The roller diameter normally ranges from 2 to 6 mm.

Rolling guides with rollers on fixed pivot pins are provided with eccentric pins for adjustment (Fig. 22.12*b*); this type of guides is used for small loads, long travels, and where the dimensional factor is not critical.

Rolling guides with recirculating roller or ball way bearings. The Series P88 antifriction way bearing [8] includes body *1* (Fig. 22.15), rollers *2* which circulate around the body, and two retainers *3* which ensure lateral guiding for the rollers and keep them from falling out. The retainers are located on the body with the aid of slots provided in them and secured to it with screws *4* and dowel pins *5*. The lateral location of the rollers safeguards them against skewing and ensures uniform movement of the bearing. The bearings are fixed to special surfaces on movable units by screws *6* and dowel pins *7*. Bearings of this type provide for a practically unlimited length of travel, and allow the ways to be effectively protected from dirt. When mounted on hardened steel ways and preloaded, these bearings have a high

34

load capacity and stiffness, and are very compact, although they are somewhat inferior in motion uniformity to guides with rolling elements in cages. Antifriction way bearings are installed in sets of two bearings on each way (at the ends).

Specifications. The out-of-straightness and twisting of the ways in preloaded assemblies should be held within 8 to 10μm for low friction. Size variation in a set of rollers (balls) to be used in one assembly should be within 2 μm, and for high-precision applications within
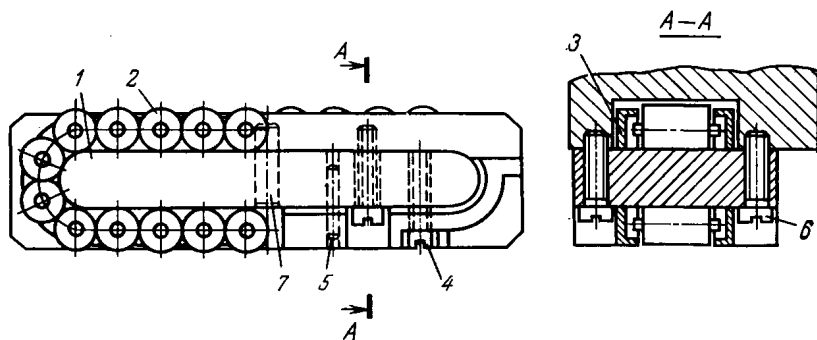
Fig. 22.15. Recirculating antifriction way bearing, Series P88 [8]

1 μm. For rollers, taper should be under 0.5 to 1 μm. Permissible form and position errors for rolling guide components are given in reference [6].

Surface roughness has a considerable effect on rolling guide performance. Better surface finish reduces friction and improves the stiffness and wear resistance of the guide. With scraped ways, a scraping depth of 15 to 20 μm reduces the stiffness by a factor of 2.5 and increases friction losses 2 times as compared with a depth of 10 μm, and 3 times as compared with that of 5 μm [12].

Requirements for surface finish of the ways are specified by a Soviet State Standard.

22.2.2. Materials

In most cases steels ШХ15 and ШХ15СГ, HRC 58-62, are recommended for use. They provide high wear resistance and show good performance under heavy working loads, in preloaded assemblies, and in applications with inadequate protection from dirt. The permissible load on one rolling element 10 mm in diameter, with steel ways hardened to HRC 60, is 6 kgf for balls and 200 kgf for short rollers. With cast iron ways, the permissible load for balls is reduced by a factor of 30 and for rollers by a factor of 10. The static load capacity of steel ways hardened to HRC 55 is lower than that of steel ways hardened to HRC 60 by a factor of 1.5 [7].

22.2.3. Selection of Oils and Greases

Rolling guides are lubricated with oils and greases. Oils are a better choice because they promote the removal of dirt and cutting fluid. Generally, the properties and amounts of lubricants in low-speed rolling guide applications are not strictly specified. The friction force is little influenced by the amount and viscosity of the lubricant. The traction force is only 10 to 15 percent higher in operation without lubrication than in that with oil lubrication. In most cases use should be made of industrial oils. Oils with a viscosity of 40 to 50 cSt at 50°C may be used for both vertical and horizontal ways.

In rolling guides operating under light loads, the resistance to motion is determined mainly by sliding friction. Hence, the use of slideway oils of the ИНСп series is advisable where static friction must be reduced, particularly for rolling guides with plain cylindrical and needle rollers (see Table 22.3). Where reliable way covers have been provided for, use can be made of greases, for example, УС-2 and УС-1. To reduce friction, specifically in antifriction way roller bearings, greases АМС-1 and АМС-3 can be recommended as having good antistick-slip properties.

Table 22.3

Oils recommended for rolling guides

Design arrangement	Slideway surface contamination			
	insignificant		substantial	
	Oil grade	Kinematic viscosity at 50° C, cSt	Oil grade	Kinematic viscosity at 50° C, cSt
Horizontal	И-40А ИНСп-40	35-45	И-20А	17-23
Vertical	ИГП-91 ИНСп-110	88-94 100-120	The same as for horizontal ways with insignificant contamination	

22.2.4. Friction in Rolling Guides

Calculation of friction losses. The friction force in rolling guides can be assumed to have two components [7]: the friction force under no-load conditions and that proportional to the load. The first component results from the friction of the rolling elements against the cage and from viscous friction associated with the lubricant. The second component is determined mainly by rolling friction as such and friction due to the difference in velocities at the contact.

The friction force T_1 on one of the way surfaces of a rolling guide is

$$T_1 = T_{in} + \frac{f_r}{r} N_1$$

where T_{in} is the initial friction force on one surface of the guide, kgf; f_r is the rolling friction coefficient, cm; r is the radius of the rolling element, cm; and N_1 is the normal force on the way surface, kgf.
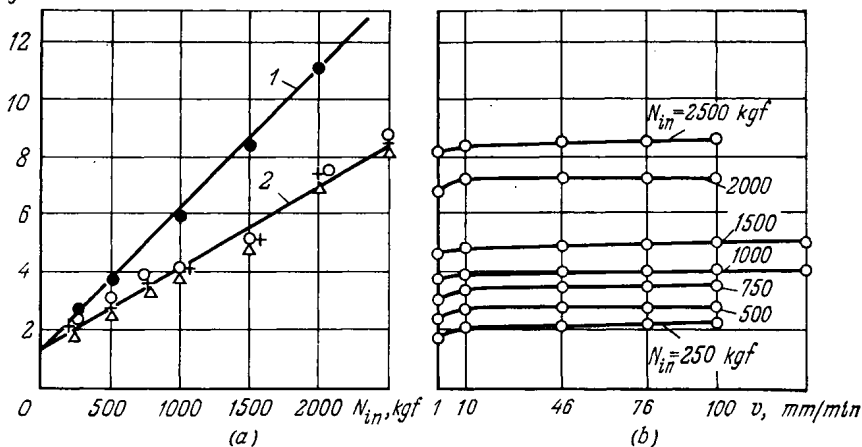
Fig. 22.16. Friction force T as a function of load N_{in} (a) and speed of motion v (b) [7]
1—7 mm dia. rollers; 2—11.3 mm dia. rollers. Ways material—hardened steel

The total friction force T (kgf) is found by adding together friction forces on all the active surfaces of the guide, using the formula

$$T = nT_{in} + \frac{f_r}{r_{ef}} N$$

where N is the total normal force acting on the guide ways, kgf; n is the number of the way surfaces; and r_{ef} is the effective radius of the rolling elements as referred to a single contact plane, cm.

In most machine tools, the working loads due to cutting forces acting on the rolling guides are not heavy, and N is determined either by the weight G of a given machine component or (for preloaded guides) by the amount of preload N_{pr}.

The friction force becomes smaller with greater diameter of rolling elements and lower working load (or preload).

The results of measuring the friction force in rolling guides are presented in Fig. 22.16.

The following design values of f_r and T_{in} can be recommended: $f_r = 0.001$ cm for hardened steel ways in combination with balls or rollers; $f_r = 0.0025$ cm for cast iron ways; for guides in medium-size machines, with rolling elements in stamped steel cages, on starting

$T_{in} = 0.5$ kgf and in motion $T_{in} = 0.4$ kgf. These values of T_{in} can also be used for cages of other designs. The force T_{in} depends on the quality of cages, especially stamped ones, in particular on the amount of pressure exerted by the cage tongues on the rolling elements.

The friction force on cast iron ways is largely dependent on the depth of scraping (see p. 35). The magnitude of T is not affected by speed, hardly affected by the lubricant viscosity, and is determined mainly by rubbing of the rolling elements against the cage. For medium-size units T does not exceed 2 to 5 kgf, and the arbitrary coefficient of friction f'_r (the ratio between the friction force and the normal load) ranges from 0.005 to 0.010, the smaller values corresponding to large loads (weights) and the larger values, to small loads.

For antifriction way bearings, the friction force is found by the formula similar to those given above [8]:

$$T = n_1 T_{01} + \frac{f_r}{r} \sum_{i=1}^{n} N_i$$

where T_{01} is the initial friction force at one bearing, kgf; n_1 is the total number of bearings; and N_1 is the total reaction force of the i-th bearing (produced by the preload and the working load), kgf.

Values of T_{01} and f_r for the P88-102 antifriction way bearings (roller diameter 8 mm) with various preloading devices are given in Table 22.4.

Table 22.4

Initial friction force in a way bearing

Mounting method	T_{01}, kgf	f_r, cm
On spring pad	0.5	0.000 4
On adjustable pad with two screws	0.6	0.000 43
On tapered gib	1.2	0.000 6

The value of f'_r for high loads ($N_i > 1\,000$ kgf) on the bearing depending on the type of preloading device ranges from 0.001 to 0.003. Decrease of the load results in sharply increased f'_r; for instance, with $N_i = 12$ kgf, $f'_r = 0.025$ to 0.030. The value of f'_r as determined by the angle φ of an inclined plane ($f'_r = \mathrm{tg}\,\varphi$) from which a bearing carrying a load of 10 to 20 kgf moves down at a uniform speed serves as a criterion of the manufacturing quality of way bearings.

The uniformity of motion and the accuracy of positioning. Rolling guides provide a very high uniformity of motion of machine components. Stick-slip occurs only if preload is excessive or the quality of the rolling guide components is poor. Guides with rolling bodies in cages assure more uniform motion than antifriction way bearings,

where the recirculating rollers are subject to instantaneous skewing and impacts on entering the working section of the path [8].

The accuracy of positioning of machine components in rolling guides, defined by the deviation from the specified position, amounts to 0.1-0.2 μm, provided the drive is rigid enough [7]. The accuracy of positioning decreases with a lower rigidity of the drive and is practically independent of the amount of preload. Positioning accuracy is interrelated with the machine response which is characterized by the sensitivity threshold, that is, the minimum motion of the driving component that sets in motion the driven component (Table 22.5).

Table 22.5

Threshold of sensitivity in positioning motion, μm

Material, heat treatment, and finish of ways	Drive stiffness, kgf/μm		
	4.6-2.2	0.8	0.2
Hardened ground steel	0.1	0.6	4
Scraped cast iron without preloading	0.1	0.4	—

22.2.5. Working Life of Rolling Guides

Rolling guide breakdowns are caused mainly by mechanical impurities and by slip of the rolling bodies, particularly rollers. Metal chips getting into the guide disrupt contact between the mating parts and cause slip and jamming of the rollers, scores and brinelling of cast iron ways, and other damage. Abrasives produce wear of the ways, often non-uniform, lobing of the rolling elements, and local wear when travels are short. The added effect of coolant with inadequate lubrication sometimes brings about considerable fretting wear.

The slip of rolling elements also results from defects of the cage and from the use of small-diameter rollers (needle rollers). Where cages are made in the form of unlinked sections, one of these may become unloaded owing to assembly defects. Under the action of vibrations this section may gradually come up to the stop and cease rolling. For this reason, cage sections should be linked.

The performance of antifriction way bearings is substantially affected by errors of mounting on machine units, e.g., the mounting height variation in a set of bearings or non-alignment in a longitudinal and a transverse direction.

With good protection and the absence of slippage, machine-tool rolling guides working usually under small loads and at low speeds provide long service life. For high-load and high-speed applications, rolling guides should be back-calculated for surface layer fatigue strength. The calculation method is given in references [7, 8].

REFERENCES

1. Выбор конструкций, материалов и методов упрочнения накладных стальных и чугунных направляющих скольжения. Рекомендации. М., ЭНИМС, 1975. 44 с. Авт.: А. С. Лапидус, Б. Н. Чижов, И. И. Ревенкова, А. С. Коновалов, М. И. Калашникова, Э. А. Майорова.
2. Крагельский И. В. Трение и износ. М., «Машиностроение», 1968. 479 с.
3. Лапидус А. С. Деформация столов в процессе эксплуатации.—«Станки и инструмент», 1961, № 7, с. 22-24.
4. Лапидус А. С. и Чижов Б. Н. Причины образования задиров на направляющих движения подачи станков и методы их предотвращения.—«Станки и инструмент», 1965, № 5, с. 22-25.
5. Лапидус А. С., Портман В. Т., Левит Г. А. Стенд для испытания антифрикционных и антискачковых свойств материалов и масел.—«Станки и инструмент», 1974, № 1, с. 20-21.
6. Левина З. М., Котляренко Л. Б., Чижова Н. В. Направляющие качения. М., ЭНИМС, 1966. 42 с.
7. Левина З. М. Направляющие качения.— В кн.: Детали и механизмы металлорежущих станков. Т. I. Под ред. Д. Н. Решетова. М., «Машиностроение», 1972, с. 344-438.
8. Левина З. М., Котляренко Л. Б., Бойм А. Г. Расчет и конструирование направляющих качения с роликовыми опорами. Рекомендации. М., ЭНИМС, 1974, 47 с.
9. Левит Г. А. Гидродинамический расчет направляющих прямолинейного и кругового движения.—«Станки и инструмент», 1958, № 9, с. 5-10.
10. Левит Г. А., Лурье Б. Г. Совершенствование методов смазки направляющих механизма подач.—«Станки и инструмент», 1961, № 11, с. 18-24.
11. Методика изучения надежности металлорежущих станков в эксплуатации. М., ЭНИМС, 1969. 187 с. Ав.: А. С. Лапидус, Л. В. Марголин, В. Т. Портман, Р. М. Пратусевич.
12. Направляющие скольжения.— В кн.: Детали и механизмы металлорежущих станков. Т. I. Под ред. Д. Н. Решетова. М., «Машиностроение», с. 88-343. Ав.: А. С. Лапидус, Г. А. Левит, Б. Г. Лурье, З. М. Левина.
13. Портман В. Т., Лапидус А. С., Александер В. Р. Повышение долговечности направляющих скольжения металлорежущих станков. М., ЭНИМС, 1971. 51 с.
14. Портман В. Т., Лапидус А. С. и Решетов Д. Н. Оптимизация формы направляющих скольжения металлорежущих станков из условий сохранения точности.—«Станки и инструмент», 1974, № 5, с. 9-12.
15. Проников А. С. Износ и долговечность. М., Машгиз, 1957. 274 с.
16. Пуш В. Э. Малые перемещения в станках. М., Машгиз, 1961. 122 с.
17. Антискачковые масла для направляющих скольжения металлорежущих станков. Рекомендации. М., ЭНИМС, 1977, с. 24.
Авт.: В. Т. Портман, А. С. Лапидус, Б. Н. Чижов, В. Р. Александер.
18. Решетов Д. Н. Расчет деталей станков. М., Машгиз, 1945. 137 с.
19. Решетов Д. Н. Детали машин. «Машиностроение», 1974. 656 с.
20. Wolf G. J. Stick-slip and Machine Tools.—"Lubrication Engineering". Vol. 21, No. 7, 1965, p. 273-275.

CYLINDER-AND-PISTON
ASSEMBLY COMPONENTS

23.1. OPERATING CONDITIONS
AND WEAR MECHANISM

In reciprocating motion, the most unfavourable conditions for the moving parts arise at the points of their reversal, i.e. where the piston moves at the minimum speed and, particularly, at the compression chamber, where the rubbing surfaces of the cylinder and the piston rings are exposed to maximum temperatures and pressures
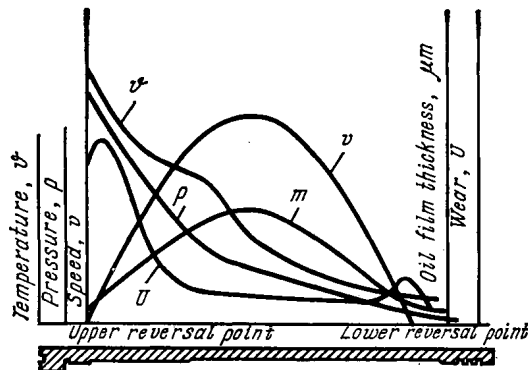
Fig. 23.1. Variation of temperature ϑ, pressure p, oil film thickness m, piston speed v, and wear U along the length of liner

(Fig. 23.1). The oil film thickness changes during the piston movement. During the suction stroke the oil film on the liner face is thinned by the fuel. During the compression stroke the oil is blasted from under the top piston rings and on ignition it burns out. This virtually destroys the oil film or makes it lose its lubricity.

Impacts during the piston strokes, vibrations of the rubbing surfaces of the piston, piston pin, piston rings, and the walls of the cylinder bore, which increase with the wear of these mating parts, greatly deteriorate the operating conditions. At the reversal points, a more or less complete destruction of the oil film is observed. In the region of the higher piston velocities, the bearing capacity of the oil film is increased, and it can reach the magnitudes found in semifluid friction. The zone of semi-dry friction covers a greater part of

the cylinder area at lower rather than at higher engine speeds. In the cylinder of an internal combustion engine, hydrodynamic friction never takes place, even in the region of the maximum piston velocity. The dry-friction area in the cylinder grows with pressures on the piston rings and temperatures of the rubbing surfaces.

Within the region of low piston velocities, the friction coefficient and wear initially decrease with increasing engine speed and then begin growing (Fig. 23.2); wear also grows with loading. In the middle of the cylinder liner the operating conditions improve. The friction force developed in sliding of the piston rings on the liner face depends on the normal pressure, sliding velocity, lubrication, and properties of the surface layers, reaching its maximum at
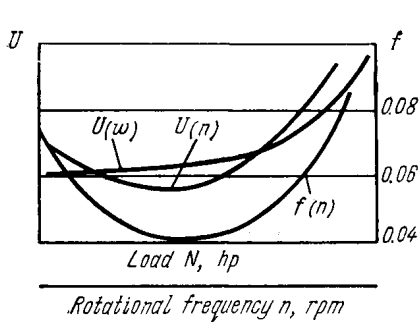
Fig. 23.2. Wear and friction coefficient of piston rings in low-speed region as functions of load (N) and rotational frequency (n)
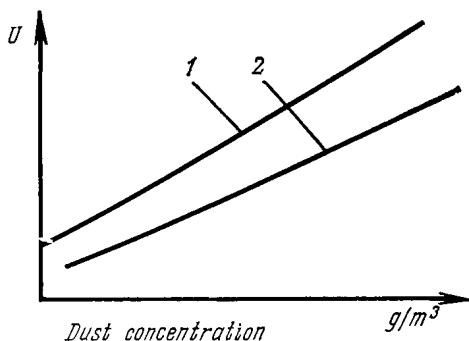
Fig. 23.3. Effect of dust in sucked air on wear of top piston ring (1) and cylinder face (2)

the reversal of piston movement. The coefficient of friction during the piston movement can vary from 0.02 to 0.2.

Among the complex phenomena of wear of the liner and piston-ring faces it is possible to discern surface failures caused by molecular seizure, fatigue, and abrasive action. These kinds of wear are closely interrelated, and show different intensity depending on the working temperature, pressure, lubrication, and properties of the materials and surface layers.

The products of combustion, particularly sulphur and vanadium compounds, have a considerable effect on wear.

Increased chemical activity of the working medium inside the cylinder may speed up fatigue and corrosion processes. The surface layers of the metals become weakened and embrittled, they crumble upon rubbing interaction and so increase the concentration of abrasive particles in the friction zone. Fuels with higher sulphur content promote rapid formation of carbon deposits on the piston head and in the ring grooves, and that impairs the exchange of heat and makes for accumulation of solid particles in the lubricant.

Abrasive particles produce a significant increase in the rate of wear through microcontact seizure. One of the sources of abrasive

particles is air. As the engine picks up speed, the amount of air delivered to the cylinder is increased, and so is the total quantity of dust. The rising concentration of dust and a larger size of dust particles lead to greater wear of the liner and the piston rings. The wear rate is in direct proportion to the concentration of dust in the air (Fig. 23.3) and to the amount of other abrasives in the friction zone. A complex relationship has been found to exist between the wear of the rubbing components in engine cylinders and the size of the abrasive particles (Fig. 23.4). Particles measuring 35 μm in cross-section
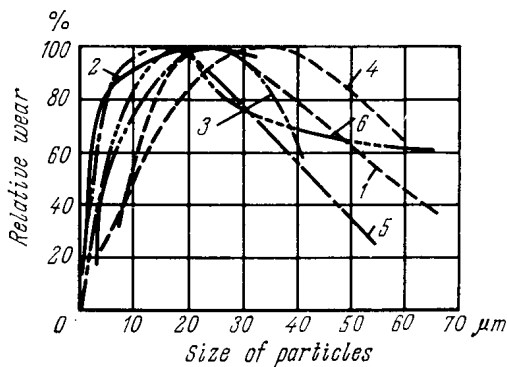
Fig. 23.4. Effect of the size of dust particles in sucked air on relative wear of a piston ring-cylinder face couple according to
1—K. Watson; 2, 3—I. F. Pochtarev; 4, 5—A. I. Nisnevich; 6—D. I. Vysotsky

produce the most rapid wear. Wear debris in the form of unoxidized hard metal particles are the most destructive abrasives. They are capable of migrating between the rubbing surfaces and, rather than decreasing in size as is often the case with mineral abrasives, they can sharply grow through metal build-up, interact with the metallic surfaces and cause severe damage. Wear can be reduced by creating conditions for a positive gradient of resistance to displacement, and by ensuring an adequate endurance of secondary structures that can limit adhesive, fatigue, and abrasive failures to minimal volumes of the surface layers.

23.2. CYLINDER LINERS

The material and processing of cylinder liners must provide for high wear resistance of the rubbing surface, structural strength, and resistance to cavitation and corrosion of the outer surface cooled by liquids.

23.2.1. Liner Materials

Cast irons. Grey low-alloy or medium-alloy perlitic cast irons (Table 23.1) have found predominant use for liners; in some cases use is also made of perlitic cast iron with globular graphite, the Ni-re-

Table 23.1

Chemical composition and mechanical properties of cast-iron cylinder liners

Chemical composition, % *								Mechanical properties		Application
C	Si	Mn	≤ P	Cr	Ni	Mo	Other elements	σ_u kgf/mm²	HB	
3.0-3.3	2.0-2.4	0.5-0.9	0.2	≤0.4	—	—	—	25-32	190-230	Automotive engines
2.8-3.4	1.8-2.4	0.8-1.2	0.2	0.5-1.0	—	0.4-0.7	1.0-1.5 Cu	28-38	241-269	
3.2-3.4	2.0-2.2	0.6-0.7	0.2-0.4	0.3-0.4	≤0.2	0.1-0.2	0.1 Cu	—	217-224	
3.1-3.3	1.8-2.0	0.5-0.7	0.4	0.3-0.5	≤0.2	Ti ≤ 0.1	0.04 V	18-22	207-255	
3.3-3.5	2.2-2.4	0.6-0.8	0.3-0.6	≤0.4	—	Ti ≤ 0.1	—	—	222-228	
3.3-3.5	2.2-2.4	0.5-0.7	0.3-0.5	≤0.1	—	0.12	—	—	229-321	
3.2-3.4	2.5-3.5	0.6-1.0	—	0.8-1.2	—	—	—	—	260-300	Medium-size liners for diesel engines
3.0-3.5	1.9-2.4	0.6-1.0	—	0.3	0.5-0.7	—	—	35-40	220-260	
2.7-3.1	1.7-2.0	0.8-1.1	0.18	0.4-0.65	0.9-1.2	0.5-0.7	0.3-0.6 Cu	35-38	207-269	Large liners for diesel engines
3.1-3.4	0.8-1.5	0.6-0.9	0.2	—	—	Ti ≤ 0.1	0.2-0.3 V	18-28	179-235	

* S under 0.08-0.15.

sist type austenitic cast iron and high-alloy cast iron with a carbide network in a perlitic or austenitic matrix.

The best service properties of liners are obtained by developing microstructures of the metal matrix and graphite with an optimal combination of parameters. It has been found that a uniform distribution in perlite of cementite inclusions measuring 0.8 to 1.5 μm and a disrupted network of phosphide eutectic inclusions having an area of 200 to 600 μm² in the form of middle-sized cells provide for better control of deformations in the surface layers and a favourable oil retaining texture. Cast iron with granular cementite inclusions in perlite exhibits these properties to a lesser degree and is more liable to wear and seizure.

In distinction to cementite, the phosphide eutectic is an active structural constituent. In the process of wear it introduces phosphorus into the surface layer, thereby increasing its separating power. The correct combination of the base microstructure, phosphide eutectic, and graphite creates conditions for the development of the optimal microgeometry and secondary structures, and provides a positive gradient of resistance to displacement.

Free ferrite or cementite in the form of large irregular inclusions, interdendritic graphite grains or an inadequate amount of graphite in cast iron adversely affect its antifriction properties, markedly increase the rate of wear and cause scoring of the rubbing components.

In perlitic cast irons used for liners of high-speed engines, a total area of free cementite in excess of 10% and its individual inclusions with an area of over 13 000 mm² are impermissible for fatigue strength reasons.

The aggregate of carbon and silicon has the greatest effect on the properties of perlitic cast iron. These properties can be varied within wide limits by varying the amount of carbon and silicon and by introducing various alloying elements. The relationship between the amount of carbon and silicon for sand-cast liners is depicted by a V-type curve with the minimum lying within 4.8 to 5.1 percent (Fig. 23.5). Deviations (plus or minus) from the optimal amount of carbon and silicon result in lower resistance to wear and scoring of liners and the mating pistons and piston rings. An increase of carbon and silicon content up to 5.2-5.4 percent improves resistance to scuffing. As the content of $C + Si$ is raised from 4.5 to 5.7 percent, the cast iron exhibits marked changes in its metal matrix and considerably increased amounts of graphite. The latter has a positive effect on wear resistance, provided that the form of the flaky graphite inclusions is favourable, their size is from 45 to 90 μm, and they are unoriented and uniformly distributed. The reason for it is that, on the one hand, graphite inclusions supply graphite to the friction zone, and on the other, they form a surface with a texture that hardly changes in rubbing; such a surface is capable of retaining some quantity of fluid lubricant. Graphite inclusions have an especially important role to play in forming

protective layers in the upper region of the cylinder and at the exhaust ports of the liner, where fluid lubricants produce little effect.

Graphite flakes uniformly distributed in the metal matrix of cast iron provide good lubrication. Spotted and globular graphites
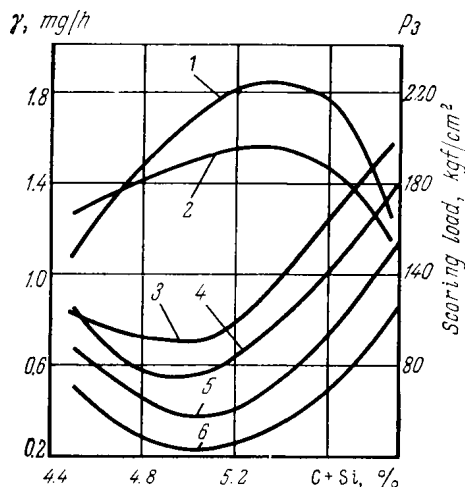
Fig. 23.5. Effect of carbon + silicon in the material of diesel-engine liners on resistance to scoring of liner and piston (1), liner and piston rings (2) and on wear of liners (3, 4), piston rings (5), and pistons (6). Materials: liners—grey cast iron alloyed with chromium, nickel, and molybdenum; piston rings—cast iron СЧХН, pistons—cast iron СЧХНД

are less effective for lubrication; that is why high-grade iron has a lower resistance to scuffing than grey iron (Table 23.2). As regards

Table 23.2

Mechanical properties and resistance to wear and scoring of cylinder-liner and piston-ring materials

Material, grade	Form of graphite inclusions	HB	σ_u, kgf/mm²	$\gamma \cdot 10^2$ mg/hr	Scoring load, kgf/cm²
Cast-iron piston ring and liner					
СЧХН/СЧХНМД	П/П	245/235	28/35	45/68	195
	П/Т	245/255	28/42	57/79	170
	П/Г	245/269	28/59	53/74	158
Cast-iron piston ring and steel liner					
СЧХН/50Г	П/—	245/610	28/85	87/128	122

Notes: 1. Microstructure of metal matrix for cast iron is perlitic and for steel martensitic; the Russian letter П stands for flake graphite, Т for dotted graphite, and Г for globular graphite.
2. The numerator gives data on piston ring and the denominator, on cylinder liner.

strength, globular graphite is the most advantageous form of graphite inclusions.

The load-carrying capacity of the layers of secondary structures and the oil films are tangibly improved as the latter becomes saturated to a definite level with dispersed-phase wear debris (graphite, metal soaps, phosphides, etc.).

For strength reasons, the cast iron used for liners should contain a minimum amount of graphite that provides dependable lubrication. An excessive amount of graphite weakens the material, reduces its wear resistance by loosening the metal matrix and, sometimes, by giving rise to a large quantity of free ferrite which promotes seizure.

Austenitic cast iron of the Ni-resist type or a high-alloy cast iron with a carbidic network, for instance a chromium-silicon cast iron, are normally used for dry liners inserted in the upper part of cylinders. These materials, particularly carbidic ones, have poor machinability. Their more common field of application is liners for small and medium piston-type engines.

Steel. For engines with small and medium cylinder diameters, use is made of steels 50Г, 55ПП, 40Х, 30Х3ВА, 35ХМЮА, 38ХВФЮ, 38ХМЮА and graphitized steels of the ЭИ336 type (1.5 to 1.75 percent C, 0.7 to 1.25 percent Si, 0.2 to 0.5 percent Mn, 0.4 to 0.6 percent Cu, 0.2 to 0.4 percent Ti).

To improve their resistance to wear and scoring, steel liners are subjected to hardening, nitriding, nitrosulphiding, chromium plating, hard nickel plating, etc.

Aluminium alloys. Cylinder blocks and liners of aluminium alloys are employed for engines with small-diameter cylinders. Use is made of alloys containing Cu, Mg, Ni, and alloys АЛ2, АЛ5, АЛ6, АЛ7, АЛ10В.

These materials make it possible to have units of reduced weight, smaller clearances between the liner and the aluminium piston, milder heating, and increased compression and horsepower of internal combustion engines. The most effective method for making the face of aluminium liners more resistant to wear is chromium plating.

A good wear resistance, approaching that of cast iron, is provided by a cylinder aluminium alloy containing 15 to 18 percent Si, copper, magnesium, titanium, iron. After anodic etching in a sodium nitrate solution this alloy acquires high resistance to scoring and good running-in ability. In addition to chromium plating, aluminium cylinders can be subjected to various surface hardening treatments, such as deposition of hard nickel, nickelous phosphate, ferrophosphorus coatings, and also such methods as anodic electroplating and metal spraying. Another solution is wear-resistant dry liners introduced into the upper region of the cylinder.

23.2.2. Methods for Improving Wear Resistance

Heat treatment

Through-hardening, normalizing, and hardening with isothermal quenching are used for steel and cast-iron cylinders as preliminary operations preceding surface hardening and as main operations for obtaining the working properties of cylinder liners.

Hardening with isothermal quenching of cast-iron and steel liners is an effective method for increasing wear resistance. The optimum treatment of cast-iron liners comprises heating to 850-870°C and isothermal quenching at 350°C. The process makes it possible to achieve the ultimate mechanical properties, sufficient wear resistance, insignificant warpage, and good machinability. In friction, the microstructure of such cast iron, comprising troostite and a substantial amount of austenite, develops quasi-equilibrium wear-resistant active layers.

The disadvantages of all methods of through hardening are warpage, which requires large machining allowances, and poor machinability with cutting tools.

Induction hardening provides high production rates, the possibility of obtaining any depth of hardening, and the minimum amount of warpage. The correct choice of heating and quenching conditions and characteristics of the hardened layer (its depth, area, and hardness) substantially increases wear resistance of steel and cast-iron liners (Table 23.3).

Table 23.3

Resistance to wear and scoring of heat treated cylinder liners

Heat treatment	HV	$\gamma \cdot 10^2$, mg/h	Scoring load, kgf/cm²
No treatment	245/255	45/68.1	195
Hardening and tempering at 220°C	249/569	41.5/51.4	220
Hardening with isothermal quenching, 350°C	249/337	37.6/48.5	241
Induction hardening, tempering at 200°C	245/528	34.4/42.8	268

Notes: 1. Piston ring of cast iron СЧХН, cylinder liner of cast iron СЧХНМД.
2. The numerator gives values for piston ring and the denominator, for cylinder liner.

Testing of cast iron liners has shown (Fig. 23.6) that through hardening reduces wear by a factor of 1.4, hardening with isothermal quenching by a factor of 1.6, and induction surface hardening by a factor of 1.7. A certain reduction in wear of the mating piston rings is also observed. The hardness of heat-treated liners has a substantial effect on the wear rate (Fig. 23.7). For example, a rise in hardness of an induction-hardened cast iron up to HB 400 markedly improves its resistance to wear and scoring. A further increase in hardness produces a weaker effect on wear resistance. The running-in of the rubbing components becomes more difficult as the hardness of liners is raised.

With steel liners, the surface layer should be hard to no lower than HRC 45, and with cast-iron liners, HRC 43. The depth of hardening

Fig. 23.6. Wear of cast iron liners and mating piston rings

Liners: *I*—unhardened, *II*—hardened and tempered at 200°C; *III*—hardened with isothermal quenching at 350°C, *IV*—induction hardened and tempered at 200°C; cast iron grades СЧХН (*1, 4, 7, 10*), СЧХНМД (*2, 5, 8, 11*); ВЧХНД (*3, 6, 9, 12*). Piston rings: unhardened cast iron СЧХН
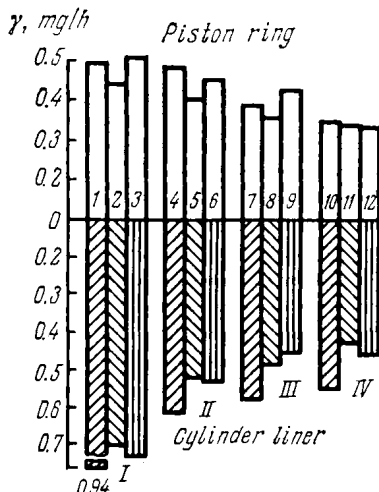
should be minimal but sufficient to ensure the required useful life of the liner; usually it is specified at 1.5 to 3.5 mm.
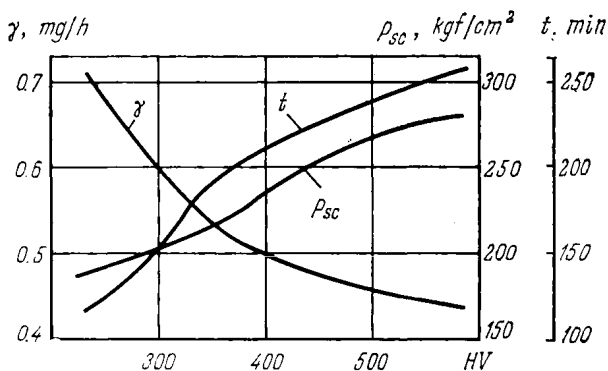
Fig. 23.7. Effect of liner hardness on wear rate (γ), running-in time (t) and scoring resistance (p_{sc}). Liner material: cast iron СЧХМ, induction hardened

Nitriding

Nitriding is more effectual for increasing wear resistance than conventional hardening, it is used to treat steel and cast-iron liners. The best results are achieved in steels 38ХМЮА, 38ХВФЮ, 38Х3ВА and cast irons with globular graphite. Additions to cast iron and steel of Al, Cr, Ni, Mo, Mn, Cu, and V upgrade the quality of the case. The microstructure of the nitrided steel is a continuous white surface layer of nitrides insensitive to etching; the layer main-

ly contains an ε-phase. A three-phase region $\varepsilon + \gamma' + \alpha$ occupies the place just under the surface layer. The number of phases rich in nitrogen decreases farther away from the surface. The most favourable is the homogeneous structure of the three-phase nitride layer.

The nitrided surface exhibits a fairly high contact strength and resistance to plastic deformation, seizure, and corrosion.

Nitriding increases fatigue strength and resistance to cavitation failures.

The principal disadvantages of nitriding are a relatively long duration of the process, warpage, and non-uniform properties through the case depth, especially so with cast iron.

The phase composition through the depth of case in cast iron changes in the direction of $\varepsilon + \gamma' \rightarrow \varepsilon + \gamma' + \alpha \rightarrow \alpha + \gamma' \rightarrow \alpha$. The most homogeneous and stable structures after nitriding are obtained in magnesium cast iron. With this material, the nitrided surface layer has the maximum hardness (H_{50} 1 100-1 400), which gradually decreases towards the core. A high hardness (H_{50} 500) holds at a depth of 250 to 450 μm. The maximum wear resistance is achieved in a cast iron alloyed with Cr, Mn, Ni, Mo, V and Cu in combination; thus, for instance, nitriding can be recommended for liners made of high-grade cast iron ВЧНМД alloyed with Ni, Mo, and Cu, and cast iron ВЧХНМД alloyed with Cr, Ni, Mo, and Cu. These materials exhibit a higher wear resistance (Table 23.4) than grey

Table 23.4

Resistance to wear and scoring of nitrided cylinder liners

Liner material	HV	$\gamma \cdot 10^2$ mg/h	Scoring load, kgf/cm²
Untreated grey cast iron СЧХНМД	245/255	45/68	195
Nitrided cast iron ВЧНМД	245/715	39/36	237
Nitrided steel 38ХНМЮА	245/907	48/47	186
Nitrided cast iron ВЧ	245/690	43/40	214

Notes: 1. Piston ring material is untreated cast iron СЧХН.
2. The numerator gives values for piston ring and the denominator, for cylinder liner.

cast iron СЧХНМД (containing Cr, Ni, Mo, and Cu), high-grade unalloyed cast iron ВЧ and steel 38ХМЮА.

Nitrided cast iron is well to phosphatize, because dissolving graphite inclusions during phosphatizing increases its oil-retaining capacity and resistance to scoring, and improves its ability to run in. Nitriding liners of high-grade cast iron gives a greater effect than hardening with isothermal quenching (850 → 350°C) and induction hardening; as regards wear resistance, it sometimes approximates chromium plating.

Cylinder liners can be nitrided in gaseous or liquid media. A promising method is ion nitriding in a glow discharge at 500 to 570°C. The hardness of the case at a depth of up to 400 μm is increased to H_{50} 500-600. The nitrided surface layer obtained in a glow discharge is more homogeneous.

Sometimes cast iron and steel liners undergo sulphidizing and nitrosulphidizing in gaseous and liquid media. It is expedient to provide in a sliding pair the combination of chromium-plated surface and a nitrided or nitrosulphidized surface.

Chromium plating

When applied to the liner face, this method proves very effective in reducing wear of the liner and the mating piston rings. The process can be used for cylinder liners and blocks of different materials (steel, cast iron, aluminium, and some other non-ferrous alloys). Electrodeposited chromium plating has a high microhardness (H_{50} 800-1 200 kgf/mm^2), high melting point (1 845°C), and good thermal conductivity ($\lambda = 0.165$ cal/(cm s °C). It provides resistance to corrosion, thermal stability, and a low coefficient of friction in sliding on many materials (Table 23.5).

Table 23.5

Coefficient of friction for electrodeposited chromium plating

Sliding pair	Coefficient of friction	
	static	sliding
Dense chrome on chrome	0.12-0.14	0.08-0.10
Dense chrome on steel	0.16-0.19	0.095-0.12
Dense chrome on cast iron	0.12-0.15	0.06-0.08
Dense chrome on bronze	0.10-0.16	0.03-0.07
Dense chrome on babbitt	0.10-0.12	0.02-0.04
Porous chrome on steel	0.14-0.16	0.07-0.10
Porous chrome on cast iron	0.11-0.13	0.05-0.09
Chrome on aluminium	0.15-0.18	0.06-0.14
Steel on steel	0.22-0.26	0.12-0.16
Cast iron on cast iron	0.14-0.20	0.09-0.12
Cast iron on steel	0.16-0.21	0.14-0.18
Babbitt on babbitt	0.13-0.14	0.07-0.09

The drawback of chromium plating is that it poorly retains oil and runs in with difficulty. Successful application of chromium plating for cylinder liners depends on the proper choice of processing conditions, plate characteristics (hardness, thickness and density), oil-retaining surface texture, and running-in method. As a result, wear is reduced not only of the plated liner, but also of the mating piston rings.

The most wear resistant coating is a bright chromium plating, deposited at 45 to 65°C with the crystal planes (111) oriented mainly

along the surface being coated. The crystal size ranges from 10^{-6} to 10^{-7} cm. Nearly all chromium platings have a network of cracks. The extent of cracking is associated with the process conditions, bath composition, plating thickness, and methods of machining the plating. The main influencing factors here are the temperature, and to a lesser degree, current density. The effect of cracking on the plating properties is dual. On the one hand, it weakens the layer of chromium; on the other, by treating the cracks with etchants it is possible to increase the ability to retain oil and to facilitate running-in.

Wear resistance and antifriction properties of a chromium plating are primarily dependent on its hardness. As the hardness grows, the wear of the chromium and the mating cast-iron part first decreases to a minimum and then goes up (Fig. 23.8). The minimum amount of wear in a sliding pair with a chromium-plated liner is observed at a chromium microhardness of H_{50} 1 000-1 050 kgf/mm², and in a sliding pair with a chro-

Fig. 23.8. Effect of chromium-plate hardness on wear of sliding pairs (solid lines—cylinder liners, dash lines—piston rings)

1—cast iron, 2—chromium
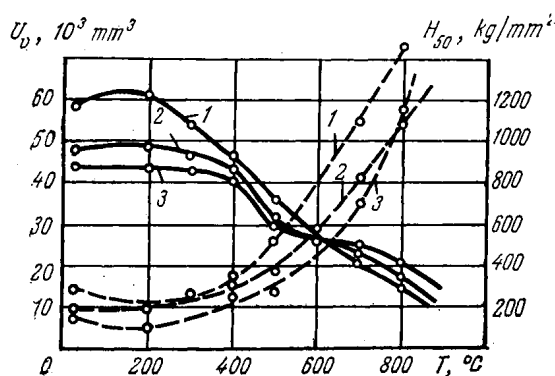
Fig. 23.9. Variation of hardness and wear resistance of chromium deposits with temperature

1—50°C, D_c (cathode current density) = 30 A/dm²; 2—58°C, D_c = 60 A/dm²; 3—66°C, D_c = 120 A/dm² (bath formulation: CrO_3 250 g/l; CrO_3 : SO_4 100-110; solid lines—hardness curves, dash lines—wear curves)

mium-plated insert, H_{50} 900-950 kgf/mm². This relation between hardness and wear resistance can be ascribed to the fact that

increased hardness reduces the volume and rate of damage due to microcontact seizure and crumbling. Hardness in excess of the optimum value increases the brittleness and stress of the plating.

A sharp drop in the wear resistance and hardness of chromium platings occurs in a temperature range of from 400 to 600°C (Fig. 23.9). Metallographical and X-ray diffraction analyses have shown
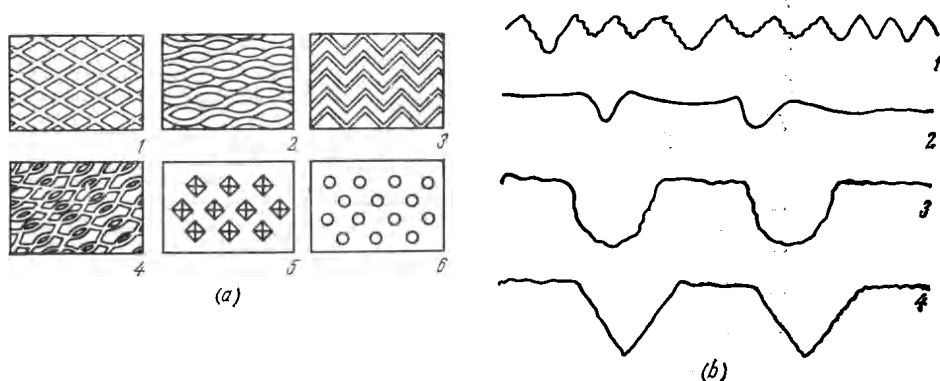
Fig. 23.10. Oil-retaining surface patterns obtained by mechanical (1-5) and electrochemical (6) methods
(a) plan view; (b) profile charts of surfaces treated by mechanical (1-8) and electrochemical (4) methods

that such a change in the properties is accompanied with stress variations, recrystallization, and loosening of the chromium layer.

The ability of the chromium-plated liner face to retain oil and resist scoring can be achieved by various methods. These consist in forming a special surface texture (dents or grooves) prior to plating (Fig. 23.10), deepening the pores in the chromium layer by etching, and etching a honeycomb-type pattern through a perforated screen. Characteristics of an oil-retaining surface texture influence the wear resistance of the plating and its running-in ability. In boundary friction, an increase in the channel-type porosity to 15-20 percent (Fig. 23.11) reduces wear of the chromium plating deposited at 58 to 66°C. A further increase in porosity (over 30-35 percent) brings about a sharp rise in the wear rate. The reason for it is that up to a point a growing porosity improves the oil-retaining ability without any significant weakening of the chromium plating. A porosity in excess of 30 to 35 percent tangibly impairs the plating strength.

Considering that chromium-plated components should run in rapidly, a chromium plating can be recommended that is porous to 25-35 percent, and hard to H_{50} 850-950 kgf/mm²; such a plating provides a fairly high wear resistance.

As the plating with channel porosity wears off, its properties approach those of a smooth chromium layer. The plating gradually ceases to keep the lubricant and to run in readily. The change of the

plating properties does not affect the performance of the mating chromium-plated piston rings. On the contrary, the wear of the sliding pair after running-in is reduced. However, for the liner, which
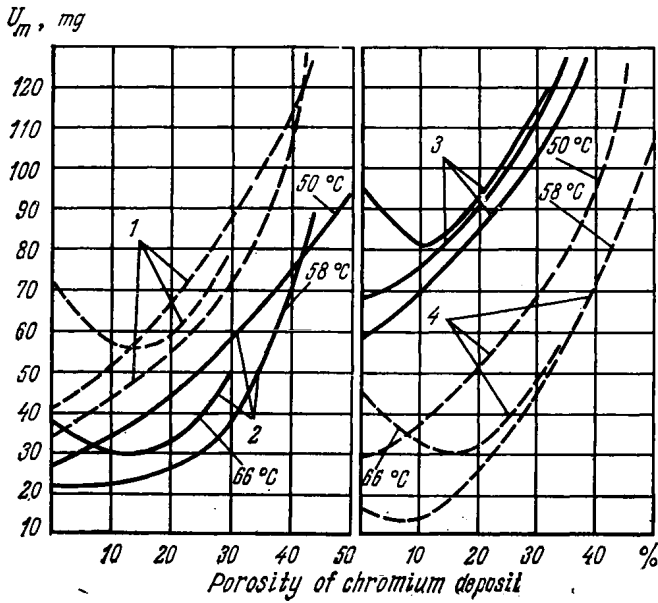
Fig. 23.11 Effect of chromium-plate porosity on wear of rubbing components
1—piston ring unplated (cast iron); 2—cylinder liner (chrome plated); 3—cylinder line (unplated cast iron); 4—piston ring (chrome plated)

should serve longer than the piston rings, to maintain the oil-retaining ability is vital.

Tests of cylinder liners and piston rings strengthened by various methods (Table 23.6) indicate that the chromium plating of liners

Table 23.6

Wear of cylinder liners and piston rings in locomotive diesel engines depending on surface treatment method

Surface treatment method	Average value of maximum wear, $U \times 10^{-4}$ µm/km	
	cylinder liners	piston rings
Chromium plating of liners	3.1	17.4
Chromium plating of piston rings	7.8	14.8
Hardening with isothermal quenching of liners	8.6	37.5
Normalizing of piston rings	15.4	44.0
No treatment	16.8	48.5

increases their wear resistance 3 to 5 times, and that of the mating piston rings, 2 to 3 times (all other things being equal). The chromium plating of piston rings is much less effective in terms of wear resis-
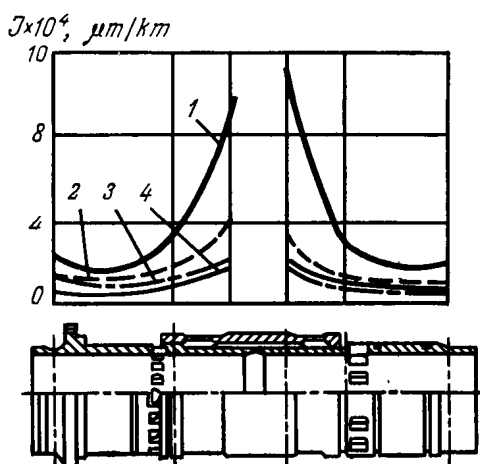
Fig. 23.12. Wear rate of cylinder liners in Type Д100 diesel engine
1—chrome-nickel-molybdenum-copper cast iron; *2*—chrome with channel porosity; *3*—chrome with etched honeycomb pattern; *4*—chrome deposited on a surface with mechanically formed oil-retaining pattern

tance. These data indicate that it is liners that should be chromium plated in the first place.

The minimum wear of a liner and the mating piston rings has been found with liners having dents formed mechanically on the face before chromium treatment (Table 23.7, Fig. 23.12).

Table 23.7

Wear of chromium plated cylinder liners in locomotive diesel engines, Type Д100

Coating	Maximum wear rate $\gamma \times 10^2$, μm/h				
	cylinder liners	piston rings			
		1	*2*	*3*	*4*
Chromium plating with mechanically formed surface pattern	5.78	15.7	9.7	8.2	4.2
Chromium plating with honeycomb surface pattern	6.45	21.8	12.8	6.9	4.7
Chromium plating with channel porosity	9.80	31.2	19.9	10.8	10.0
Untreated chromium-nickel-molybdenum-copper cast iron	22.7	47.1	24.0	13.8	10.7

The two top piston rings in chromium plated liners (Fig. 23.13) exhibit a smaller and more uniform rate of wear than they do when working in unplated cast-iron liners.

A dense layer of chrome has a low coefficient of friction at low specific pressures. However, at pressures of over 70 to 80 kgf/cm^2, the friction coefficient has been found to rise rather sharply. That points to the disruption of the oil film and increased friction due to direct metal contact of the rubbing surfaces (Fig. 23.14).

Of all the chromium deposits tested, that with channel porosity exhibited the highest values of friction coefficient; it was also less responsive to overloading than the plating deposited on the surface with a mechanically formed pattern.

A locally deposited chromium plating or a chrome-plated lining insert pressed into a cylinder bore prove to be effective for reducing wear of the cylinder and the piston rings. It is advisable to form an oil-retaining surface pattern in this region.

Fig. 23.13. Distribution of wear rate along the perimeter of piston rings working in liners with different kinds of chromium deposit

1—no deposit; 2—chrome with channel porosity; 3—chrome with etched honeycomb pattern; 4—chrome deposited over mechanically formed pattern

Fig. 23.14. Variation of friction coefficient with pressure for different oil-retaining surface patterns of chromium plating

—dense chrome; 2—chrome with dents formed on substrate; 3—chrome with channel porosity; 4—unplated liners, cast iron СЧХН

The macro- and microgeometry of the cylinder face, both initial and acquired in service, have a substantial effect on the performance and wear of the rubbing components (Fig. 23.15).

In this respect, the most important individual factor is ovality of the cylinder bore. Piston rings in cylinders with excessive ovality take a longer time to run in. The rubbing components work at increased local pressures and temperatures for a considerable period of time. Dry friction developing on large surface areas leads to scoring and severe wear.

The cylinder-bore geometry deviations may be brought about by thermal instability of the material, and by machining and assembly errors.

The surface roughness of the cylinder bore should be held about an optimal value that provides the running-in without excessive wear and scoring. The initial surface roughness depends on the bore diameter, geometrical deviations, operating conditions, materials of the liner, piston, and piston rings, lubrication, production costs, etc.

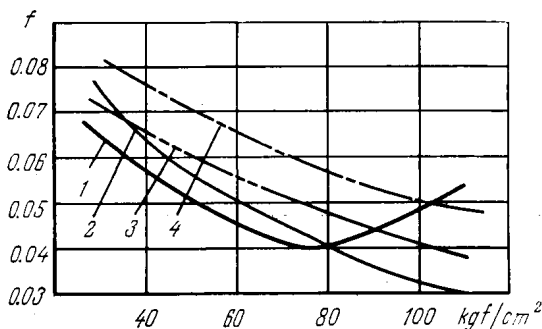For cylinders in internal combustion engines, compressors, pumps, steam engines, pneumatic hammers, presses and other machines with a cylinder bore of 150 to 500 mm in diameter, the surface finish should be 0.2-0.5 µm Ra.

A further reduction in surface roughness involves higher machining costs and, sometimes, impairs the retention of oil and makes for increased tendency to scoring. A greater surface roughness is also undesirable, because it results in more intensive wear of the rubbing surfaces during the running-in period. The optimal surface roughness for automobile engine cylinders is 0.15 to 0.4 µm Ra.

Fig. 23.15. Wear rate for piston rings and cylinder liners in Type Д100 diesel engines as a function of linear ovality

In the course of running-in, the cylinder face develops a surface roughness that during regular service varies about the optimal values. With automotive engine cylinders, the surface roughness in the upper region of the cylinder bore comes to 0.1 to 0.8 µm Ra and in the middle, 0.05 to 0.3 µm Ra. Cylinder liners in high-power transport diesel engines after running for over 1 000 h exhibit a surface roughness of 0.3 to 0.6 µm Ra in the upper region and 0.1 to 0.4 µm Ra in the middle.

Some applications where operating conditions are extremely severe (high pressures and temperatures, lubricant starvation, etc.) require a special oil-retaining surface pattern maintained over a long period of service. This pattern should provide a reliable lubri-

cant film between the rubbing components under regular and critical working conditions. The choice of a method for making the surface pattern and of its characteristics is governed by the frictional conditions, design features, and specified life of the machine.

An irregular surface pattern is formed by shot blasting and chemical or electrochemical etching. A regular pattern is usually formed by a multitooth tool or etched through a perforated screen (see Fig. 23.10). Helical, circular, or spiral grooves are made by a cutter, a diamond sphere, or cemented-carbide balls. The oil-retaining patterns are most advantageous for a strengthened cylinder surface which is difficult to run in (hardened, nitrided, etc.) and which keeps the lubricant poorly (chromium-plated, steel, etc.).

Fig. 23.16. Variation in wear rate (1), (2) and resistance to scoring (3) with ratio between the area of dents and the total area of surfaces in contact (A_d/A_0) for liners (1) and piston rings (2)

The rate of wear of the liner and the piston rings decreases up to a certain point as the liner area covered with oil-retaining dents is increased (Fig. 23.16). Beyond that point the wear rate goes up. This minimum-wear point agrees with the maximum resistance to scoring. The character of this phenomena is due to the fact that the dented area in excess of the optimum value gives rise to a contact pressure that is greater than the maximum load carrying capacity of the oil film.

23.3. PISTON RINGS

Piston rings of rectangular and trapezoidal cross-sections (Table 23.8) with a pear-shaped radial pressure diagram (Fig. 23.17) find the most extensive application. For cylinders with large ports, better results are achieved with rings having an apple-shaped pressure diagram.
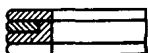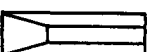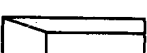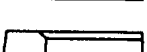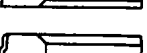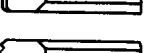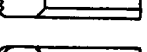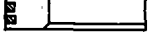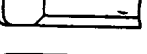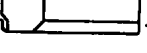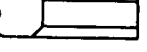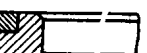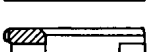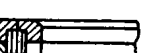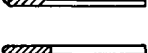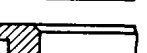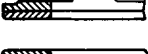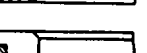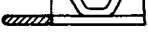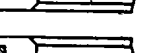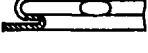
Medium-speed engines are provided with piston rings featuring a round or slightly oval pressure diagram.

Compression rings may be used without surface hardening (type К1-К3), with a convex (К4), tapered (К5), stepped (КР1, КРУ1), roughed (КР2) or grooved (КР3, КРУ2) face that facilitates running-in; with wear-resistant or run-in coatings, types КРУ, КРУ1, КРУ2 КВУ1, КРУ3, КРУ4, etc.

For severe lubricating conditions, use is made of piston rings with antifriction inserts (types КВ1, КВ2, КВ3, КВ4, КВ5, КВУ1)

Table 23.8

Types of piston rings

Designation	Face shape		Designation	Face shape
Compression rings			КСП	
К1			КР4	
К2			КРУ3	
К3			КР5	
К4			КРУ4	
К5			КР6	
КР1			КРУ5	
КР2			КСТ	
КРУ			*Oil scraper rings*	
КРУ1			М1	
КР3			МУ1	
КРУ2			М2	
КВ1			МУ2	
КВ2			МСП1	
КВ3			МСП2	
КВ4			МСФ	
КВ5			МСР	
КВУ1				

and of multipiece laminated steel rings КСП. The inserts are made of tin-phosphorus or tin-lead bronzes, and polymer materials.

Roughness (КР4), undulations (КРУ3) or various grooves (КР5, КРУ4, КР6) ensure oil retention and thereby better performance. Such grooves are sometimes filled with a solid lubricant (КРУ5).
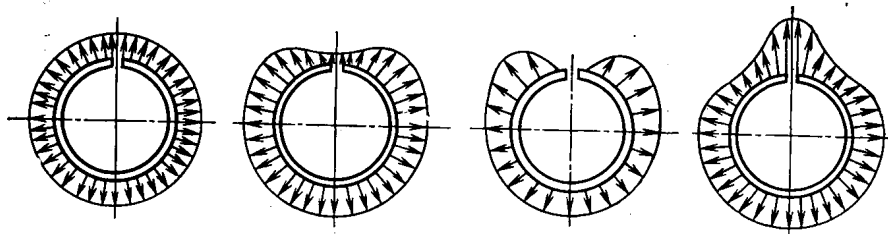
Fig. 23.17. Piston-ring radial pressure diagrams

Axially elastic disk-type steel rings (КСТ) easily run in and seal the cylinder.

Oil scraper rings come in different types, e.g. solid (М1, МУ1), box-type (М2, МУ2), multipiece laminated (МСП1, МСП2), special-section non-expansible type (МСФ), elastic expansible type (МСР). These rings are heat treated, case hardened, and also specially coated to facilitate running-in and improve wear resistance.

23.3.1. Piston-Ring Materials

The material of piston rings should easily lend itself to running-in and provide high resistance to wear, scoring and corrosion; high elasticity, static and fatigue strength; high heat capacity and heat conductivity. There is no material as yet that could meet all these requirements, and therefore piston rings are often subjected to a number of treatments.

Cast iron. Regarding the complex of properties, this group of materials (Table 23.9) is the most suitable for piston rings.

In heavy-duty applications, the need arises for a complex alloying and inoculating of grey cast iron; sometimes it should be replaced with globular-graphite cast iron, alloy steel, and special alloys.

The metal base of grey cast iron should be thin-plate perlite, sometimes thin-plate sorbite; the graphite inclusions should be medium-sized, lamellar in structure, straight or slightly curved in shape, and scattered.

Coarse or fine-grained structures are impermissible; free cementite, ferrite, and graphite of pseudoeutectic, dendritic, streak-type and large-flake varieties must be reduced to a minimum.

Grey cast iron for piston rings should have the structure of lamellar pearlite with a distance between cementite lamellae of 0.5 to 166 μm, with a disrupted network of phosphide eutectic inclusions having an area of 2 000 to 12 000 μm², with a uniform distribution

of flaky graphite inclusions measuring from 40 to 90 μm and with a total area of graphite of 3 to 6 percent. Cast iron with globular graphite should have a perlitic matrix with no more than 5 percent ferrite, with dispersed cementite inclusions spaced at 0.5 to 1.2 μm, and with uniformly distributed globular graphite inclusions measuring from 30 to 100 μm. Piston rings of high-alloy cast iron can in some cases have the metal base structure of austenite or acicular bainite.

To improve their strength and wear resistance, piston rings are sometimes oil hardened at 850-870°C and tempered at 350-500°C. Still better results are obtained by hardening with isothermal quenching at 850 → 350°C with a holding time of 2 to 3 hours.

Grey cast irons, including alloyed grades, have low fatigue strength. Piston rings working at high temperatures and loads are expedient to make of globular-graphite cast iron, whose cyclic strength is two times that of grey cast iron. However, the low antifriction properties and poor resistance to scoring of cast iron with globular graphite (see Table 23.10) necessitate the use of special remedial measures, such as chromium plating, plasma spraying, or thermodiffusion treatment.

Steel. The mechanical properties of the steels used for piston rings (Table 23.11) are much better than those of the cast irons. For instance, a chromium-vanadium steel has four times the fatigue strength of a chromium-nickel grey iron. The elastic modulus of steel is two times that of cast iron, which makes it possible to use, for the same radial pressures, steel piston rings of smaller radial thickness than cast iron rings. Steel piston rings find extensive application in internal combustion engines, compressors, pumps and other piston-type machines because they are more simple in manufacture and have wide design potentialities. The rings that undergo no surface treatment (chromium plating, nitrosulphidizing, etc.) should be made of high-carbon steels for better wear resistance. Depending on the chemical composition and heat treatment method, steel piston rings may have the structure containing sorbite, troostite, or bainite with fine-grained carbide inclusions. Steel piston rings are produced from tubular blanks, special-section wire or band. They are made solid, multipiece and with expanders.

Because steel rings feature a low resistance to wear and scoring, they are normally subjected to surface hardening. Another method for improving the antifriction properties and resistance to scoring is to interpose phosphor bronze, cast iron, or fluoroplastic inserts between steel rings (Table 23.8). Steel rings without surface hardening are used in compressors, scavenge pumps, hydraulic equipment, and grey-iron cylinders. In internal combustion engines, such rings are placed into the piston bottom grooves.

Metal-ceramic sintered alloys. Piston rings of iron-base sintered alloys (Table 23.12) are coming into practical use. These are alloyed with Cr, Ni, Cu, P, Zn, V, Sb, Sn, Mg, Si, etc. Additions of graphite,

Chemical composition and mechanical properties of cast irons for piston

Chemical composition, %*							
C	Si	Mn	P	Cr	Ni	Mo	Mg
3.0-3.4	1.5-2.0	0.6-0.9	0.3-0.4	—	—	—	—
2.7-3.1	1.3-1.8	0.8-1.4	0.3-0.5	0.2-0.45	0.3-0.7	—	—
3.7-3.9	2.4-2.6	0.5-0.75	0.3-0.5	0.25-0.35	—	—	—
3.2-3.8	2.1-2.6	0.7-1.2	$\leqslant$0.1	0.1-0.4	0.7-1.2	0.6-0.9	0.04-0.1
3.4-3.7	2.5-3.2	0.5-0.8	0.35	0.4-0.7	0.5-0.8	0.8-1.3	0.04
3.3	1.9	0.8	0.3	—	—	—	—
3.0	1.7	1.25	0.55	0.55	0.4	—	—
3.05	2.4	1.0	0.5	0.85	—	—	—
2.8-3.25	1.7-2.2	1.0-1.5	0.4-0.7	0.4-0.7	$\leqslant$0.4	—	—
3.5-3.8	2.6-3.1	0.6-0.8	0.5-0.7	—	—	—	—
3.6-4.0	2.5-3.0	0.5-0.8	0.4-0.6	$\leqslant$0.3	—	—	—
3.7-3.9	2.4-2.6	0.6-0.8	0.3-0.5	0.25-0.35	—	0.3-0.5	—

* S under 0.03-0.1.

Sb, Sn, Zn, P. Pb and Cu reduce the friction coefficient and increase the resistance to wear and scoring. Alloying with carbide-forming elements (Cr, V, Mo, Mn) improves the wear resistance, thermal stability, and mechanical properties of sintered alloys.

The antifriction properties of piston rings made of these alloys are strongly influenced by the porosity, which should be within 5 to 25 percent, depending on working conditions. Each application has its optimum in porosity; however, for strength reasons porosity should be kept down to a minimum that ensures reliable lubrication.

Table 23.9

rings

Other elements	Mechanical properties				Casting method
	σ_u, kgf/mm²	σ_{-1}, kgf/mm²	HB	E kgf/mm²	
—	28-32	8-10	207-235	6 000-8 000	Sand casting of multipiece tubular blanks
—	35-40	9-11	235-245	8 000-10 000	
0.35-0.5 Cu 0.08-0.18 Ti	38-45	12-14	255-286	9 000-11 000	
0.3-0.7 Cu	55-60	22-26	269-321	16 000-18 000	
0.8-1.2 Cu 0.1-0.3 V	56-62	24-28	255-297	16 000-18 000	
— 0.75 W 0.22 Ti	30 35	12 14	230 262	10 000 12 000	Centrifugal casting of multipiece tubular blanks
0.4 V	35	12	262	13 000	
0.5-1.0 W 0.15-0.3 Ti	38-40	13-16	245-265	12 000-14 000	
— 0.2-0.4 V 0.3 Cu	30-40 35-45	9-12 8-13	235-260 229-262	9 000-11 000 10 000-12 000	Individual ring blanks
0.25-0.5 Cu 0.1-0.2 Ti	40-45	9-14	245-269	10 000-14 000	

Among the self-lubricating compacted sintered materials, metal-graphite compositions based on copper, iron and their alloys are of interest. Colloidal graphite in these materials makes it possible for the piston rings to operate at high temperatures, with scant lubrication or the lack of a fluid lubricant. Impregnation with Sn, Cd, Pb increases wear and scoring resistance, and that with Cu and its alloys also adds strength and resistance to corrosion.

Some positive effect is achieved by phosphatizing and by oxidizing with dry steam at 560 to 580°C and impregnating with fluid

Table 23.10

Results of wear tests of cast-iron and steel piston rings]

Material, grade	HB	$\gamma \times 10^2$ mg/h	Running-in time, min	Scoring load, kgf/cm²
СЧХН/СЧХНМД	245/235	47/72	120	188
СЧХНМД/СЧХНМД	255/235	36/64	132	205
ВЧ/СЧХНМД	264/235	61/99	147	145
ВЧНМД/СЧХНМД	278/235	50/83	166	162
65Г/СЧХНМД	432/235	77/140	151	103

Note. The numerator gives data on piston rings and the denominator, on cylinder liners.

and solid lubricants. Metal-ceramic piston rings are also subjected to sulphidizing, sulphocyaniding and other methods of thermochemical treatment, which materially improve their wear resistance (Table 23.13).

The ease of running-in, good oil retention, and, in some cases, high wear resistance of sintered-alloy piston rings make them promising.

They can be recommended for internal combustion engines, compressors, hydraulic cylinders, etc.

Bronze. Bronze piston rings are employed in unfavourable lubricating conditions, where the working medium may cause corrosion, or where the piston unit is brought into action only occasionally and therefore corrosion of the rubbing surfaces may set in. Such rings come in several versions, such as elastic solid or multi-piece with expanders, or they are used in combination with steel or cast-iron rings.

A tin bronze [13] containing 86 percent Cu, 14 percent Sn and some addition of P can be universally used for piston rings. This bronze, sand and centrifugally cast, features $\sigma_u = 20\text{-}25$ kgf/mm², $\delta = 8$ percent, HB 75-115, $E = 6\,000\text{-}7\,000$ kgf/mm² and can be used for elastic rings.

A tin bronze [13] with 10 percent Sn and 15 percent Pb, and that with 5 percent Sn, 20 percent Pb and 3 percent Ni have poor elastic properties. However, they surpass the above-mentioned grade in wear and scoring resistance and in antifriction properties under conditions of lubricant starvation; hence they are used for solid or, better still, multipiece rings with expanders in steam engines and compressors.

Where high elastic properties are required, use should be made of a berillium bronze with 2.5 percent Be [13]. After forging and tempering the bronze exhibits high mechanical properties ($\sigma_u = 80$ to 120 kgf/mm²; $\delta \leqslant 20$ percent; HB 280-350). Good elastic properties are also provided by a silicon-nickel bronze with 1 percent Si and

Table 23.11

Chemical composition and mechanical properties of steel piston rings

	Chemical composition, %*					Mechanical properties			Application
C	Si	Mn	Cr	Other elements		σ_u, kgf/mm²	σ_{-1}, kgf/mm²	HB	
1.45-1.7	⩽0.4	⩽0.35	11.0-12.5	0.15-0.30 V 0.4-0.6 Mo		125-140	65-76	324-381	High tempera-tures and loads
0.8-0.95	0.35-0.5	0.25-0.4	17-18.5	0.08-0.15 V 1.0-1.25 Mo		130-150	60-70	363-415	
0.95-1.10	0.2-0.3	0.25-0.45	1.3-1.6	<0.08 Mo <0.35 Ni <0.25 Cu		126-140	50-60	353-405	
0.4-0.5	3.0-3.5	0.4	8.0-9.0	—		110-140	55-65	341-401	
0.5-0.65	0.2-0.4	0.7-0.9	0.9-1.20	0.15-0.2 V		110-130	48-55	309-343	Medium tempera-ture and loads
0.95-1.04	0.15-0.3	0.15-0.3	⩽0.45	—		100-120	48-52	324-372	
0.62-0.70	0.17-0.37	0.7-1.0	⩽0.10	—		90-110	45-50	410-442	

* P and S under 0.025-0.04%.

Table 23.12

Chemical composition and physico-mechanical properties of sintered metal-ceramic piston rings

Chemical composition, %*							Porosity, %	Mechanical properties	
C	Si	Mn	Cr	Ni	Cu	Other elements		Elasticity modulus, $E \times 10^{-3}$, kgf/mm²	HB
2.8	—	—	1.4	—	1.3	Powdery iron 94,5 ПЦЛ-18ХСНД	12-15	9-12	163-187
3.0	—	—	1.5	—	1.5	94ПЦЛПКП	12-15	10-13	165-210
1.0-1.5	0.1-0.3	≤0.1	1.5-5.0	0.1-1.5	3.0	0.1-0.5 Mo**	6-8	9.5-13	173-203
0.8-1.2	0.3-0.8	0.4-0.6	—	—	4-6	0.4-1.2 Sn	10-12	8-11	142-167
0.52	0.16	0.19	—	—	0.52	0.36 Sn / 4.50 Pb	7-10	12-14	195
0.7	0.12	0.33	0.07	—	9.8	3.55 Pb	7-12	12-15	167
1.25	0.2	0.5	—	—	3.0	0.9 Mo	9-15	9-13	148
1.2-1.3	0.1	0.3	—	—	3.5	0.6 Mo	8-12	10-12	155-212

* S and P under 0.01-0.1.
** Data given here and below are according to sources in this and other countries.

Table 23.13

Data on wear of sintered metal-ceramic top compression piston rings in automobile engines

Treatment method	$I \times 10^3$, μm/km		
	decrease in radial thickness	decrease in perimeter	increase in end clearance
No treatment	5.4	82.1	39.1
Tinning	4.9	30.8	35.0
Oxidizing in steam	4.5	26.5	32.8
Sulphidizing	4.0	25.2	30.8
Sulphocyaniding	3.8	21.2	25.4

2 percent Ni [13] which after forming and heat treatment has $\sigma_u = 40$ to 80 kgf/mm²; $\delta = 8$ to 15 percent; and HB 150-200.

Good performance in steam engines, internal combustion engines and pumps is shown by combination-type rings comprising bronze, elastic steel and cast iron components.

Non-metal materials. The use of non-metals for piston rings has been known quite a long time. Various fibrous materials in the form of elastic packing and seals impregnated with self-lubricating materials (graphite, MoS_2, etc.) are used in centrifugal pumps, centrifuges, air turbo-blowers and some other equipment.

Solid high-grade carbon materials with a friction coefficient of 0.1 to 0.17 on steel and 0.18 to 0.25 on copper are recommended for seals. Self-lubricating graphite rings can be used without fluid lubricants in cylinders made of cast iron, steel, Monel metal, etc.

In applications with graphite rings, a working medium coming into the cylinder must be carefully cleaned of abrasives. Inadequate filtration will result in rapid wear of the cylinder and the rings.

A recent development is substantial improvements in antifriction properties of wood achieved by impregnating it with polymer compounds, graphite, and MoS_2, which allows it to be used for piston rings and seals.

Wooden piston rings impregnated with graphite can operate at up to 600°C. Such rings can be employed for thermocompressors and refrigerant compressors.

Piston and seal rings can be made of polymer materials, such as fluoroplastic-4. Rings of graphite- or glass-filled fluoroplastic have sufficient strength and thermal stability, a low coefficient of friction and high wear resistance. Tests have shown that cylinders and piston rings wear much less, and engine start-up becomes easier.

Piston rings of fluoroplastic filled with bronze powder and combination rings consisting of steel or cast-iron rings with fluoroplastic inserts have proved advantageous. Such rings are normally used with elastic expanders. Their field of application is pumps, compressors, and steam engines.

For pumps handling cold, hot, saline, and marine water, brines, acids, alkalis, ammonia, oils, etc., at pressures up to 100 kgf/cm², the use of graphitized vulcanite rings can be advised.

23.3.2. Wear-Resistant Coatings

Methods for improving the wear resistance and antifriction properties of piston rings include coating with metals and non-metals. The most efficient are electroplating with chromium and plasma or flame spraying with molybdenum and composite alloys.

Chromium plating. Depending on design features and frictional conditions, poreless or porous chromium deposits can be used. Dense chromium is normally employed for small-diameter piston rings and accurate fits of the rings in the cylinder. Piston rings with dense chromium deposits are additionally provided with special coatings which facilitate running-in.

A porous chromium plate, obtained by anodic etching of an initially dense chromium deposit, has channels 20 to 40 μm deep. Such a plate shows a good running-in ability and resistance to scoring. The porous layer of the plating wears relatively fast at the initial stage of operation and so runs in against the cylinder bore, whose geometry errors may be as high as 30 to 50 μm.

Piston rings are finished by various methods, e.g. honing, superfinishing or lapping in holes simulating cylinder bores, which are sometimes charged with diamond powder. Piston rings for tractor engines undergo electrolytic lapping or electroplating by means of reverse current.

Piston rings over 200 mm in diameter and 3.5 mm thick should have a special face profile and microgeometry which facilitate running-in and the retention of oil. This is achieved either by forming the profile before chromium plating or by grinding it after plating. It is good practice to cut V-grooves on wide rings for better lubrication. The chromium plated face retains the initial profile, and the grooves left after lapping ensure the proper functioning of the rubbing surfaces.

Another method is roughing the rings with a turning tool at feed rates of 0.1 to 0.25 mm/rev prior to chromium plating. The rings are then honed or lapped to remove the peaks of the surface irregularities.

A single chromium-plated ring per piston is quite enough to markedly reduce wear in petrol engines (Table 23.14).

In heavy-duty transport diesel engines, it is advisable to use no less than two rings with a plating over 150 μm thick.

Sprayed metal coatings. In addition to chromium plating, the flame and plasma spraying methods are used for depositing wear-resistant metal coatings on piston rings. These coatings run in easily and provide good resistance to wear and scoring.

Among the metals used for spraying, the most remarkable is molybdenum. A high melting point (2 625°C) and heat conductivity, and special properties of the oxide forming on the surface determine

Recommended thickness of chromium plating

Type of engine and diameter of cylinder bore, mm	Plating thickness, μm	Number of chromium-plated rings per piston
Petrol engines	60-120	1
Diesel engines:		
≤ 150	80-140	1-2
≤ 350	150-300	2-3
> 350	300-600	3

a fairly high resistance of molybdenum coatings to seizure in oxidizing atmosphere. The hardness of molybdenum coatings ranges from 300 to 1 000 HV. However, the properties of the coating change in actual engine conditions.

The molybdenum coatings deposited in the flame spraying process have a hardness of HV 500-1 000, which drops to HV 400-800 after operation in an engine at 300°C. With these deposits, resistance to flaking varies from 1.5 to 3.0 kgf/mm^2 and porosity, from 16 to 20 percent.

The molybdenum coatings deposited in the plasma spraying process provide a better adhesion to the base and somewhat lower porosity (10 to 18 percent). The initial hardness of the plasma-sprayed coatings (HV 600-800) drops in operation under the same conditions to HV 400-600. The two kinds of molybdenum coating do not differ in scoring resistance.

A typical drawback to all sprayed metal coatings is their low strength of adhesion to the metal base, which becomes even lower under the action of the high working temperatures and corrosive medium within the cylinder.

Composite coatings are now being developed which contain Mo, Cr, Ni, W, etc. Their microstructure consists of the matrix with a hardness of HV 600-1 000 and hard inclusions in the form of molybdenum, tungsten and chromium carbides, intermetalloids, etc., having a hardness of HV 1400-1 800 and a 10-15 percent porosity. The wear resistance and adhesion strength of the plasma-sprayed composite coatings are higher than those of the single-phase molybdenum coatings. The best performance is exhibited by composite coatings with the bottom layer for good adhesion, the main wear-resistant working layer, and the upper layer for running-in. The wear-resistant matrix of such a coating may have inclusions hard to HV 2 000.

23.3.3. Running-in and Antifriction Coatings

Running-in is facilitated through the use of antifriction and anti-scoring coatings. These include deposits of tin, lead, cadmium, copper, indium, pseudoalloys, films of phosphides, sulphides, oxides, etc. Use is also made of mechanical loosening and etching of the surface layer.

Running-in coatings are deposited on rubbing surfaces by various techniques; the chemical, electrochemical, mechanical, and plasma methods are among the most commonly used. The electrochemical method is employed for depositing pure metals and multicomponent alloys.

Films of compounds based on epoxy and silicon resins and other composite materials containing substances capable of generating solid lubricant films with a low shear strength also find application.

Piston rings are often phosphatized or tinned. Although these coatings are different in nature and action, both have proved to be efficient when used for running-in on unhardened and chromium-plated mating surfaces (Table 23.15).

Table 23.15

Test data on wear behaviour of antifriction and running-in coatings for piston rings

Coating	Running-in time, min	$\gamma \times 10^2$, mg/h		Scoring load, kgf/cm²	
		liner	piston ring	onset of damage	scoring
Uncoated cast iron СЧХН	125	68.1	45	152	195
Phosphatizing in cold baths	89	72.4	49.4	160	228
Phosphatizing in hot baths	40	84.0	66.9	210	310
Sn	64	58.5	36.6	195	230
Cd	78	64.2	43.5	123	226
Pb	67	66.0	41.8	135	218
Cu	86	62.1	43.7	107	201
Cu + Sn	53	57.7	38.4	220	255
Cu + MoS₂	72	58.0	34.1	204	271
ВАП (MoS₂)	55	63.8	42.0	230	294
ВНИИ НП-220 (MoS₂)	60	65.0	44.3	155	230
Phosphate + MoS₂	32	72.3	54.5	236	344
Cr	460	49.0	26.4	160	234
Cr + Sn	263	44.5	22.5	198	260
Cr + Cu	330	42.3	20.0	176	265
Cr + Cu + Sn	280	41.0	19.4	203	280
Cr + Cu + MoS₂	286	40.0	18.6	230	302
Mo (plasma sprayed)	145	62.4	32.5	230	298
Mo (flame sprayed)	160	65.3	38.1	210	265
Mo composite deposit (plasma sprayed)	180	56.0	28.3	255	314

Phosphate coatings tangibly improve resistance to scuffing. The coatings deposited in hot baths have a considerable surface roughness (6-10 μm Rz) and therefore intensively wear at the initial stage of running.

A layer of a molybdenum disulphide composition based on epoxy resin 10 to 12 μm thick deposited on a preliminarily phosphatized surface makes it possible to markedly increase the efficiency of running-in.

Tin plating eliminates seizure at considerable contact pressures by localizing contact surface damage within the tin layer (Table 23.15) and facilitates the running-in process, provided that the deposit has good adhesion to the base.

An important feature of the tin coating is its ability to spread over the rubbing surface and to fill surface irregularities. This levels out the contact pressures and so excludes critical loads. The presence of tin in the hot zones brings about a sharp drop in the friction coefficient (to 0.04).

Lead coating, which has sufficient plasticity and a low melting point, is nearly as effective as tin in improving the resistance to scoring and in facilitating the running-in process. However, it is subject to rapid oxidation in engine cylinders, has a short wear life, and in its pure form is rarely used as a means for piston ring running-in.

Cadmium is close to tin in its properties but has a lower plasticity.

As seen from Table 23.15, electrodeposited copper platings shorten the running-in period and improve scoring resistance. Still greater effect is provided by combination coatings of copper and MoS_2 deposited simultaneously and by double-layer coatings of copper and tin.

The composite $Cu + MoS_2$ coating has very valuable properties; MoS_2 in the copper matrix drastically reduces resistance to displacement in the real contact area, and that ensures a relatively short duration of running-in and high scoring resistance. The principal advantage of this coating over tin platings is the longest wear life.

Polymer coatings promote the running-in process and increase scoring resistance. Their useful life, however, has proved to be shorter than that of the composite metallic coatings.

Chromium platings, even the porous ones, need greater efforts to enhance their ability to run in than cast iron. Electrodeposited chrome takes the longest time to run in. Deposition of tin over the chromium plating makes it possible to cut this time by a factor of 1.7 and to some extent improve the load-carrying capacity of the sliding pair. The tin layer on chromium lives shorter than on cast iron because of poorer adhesion. Copper provides a better adhesion to chrome, although the running-in process is longer. The composite $Cu + MoS_2$ coating has proved to be the most advantageous for chromium-plated piston rings; compared with tin it has a higher scoring resistance and longer useful life. For instance, the compo-

site coating on chrome-plated piston rings in diesel engines lasts from 100 to 300 hours. Under the same conditions a tin coating wears away in 2 to 4 hours.

All running-in coatings eliminate scoring at the initial working stage and increase the load-carrying capacity of the rubbing components. Later, the resistance to wear and scoring is determined by the properties of their basic materials.

23.4. PISTONS

Pistons wear at the ring grooves, skirt, and piston-pin bores. Monometal pistons made of aluminium alloys fail mainly due to the wear of the two top ring grooves. Other piston failures include
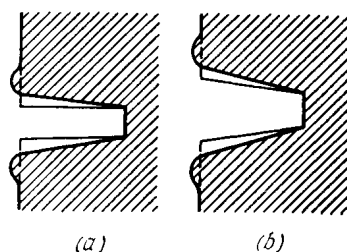
Fig. 23.18. Shape changes in piston-ring grooves of aluminium pistons due to wear
(a) rectangular groove; (b) trapezoidal groove

scoring and cracking caused by thermal, fatigue and corrosive factors. Gross malfunctions in internal combustion engines can involve the burning-out of the piston heads. This failure is typical of aluminium alloy pistons.

Repeated radial displacements of piston rings accompanied by impacts produce plastic deformations at the edges of the grooves and a flow of thin metal layers outwards.

Rubbing between the piston-ring and groove surfaces may take place at elevated temperatures (200 to 250°C), in the presence of carbon and abrasive particles getting in from outside.

Greater wear is observed on the bottom surfaces of ring grooves due to the action of gas pressure during the expansion stroke.

The main factor that gives rise to distortions of the shape of ring grooves in aluminium pistons is the bulk deformation, which grows as the piston is heated to the working temperature (Fig. 23.18).

The piston skirt wears unevenly, mainly in the maximum-pressure areas. Its wear rate, however. is much lower than that of the top grooves.

The skirts of aluminium pistons wear slower than those of cast iron, steel, and non-ferrous alloy pistons. This is usually ascribed to

greater inertial forces and specific loads which arise in interaction of the heavier pistons with the cylinder face.

Shape changes of the rubbing surfaces in the piston assembly components due to wear-in at the initial stage of operation enhance the assembly performance and especially its sealing function. At that stage the engine usually shows its maximum efficiency.

As the clearances grow as a result of further wear, the optimal fit of the piston in the cylinder is impaired, giving rise to impacts, vibrations, and loosening of the rings in the grooves.

The loose top compression rings inevitably produce rapid wear, impair tightness, and reduce efficiency of the unit.

23.4.1. Piston Materials

Pistons for internal combustion engines should be made of materials having sufficient strength and wear resistance, high thermal conductivity, low thermal expansion coefficient, low density and high heat resistance.

Aluminium alloys. Pistons made of aluminium alloys have found wide application because of the smaller mass. This reduces inertial action on the crankshaft assembly components, friction forces, and wear. Owing to their high thermal conductivity, aluminium-alloy pistons are heated in operation less than cast-iron and steel pistons. Their heads collect less carbon, and the skirts carry a stronger oil film, which creates favourable frictional conditions on the cylinder face.

The drawbacks to aluminium alloys are their low strength at elevated temperatures and high linear expansion coefficient.

Extensive use has been made of eutectic and hypereutectic aluminium alloys with Cu, Ni, Mg, and Fe. For high-speed internal combustion engines, it is common practice to employ wrought alloys AK2, AK4, AK4-1, AK9 and an alloy known as forged silumin whose wear resistance is higher and linear expansion coefficient is lower than with the other piston wrought alloys. But in terms of high-temperature strength, this alloy is second to the AK2 and AK4. Fairly good antifriction properties of these alloys result from the microstructure that consists of low-alloy ductile matrix and hard second-phase inclusions.

Cast irons. Cast irons used for pistons (Table 23.16) have lamellar, spot, and globular graphite inclusion. The metal matrix is commonly a perlitic one. Alloy cast irons can have the structure of austenite or bainite. Cast irons intended for pistons in internal combustion engines should have not only an adequate strength and wear resistance, but also dimensional stability, resistance to burning cracks, corrosion, and fatigue.

The close-grained structure of the metal matrix and graphite and, especially, alloying with Mo, V, Cr, Ni, and Cu, increase the resistance of cast iron to the above-mentioned failures. The greatest

Table 23.16

Chemical composition and mechanical properties of cast-iron pistons

Chemical composition, %*					Mechanical properties	
C	Si	Mn	P	Other elements	σ_u, kgf/mm²	HB
Small and medium pistons						
3.3-3.5	2.0-2.3	0.6-0.9	⩽0.2	Cr, Mo, Cu,	24-30	197-250
3.2-3.4	1.9-2.2	0.6-0.9	⩽0.2	Ni	21-28	187-228
Large pistons						
3.3-3.5	1.3-1.8	0.6-0.9	⩽0.2	0.2-0.4 Mo, ⩽0.1 Ti, 0.2-0.3 V	24-30	170-190
2.9-3.2	1.6-2.1	0.8-1.2	⩽0.2	⩽0.5 Ni 0.4 Cr	27-30	197-241
3.1-3.4	0.8-1.4	0.6-0.9	⩽0.2		18-25	170-190
High-speed engine pistons						
2.7-3.0	1.6-2.0	0.9-1.2	0.06	0.7-0.9 Ni, 0.25-0.35 Cr, 0.2-0.3 Mo, 0.2-0.3 Cu	30-35	196-235
3.35-3.8	1.3-52.0	0.8-1.3	0.15-0.4	0.5-0.8 Cr, 0.4-0.8 Mo, ⩽0.3 Ni	30-35	207-255
3.4-3.8	2.0-2.8	0.3-0.6	⩽0.08	⩽1% Mo, ⩽0.07 Mg	60-74	200-260

* S under 0.02-0.08.

strength is typical of pistons that are made of cast iron with globular graphite.

Alloying considerably improves the dimensional stability and strength of cast iron, but not necessarily its antifriction properties. When selecting a cast-iron grade, it must be taken into account that cast iron with globular graphite is inferior in thermal conductivity and antifriction properties to grey cast iron.

High strength of cast irons, a rational design and casting technique make it possible to obtain pistons that have better wear resistance and thermal stability than aluminium pistons, and roughly the same mass.

23.4.2. Methods for Piston Strengthening

These include heat treatment, the use of metal and non-metal coatings, various inserts, and combination-type piston designs of different materials.

Coating with Sn-, Cu-, and Pb-base antifriction alloys, phosphate and oxide films, and also oil-retaining surface patterns improve wear and scoring resistance and simplify running-in. Protection of piston heads against burning-out, corrosion and fatigue failures, and reduction of temperature in the top-grooves area can be effected with ceramic plasma coatings and also, for aluminium pistons, by anodizing.

Chromium plating can be recommended for protecting piston heads against combustible gases and corrosive attack and for increasing the wear resistance of the ring grooves. In cast-iron and steel piston heads, the ring grooves are also strengthened by induction hardening, nitriding, and nitrosulphidizing.

Ceramic and oxide coatings are used predominantly in protection of cast-iron and aluminium piston heads. Having good anticorrosion properties, high thermal stability, and low thermal conductivity, these coatings reduce the heat flux from the combustion chamber, and level out the piston temperature field by intensively reducing the temperature in the highly heated areas.

As a rule, pistons with non-metal coatings exhibit low surface temperatures and wear.

Ceramic coatings based on oxides of zirconium (ZrO_2) and aluminium (Al_2O_3) are deposited by enamelling, and by the plasma and flame spraying techniques. The thickness of the coat is specified at 100 to 400 μm.

To ensure effective piston-head protection, the thermal conductivity of the coat should be no lower than $\lambda = 1.5$ kcal/(m h °C) and heat reflection factor no lower than 0.75.

The use of heat-protection coatings on aluminium pistons is important for controlling not only the burning-out of the head and the piston thermal distortion, but also the wear of the top ring grooves, holes, bosses, and skirt through reducing the temperature of the rubbing surfaces.

Oxide coatings obtained by anodizing are similar in properties to ceramic deposits, but their density and strength of adhesion to the metal base is higher. Their hardness ranges from 300 to 600 H_{50}.

The antifriction properties and wear resistance of oxide films can be increased by the application of solid lubricants (graphite, MoS_2, etc., Table 23.17).

The most effective way of reducing the wear of the top ring grooves is to make the piston composite or to reinforce it with wear-resistant inserts. Usually, an insert of austenitic cast iron or steel is introduced in the area of the top rings. The austenitic cast iron (Ni-resist) provides a high resistance to wear and scoring (Table 23.18).

A valuable feature of the Ni-resist is that its linear expansion coefficient (19×10^{-6}, 1/°C) is close to that of aluminium piston alloys (20×10^{-6}, 1/°C). Therefore a reliable assembly of the insert with the piston is secured. The hardness of the Ni-resist is HB 150-220.

Table 23.17

Resistance to wear and scoring of alloy-AK4-pistons subjected to anodizing, graphite coating, and coating with MoS₂

Treatment	HB	Coating thickness, μm	γ, mg/h	Resistance to scoring, kgf/cm²
No treatment	112	—	0.86	49
Anodizing	447	105	0.61	79
Anodizing and coating with graphite	438	125	0.54	85
Anodizing and coating with MoS₂	455	134	0.48	120

Table 23.18

Resistance to wear and scoring of piston materials

Material	HB	γ, mg/h	Resistance to scoring, kgf/cm²
Chromium-nickel cast iron	229	0.52	174
Aluminium alloy AK4	112	0.86	49
Aluminium alloy AK4 anodized and coated with MoS₂	455	0.48	120
Ni-resist	217	0.37	228

The insert can be soldered or mechanically fixed to the piston body. Various forms of inserts are in use, from a solid annular piece to individual elements (Fig. 23.19). Sometimes, for cost reasons,
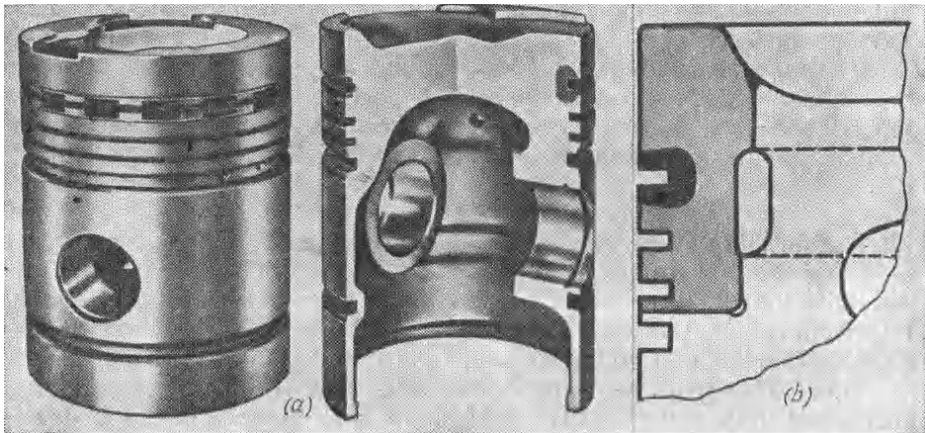
Fig. 23.19. Pistons with wear-resistant inserts for diesel engines
(a) wear-resistant ring or individual inserts; (b) combination-type annular insert

the top ring grooves are reinforced by steel helical wire inserts introduced in the process of casting (Fig. 23.20).

Actually, the use of pistons with inserts in various machines has shown that wear of the top ring grooves dropped by a factor of 2 to 6.

This method, however, has its disadvantages, namely, an involved manufacturing process, increased costs, and an insufficiently reliable mounting of the insert on the piston.

Methods have been developed for hard facing and plasma spraying of the piston-ring grooves with wear resistant alloys. The grooves can also be protected against wear by using piston rings with chrome-plated sides. In engines with medium loads and temperatures, this method allows the wear of the grooves to be reduced by a factor of 1.5 to 2.5.
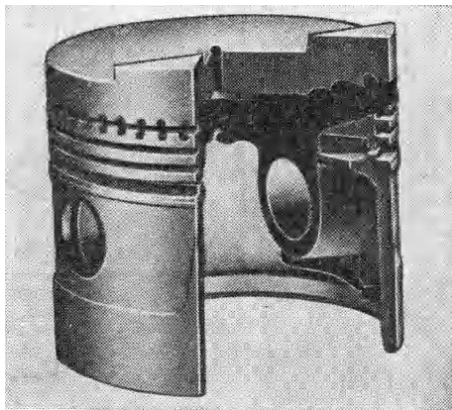
23.5. PISTON PINS

Fig. 23.20. Piston with top ring groove reinforced by steel helical wire

Piston pins may be movable both in the piston and in the connecting rod, or they may be fixed in one of these.

The first type of mounting is more advantageous as regards friction; the wear of the pin and its mating surfaces is less intensive, both on the diameter and along the length. The assembly is more reliable in operation, because if the pin seizes in the piston bores or in the connecting-rod bushing, the rocking of the connecting rod will continue.

Wear of the pin surface, as it rubs against the mating surfaces, is due to molecular seizure resulting from oil film disruption that occurs on instant local overheatings and vibrations; abrasive action of hard particles in the soft metal of the piston-pin bosses and the connecting-rod bushings; and irreversible processes running in the subsurface layers of the pin.

Geometry errors of the pin and its mating surfaces have a considerable effect on their wear life. Thus, the wear of the pin and the connecting-rod bushing grows with the height of the pin-surface waviness (Fig. 23.21). The wear life of this joint can be prolonged by increasing the real contact area through better surface finish and geometry of the mating surfaces.

Initially, piston pins are finished to 0.12-0.3 μm Ra. As they run in, the surface roughness decreases to 0.02-0.3 μm Ra.

For automobile-engine piston pins sliding in bronze connecting-rod bushings, the surface roughness comes to 0.07 to 0.09 μm; for pins sliding in aluminium-piston bosses, it is 0.08 to 0.1 μm Ra. The oil film thickness in such joints amounts to 0.7-0.85 μm. At extremely low sliding speeds, the oil film thickness may be much smaller
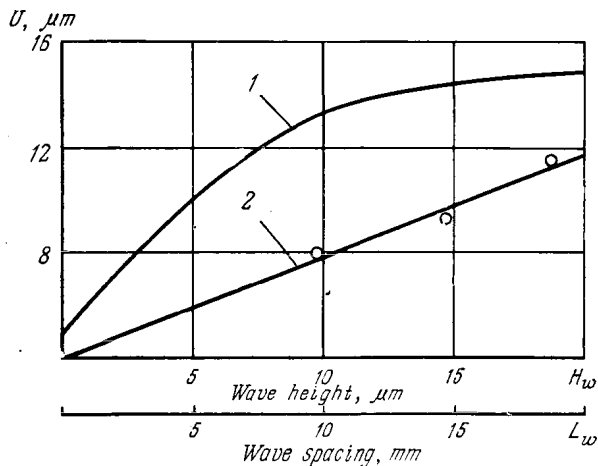
Fig. 23.21. Wear of piston pins as a function of surface waviness
1—wave spacing; 2—wave height

than that, i.e., the pin will work in the boundary lubrication conditions. The initial surface roughness of the pin hole and the connecting-rod bushing should be greater than that of the pin.

In automotive engines, the rational value for pins is 0.16 μm Ra and for pin holes in pistons 0.3-0.4 μm Ra.

The most effective way to improve wear resistance is to increase the hardness and load-carrying capacity of the oil film. A uniform lubricant film and proper clearances make it possible to mitigate impacts in the joint for better performance and trouble-free service over a long period of time.

The piston pin wears non-uniformly along its periphery, and this can be put down to varying frictional conditions due to distortions of the mating parts, varying temperatures, loads, and antifriction properties of the materials.

A low resistance to seizure, as, for instance, in chrome-plated piston pins rubbing against lead-bronze bushings, may give rise to intensive wear of the surfaces.

The pin material should effectively resist wear, impacts, and cyclic loads. The wear resistance and strength of the pin are secured by case hardening, so that it has a hard surface and a tough core. The carbon and alloy steels used for pins are subjected to carburizing, nitriding, carbonitriding, or induction hardening (Table 23.19).

78

Table 23.19

Wear resistance of piston pins according to laboratory and field tests

Material	Strengthening method	HRC	U_m, mg, in laboratory	$I \times 10^4$, μm/km, in service
55ПП	Induction hardening	57	86	48
50ХФ		59	72	—
12ХН3А	Carburizing	62	63	40
27ХГР	Carbonitriding	63	50	20
38ХМЮА	Nitriding	65	44	15

The following steel grades are recommended for pins: low-carbon steels 15, 15Х, 20ХН, 12ХНВА, 12ХН3А, 15ХНА, 38ХМЮА which are carburized, nitrided, and carbonitrided; induction-hardened steels 40, 40Х, 40ХН, 50Г, 50ХФА.

Other methods to increase wear resistance and also to restore the dimensions include hard chromium plating, nickel plating, acierage, plasma spraying, hard facing, etc. (Table 23.20).

23.6. SURFACE FINISH REQUIREMENTS

The initial surface roughness of the piston assembly components should provide for a short running-in period, minimum wear, optimum surface texture stability, high load capacity, and specified compression.

As the piston skirt and rings wear somewhat faster than the cylinder, their initial surface roughness must be greater than that of the cylinder face, or their surfaces should have a special oil-retaining texture (Table 23.21).

Strict requirements are also placed on the sides of the rings and the ring grooves, since these are often subject to rapid wear, and that shortens the useful life of the machine.

The pin surface finish should be fairly high, but it must be borne in mind that a surface roughness smaller than 0.1 μm Ra may impair the load capacity of the joint. The surface roughness of the piston pin holes and the connecting-rod bushing should be greater than that of the pin.

The recommended limiting values of surface roughness are established with regard to the permissible clearances, wear rate, running-in time, and the cost effectiveness of finishing operations. The optimal surface roughness retained during service helps to achieve and maintain the rated characteristics of a piston-type machine over the specified service life.

Table 23.20

Wear resistance of piston pins made of steel 15X with different coatings

Treatment	Coating thickness, mm	HV	μm, Ra	Material		Vehicle run, thousands of km	Increase in fit clearance after run, μm		Comparative wear resistance of joint, %	
				connecting-rod bushing	piston boss		pin/boss	pin/bushing	pin/boss	pin/bushing
Carburizing	—	840	0.16-0.32	Bronze OЦC4-4-25	Aluminium alloy HB115-140	87.6	26	63	100	100
Dense chromium plating	0.15	770	0.32-0.63			24	23	63	31.2	27.4
Porous chromium plating	0.15	—	—			30.8	20	50	46.3	44.2
Acierage	0.20-0.23	568	0.32-0.63			30	30	60	30.8	36.8

Table 23.21

Recommended and optimal surface roughness for cylinder-piston assembly components

Rubbing surface	Values of Ra, μm	
	recommended	optimal
Cylinder face	0.2-0.63	0.15-0.32
Piston-ring face	0.63-2.5	0.4-0.6
Piston-ring side	0.15-0.5	0.15-0.3
Piston skirt	0.6-1.25	0.25-0.5
Piston-ring groove	0.32-0.63	0.2-0.5
Piston-pin bore in piston boss	0.3-0.5	0.2-0.32
Piston pin	0.12-0.3	0.04-0.1
Connecting-rod bushing	0.4-0.8	0.25-0.4

REFERENCES

1. Асташкевич Б. М. Вопросы повышения износостойкости цилиндровых втулок и поршневых колец транспортных двигателей.—«Вестник машиностроения», 1976, № 3, с. 9-12.
2. Асташкевич Б. М., Ларин Т. В. Оптимальный состав и структура чугуна цилиндровых втулок тепловозных дизелей.—«Литейное производство», 1970, № 6, с. 30-33.
3. Асташкевич Б. М., Ларин Т. В. Восстановление трущихся деталей транспортных двигателей износостойким хромированием. М., «Транспорт», 1967, 147 с.
4. Гаркунов Д. Н., Поляков А. А. Повышение износостойкости деталей конструкций самолетов. М., «Машиностроение», 1974, 198 с.
5. Гурвич И. Б. Долговечность автомобильных двигателей. М., «Машиностроение», 1967, 104 с.
6. Карпов Л. Н. Надежность и качество судовых дизелей. Л., «Судостроение», 1975, 231 с.
7. Крагельский И. В. Трение и износ. М., «Машиностроение», 1968, 480 с.
8. Ларин Т. В., Асташкевич Б. М. Оценка износостойкости материалов на машине трения с возвратно-поступательным движением.— В кн. Трение и износ в машинах. Сб. XV. М., Изд-во АН СССР, 1962, с. 114-130.
9. Лахтин Я. Д., Коган Я. Д. Азотирование стали. М., «Машиностроение», 1976. 254 с.
10. Мишин И. А. Долговечность двигателей. М., «Машиностроение», 1976, 288 с.
11. Михайлов-Михеев П. Б. Справочник по металлическим материалам турбино- и моторостроения. М.-Л., Машгиз, 1963, 838 с.
12. Повышение износостойкости деталей двигателей внутреннего сгорания. Под ред. М. М. Хрущова. М., «Машиностроение», 1972, 176 с. Авт.: Б. М. Асташкевич, М. А. Григорьев, Н. Н. Пономарев и др.
13. Энглиш К. Поршневые кольца. Т. 1 и 2. М., «Машиностроение», 1963, 951 с.
14. Юргенсон А. А., Зеленская Г. И. Материалы быстроходных дизелей и их термическая обработка. М., «Машиностроение», 1964, 267 с.

24.1. GENERAL PRINCIPLES OF SEALING

24.1.1. Basic Definitions

A *seal* (*packing*) is a combination of components which provides for tightening effect.

The *sealing capacity* is the main characteristic of the performance of a seal; it is measured by the mass of a substance escaping through the seal (leakage rate).

Tightness specifications are dictated by the reliability and service-life requirements for a particular piece of engineering equipment.

The *seal performance factor* is expressed by the relationship

$$i = 1 - \frac{m}{m_p} = 1 - \frac{1}{m_p} \int_{t_0}^{t_r} m\,(t)\,dt$$

where m and m_p are respectively the actual and permissible masses of leaking substance over the rated service life t_r, $m\,(t)$ is a function describing the variation of leakage with time, t_0 is the moment at which the seal begins to leak, determined by a particular tightness checking method.

If the leakage mass $m < m_p$ over the time $t = t_r - t_0$, then the factor $i > 0$. In the inoperative-failure conditions when $m > m_p$, the factor $i < 0$.

24.1.2. Classification and Characteristics

With reference to wear and lubrication, engineering seals may be classified as follows:

—regarding the relative motion between the mating surfaces, as *dynamic* or *static*;

—regarding the external friction at least at separate portions of the contact region at some moments of time, as *contact* or *clearance* seals.

Dynamic seals may also be divided by the character of relative motion into the rotary, reciprocatory, and complex types. There are also the following divisions: for contact seals—stable-shape, va-

Classification of seals

Table 24.1

Classification characteristics	Design types	Figure No.	Classification characteristics	Design types	Figure No.
Dynamic, contact-type, stable shape	Lip seals, face seals, piston rings, segmental rings	24.1	Dynamic or static, clearance-type, gas	Buffer-fluid seals	24.5
Dynamic, contact-type, variable shape	Diaphragms, bellows, inflation-type seals	24.2	Dynamic or static, clearance-type, combined	Magnetic-fluid seals	24.6
Static, contact-type, variable shape	Inflation-type seals		Static, contact-type, stable shape	Metal gaskets, rubber rings	24.7
Dynamic, contact-type, shapeless	Groove packings, stuffing boxes	24.3	Static, contact-type, shapeless	Groove packings, stuffing boxes, sealants (pastes)	24.8
Dynamic, clearance-type, liquid	Labyrinth seals, screw-pump seals, impeller seals, ejector-type seals, centrifugal fluid seals	24.4	Static, contact-type, liquid	Buffer-fluid seals	24.9

riable shape and shapeless (filling) seals (classification basis is the stability of geometric shape); and for clearance seals— liquid, gaseous, and combined seals (classification basis is the physical nature of the separating medium).

Table 24.1 lists some seal designs shown in Figs. 24.1 to 24.9. Many up-to-date sealing devices are combined: they incorporate structural components characteristic of various types of seals.

Seals generally include the following elements: surfaces to be tightened, for instance, the cylindrical surface of a shaft or housing;
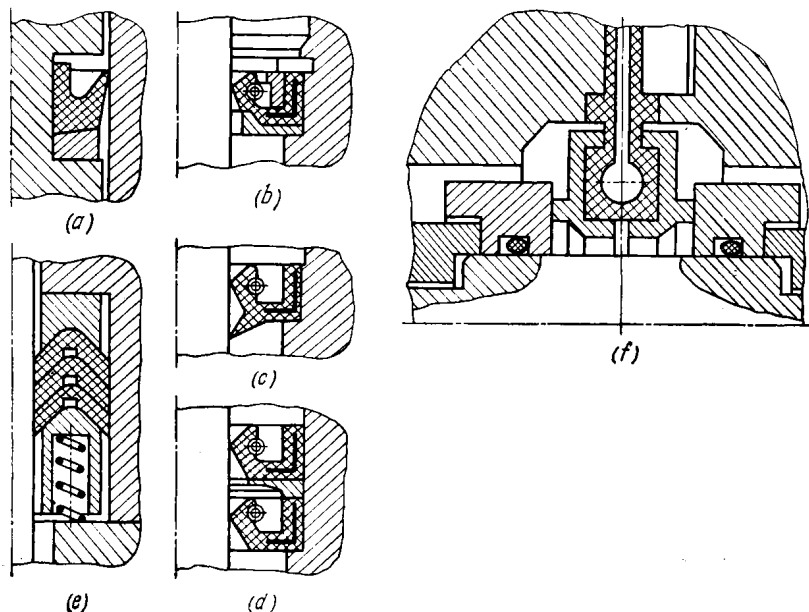
Fig. 24.1. Dynamic contact seals of stable shape
(a), (b), (c), (d) lip-type packings; (e) inflation-type double-end face seal

a sealing component such as a rubber ring; and auxiliary elements (secondary sealing components, reinforcing components, etc.).

The main sealing problems and main techniques used to solve them are as follows:

—reducing leakage through the clearance by improving the hydraulic resistance of the seal;

—preventing leakage by reducing the clearances with the use of accurately matched parts and elastic materials, or by the application of heavier compressive loads;

— filling the clearance with a packing material or sealant and applying a force field to the sealing medium;

—separating the media with a tight partition in the form of diaphragms, bellows or couplings of various types.

The performance of any seal is influenced by numerous and varied factors, which are often interactive. For instance, about 30 dif-
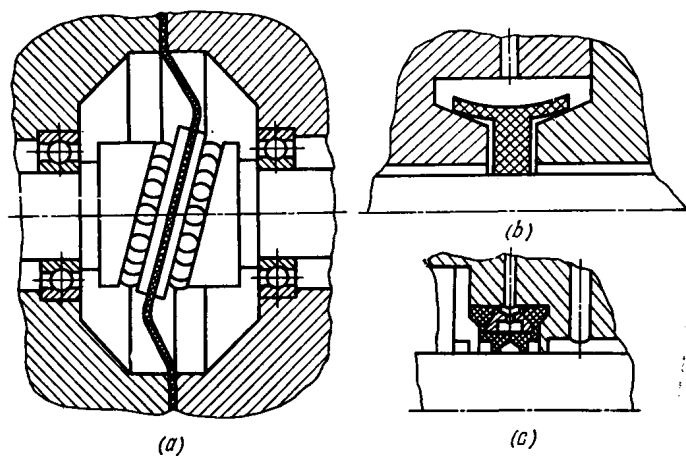
Fig. 24.2. Dynamic contact seals of changeable shape
(a) diaphragm; (b) and (c) inflation-type radial seals
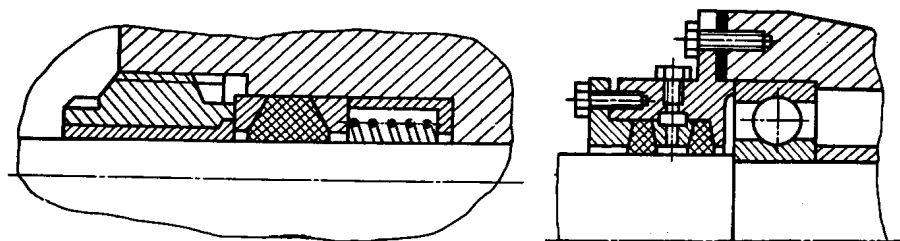
Fig. 24.3. Stuffing boxes
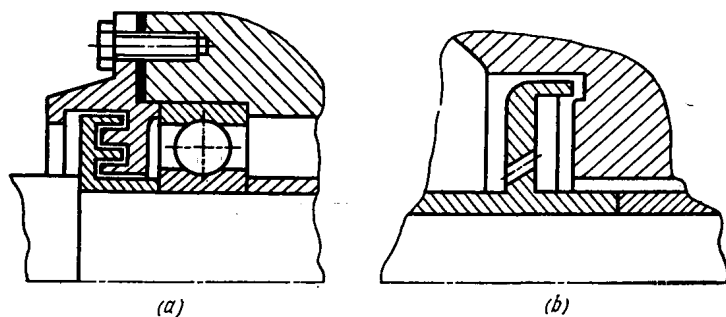
Fig. 24.4. Clearance seals
(a) face labyrinth; (b) impeller

Fig. 24.5. Clearance-type buf-
fer-gas seal

1—supply of oil to bearing; *2*—gas
inlet; *3*—gas outlet
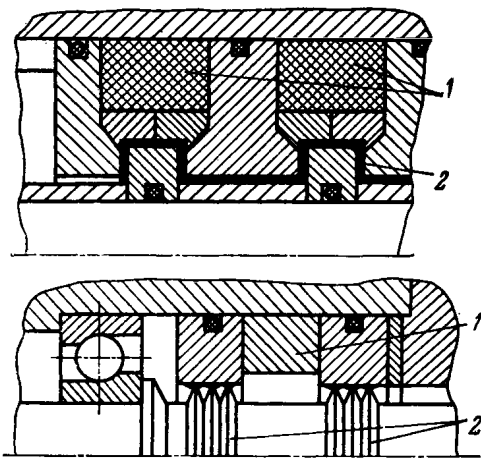
Fig. 24.6. Magnetic-fluid seals

1—annular magnets; *2*—magnetically-active li-
quid
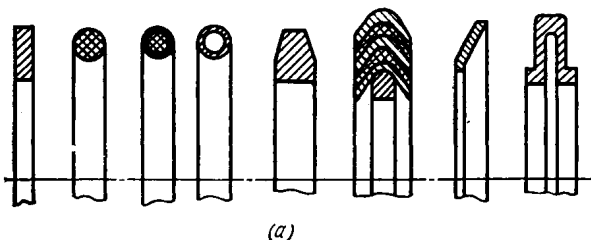
(a)   (b)

Fig. 24.7. Sealing gaskets

(a) types of gaskets; (b) stable-shape static contact seal in a machine unit; *1*—round-section
annular gasket; *2*—PTFE gasket completely filling its groove; *3*—reserve space

Fig. 24.8. Application of
anaerobic sealant (*2*) for
sealing screw thread and
locking nut (*1*) on screw (*3*)

Fig. 24.9. Buffer-liquid seal for lubricating,
cooling, and relieving lip packing from load
in motion and at rest

1—chamber being sealed; *2*, *3*—inlet and outlet
of buffer fluid

ferent factors have a major effect on the operation of oil seal units, and these factors can be grouped in the following way.

Operating conditions: rated life, temperature, load, sliding speed, storage and transportation conditions, vibrations, variations of the performance characteristics, etc.

The properties of the fluid to be sealed: freezing and boiling temperature, thermophysical properties, chemical aggressiveness, viscosity, and its dependence on temperature and pressure, behaviour in narrow clearances, etc.

The properties of the materials of the mating parts and their coatings: strength characteristics (in particular, fatigue and relaxation), thermophysical properties, etc.

The design of the product that incorporates the seal: configuration, surface geometry and mass of the components, their thermophysical properties, lubricating and cooling conditions, shaft misalignment and runout, etc.

The seal's manufacture and assembly: surface treatment methods, machining conditions and accuracy, correct assembling sequence, etc.

Proper handling and maintenance: correct operating conditions, periodic inspection and change of lubricant, etc.

Physico-chemical processes in the area of contact: film formation, changes in the properties and structure of the materials, distortions of the geometry of components due to wear or deformation, etc.

The performance of seals is characterized by the degree of tightness, service life, power losses, by the extent of damage to the contacting surfaces in operation, etc. The degree of tightness, wear life t_w, and performance factor i are the most important characteristics of seal performance. In addition to the above factors, temperature, whose level is determined by their joint action, also affects the performance of dynamic seals. Whereas temperature has the major influence on the frictional effects in the contact area, the leakage is caused by reduction in the contact pressure and distortions in the geometry of the rubbing surfaces due to wear, increased thermal deformations, etc. In some instances, these factors are interdependent.

The service conditions of sliding contact seals in machinery, determined by combinations of the above factors, are very diverse. Some idea of their variety can be gained by reference to Table 24.2, in which several major factors are presented in a general form. It can be seen that increasing pressure of the sealing medium p_s, sliding speed v, and their product $p_s v$ tend to reduce the seal service life at $i > 0$.

The most important present-day problems of sealing are indicated in Fig. 24.10.

The principal way of improving the design calculation of dynamic and static seals for long service life, friction, and wear is to relate in each particular instance the geometric parameters of the contacting surfaces, the properties of the medium to be sealed, and the external

Table 24.2

General characteristics of seal operating conditions in some technology fields

Field of application	Operating conditions			Fluid to be sealed	Reliability requirements	Required service life. h (approximately)	Maintenance	Applications
	p_s, kgf/cm²	v, m/s	$p_s v$					
General engineering	0-4	2-10	35	Non-aggressive, temperature 0-35°C (water, oil, etc.)	Average; low-rate leakages (e. g. 0.002 g/h) are admissible	15 000	Inspection, repair, and replacement of seal are feasible	Machine tools, speed reducers, electric motors
Transport	0-10	5-10	80	Non-aggressive, temperatures -60-+110°C (oil, kerosene, etc.)	Average; low-rate leakages (e. g. 0.005 g/h) are admissible	10 000	Periodic inspection and replacement are admissible	Automobile and excavator units
Chemical and petroleum engineering	0-450 (vacuum not excluded)	10-150	500	Aggressive, temperatures -50-+200°C (acids, alkalies, etc.)	High; insignificant leakages into a closed chamber are allowable	5 000	Inspection is difficult; replacement is possible during machine assembly	Pumps, compressors, reactors
Aviation	0-200	20-100	500	Both aggressive and non-aggressive (oil, fuel, etc.)	Very high; leakage is practically inadmissible	1 500	Inspection is difficult; replacement is possible during machine reassembly	Engine components, control instruments
Nuclear engineering	50-200 (vacuum not excluded)	10-50	500	Both aggressive and non-aggressive (water, steam, etc.)	Very high; leakage is inadmissible	1 000	Replacement in service is impossible. Danger of radiation	Pumps in nuclear power plants, system components
Space technology	0-200 (vacuum not excluded)	20-300	1 000	Aggressive (fuel)	Very high; leakage is practically inadmissible	100	Replacement is impossible. Seal is subject to space-flight effects	Pumps, control instruments

conditions (temperature, pressure difference, normal load, etc.) to the amount of leakage through micro-clearances between the mating surfaces.

Let us consider the characteristics of the most frequently used types of seals and packings.
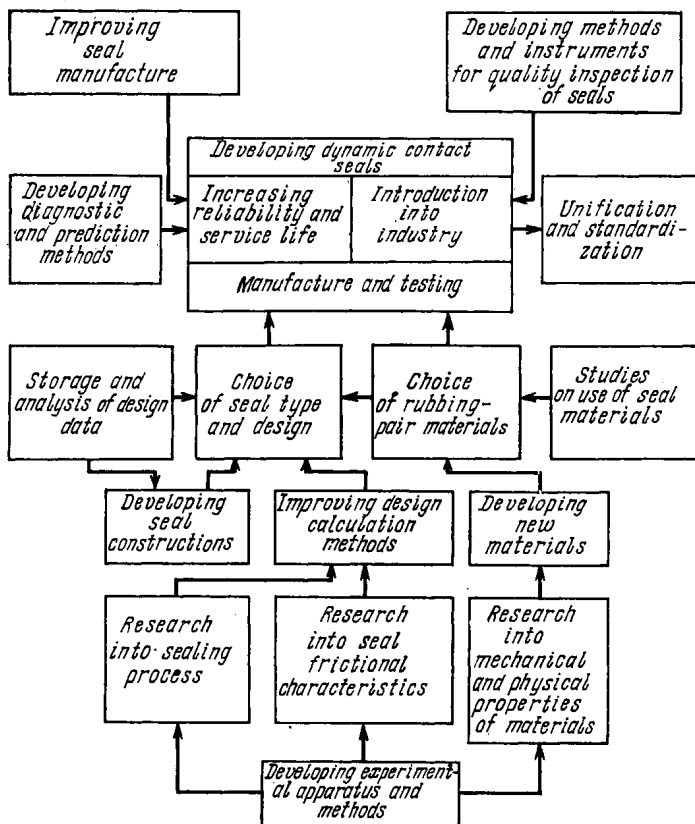
Fig. 24.10. Some sealing problems

Dynamic and static clearance seals. The advantages of these types of seals are a practically unlimited life and insignificant friction losses. Where the temperature of a seal needs to be maintained at a constant level, and the leakage of the fluid sealed or the ingress of dirt, moisture, or abrasive particles from the environment into the product must be fully excluded, use is made of clearance seals with a chemically neutral buffer fluid. The temperature, pressure, flow rate and properties of the fluid are chosen depending on the seal application. Used as the buffer fluid are water, steam, air, nitrogen, helium, and the like (see Figs. 24.5 and 24.9).

89

Among dynamic clearance seals that have found the most extensive use are the labyrinth, screw-pump (viscoseal), and centrifugal types. Their design calculation consists in the choice of dimensions for the specific number of shaft revolutions and specific properties of the liquid to be sealed so as to ensure the required pressure difference. The design recommendations are given in references [9, 19].

A relatively new design is an ejector seal [9].

Clearance seals using magnetically-active liquid find ever increasing application both in the USSR and other countries. The liquid is a colloidal suspension of solid particles of a magnetic material (for instance, magnetite) from 0.2×10^{-2} to 1.0×10^{-2} μm in size in conventional lubricating oils or other liquids (water, kerosene, or glycerine). The magnetic fluid is held in the clearance between the product's shaft and housing by the magnetic field set up by an annular magnet surrounding the shaft (see Fig. 24.6). This seal gives the benefits of a practically unlimited service life and excellent tightness at high pressure differentials (for example, 100 kgf/cm²) and shaft rotational speeds (say, 60 000 rpm). A magnetic-liquid seal can operate at temperatures from −60°C to +150°C and over, in a vacuum of 1×10^{-9} mm Hg, at large radial runouts and considerable surface roughness of the shaft [7, 27].

Static contact seals. Rubber annular gaskets of various cross-section profiles have been widely used over the past 20 years. Rubber "O" rings (see Fig. 24.7) can be applied successfully for packing at temperatures from −50 to +200°C at pressure differentials up to 1 000 kgf/cm²; to prevent extrusion of rubber into the clearance between the parts, it is good practice to install a stiff bearing washer together with the rubber ring. The choice of rubber for packing rings is dictated by the properties of the fluid to be sealed. A theory has been devised [11] to provide a basis for the design of seals with "O" rubber rings. Elastic metal rings of various cross-section forms (see Fig. 24.7) are very promising. Use is also made of still more complex, reinforced metal-asbestos or metal-polymer gaskets.

Machine units operating at variable temperatures (ranging, for instance, from −196 to +800°C) are tightened with elastic gaskets made from a metal whose coefficient of volume expansion is equal to that of the housing. Such a design [22] excludes the loss of tightness due to dissimilar thermal deformations of the mating parts.

Stationary joints are also tightened with sealants, such as anaerobic resins (substances whose polymerization only occurs in the absence of oxygen, say, in narrow gaps where the access of air is restricted).

Dynamic contact seals. These operate with external friction. In some types, for instance, in lip packings for rotary and reciprocatory shafts and rods, in face (axial) seals, or in piston rings, friction is continuous. In many other types, however, external friction

and the contact of surfaces occur intermittently or at separate surface portions, which, while offering reduced wear and frictional force, makes the provision of tightness more difficult. Related to such seal types are segmental rings (with an embracing garter spring), floating-bush seals, hydrostatic (or aerostatic) and hydrodynamic (or aerodynamic) face seals, lip-type hydrodynamic seals, and the like [10, 16, 21].

Continuous external friction over the whole contact area imposes more severe operating conditions. This primarily concerns seals in which the coefficient of mutual overlap $K_{ov} = 1$ (lip and face shaft seals). The value of $K_{ov} < 1$ provides beneficial conditions for the supply of lubricant to the friction area and ensures better cooling (lip packings or piston rings for reciprocating joints).

Air or hydraulic inflatable seals can be successfully used in many vital engineering applications. In these units, an elastic ring made of an antifriction material is installed in a circular recess in the stationary housing so as to embrace the shaft (or rod). The elastic ring is loaded radially by a gas or liquid supplied into the circular recess. Changing the pressure in the recess and the consumption of air or liquid allows the normal contact pressure and the operating temperature to be adjusted for the specified values (see Fig. 24.2).

Fig. 24.11. Combined sealing unit
1, 5—inlet and outlet of buffer fluid; *2*—face packing elements; *3*—garter spring; *4*—labyrinth grooves on shaft

Figure 24.11 shows a more complex combined seal design with a chamber in which the required pressure is built up; the shaft has circular grooves forming a labyrinth, and the packing elements are cups that take up radial and axial load from a garter spring. Since the gas or liquid is discharged through the shaft, this seal may be classed with a buffer-fluid type.

The efficiency of lip seals for shafts can be improved if two packing rings are installed in the unit (with their lips toward the chamber sealed). It should be noted that the wear of the second packing can be reduced and the seal life extended, if the packing rings are spaced apart at an optimum distance and a proper amount of lubricant is put into the cavity formed by the rings [17].

Face seals can be made more effective by reducing K_{ov} of the sliding pair (one of the rings is shaped as an ellipsis or given some other configuration). Other routs to increase efficiency include the use of hydrodynamic effect (the joint surface is provided with grooves of different configurations), hydro- and gas-static effect (a liquid or gas is directed to the contact area), better cooling, etc.

The sealing capacity is improved by installing several identical seals in tandem.

Data on packing materials can be found in references [6, 8, 10, 16, 21, 24].

24.1.3. Design of Dynamic Contact Seals for Improved Performance

The general seal development sequence is discussed in [17]. In a simplified form, it is like this: design calculation and development, manufacture and quality inspection, performance tests on special
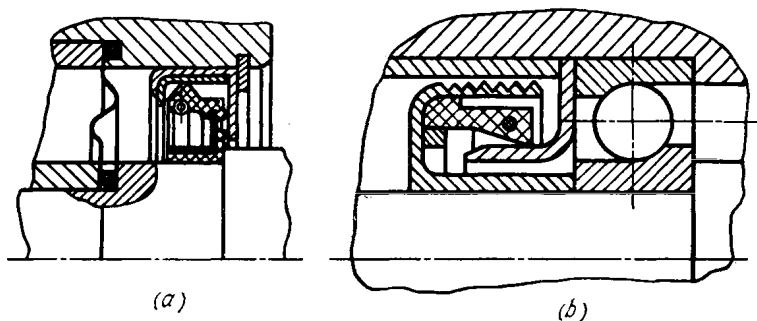
Fig. 24.12. Seal units with separate static and dynamic packing elements

(a) diaphragm (static element), centrifugal-action lip packing (dynamic element); (b) lip packing (static element), screw pump (dynamic element)

test beds (the experiments are planned on the basis of wear and friction modelling theory), and field tests.

When developing a seal, the product designer should consider the following factors:

—effective tightening can be achieved through better seal design as well as with improved antifriction sealing materials;

—the optimum operating conditions must be a goal in the development of the product using the seal; in some cases, re-design of the whole product to achieve this goal may prove essential;

—the requirement for a high degree of tightness actually means dry rubbing or boundary friction, with the result of a reduced seal life;

—tightness is often achieved in practice by employing seals of various types in combination.

The general guidelines for the development of dynamic contact seals are as follows [17].

(1) *Separation of functions*, that is, the use of a few seals together, each serving a different function. For instance, to seal a product at rest and in motion, packing devices of various types are applied in combination: static contact lip-type radial or axial seals, which are automatically disengaged as the shaft is set in motion, and clearance seals, such as a labyrinth, a viscoseal, or an impeller (Fig. 24.12).

(2) *Elimination of adverse factors.* It is essential to prevent or alleviate the adverse effect of the factors mentioned before (see p. 87). For example, methods are known for reducing the influence of such factors as sliding speed, high fluid pressures, shaft runout, the action of aggressive media, or the entry of dust and moisture from the atmosphere into the contact area (Fig. 24.13).

(3) *Minimizing the heat generated by friction.* There are a number of methods to reduce friction, wear and loss of tightness of the rubber
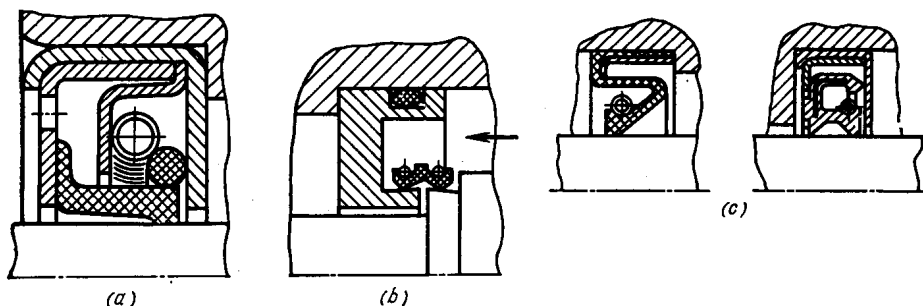
Fig. 24.13. Reducing the effect of high fluid pressure (*a*), speed (*b*), and shaft runout (*c*) on lip packing

lip packings for rotary shafts; among such methods are improving the antifriction properties of rubber and the lubricating conditions in the contact zone; producing shafts with optimum surface roughness and hardness by such manufacturing methods as vibro-rolling, roller-burnishing, or grinding for a specified surface lay; the use of antifriction coatings, i.e. silver plating, gilding; setting up predetermined vibrations in the sealing lip; etc.

(4) *Making use of the hydrodynamic effect,* that is, using devices with a lubricant film between the shaft and the sealing element in operation. Although it is essentially a particular case of the previous principle, it requires a special attention. For example, the contacting surfaces of shafts or packing elements are so shaped as to form a physical wedge in the contact region. To this end, the shaft can be provided with small projections or helical serrations, and the packing, with helical grooves, projections, or recesses (Fig. 24.14). The hydrodynamic effect can also be achieved by applying the normal load non-uniformly.

(5) *Improving the removal of heat from the contact area.* This measure is as important as keeping the heat generation to a minimum. Some proven ways toward this end in lip-type shaft seals are: increase in the heat-emitting area (e.g., the edge of the sealing lip) and the mass of components; the use of highly heat-conductive parts and coatings (a copper sleeve fitted over the shaft can be employed as the mate to the lip packing); more intense cooling of the contact re-

gion with the fluid being sealed or with another fluid (a positively directed fluid flow); the use of heat-removing tubes, etc. (Fig. 24.15).
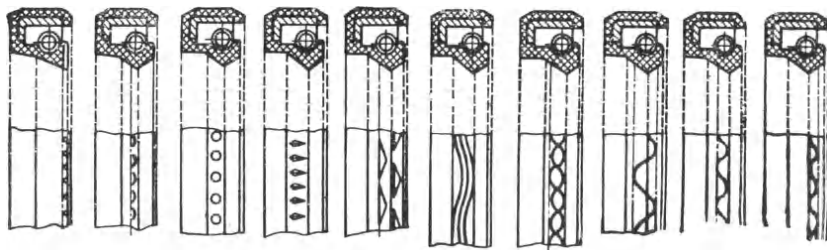
Fig. 24.14. Some rubber lip-seal designs for achieving hydrodynamic effect

Decreasing the heat generated in friction and intensifying its transfer from the contact region, so as to keep the seal operating
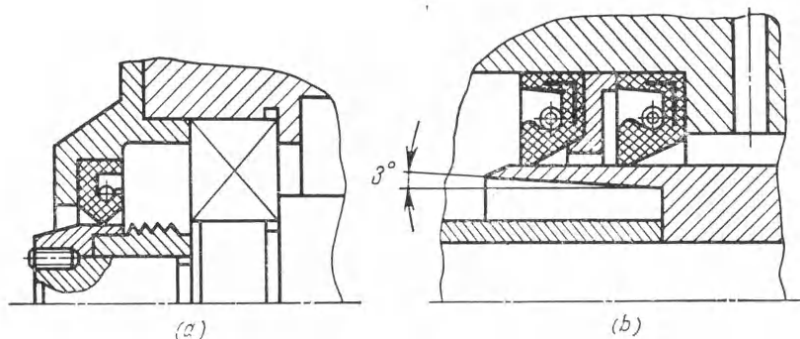
Fig. 24.15. Seal units with improved heat removal from lip-shaft contact zone
(a) use of sleeve from material of high thermal conductivity; (b) cooling shaft portion contacting the packing rings

temperature below the prescribed limit (the heat-distortion temperature for polymers), is one way to achieve better performance of contact seals. Another way is developing packing materials of higher thermal resistance (that is, a higher heat-distortion temperature for polymers, which is established in frictional heat-resistance tests).

24.1.4. Friction and Wear in Dynamic Contact Seals

A great diversity of contact-seal designs, materials, operating conditions, and factors that affect their performance have not yet allowed the general conclusions on friction and wear of these seals to be drawn. At the same time, the results of studies of particular cases may often lead the design engineer to an erroneous decision if the seal he develops is different in some way from that he has taken as a prototype.

Case studies of specific seal applications are very numerous [8, 10, 16]. We shall, therefore, summarize some results of experimental and theoretical research into lip- and face-type shaft seals only, that is, the types that have found the most extensive application in the various branches of engineering.

Lip-type seals ($K_{ov} = 1$). (1) It has been established experimentally that the apparent area of contact of the lip packing with the shaft depends on the time the preliminary static contact takes, the fluid pressure in the chamber being sealed, and the wear of the mating surfaces.

For most sealing rubbers the apparent and the real area of contact (A_a and A_r) are formed largely during the first 15 min after assembly.

With increasing pressure of the fluid being sealed, p_s, the apparent contact area A_a is found to grow linearly; this linear relationship holds with the growth in A_a due to wear.

The grease put into a seal in assembly is gradually forced out during static contact (in 5 to 10 days in general-engineering applications), and the magnitude of the starting moment M_f proves close to that in an unlubricated seal (the Denny effect).

(2) Diagrams which show a maximum have been obtained experimentally for the distribution of pressure p and the temperature across the width of the contact area.

The magnitude of the normal load depends on the packing design, the properties of the material, the pressure of the fluid sealed, p_s, and the spring pressure, and varies along the shaft perimeter (if the shaft is misaligned at rest) and in time (if the shaft has radial runout).

(3) Methods of design calculation of a rubber lip packing for strength, calculation of pressure p, of thermal conditions, and of some other parameters have been developed [17]. A pressure calculating method has been devised by modelling the lip packing with a 'beam' according to the Davletbaev-Sell scheme, or with a cylindrical or a conical shell.

(4) Data on frictional behaviour of lip packings at high sliding speeds (specifically, at $v \geqslant 30$ m/s, that is, a speed close to that of the propagation of sound in rubber) have been obtained.

(5) Experimental research has been conducted on friction, wear, variation of fluid film thickness between the lip packing and the shaft depending on shaft runout, the properties of the fluid, lubricating conditions, load, speed, temperature, design, the properties of packing material, and the shaft surface roughness.

In sealing against liquids, either boundary or nearly-fluid friction occurs, although the lubricating conditions across the contact area and along the shaft circumference are different and can vary with time.

According to the results obtained in the USSR and other countries in testing lip packings for various applications, the $p_s v$ factor

may be considered a constant for a certain temperature of the lip. The heat-distortion temperature ϑ for the packing material being known, it is possible to find the limiting value of $p_s v$. Experiments were conducted at $p_s \leqslant 8$ kgf/cm² and $v \leqslant 70$ m/s. It was found that for nitride rubbers which provide the material for not less than 80 percent of all lip packings, the heat-distortion temperature does not exceed 300°C, and the $p_s v$ value in short-time operation and at a 80 mm shaft diameter should not be over 250 kgf m/(cm² s). An excess of this value leads to overheating, severe wear (seizure and, in some cases, cracks) and considerable leakage ($i < 0$). The relationship between $p_s v$ and the leakage rate for different types of lip packing is still to be studied.

(6) Wear is often observed on the working surface of loaded lip seals ($p_s > 0.5$ kgf/cm²) at a high speed ($v > 30$ m/s), the shape of the worn portion in the lip cross-section well conforming to the shape of the p and ϑ diagrams.

Lip packings may be calculated for wear in the following sequence: break down the contact zone into separate sections and find the mean values of p and ϑ for each section, determine the rubber strength characteristics on the basis of the found values of p and ϑ, determine the surface roughness parameters for the shaft and the rubber, calculate the wear rate for each of the sections by the formulas given in Chapter III, calculate the amount of wear in terms of mass on each of the sections over the period of the seal service, plot a diagram of the wear across the contact area, and compare the found values with experimental results in order to refine the calculation.

The seal life does not lend itself to calculation by the wear diagram at the design stage because the distribution of load p, temperature ϑ, and the coefficient of friction are unknown during operation as well as changes in the surface roughness and width of the contact area.

Face seals ($K_{ov} = 1$). (1) Design calculation methods have been devised for the assessment of fluid pressure (with regard to out-of-squareness of the faces and to pressure in the clearance), behaviour of the fluid sealed in face clearances, hydrodynamic effect for the sealing rings of various designs (with annular or helical grooves, recesses in one of the rings, for an elliptical ring, for an eccentric ring, etc.), deformations of the rings due to pressure and temperature, and also temperature fields in the rings of the rubbing pair.

(2) Face seals with a small sealed-fluid chamber that are used for high-speed shafts require taking into consideration the amount of heat evolved owing to friction between the rotating components and the fluid, which, in such seal designs, may prove commensurable with the heat due to friction between the seal rings. Recommendations are available for calculating the fluid flow rate through the chamber to prevent overheating [17].

(3) Variation of the coefficient of friction, wear rate, and leakage rate with load and speed for different fluids and seal designs has

been studied experimentally. Relationship between the leakage rate and the main factors on which it depends has been obtained by dimensional analysis for a particular seal design. The frictional behaviour of seals has been investigated under various operating conditions.

(4) Antifriction materials suitable for face seal rings have been developed; among them are metal alloys, non-metal composite materials based on resins and polymers, graphite-base materials, etc. [17].

Contact seals with rubber-metal sliding pairs have found extensive application. The frictional properties of such combinations of materials are discussed below.

24.2. FRICTIONAL PROPERTIES OF RUBBER-METAL SLIDING PAIRS IN SEALS

24.2.1. Physico-Mechanical Properties of Sealing Rubbers

Depending on application, sealing rubbers should be strong, heat resistant, cold resistant, or resistant to chemical attack. These characteristics must often be combined; some of them are mutually incompatible. Anyhow, all sealing rubber applications require good friction properties: high wear resistance and a low coefficient of friction.

A large part of engineering seals must be oil- and fuel-resistant. These properties of sealing rubbers improve in the following order of base elastomers: polychloroprene, nitrile, polyacrylic rubber, and fluoroelastomers. With nitrile rubbers, the higher the content of nitrile groups in the molecular chain of the rubber, the higher the oil- and fuel resistance. Heat resistance is also an important requirement to be placed on sealing rubbers.

By heat resistance, sealing rubbers can be arranged in the following order: ϑ = 110 to 130°C for nitrile rubbers, ϑ = 130 to 150°C for polyacrylic rubbers, and ϑ = 200 to 250°C for fluoroelastomers and silicone rubbers, ϑ being the bulk-temperature performance limit.

At low temperatures about —70°C, most rubbers and their vulcanizates lose elasticity and become hard. The lower temperature limits at which rubbers still remain elastic are: for nitrile rubbers —40°C, for polyacrylic rubbers —30°C, for fluoroelastomers —30°C, and for silicone rubbers —70°C.

Mechanical properties of the most frequently used sealing rubbers are listed in Table 24.3.

Table 24.3

Physico-mechanical properties of rubbers

Grade of rubber	Tensile strength, kgf/cm²	Percent elongation		Hardness by TM-2
		per unit length, min	permanent, max	
СКН-26	115	150	15	75-85
СКН-18 + СКН-26	90	130	6	75-85
СКН-40	100	150	28	70-85
СКФ-26	130	80	10	75-85
СКФ-32	140	130	15	75-90

Note. Physico-mechanical properties of rubbers are given in more detail in handbook [24].

24.2.2. Influence of External Factors on Performance of Seals *

The temperature operating conditions for seals are determined by the temperature of the fluid being sealed and the amount of heat generated by friction.

In severe operating conditions, the friction temperature can exceed the fluid temperature by 80 to 100°C. The measurement of the
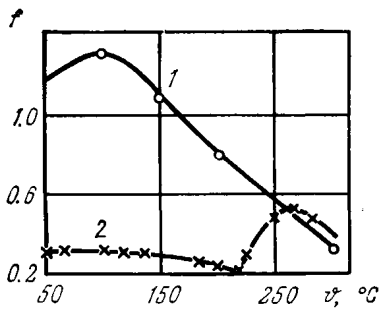
Fig. 24.16. Coefficient of friction of face-type rubber-metal sliding pair as a function of temperature (sliding conditions; $p = 2$ kgf/cm²; $v = 1.0$ m/s; rubber СКН-18 + СКН-26)
1—dry friction; 2—lubrication with grease ЦИАТИМ-221

temperature on the rubbing surfaces is difficult, and the seal's operating conditions and service life are often assessed in practice by the temperature near the contact area; however, being lower than the actual one, its value can lead to large errors.

The relationship between the coefficient of friction of rubber and the temperature both in unlubricated conditions and with grease lubrication is shown in Fig. 24.16. In dry rubbing (curve *1*), the maximum values of the coefficient of friction occur over a 50 to 150°C range, past which the coefficient becomes lower. The character of the relationship can be accounted for by change in the polymer

* Apart from those discussed in this paragraph, some other factors can have a marked effect on seal performance in particular cases. *Ed.*

tructure, attended by decrease in the coefficient of friction; this change is due to the effect of mechanical and chemical processes at temperature of 150°C and higher, activated by the repeated deformation of the surface layer. With the presence of grease in the contact area (curve 2), two characteristic regions can be distinguished. The first region exhibits a monotonous reduction in the coefficient of friction with temperature rising up to a certain critical value ϑ_{cr}. In the second region, the continuing growth in temperature brings about a stepwise increase in the coefficient of friction. The fall in the first region is caused by a decline in the resistance of the lubricant film to shear, and the sharp increase in the second region, by decomposition of the lubricant at high critical temperature and, hence, transition to dry friction.

Thermal-oxidative processes, which occur in the area of severe wear, lead in some cases to destruction of the polymer. Being a thermally activated process, this destruction sharply intensifies in a certain sufficiently narrow temperature range (critical temperatures). Above this range, which is 150 to 250°C, the character and the mechanism of wear change. Wear, largely induced by temperature, becomes catastrophic. All the other factors—sliding speed, pressure, and the coefficient of friction—affect wear mainly through temperature changes. This suggests that control of the temperature (for instance, its reduction by properly cooling the seal unit) is an effective way towards the lessening of wear at increased sliding speeds and pressures.

The critical temperatures limiting the lubricating action of greases in rubber-metal sliding pairs are given in Table 24.4. The material of the mating metal component is steel 45.

Table 24.4

Critical temperatures for rubber-metal sliding pairs

Base lubricant	Temperature, °C	
	nitrile rubbers	fluoroelasto-mers
Synthetic mineral oils	200-250	150-180
Polyethylene silicone liquid	200-250	200-250
Petroleum oils	150-200	200-250

Sliding speed. Increased sliding speed leads to growth in temperature in the contact zone. At high sliding speeds, it is advisable to use materials that have good heat and wear resistance.

The influence of sliding speed on the coefficient of friction is illustrated in Figs. 24.17 and 24.18. An increase in sliding speed in the region of high speeds has the effect of reducing the coefficient of friction for both dry and boundary friction processes. This character of the relationship for dry friction is linked

with the rheological processes occurring in the contact zone because the time during which separate surface areas are in contact shortens and, hence, the real pressure increases with higher sliding speeds.

The reduction in the coefficient of friction with sliding speed is also induced by the growth in temperature due to higher speed.
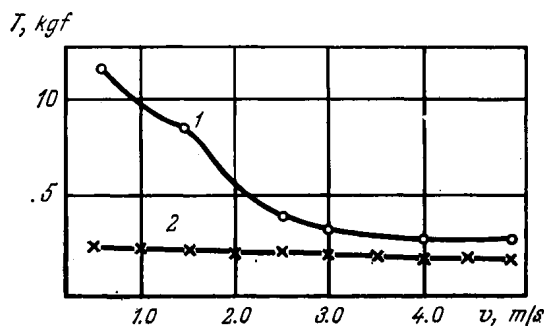
Fig. 24.17. Friction force in face-type rubber-metal sliding pair as a function of sliding speed (sliding conditions: $p = 2$ kgf/cm²; rubber СКН-18 + СКН-26) *1*—dry friction; *2*—lubrication with grease ЦИАТИМ-221

For boundary friction, the decrease in the coefficient of friction with higher sliding speeds is brought about by the corresponding temperature rise that affects the lubricant viscosity.
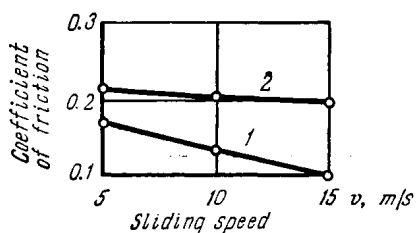
Fig. 24.18. Coefficient of friction of radial-type rubber-metal sliding pair *vs* sliding speed
1—rubber СКН-18 + СКН-26; test temperature 175°C; grease ЦИАТИМ-221; *2*—rubber СКФ-32; test temperature 200°; dry friction

The influence of sliding speed on wear is indirect, through changes in the elastic properties and strength of the rubber and changes in the coefficient of friction. Since temperature also grows with the sliding speed, the effect of the speed on wear can only be estimated either at a low speed (the heating of the surface can be ignored) or at a constant temperature. In the range of high sliding speeds, where the coefficient of friction lowers with rising speed, wear also decreases as the speed grows (at a constant friction temperature).

At first such a relation between wear and sliding speed may seem to contradict a widely held view that wear varies directly with

the power factor since increase in sliding speed normally leads to growth in temperature and wear.

However, if the temperature is maintained constant, increase in sliding speed causes the coefficient of friction to diminish.
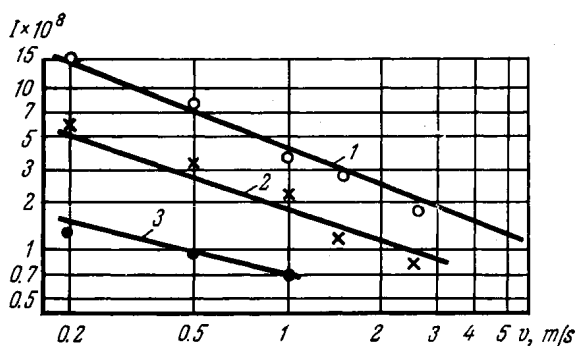
Fig. 24.19. Wear rate of face-type rubber-metal sliding pair *vs* sliding speed (sliding conditions: $p = 2\text{kgf/cm}^2$, $v = 1.0$ m/s; rubber СКН-18 + СКН-26 at temperatures *1*—200°C; *2*—150°C; *3*—100°C)

The experimental results presented in Figs. 24.19 and 24.20 indicate that increase in sliding speed under invariable temperature conditions results in reduced wear rate.

The pressure and the nature of the fluid being sealed. Growing pressure of the fluid being sealed increases the radial force, restricts
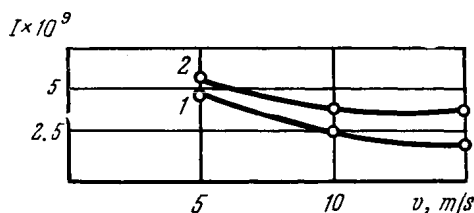
Fig. 24.20. Wear rate of radial-type rubber-metal sliding pair *vs* sliding speed *1*—rubber СКН-18 + СКН-26; temperature 175°C; grease ЦИАТИМ-221; *2*—rubber СКФ-32; temperature 200°C; dry friction

the supply of the lubricant to the contact region, enlarges the part of the contact area where dry rubbing takes place, and raises the friction force and contact temperature. These conditions result in weakened tightness and shorter seal life.

The physico-mechanical properties of the rubber can undergo substantial changes under the action of the fluid being sealed. The sulphur- and chlorine-containing substances in the additives, which are activated by heat cause a speeded ageing of the rubber. The degree of swelling of oil-resistant rubbers mainly depends on the content of aromatic components in the oil. An aggressive fluid can destroy the packing element partially or completely.

The radial force that presses the sealing lip against the shaft is an important parameter of a seal unit. An insufficient radial force leads to formation of a thicker lubricant film and makes for leakages. Excessive radial forces deteriorate the lubricating conditions for the rubbing surfaces, set up more severe temperature conditions in the contact region, and speed up the ageing and wear of the rubber.

Difference in radial forces is a major cause of unsteady operation of seals having similar specifications. The radial force related to a unit contact area (radial pressure) depends on the width of the contact zone, which is determined by many factors and varies during the service of a seal; for this reason, the parameter commonly used as a substitute is the radial force related to a unit length of the shaft circumference.

24.2.3. Effect of Surface Roughness on Performance of Seals

Because of substantial difference in the mechanical properties (hardness, elastic modulus) of the rubbing materials, the roughness of the metal surface has the major effect on the friction and wear of rubbers. As a rule, rubbers are readily deformable, which leads to closer approach of the contacting surfaces and growth in the real contact area. Owing to low thermal conductivity of rubbers, these factors lead to temperature rise in the contact zone during boundary friction and to increase in the coefficient of friction and wear rate.

Very smooth surfaces (0.04 to 0.16 μm *Ra*) are incapable of holding a low-viscous lubricant and bringing it to the contact region; the resulting phenomenon known as "film starvation" gives rise to a high shear resistance. Moreover, the increased real area of contact causes the molecular component of friction force to grow.

A rough shaft surface (2.50 to 1.25 μm *Ra*) holds the lubricant; however, the normal and tangential forces applied to the seal originate large deformations of the surface layer in the softer member of the sliding pair. The coefficient of friction rises because of increase in f_{mc}, and disruption of the lubricant film is possible. As a result, the shaft and the seal wear away more severely. A maximum lip-seal life is achieved with a shaft surface roughness of 0.16 to 0.63 μm *Ra*.

Apparently, to reduce the wear rate during the running-in and service periods, it is essential to specify an optimum, steady-state roughness for given operating conditions.

The following analytical method may be helpful for predicting the steady-state roughness. The coefficient of friction in elastic contact can be expressed through the roughness parameters of the mating part made of steel and through the mechanical properties of the sealing component [13]:

$$f = A\Delta^{-\nu/2\nu+1} + \beta + B\Delta^{\nu/2\nu+1} \qquad (24.1)$$

where

$$A = \frac{\tau_0 \, (k_1 \Theta)^{2v/2v+1}}{2 p_s^{1/2v+1}}, \quad B = 0.19 \alpha_h K_v \, (k_1 p_s \Theta)^{1/(2v+1)}$$

$$k_1 = 2 \sqrt{\pi} \, \frac{\Gamma(v+3/2)}{\Gamma(v+1)}; \quad K_v = \frac{8}{3 \sqrt{\pi}} \, \frac{\Gamma(v+3/2)}{\Gamma(v+1)}$$

A and B are constant factors for the specified load p_s, lubricating conditions τ_0, and mechanical properties of the materials α_h and Θ.

The steady-state roughness corresponds to a minimum of friction ($b = 2$; $v = 2$)

$$\Delta = 15 \left(\frac{\tau_0}{\alpha_h} \right)^{5/4} p_s^{-1/2} \Theta^{3/4} \tag{24.2}$$

and

$$f_{min} = 1.5 \sqrt{\tau_0 \alpha_h \Theta} + \beta \tag{24.3}$$

The frictional properties of some rubbers used in seals and the results of calculation of the steady-state roughness are given in Table 24.5.

Table 24.5

Frictional properties of rubbers on steel 45 (dry rubbing) [13]

Grade of rubber	E, kgf/cm²	f	τ_0, kgf/cm²	Steady-state roughness* Ra, μm	
				experimental data	calculated data
СКН-40	85	0.41	5.7	0.58	0.47
СКН-18 + СКН-26	100	0.5	8.0	0.42	0.55
СКЭП	90	0.31	8.4	0.68	0.69
СКН-26	150	0.36	6.7	0.30	0.43

* Parameter Ra is calculated by formula $Ra = 4.3 \, \Delta^{1/2}$.

24.2.4. Calculation for Wear

Fatigue wear predominates in the friction of rubbers against hard surfaces. This type of wear is caused primarily by a discrete character of frictional contact, whereby the rubber is repeatedly deformed at separate spots of real contact with the result of destruction and breakaway of the material's particles. The extent and frequency of the deformation depend on the surface properties and geometry as well as on temperature, sliding speed, and pressure.

The main peculiarity of friction of rubber seals against steel at higher sliding speeds is high contact temperatures, ranging from 100 to 250°C and over, that result from the repeated deformation of

rubber while in contact with the surface irregularities of its metal counterpart.

The theory of wear for polymers allows the amount of wear to be predicted analytically. The necessary data are the physico-mechanical properties of the rubber, the value of the coefficient of friction characteristic of the sliding pair, and the surface roughness of the metal counterbody.

The wear rate is calculated [18] by the formula

$$I = C \left(\frac{P_a \Theta}{K_v'} \right)^{1+\gamma t_y} \Delta^{\frac{t_y}{2}(1-\gamma)} \left(\frac{K_f^y}{\sigma_v \Theta} \right)^{t_y} \qquad (24.4)$$

where

$$C = \frac{v^{1/2} \Gamma(v) \Gamma(1+t_y/2)}{4(v+1) \Gamma(v+t_y/2)}, \qquad K_v' = \frac{K_v}{2\sqrt{\pi}},$$

$$\gamma = \frac{1}{2v+1}, \qquad K_f^y = \frac{4kf}{3\pi}$$

According to data by E. F. Nepomnyashchy, the coefficient K_f^y for rubbers is equal to 3. It should be noted that formula (24.4) is valid for $\frac{P_a}{E} \leqslant 0.02$ to 0.05.

Before using formula (24.4), it is necessary to determine f and σ_0 as functions of temperature since the sliding velocity leads to self-heating of the rubber frictional surface.
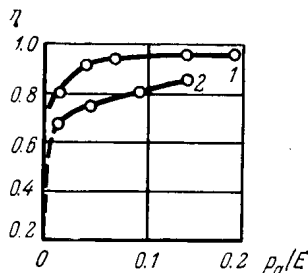
Fig. 24.21. Relationship between relative real area of contact and $\frac{p}{E}$ criterion for surface-roughness parameter
1—0.16 to 0.63 µm Ra; 2—1.25 to 2.5 µm Ra

As regards t, the parameter of the Wöhler curve [that is, $n = \left(\frac{\sigma_0}{\sigma_x} \right)^t$ where σ_x is the value of stress amplitude] which is found experimentally, its value is not significantly dependent on temperature and usually equals from 3 to 6.

The real area of contact is determined by comparing profile graphs of the contacting surfaces of metal and rubber, which are formed under load.

The relationship between the real contact area of rubber and the parameter p_a/E, which characterizes the loading of the seal for metal surfaces with different surface roughness, is presented in Fig. 24.21.

During contact of rubber with a metal surface having a roughness of 0.32 to 0.63 µm Ra and smaller, the relative area of contact for

p_a/E increasing from 0.05 to 0.2 becomes stabilized and little depends on load; it may be assumed constant and equal to 0.90-0.95.

Therefore, the rate of wear for rubber seals during dense contact, that is, at $p_a/E > 0.05$ may be calculated by the simplified formula

$$I = 0.03 \left(\frac{3fp_a}{\sigma_0 0.9} \right)^{t_y}$$

The calculated and experimental wear rates for two rubber seals operating in various rubbing conditions are given in Table 24.6.

Table 24.6

Experimental and calculated data on wear of rubber seals

Grade of rubber	Rubbing conditions				Wear rate	
	v, m/s	p, kgf/cm²	ϑ, °C	f	experimental	calculated
СКН-18+СКН-26	5	1	100	0.17	7×10^{-10}	5×10^{-10}
		3	200	0.2	2×10^{-10}	1.1×10^{-10}
СКФ-32		1	150	0.33	2×10^{-9}	9×10^{-10}

According to the principle of independent action of forces, the force Q_{rad} that presses the sealing lip against the shaft consists of three components:

$$Q_{rad} = Q_{el} + Q_{spr} + Q_{fl}$$

The component Q_{el} arises in the contact because of an interference fit between the shaft and the lip seal, Q_{spr} is the force exerted by the garter spring, and Q_{fl} is the force induced by the fluid being sealed. These forces are determined on the assumption that the deformation of rubber in a lip seal agrees with the linear theory of elasticity and the rubber is isotropic and incompressible [4, 14].

To find Q_{el}, the sealing lip is divided into two parts, namely, a ring and a root (Fig. 24.22). Thus, Q_{el} is made up of two components: Q_r, which is the force exerted by the ring expanding as it is fitted over the shaft, and Q_{df}, the force that arises from deflection of the root.

Fig. 24.22. Design calculation diagram for lip seal
1—ring; *2*—root

The component Q_r is determined by the formula

$$Q_r = \frac{\pi \delta l E}{\dfrac{1 + (r/R)^2}{1 - (r/R)^2} + \mu}$$

where δ is the amount of the diametrical interference between the seal and the shaft, l is the thickness of the ring, E is the static modulus of elasticity for the rubber, μ is Poisson's ratio equal to 0.5 for

rubber, R is the outer radius of the ring, and r is the inner radius of the ring.

The component Q_{df} is found by regarding the sealing lip as a variable-section cantilever (Fig. 24.23) loaded by a concentrated
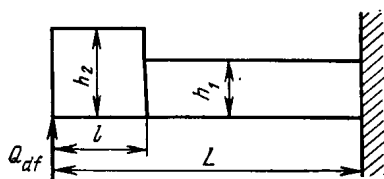
Fig. 24.23. Diagram for calculation of root deflection force

force and having two portions with the heights h_1 and h_2 and the respective moments of inertia J_1 and J_2.

According to elasticity theory, the equation for calculating the second component, Q_{df}, of Q_{el} has the form

$$Q_{df} = \frac{\delta}{2\left[\dfrac{L^3}{3EJ_1} - \dfrac{l^3}{3E}\left(\dfrac{1}{J_1} - \dfrac{1}{J_2}\right) + \dfrac{h_1^2}{8GJ_1}(L-l) + \dfrac{h_2^2 l}{8GJ_2}\right]}$$

where G is the shear modulus of rubber $[\sim 1/3E]$.

For determining Q_{spr}, the sealing lip is assumed to be a cantilever beam that bears on the shaft by its free end and is loaded with
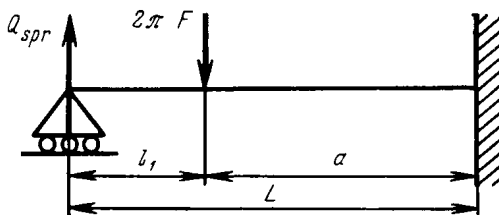
Fig. 24.24. Diagram for calculation of garter-spring force

a concentrated force Q_{spr} (Fig. 24.24). The radial force due to extension of the spring

$$Q_{spr} = \frac{2\pi F a^3}{L^3}\left(1 + \frac{3l_1}{2a}\right)$$

where F is the axial spring force at the specified deformation.

The force exerted by the fluid being sealed is found by the formula

$$Q_{fl} = 0.625\pi pRL$$

where p is fluid pressure.

The variation of radial force with the amount of interference is shown in Fig. 24.25.

If the seal is mounted on the shaft with some eccentricity, then the radial force per unit length of circumference of the shaft will be given by

$$p_r = KE \left(\delta_0 + \beta \sin \varphi \right) + p_{spr} + p_{fl}$$

where δ_0 is the amount of radial interference, β is eccentricity, φ is the angular coordinate of the given point of the lip, which depends
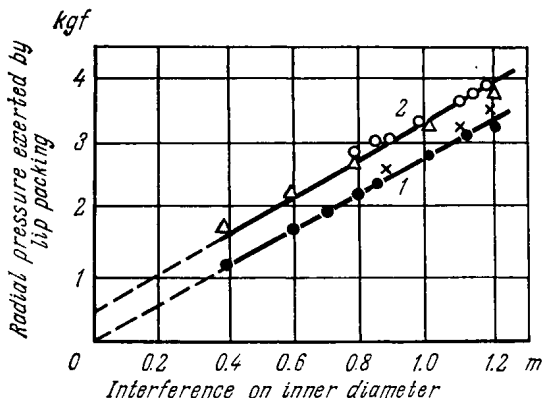
Fig. 24.25. Radial force *vs* amount of interference for lip seals ($\triangle$,●—design data; $\bigcirc$, ×—experimental data)
1—without spring; *2*—with spring

on the chosen origin, p_{spr} is the garter-spring force per unit length, $p_{spr} = Q_{spr}/2\pi r$, and p_{fl} is the fluid force per unit length, $p_{fl} = Q_{fl}/2\pi r$.

With the presence of radial runout (dynamic eccentricity), the radial force per unit length will be

$$p_{r.dyn} = p_r + KE_{dyn}\beta_{dyn} \sin \left(\alpha_0 + \omega t \right)$$

where α_0 is the angle of shaft revolution in the chosen coordinate system at $t = 0$.

24.2.5. Methods for Improving Wear Resistance

The basic conditions for increasing the wear resistance of contracting materials are that the gradient of mechanical properties must be positive and the penetration of a solid into the mating surface must be a minimum. A positive gradient of mechanical properties in rubber products is achieved by manufacture in press moulds having the appropriate surface roughness. The hardness and smoothness

of the metal surface in a sliding pair makes for a minimum penetration of the mating parts into each other. With regard to sealing rubbers the requirements to be met for better wear resistance are:

—the rubber must have a low coefficient of friction;

—the temperature of the friction surface in the contact region must not exceed the limit beyond which the rubber is destroyed; and

—in the process of friction over a wide temperature range, a thin, weak-structure layer must continually re-form on the rubber's surface.

Since the coefficient of friction not only affects the wear process by itself, but also determines the temperature conditions for tribological units, its reduction provides an effective way to improve the wear resistance of rubber-metal sliding pairs. This reduction can be achieved by two methods:

(1) surface treatment of rubber, for instance, halogenation (specifically fluorination, chlorination, or bromination); and

(2) introduction of antifriction additives into a rubber composition.

The frictional properties of sealing rubbers subjected to halogenation are given in Table 24.7.

Table 24.7

Frictional characteristics of rubbers.
Rubbing conditions: $p = 2$ kgf/cm², $v = 1.5$ m/s

Grade of rubber	Surface treatment	Frictional characteristics		
		$I \times 10^8$	f	ϑ, °C
CKH-18	Fluorination No treatment	0.2 to 0.4 3.5	0.35 1.25	70 220
CKH-40	Fluorination Chlorination Bromination No treatment	0.35 0.4 1.18 3.8	0.36 0.42 0.84 1.2	91 104 138 210

From the table it follows that fluorination, chlorination, and bromination, apart from improving other properties of rubber, substantially reduce the coefficient of friction and increase the wear and temperature resistance.

The halogenation of seal surfaces not only improves their frictional characteristics, but also stabilizes the radial force to some extent, and thus makes seals more dependable.

The magnitudes of radial force for seals produced from CKH-40 halogenated rubber are indicated in Table 24.8.

The chemically-modified rubber seals are particularly effective at the initial stage of operation, and this is very important for their

Table 24.8

Radial force of seals made from rubber СКН-40

Surface treatment	Radial force, gf		Surface treatment	Radial force, gf	
	start of test	end of test		start of test	end of test
No treatment	2 610	1 945	Chlorination	3 210	2 960
Fluorination	2 990	2 730	Bromination	3 460	2 830

further service. The variation of frictional force in the process of testing seals made from reinforced СКН-40 nitrile rubber with the chemically-modified surface is shown in Fig. 24.26.

A method for chemical treatment of seal surfaces should be chosen with regard to processing factors as well as to the result it produces. These factors may include the complexity of equipment, the difficulty of neutralizing solutions, the availability and costs of starting materials, toxicity, etc.

Along with the chemical modification of the friction surfaces of rubbers, introducing antifriction additives is also an effective way to increase wear resistance. The most advantageous additives for this purpose are carbon cloth, graphite, fluoroplastic, molybdenum disulphide, etc.

Some rubbers containing fluorine, ethylene, and propylene change their structure at high temperatures and wear away from galling.

This undesirable phenomenon can be prevented by using some antifriction additives, such as silicon nitride or carbon cloth, which improve the frictional heat resistance of sealing rubbers.

Fig. 24.26. Variation of frictional force in testing seals from reinforced modified-surface rubber СКН-40 in dry-friction conditions

1—unmodified rubber; *2*—fluorinated rubber; *3*—chlorinated rubber; *4*—brominated rubber

The frictional characteristics of СКФ-32 rubber containing graphite in combination with low-molecular-weight polytetrafluorethylene are listed in Table 24.9.

A combination of graphite and polytetrafluorethylene results in that the pressure, particularly a high one, has no marked effect on wear resistance. The use of elastoplastics as wear-resistant seal-

Table 24.9

Frictional properties of rubber СКФ-32 filled with graphite and fluoroplastic.
Sliding speed $v = 1.5$ m/s

Pressure p_a, kgf/cm²	Frictional characteristics			Pressure p_a, kgf/cm²	Frictional characteristics		
	$I \times 10^8$	f	ϑ, °C		$I \times 10^8$	f	ϑ, °C
2	9	1.1	205	13	2.25	0.23	242
4.5	11	0.53	235	17	2.5	0.17	245
9	6	0.3	240	21	2.4	0.14	260

ing materials carries much promise for the development of new materials for sealing applications.

Seals with various types of serrations or knurling on the frictional packing surfaces are extensively used since they produce the hydrodynamic effect and thereby have a longer life.

REFERENCES

1. Белова И. С., Гридунова Е. Б., Литвинова Т. В. Применение твердых смазок в рецептуре резины из фторкаучука для повышения ее износостойкости.—«Каучук и резина», 1973, № 12, с. 24-25.
2. Бартенев Г. М., Лаврентьев В. В. Трение и износ полимеров. М., «Химия», 1972, 240 с.
3. Бартенев Г. М., Цыбук Б. С., Гридунова Е. Б. Исследование смазочного действия консистентных смазок при скольжении резины по металлу в области высоких температур.—«Механика полимеров», 1968, № 5, с. 876-880.
4. Бартенев Г. М., Цыбук Б. С., Коморницкий-Кузнецов В. К. К вопросу расчета радиальных усилий резиноармированных манжетных уплотнений.—«Каучук и резина», 1966, № 10, с. 25-28.
5. Васильцов Э. А. Бесконтактные уплотнения. Л., «Машиностроение», 1974, 160 с.
6. Ганз С. Н., Пархоменко В. Д. Антифрикционные химически стойкие материалы в машиностроении. М., «Машиностроение», 1965, 148 с.
7. Герметичный ввод вращательного движения с магнитожидкостным уплотнением.—«Приборы и техника эксперимента», 1975, № 3, с. 191-192. Авт.: А. З. Аврамчук, А. К. Калинкин, Ю. О. Михалев и др.
8. Голубев Г. А., Кукин Г. М. Уплотнения вращающихся валов. М., «Наука», 1966, 96 с.
9. Голубев А. И. Современные уплотнения вращающихся валов. М., Машгиз, 1963, 216 с.
10. Голубев А. И. Торцовые уплотнения вращающихся валов. М., «Машиностроение», 1974, 214 с.
11. Добрушкин Д. Б. Проектирование эластичных торовых уплотнений.—«Вестник машиностроения», 1970, № 12, с. 38-41.
12. Евстратов В. Ф. Фрикционный износ резин. М.-Л., «Химия», 1964, 272 с.
13. Комбалов В. С. Влияние шероховатости твердых тел на трение и износ. М., «Наука», 1974, 112 с.
14. Коморницкий-Кузнецов В. К., Лепетов В. А., Цыбук Б. С. Исследование изменений радиального усилия уплотнений валов в динамическом режиме.—«Каучук и резина», 1974, № 6, с. 31-33.

15. Коморницкий-Кузнецов В. К., Рыбалов С. Л., Юровский В. С. Фрикционные свойства резиноармированных манжет, уплотняющих вращающиеся валы.—«Каучук и резины», 1971, № 11, с. 36-38.
16. Кондаков Л. А. Уплотнения гидравлических систем. М., «Машиностроение», 1972, 240 с.
17. Контактные уплотнения вращающихся валов. М., «Машиностроение», 1976, 264 с. Авт.: Г. А. Голубев, Г. М. Кукин, Г. Е. Лазарев, А. В. Чичинадзе.
18. Крагельский И. В., Добычин М. Н., Комбалов В. С. Основы расчетов на трение и износ. М., «Машиностроение», 1977, 526 с.
19. Краев М. В., Овсянников Б. В., Шапиро А. С. Гидродинамические радиальные уплотнения высокооборотных валов. М., «Машиностроение», 1976, 104 с.
20. Нудельман З. Н., Алябина Е. А., Прокудин И. П. Об увеличении износостойкости резиновых деталей путем фторирования их поверхности. «Каучук и резина», 1969, № 3, с. 21-23.
21. Макаров Г. В. Уплотнительные устройства. Л., «Машиностроение», 1973. Изд. 2-е доп. и перераб. 232 с.
22. Пономарев А. С. Новые уплотнительные устройства неподвижных соединений и трубопроводов. «Вестник машиностроения», 1971, № 7, с. 27.
23. Рыбалов С. Л., Крагельский И. В. О механике износа уплотнительных резин.— В сб.: Резина — конструкционный материал современного машиностроения. М., «Химия», 1976, с. 286-295.
24. Справочник резинщика. М.-Л., «Химия», 1971, 608 с.
25. Черский И. Н. Полимерные материалы в современной уплотнительной технике. Якутск, Якутское книжное изд-во, 1975.
26. Юровский В. С., Рыбалов С. Л. Коморницкий-Кузнецов В. К. Фрикционные характеристики резиновых уплотнений с галоидированной поверхностью. «Каучук и резина», 1974, № 4, с. 37-39.
27. Moskowitz R. Dynamic sealing with magnetic fluids. "ASLE Trans", 1975, vol. 18, N 2, p. 135-142.

FRICTION DEVICES

25.1. CLASSIFICATION

Dynamic friction devices include brakes, stops, clutches, and friction (e.g. centrifugal) governors. These devices are intended to change, say, to reduce, the speed of a solid (or a machine drive) by converting the kinetic energy into heat through the friction forces and to dissipate this heat.

Dynamic friction devices are used for accelerating (clutches) and stopping (brakes of all kinds) vehicles, and for transmitting motion
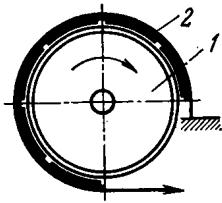
Fig. 25.1. Band brake
1—drum (rotates); 2—band with linings
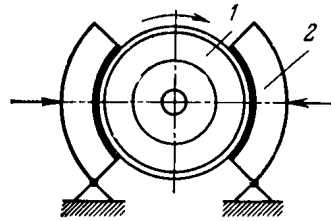
Fig. 25.2. Shoe brake
1—drum (rotates); 2—shoes

and changing its direction (friction clutches and governors) in industrial equipment.

Friction devices are distinguished by the features described below.

The kind of contact. Friction contact can be effected between flat rubbing surfaces, with $K_{ov} = 1$ (disc brakes and clutches) and $K_{ov} < 1$ (disc brakes, clutches, track brakes, friction governors); and between cylindrical and conical internal ($K_{ov} \leqslant 1$) and external ($K_{ov} < 1$) surfaces (shoe and band brakes, clutches, and friction governors).

As regards construction, brakes come in the following varieties: band brakes (Fig. 25.1), shoe brakes (Fig. 25.2), chamber-type brakes (Fig. 25.3), single-disc and multiple-disc brakes (Figs. 25.4 and 25.5), and track brakes (Fig. 25.7). Clutches and governors include disc and shoe types, and also magnetic-particle clutches (Fig. 25.6).
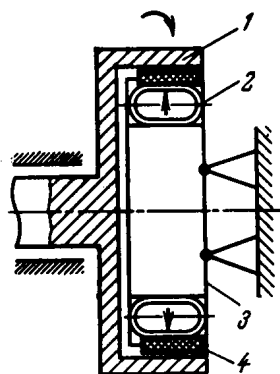
Fig. 25.3. Chamber brake
1—drum (rotates); *2*—inflating chamber;
3—body; *4*—lining
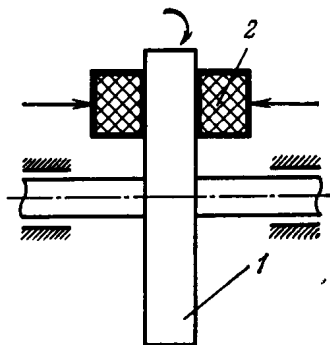
Fig. 25.4. Single-disc brake
1—disc (rotates); *2*—blocks
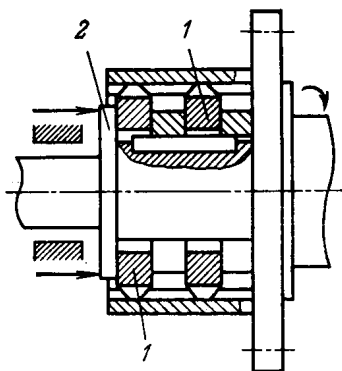
Fig. 25.5. Multiple-disc brake
1—discs (rotate); *2*—shaft connected with
stationary discs
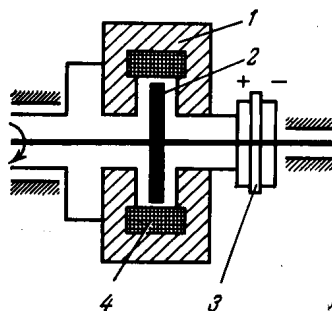
Fig. 25.6. Magnetic-particles clutch
1—body; *2*—rotor; *3*—current collector;
4—winding
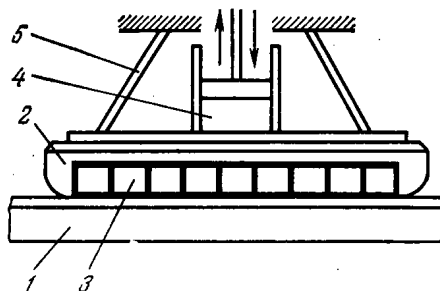
Fig. 25.7. Track brake
1—rail; *2*—casing; *3*—block; *4*—actuating cylinder: *5*—suspension

8—01462

Each of these devices, except the track brake, consists of the driving and the driven member. In brakes, as distinct from clutches, the driven member is always stationary. In band and shoe brakes, contact is effected by pressing the friction element, a lining fixed on a flexible band or a rigid shoe, to the rotating drum or shaft. Here, the friction element contacts the part being braked on a single surface, external or internal. In disc-type devices, friction is effected on both sides of the friction element, and that requires less construction space and increases the capacity of the unit. In multiple-disc constructions, working either in an oil bath or without oil, the moment of friction is the sum of the moments developed by each pair of the discs (rotating and stationary). This is the most compact design.

Contact rigidity of the friction device depends on the surface roughness and waviness of its components, the compliance of the
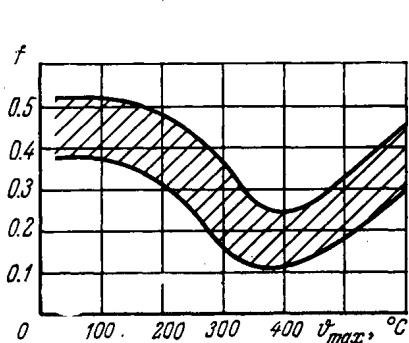
Fig. 25.8. Frictional thermal stability curve for asbestos-rubber compositions
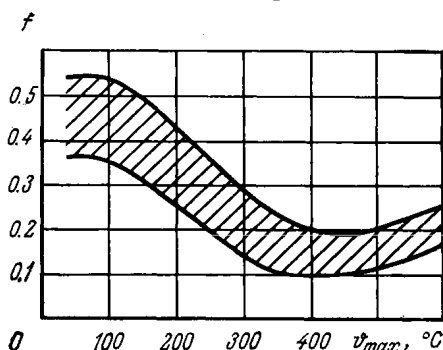
Fig. 25.9. Frictional thermal stability curve for asbestos-bakelite compositions

materials in the direction of force application, and the compliance of the structure carrying the friction material. Compliance is provided by introducing an elastic underlayer (such as porous rubber), by increasing the number of independent-action elements, by arranging slots in structural parts, etc.

The higher and most stable values of the friction coefficient, irrespective of the kind of contact, are observed with a high compliance of the friction element in a normal and tangential directions. Such a compliance ensures the most uniform distribution of actual loads on the contact, and thereby reduces its temperature, the temperature gradient and the thermal stresses. Normally, relationship between the friction coefficient and the temperature is described by a drooping characteristic (Figs. 25.8 to 25.11), and a decrease in the contact temperature brings about an increase in the friction coefficient.

It must be noted that high-compliance friction elements make it possible to reduce the inertia t_{in} of the friction device (that is, the time in which the friction moment M_{fr} mounts upon application of the load or drops to zero upon its removal). This is of special impor-

tance to clutches that work in a dynamic regime. With operation in oil, t_{in} can be cut by making grooves on the rubbing surfaces. The shortest t_{in} is obtained in devices with circular grooves on the rubbing surfaces or with a large number of friction elements, and the longest, in those with grooveless rubbing surfaces. The grooves promote the removal of heat and wear debris.

Access by film-forming media to the friction contact. With the friction elements closed on the counterface of a pulley or disc,
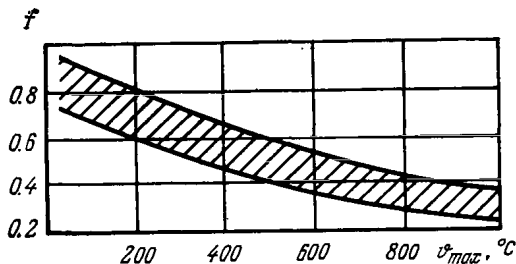
Fig. 25.10. Frictional thermal stability curve for sintered metal-ceramic compositions

some area of the latter remains exposed to the ambient medium, which contains gas, dust and moisture. This gives rise to chemical reactions and adsorption processes on the rubbing surfaces. A high temperature caused by friction and high contact pressures intensify these phenomena. Thus, exposure to hydrogen-containing media
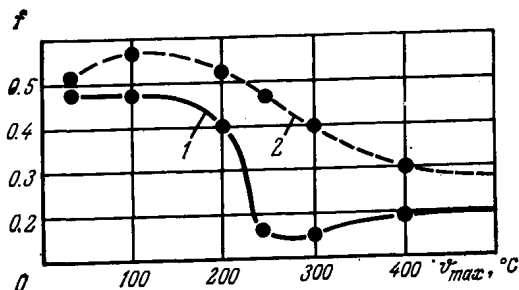
Fig. 25.11. Frictional thermal stability curves for untreated (1) and heat treated (2) asbestos-resin materials

brings about an intensive saturation of steel with hydrogen, a change in its properties, embrittlement, and, finally, wear.

Nitrogen and carbon dioxide produce a favourable effect on the frictional properties and wear resistance of asbestos-rubber compositions in rubbing on steel. The use of ammonia is advisable for sintered metal ceramic-on-cast iron sliding pairs.

Excessively wide friction elements in high-speed friction devices prevent the active media from getting into the contact zone. After the existing surface film has worn off, seizure or severe wear is likely to occur.

The duration of sliding. The operating conditions for a friction device are assessed from two parameters which are important for selection of friction couples. These are the duration of sliding and the heat exchange factor (Table 25.1). The latter can be overlooked

Classification by sliding time

Character of sliding	Sliding time, t_{fr}, s	Heat exchange factor
Short-time sliding	$t_{fr} < 60$	Negligible
Prolonged sliding Sliding in quasi-steady conditions Sliding in steady-state conditions	$60 < t_{fr} < 300$ $300 < t_{fr} < 1\,000$ $t_{fr} > 1\,000$	Significant

for normal conditions, in which the coefficient of heat transfer is $\sigma'_{cool} = 20$ to 60 kcal/(m² h °C), up to Fourier numbers of Fo $\leqslant 10$.

Working conditions. Normal operation of friction devices is considerably affected by external energy fields (Table 25.2) and other

Effect of external fields

Energy field	Action	Change in frictional characteristics due to extreme energy changes	
		f	I
Thermal	Heating or cooling the ambient medium	Variation by a factor of 2-3	Variation by a factor of 5-10
Electrical	Passage of electric current through friction couple	Variation by a factor of up to 5	Increase by a factor of 5-10
Electromagnetic	Friction in strong magnetic field	Increase by 40-50%	Increase by 40-50%
Chemical	Exothermic and endothermal reaction within friction-element bulk	Variation by 15-20%	Decrease by a factor of 2-3
Nuclear	Preliminary treatment of rubbing surfaces by radiation	Decrease by a factor of several hundreds	

factors, which should be in agreement with working properties of friction materials (Table 25.3).

Cooling method. Use is made of air, liquid, emulsion, or chemical cooling. Air cooling is effected either through natural convection or by blasting the friction unit with an air stream from a fan or compressor, in which case the air must be cleaned of impurities (oil, etc.).

Table 25.3

Recommended application for friction couples used in friction devices

Operating conditions	Materials	p_a, kgf/cm², not over	Temperature range of application, °C		Approximate value of friction coefficient (for calculations)
			ϑ_A^*	ϑ_V	
Light, no lubrication	Asbestos-rubber compositions, sintered copper-base and aluminium-base alloys, natural polymers (leather, processed wood) on steel	8 (10)	60-200	⩽ 120	0.3-0.35
Medium, no lubrication	Asbestos compositions with complex binder, sintered copper-base and iron-base alloys on steel or cast iron	15	⩽ 400 (450)	⩽ 250	0.25-0.28
Heavy, no lubrication	Sintered iron-base alloys, composite materials, carbon materials, and asbestos-resin materials on steel or cast iron	60	⩽ 1 200	⩽ 600 (800)	0.22-0.25
Light, with lubrication	Sintered copper-base and aluminium-base alloys, asbestos-resin compositions on steel, cast iron, bronze, molybdenum	35	⩽ 100 (120)	⩽ 100	⩽ 0.12
Heavy, with lubrication	Sintered iron-base materials on steel, titanium alloys, and molybdenum	60-70	⩽ 120 (150)	⩽ 100	⩽ 0.1
Special heavy-duty applications	Steels, titanium alloys, and sintered alloys on steel	1 500	−60 to +50	−40 to +40	0.22-0.25

Note. Given in parentheses are rubbing surface temperatures ϑ_A^* and bulk temperatures ϑ_V permissible for short-time operation.

However, water has four times the specific heat of air, and therefore friction devices with liquid (usually water) heat exchangers have found extensive use. These are arranged as metallic friction elements with a large number of channels.

The rubbing-surface temperature is effectively reduced by an air-liquid emulsion delivered there through a nozzle. The proper choice of the ratio of mixture components and control of the flow by the actuation time make it possible to avoid the formation of a fluid film reducing the coefficient of friction. The artificial cooling helps to lower the temperature in the friction zone, in some cases by 40 to 50 percent, to reduce the mass of the brake and to prolong its service life.

The friction elements can also be filled with chemically active agents which develop reversible reactions on heating caused by braking and later on natural cooling.

Stability to vibration. This is provided by the use of materials with a high damping capacity and by a structural stiffness that excludes vibroresonant phenomena in the working frequency region.

25.2. REQUIREMENTS PLACED ON FRICTION MATERIALS

Typical specifications of friction materials include the parameters given in Table 25.4.

Table 25.4

Friction couple specifications

Parameter	Designation	Dimension
Speed at the beginning and the end of engagement on application	v_{in}, v_{fin}	m/s
Load	N, P	kgf
Predicted specific load	p_a	kgf/cm^2
Mean coefficient of friction	f_m	—
Stability of friction force (friction coefficient)	α_{st}	—
Duration of sliding	t_{fr}	s
Bulk temperature of friction elements	ϑ_V	°C
Mean temperature of rubbing surface	ϑ_A^*	°C
Number of applications per hour	n	—
Moment of inertia of rotary driving and driven parts	J_m	kgf m s^2
Thermal diffusivity coefficient	a	m^2/s
Mean friction power and its variation	$N_{fr\,m}$, τ_N	kgf m/s
Mean friction work and its variation	$W_{fr\,m}$, τ_W	kgf m
Wear rate	I, $I_{permissible}$	—

Apart from these, specified are the kind of contact, the mutual overlap coefficient, contact stiffness, method of cooling, lubrica-

tion requirements, flame resistance, moisture resistance, and the quality attributes according to GOST 18090 — 72.

In addition, provision is made for rapid running-in of the rubbing components (for instance, the initial braking torque should amount to 80 percent of the rated value); the probability of failure-free operation is evaluated; design measures are taken to assure safety against fire, resistance to seizure in hot and cool conditions, high stability in oil, the absence of screeching, and the freedom from pick-up and smearing of the material.

It should be borne in mind that most of these requirements are met by friction materials where changes in the chemical and phase composition and structure run steadily and uniformly, and, consequently, the properties of the surface layers remain stable during service.

The effect of the work of friction on friction materials, according to F.K. Germanchuk, is shown diagrammatically in Fig. 25.12; it can be applied practically to any combination of such materials.

The requirements for friction materials (see Table 25.4) are worked out from the following considerations.

The initial speed of sliding in modern friction devices varies in a wide range from several cm/s to 50 m/s and, rarely, over. The sliding speed at disengagement also varies considerably. It drops by several percent as against the initial speed in clutches, and to zero in most brakes. The sliding speed has a substantial effect on power, friction work, and temperature. The latter, in turn, together with load, determines the frictional and wearing characteristics.

The load on friction devices also varies over a wide range, from dozens of tons to dozens of grammes. Where loads are heavy, more compact multiple-disc designs are recommended for use. The anticipated specific load is calculated for given overall dimensions of the device. Its magnitude for medium operating conditions should not exceed the values given in Table 25.3. This parameter, however, should be updated after the mean bulk temperature and the mean surface temperature have been estimated (their recommended limits are given in Table 25.3).

The coefficient of friction should be sufficient to provide the required friction force under working loads acting on the friction device. For friction materials rubbing against metal, the friction coefficient ranges from 0.2 to 0.5. The friction material should have a stable value of the friction coefficient during engagement.

The coefficient of friction f depends on the acting load, temperature, design arrangement, surface finish, and type of material.

The longest wear life of the friction couple is observed under operating conditions within the region of elastic or plastic-elastic contact. To provide for such conditions, the designer has either to develop a design with extended rubbing surfaces and relatively small permissible loads or to resort to friction materials (often the latest pilot brands) which exhibit high wear resistance. Roughly, the

119

```
                                    ┌─────────────────────────────┐
                                 ┌─▶│   Surface texture changes   │
                                 │  └─────────────────────────────┘
                                 │  ┌─────────────────────────────┐
                                 ├─▶│  Current phase and structural│
                                 │  │           changes            │
                                 │  └─────────────────────────────┘
        ┌──────────────┐         │  ┌─────────────────────────────┐
        │Processes running│      ├─▶│Diffusion and chemical processes│
        │  in surface   │────────┤  └─────────────────────────────┘
        │layers during  │        │  ┌─────────────────────────────┐
        │   braking     │        ├─▶│Expansion and compressive stress│
        └──────────────┘         │  └─────────────────────────────┘
```

Surface texture changes

Current phase and structural changes

Diffusion and chemical processes

Expansion and compressive stress

Softening of materials and deterioration of mechanical properties

Seizure

Changes in friction coefficient

Work of friction W_{fr}

Shape changes in surface layer

Rise in temperature of friction couple

Processes running in surface layers during braking

Residual phenomena in surface layers

Changes in surface texture

Permanent phase and structural changes

Chemical composition changes

Plastic contraction and tensile stresses in surface layer

Changes in mechanical properties (hardening and softening)

Non-uniform wear of rubbing surface

Warpage, shrinkage and cracking of friction elements

Fig. 25.12. Diagram of action of frictional heat on friction materials (according to F. K. Germanchuk)

friction coefficient f for metal rubbing on composite materials is taken to be 0.28-0.30, for metal on metal-ceramic materials 0.20-0.23, and for metal on metal 0.15.

The stability α_{st} of the friction coefficient is defined by the ratio between the effective moment of friction forces $M_{fr\ ef}$ and the maximum moment $M_{fr\ max}$ (Fig. 25.13). The effective value (ordinate) is found as the area confined between the moment variation
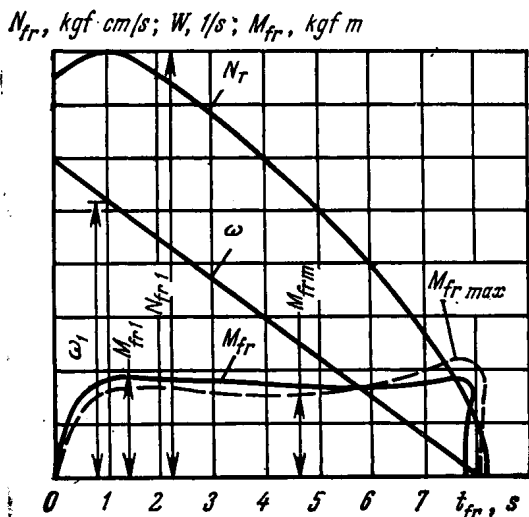
Fig. 25.13. Graphical estimation of friction power and braking work

curve $M_{fr} = f\ (t_{fr})$ and the axis of abscissas is divided by the process time (the abscissa), taking into account the chart scale. The stability characterizes the safety factor of the friction device. For friction elements made of asbestos-base composition $\alpha_{st} \approx 0.9$, for those of metal-ceramic compositions $\alpha_{st} = 0.75$-0.85, and for metal rubbing against metal $\alpha_{st} = 0.4$-0.5 only. That signifies, that the latter combination may generate intensive friction oscillations, and, in addition, it requires a twofold increase in safety factor for the fastening elements (bolts, connecting links, etc.). Variations of the friction coefficient during braking are defined by the ratio

$$\gamma_m = \frac{M_{fr}\text{max} - M_{fr}\text{min}}{M_{fr}\text{max}}$$

and the braking efficiency over useful life, by the ratio $\beta_{ef} = \dfrac{\alpha_{st}}{t^2_{fr}}$ and the factor $\varkappa = \dfrac{\beta_{ef}}{I_l}$, where I_l is wear in metres per metre of sliding distance.

The stability of the friction coefficient is a critical factor; its decrease with rising speeds (temperatures) results in the loss of

efficiency of the friction device. This effect can sometimes be observed in brakes, when prolonged and repeated braking fails to stop the vehicle.

Some materials exhibit an irreversible deterioration of frictional properties and wear resistance after heating. Such materials cannot be used in friction devices. Only special materials designed for frictional applications are recommended for use in friction devices.

The sliding time and the sliding speed and power variation laws provide the most important initial data for calculating the temperature of the rubbing surfaces and, later, for developing equations of frictional thermodynamics. These equations enable one to predict at the developmental stage variations in the braking torque, speed, and temperature.

Among the data on operating properties of friction couples, the average specific power of engagement and sliding $N_{A\ fr} = \dfrac{M_{fr}\omega}{A_{a1}}$ is of importance, since it has a substantial effect on the output characteristics.

The bulk temperature of the friction element is found by the formula

$$\Delta\vartheta_{V1} = \frac{\alpha_{hf}W_{fr}}{m_1 c_1} \text{ or } \Delta\vartheta_{V2} = \frac{(1-\alpha_{hf})\,W_{fr}}{m_2 c_2} \qquad (25.1)$$

where m is the mass of the element; α_{hf} is the coefficient of the heat flow distribution; W_{fr} is the total work of friction.

Formulas for calculating α_{hf}, and also physical and mechanical properties of some commercial friction materials are given in Tables 25.5 through 25.7.

The figures presented in Tables 25.6 and 25.7 are to some extent approximate and averaged values. They are considerably influenced by the heat treatment and ageing of the materials.

When a brake is repeatedly applied for a short time, with the number of applications per hour being n, the components of the brake get cooled between the application. The bulk temperature at the end of the cooling interval before the nth application is determined by the formula

$$\Delta\vartheta_{V_{fr}} = \vartheta_0 + \frac{\alpha_{hf}W_{fr}}{Gc} \left(\frac{e^{-kt_{cool}} - e^{-nkt_{cool}}}{1 - e^{-kt_{cool}}} \right) \qquad (25.6)$$

where ϑ_0 is the initial temperature of the unit equal to the ambient temperature, $k = \sigma^1_{cool}A_{cool}/G$, G is the mass of the friction element, A_{cool} is the cooling area of the friction element; σ_{cool} is the heat transfer coefficient, and t_{cool} is the time of cooling.

The formula has been derived on the assumption that cooling runs in accordance with the Newton Law, i.e.

$$\Delta\vartheta_{V_m} - \vartheta_0 = (\Delta\vartheta_{V_m}^{max} - \vartheta_0)\,e^{-kt} \qquad (25.7)$$

Table 25.5

Heat flow distribution coefficients

Formula	Range of application
$$\alpha_{hf}^{\mathrm{I}} = \frac{\sqrt{\lambda_2 c_2 \rho_2}}{\sqrt{\lambda_1 c_1 \rho_1} + \sqrt{\lambda_2 c_2 \rho_2}} \qquad (2)$$ where $\rho_{1,2}$ = density, kg/m^3	$K_{ov} \approx 1$, $v \leqslant 3$ m/s, Pe= $=\dfrac{v d_r}{a} \leqslant 0.4$ $(d_r =$ mean diameter of spot of macro- and microcontact) Friction elements are nearly equal in volumes
$$\alpha_{hf}^{\mathrm{II}} = \frac{1}{1 + \dfrac{b_1 c_1}{b_2 c_2} \sqrt{\dfrac{a_1}{a_2}}} \qquad (3)$$ where $b_{1,2}$ = friction-element dimension along the linear heat flow, $a_{1,2}$ = thermal diffusivity coefficients, m^2/s	$0.6 < K_{ov} < 1$, $v \geqslant 3$ m/s, Pe > 0.4 Friction elements may be substantially different in volumes
$$\alpha_{hf}^{\mathrm{III}} = \frac{1}{1 + \dfrac{\lambda_1 \sqrt{a_2}}{K_{ov} \lambda_2 \sqrt{a_1}}} \qquad (4)$$ $$b_{ef} = 1.73 \sqrt{a t_{fr}} \qquad (4a)$$ The friction-element dimension is greater than the effective depth b_{ef} or heat diffusion	$0.2 < K_{ov} < 1$, $v \geqslant 3$ m/s, Pe > 0.4 Friction elements are substantially different in volumes
$$\alpha_{hf}^{\mathrm{IV}} = \frac{4\lambda_1}{4\lambda_1 + \pi^{1/2}\lambda_2 \mathrm{Pe}^{1/2}} \qquad (5)$$	$K_{ov} \ll 1$, Pe$= \dfrac{v d_r}{a} \geqslant 20$, $v \geqslant 3$ m/s
$$\alpha_{fr}^{\mathrm{V}} = \left\{ 1 + \frac{\psi_{V2} b_2 \lambda_1}{\psi_{V1} b_1 \lambda_2} \left[\frac{\mathrm{Fo}_2}{\mathrm{Fo}_1} - \frac{\mathrm{Fo}_1 - \mathrm{Fo}_2}{3\mathrm{Fo}_1^2 A} \left(\frac{1}{3} \ln \times \right. \right. \right.$$ $$\left. \left. \left. \times \frac{(1/3 - A)}{(1/3 + A)} \frac{1/3 - \mathrm{Fo}_1 + A}{1/3 - \mathrm{Fo}_1 - A} - A \ln 3/2\mathrm{Fo}_1 \right) \right] \right\}^{-1}$$ where $A = \left(\mathrm{Fo}_1^2 + \dfrac{1}{9} \right)^{1/2} \qquad (6)$ ψ_V = coefficients that allow for effective heated volumes of friction elements *1* and *2* (Fig. 25.1 and 25.2) $\mathrm{Fo}_i = a_i t_{fr}/b_i^2$, $t_{fr} = \dfrac{2W_{fr}}{f_0 p_0 v_0 A_c}$	Mean integral α_{hf} per braking at $0.1 \leqslant K_{ov} \leqslant$ $\leqslant 1$, v varies from maximum to zero, Pe > 0.4

where $\Delta \vartheta_{Vm}^{\max}$ is the mean bulk temperature of a body at the beginning of cooling.

Usually, if $n \geqslant 10$, the heat transfer conditions can be regarded as steady, and in formula (25.6) the expression $\dfrac{e^{-kt_{cool}} - e^{-nkt_{cool}}}{1 - e^{-kt_{cool}}}$ can be replaced with (10 to 45) kt_{cool}. The most difficult quantity

Table 25.6

Some physical properties of commercial metallic friction materials

Material	λ, kgf m/(m s°C)	c, kgf m/(kg °C)	$\rho \times 10^{-3}$, kg/m³	$a \times 10^5$, m²/s	Temperature saturation coefficient $\sqrt{\lambda c \rho} \times 10^{-2}$, kgf m/(m² s$^{1/2}$°C)
Sintered friction materials:					
iron-base (ФМК-11)*	3.5/3.1	51/62.2	5.5/6.0	1.24/0.82	9.86/10.8
			5.6-6.3		
copper-base	3.0/3.5		5.6-6.3		
Alloy steels:					
grade 30ХГСА	3.9/3.9	47/49	7.8	1.07/1.01	12.1/12.2
grade 65Г	4.6/2.9	46/51	7.8	1.28/0.7	12.8/10.9
Structural steels:					14.7/15.3
grade 10	5.92/4.9	47/60.2	7.8	1.61/1.04	13.4/13.0
grade 45	4.9/4.2	48/53	7.8	1.3/1.01	7.3/8.9
Stainless steel, grade 12Х18Н9Т	1.3/1.8	51/56	7.9	0.34/0.43	
Bronze БрАЖМц 10-3-1.5	6.0/7.8	39/44	8.9	1.74-2.01	14.5/17.6
Cast irons:					
grade ЧНМХ	5.1/4.7	51/60.2	7.1	1.41/1.10	13.6/14.1
grey irons	4.3/5.1	55.1	7.15	1.09-1.30	13/14.2
Titanium (grade ВТ-14)	0.8	57	4.5	0.33	4.54
Berillium	15.3/12.2	194/240	1.8	4.3/2.7	23.1/23.3
Chromium	6.8/4	46/51	7.2	2.0/1.25	14.8/12.9

* used in combination with cast iron ЧНМХ.
Notes: 1. Values in the numerator hold at 20°C, in denominator at 300°C. 2. Hardness *HB* 61.2-96.9 is for sintered materials, *HB* 163.2-224.4 for cast irons, and *HB* 204-224.4 for steels.

---

to find is the coefficient of external heat transfer σ^1_{cool} which depends for its magnitude on the kind of coolant, its velocity, the size of the area being cooled, and $\Delta\vartheta_m^{max}$.

The mean temperature at the sliding interface. The maximum temperature (in unsteady conditions) is roughly estimated by the following formula, which is valid at $\frac{t_\vartheta}{t} = 0.055$, Fo ≈ 0.333 (the Fourier number), and with the heat flow normal to the sliding interface (t_ϑ is the time coordinate corresponding to the maximum power):

$$\vartheta_{A\,fr} = \frac{(1 - \alpha_{hf})\,W_A b_1}{3\lambda_1 t_{fr}}(\tau_N + \tau_W) \qquad (25.8)$$

where W_A is the specific energy, that is, the ratio between the predicted work and the nominal friction area.

Table 25.7

Some physical properties of commercial non-metal friction materials

Type of material	λ, kgf m/(m² s °C)	c, kgf m/(kg °C)	$\rho \times 10^{-3}$, kg/m³	$\alpha \times 10^7$, m²/s	Coefficient of temperature saturation $\sqrt{\lambda c \rho}$, kgf m/(m² s 1/2 °C)	σ_{com}, kgf/mm²	HB
Asbestos composition							
with rubber binder	0.0408-0.052	91.8-122.4	2-2.5	1.7-2.8	86-126	5.1-10.2	16.3-27.5
with compound binder	0.041-0.061	91.8-117.3	2-2.6	1.3-3.4	86.7-136	41-15.3	17.3-51.0
with resinous binder	0.0765-0.082	97.9-102	2.3-2.5	3.0-3.5	131-145	7.14-7.65	47.9-49.0
Elastic asbestos composition	0.046-0.051	89.8-102	2.1	2.4-2.7	97.7-104.4	2.55-3.57	2.04-3.57
Cardboard-latex composition	0.036	111.2	1.6	2.0	80×10^3	7.45	14.3
Cardboard-bakelite composition	0.036	107.1	2.0	1.7	87.9	10.6	38.8
Fabric-bakelite composition	0.046	124.4	2.0-2.1	1.8	107-110	10.2	32.6-33.7
Spirally wound material	0.039	127.5-137.7	1.5-1.8	1.6-2.0	86.6-98.6	37.7-5.8	11.2-12.2
Carbon-graphite	10.2-25.5	61.2-81.6	1.5-2.2	14-28	$(9.67\text{-}21.4)10^3$	—	—

For rough estimation, the expression $(\tau_N + \tau_W)/3$ in formula (25.8) can be replaced by a coefficient of 0.65.

The heat is transferred from the outer surface of the friction device to the ambient medium mainly through natural or forced convection. The effect of the heat radiation from nearby parts will be substantial where these are heated to a level different from that of the friction-device outer surface, and where the ambient medium comprises so-called industrial gases. In such situations, the heat components due to convection and radiation must be added up. However, such cases are rare in conventional friction devices.

If the bulk temperature exceeds 500 to 600°C, forced cooling must be resorted to.

Moments of inertia of gyrating masses and the average amount of friction work. When determining the average amount of work expended on friction, account must be taken not only of the mass of all drive components having a translatory motion, but also of the moment of inertia of the rotating parts. For instance, the kinetic energy balance for a moving railway vehicle relative to each of its n brakes can be expressed as

$$W_{fr} = \frac{1}{n}\left[W_v - (W_{bear} + W_{air} + W_{sk}) + 4W_{J_M}\right] \qquad (25.9)$$

where W_v is the energy of the vehicle in movement, $W_{bear} + W_{air}$ is the work expended on overcoming the aerodynamic resistance and friction in bearings, W_{sk} is the work expended on skidding of the wheel on the rail (2 percent in normal braking), and $4W_{J_M}$ is the energy of gyrating masses for the four wheel pairs of the vehicle.

The energy of gyrating masses is found by the formula

$$W_{J_M} = \frac{J_M \omega^2}{2} \qquad (25.10)$$

The magnitude of the inertia moments J_{1M} and J_{2M} of the rotating driving and driven parts, respectively, has an effect on the moment of friction during the engagement of the clutch placed between the motor and the transmission:

$$M_{fr} = M_m \frac{J_{2M}}{J_{1M} + J_{2M}} + M_l \frac{J_{1M}}{J_{1M} + J_{2M}} \qquad (25.11)$$

where M_l is the useful torque of the output mechanism.

In brakes and clutches operating in a braking mode, M_{fr} is affected by J_{2M} only. The power of friction is calculated by the formula $N_{fr} = M_{fr}\omega$.

The mean values of power $N_{A\,fr}$ and friction work $W_{A\,fr}$ per unit area of the rubbing surface, and also this work per volume of the friction element, $W_{V\,fr}$, are specific characteristics used to evaluate the efficiency of a given friction material in a given design.

Thermal diffusivity. Friction couples where both elements have low thermal diffusivity (for instance, plastic on plastic) can be

126

found exceptionally rarely. As a rule, one or both elements are made of materials with high thermal diffusivity (metals, alloys, graphite compositions), which provide for intensive removal of heat from the friction zone. However, with one of the mating elements made of a material with a low thermal diffusivity and having a high contact rigidity, there is a chance that high-temperature ($\vartheta_A = 800$ to $1000°C$) friction zones arise on the rubbing surfaces.

In these zones or somewhere nearby, local wear spots, cracks, pick-up and smears of material on the metal counterface are likely to occur. To prevent this, special measures are outlined in design documentation.

The rate of wear. This should be specified with regard to the wearing qualities offered by present-day friction materials.

The friction element (brake shoe, etc.) and the counterface (a metal drum, disc, etc.) operate under conditions involving repeated heating and cooling. The resulting thermal stresses are much higher than the mechanical stresses. Therefore, the friction materials selected should effectively resist thermal fatigue. For such materials the wear rate can as a first approximation be calculated by the formula $I = i_h p/HB$, where I is the wear in metres for 1 metre of sliding path.

If the friction couple has been chosen properly and it works within the temperature region specified for it in Table 25.3, i_h will range from 10^{-6} to 10^{-7}. The hardness of friction materials is given in Table 25.7. It is enough for wear-life prediction to divide the design wear allowance by the magnitude of I. The result will be the sliding path on which the friction element is expected to provide normal performance during its service life. In such estimations, however, allowance should be made for considerable variations in hardness and wear resistance observed in different batches of friction materials.

After all requirements on the friction couple have been determined, the materials are selected from catalogues.

25.3. DESIGN OF FRICTION DEVICES

Considered below is an algorithm for designing a friction device in accordance with the friction couple specifications (see Table 25.4).

Tentative choice of friction materials. (1) From reference data, using the HB δ_p criterion (δ_p is elongation at rupture), the most wear-resistant material is selected for the friction counterface; wear resistance is proportional to this criterion.

(2) The friction couple that meets the specifications is selected by analyzing respective curves of frictional thermal stability (relationships $f = f (\vartheta_{max})$ and $I = I (\vartheta_{max})$, where f is the friction coefficient, I is the wear rate and ϑ_{max} is the maximum surface temperature). Examples of such relationships are presented in

Figs. 25.8 through 25.11. For a completely new combination of materials, such relationships are obtained by testing on friction machines, e.g. types УМТ-1, ИМ-58, И-47, МФТ-1, МИФИ-1 and МИФИ-2. Tests are carried out over a wide range of expected loads on the nominal area of friction.

(3) The type of friction device and the mode of operation (Figs. 25.1-25.7), the coefficient of mutual overlap K_{mo}, the friction-element dimensions, the duration of sliding, and the cooling method (Table 25.1, and pp. 118, 122) are decided upon.

(4) The friction thermodynamics equation is set up and solved to determine variations of the friction force (friction force moment), speed, and temperature with time.

(5) In situations where commercially available materials do not meet the requirements, laboratory tests of new pilot materials are provided for.

(6) A full-size friction-device prototype is designed and built in accordance with the general recommendations [see point (2)] or with those resulting from the tests mentioned in point (5), taking into account the scale factor. Methods for calculating the scale factor are shown in Fig. 25.17, and formulas to calculate the scale factor for testing conditions are given in Table 25.11.

(7) The prototype of the friction device is tested under laboratory conditions on a test bed, with recording of its frictional, wearing, and temperature characteristics.

(8) The prototype is then field tested in the machine it has been designed for.

(9) The errors of the experiment are evaluated.

(10) The data obtained is prepared for use in condensed form by mathematical treatment, e.g. by means of a regression equation.

Some steps of this algorithm are considered below in detail.

For critical heavy-duty applications, both materials of the friction couple are developed and produced by specialized organizations. If a friction couple is intended for light and medium working conditions and one of its elements is of a rubber-asbestos or resin-asbestos composition, the second element, i.e. the counterface, is made of a metal, which is normally chosen from catalogues.

The friction material certificate must include the value of the friction coefficient. In practice, this important parameter is often determined on a Type И-32 test machine at temperatures of up to 100°C only, rather than on advanced testing equipment (Types МФТ-1, И-47, ИМ-58 machines), which may not be available. As friction coefficients are known to drop substantially with rising temperatures, the values that the designer has for reference are considerably greater (two times and more) than the actual values. When using the frictional thermal stability curves given in the literature, it must be born in mind that most of them were obtained for materials which had undergone no thermal action arising in rubbing. Such an action sometimes results in definite transform-

tions of the surface layer (see Fig. 25.11), that ensure stable frictional and wearing characteristics as compared with the initial values.

Frictional thermodynamics calculation. In hard braking, frictional properties of the rubbing materials substantially vary with the operating temperature, speed, and load of the brake. Variations of the braking-process characteristics are interdependent, as can be seen, for instance, from the expression of the dynamics of motion during braking:

$$v_t = v_0 - \frac{A_a v_0^2}{2W_{fr}} \int\limits_0^t f_t p_t \, dt \tag{25.12}$$

Analysis of the effect that the sliding speed, load, temperature and its gradient have on the friction coefficient during braking has shown a predominant influence of the temperature. For this reason, calculations from the average value of the friction coefficient usually prove inconsistent, particularly so in the absence of similar cases that could be used as reference. In order to predict variation of the friction coefficient (braking torque) with the contact temperature, load, speed, specified operating conditions, physical, mechanical and frictional properties of the friction-couple materials, short-term operation and heat removal conditions, a system of equations of frictional thermodynamics has been developed at the Institute for the Study of Machines (IMASh), of the USSR Academy of Sciences.

The system comprises a dynamics equation, an expression for variation of the friction coefficient with temperature as obtained from standard tests for frictional thermal stability, expressions for variation of pressure, mean frictional contact temperature, bulk temperature before the n-th brake application, a relationship between the hardness of the weakest member of the friction couple and the bulk temperature (hot hardness), and an expression for variation of temperature at the points of real contact. For different friction devices (brakes, clutches, etc.) these expressions will differ in character. Given below is a system of frictional thermodynamics equations for an intermittent duty, involving repeated short-time brake applications (a single-application duty has $n = 1$)

$$v_t = v_0 - \frac{A_{ac} v_0^2}{2W_{fr}} \int\limits_0^t f_t p_t \, dt$$

$$f_t = f_0 \left\{ K_1 + \frac{K_2}{[K_3 (\vartheta^* + \vartheta_{fl} + \vartheta_V - \vartheta_m]^2 + 1} \right\}$$

$$N_t = N_0 (1 - e^{-\frac{t}{T}})$$

$$\vartheta^* = \frac{\alpha_{hf} v_i b_i A_{ac} \left[f_t p_t v_t \left(\frac{1}{3} - \frac{2}{\pi^2} \Sigma \right) + \frac{a_t}{b_i^2} \int\limits_0^t f_t p_t \, dt \right]}{A_{ai} \lambda_i}$$

$$\vartheta_{fl} = \frac{1.73 d_r a_2^{1/2} A_{ac} f_t p_t v_t}{A_r \left[4\lambda_1 a_2^{1/2} + \lambda_2 \left(\pi d_r v_t \right)^{1/2} \right]}$$

$$\vartheta_V = \frac{\alpha_{hfi} W_{fr}}{G_i c_t} \left(\frac{e^{-Kt_{cool}} - e^{-nKt_{cool}}}{1 - e^{-kt_{cool}}} \right)$$

$$HB_{2t} = HB_{20} \left\{ m_1 + \frac{m_2}{[m_3 \left(\vartheta^* + \vartheta_V - \vartheta'_m \right)]^2 + 1} \right\}$$

$$(i = 1,\ 2),\ K = \frac{\sigma' A_{fl}}{G_i c_t}$$

In these formulas A_{ac} is the nominal area of contact for designs where $A_{a1} \neq A_{a2}$ owing to different widths of the rubbing surfaces or grooves, ϑ_{fl} is a temperature flash; ϑ_i^* is the mean temperature at the sliding interface: $\sum = \sum\limits_{n=1}^{\infty} \frac{1}{n^2} e^{-(\pi n)^2} \frac{a_i t}{b_i^2}$. For practical purposes $n = 3\text{-}4$ will suffice.

To facilitate the solution, the equations are expressed in relative units by means of the following formulas:

$$\left.\begin{aligned}
&\tau = \frac{t}{t_{fr}}, \quad \omega = \frac{v_t}{v_0}, \quad \varepsilon = \frac{f_t}{f_0}, \quad \gamma_t = \frac{p_t}{p_0} \\[4pt]
&B'_2 = \frac{B_2}{t_{fr}}, \quad \delta = \frac{T}{t_{fr}}, \quad \theta_{fl} = \frac{\vartheta_{fl}}{\varkappa} \\[4pt]
&\theta^* = \frac{\vartheta^*}{\sigma}, \quad \theta_{V\,tot} = \frac{\vartheta_{V tot}}{\sigma}, \quad \theta_{fr} = \frac{\vartheta_{fr}}{\sigma} \\[4pt]
&\theta'_{fr} = \frac{\vartheta'_{fr}}{\sigma}, \quad \varphi = \frac{HB_{2t}}{HB_{20}} \\[4pt]
&\mathrm{Fo}_i = \frac{a_i t_{fr}}{b_i^2}, \quad t_{fr} = \frac{2 W_{fr}}{f_0 p_0 v_0 A_{ac}} \\[4pt]
&\sigma_i = \frac{\alpha_{hfi} \psi_{Vi} b_i A_{ac} f_0 p_0 v_0 \mathrm{Fo}_i}{A_{ai} \lambda_i} \\[4pt]
&\varkappa = \frac{1.65 f_0 \left(a_2 v_0 \right)^{1/2} HB_{20}}{\lambda_2} \left(\frac{r_1 h_1 M}{v_1} \right)^{1/4} \left(\frac{p_0}{b_{01} HB_{20}} \right)^{1/4 v_1} \\[4pt]
&\mu = \frac{1.33 \lambda a_2^{1/2}}{\lambda_2 v_0^{1/2}} \left(\frac{v_1}{r_1 h_1 M} \right)^{1/4} \left(\frac{b_{01} HB_{20}}{p_0} \right)^{1/4 v_1}
\end{aligned}\right\} \quad (25.14)$$

For an intermittent duty, the system of frictional thermodynamics equations in relative units takes the following form

$$\omega = 1 - \int_0^\tau \varepsilon \gamma_{fr} d\tau'$$

$$\varepsilon = K_1 + \frac{K_2}{[\beta_1 \left(\theta^* + \theta - \theta_{fr} \right) + \beta_2 \theta]^2 + 1}$$

$$\gamma_{fr} = 1 - e^{\frac{\tau}{\sigma}}$$

$$\theta^* = \left(\frac{1}{3\mathrm{Fo}_i} - \frac{2}{\mathrm{Fo}_i \pi^2} \, \Sigma \right) \varepsilon \gamma_{fr} \omega + \int_0^\tau \varepsilon \gamma_{fr} \omega \, d\tau$$

$$\theta_{fl} = \frac{\varepsilon \varphi \omega}{\sqrt{\bar{\omega} + \mu}}$$

$$\theta = \frac{\alpha_{hti} W_{fr}}{\sigma G_i c_i} \left(\frac{e^{-K t_{cool}} - e^{-n K t_{cool}}}{1 - e^{-K t_{cool}}} \right) \tag{25.14a}$$

$$\varphi = m_1 + \frac{m_2}{[\alpha \, (\theta^* + \theta_V - \theta'_{fr}) \,]^2 + 1}$$

where $\beta_1 = K_3 \sigma$, $\beta_2 = K_2 \varkappa$, $\alpha = m \sigma$.

Depending on v and p, conditions may arise where the frictional temperature is mainly influenced by ϑ_{fl}. In other conditions ϑ_{fl} has little effect on the mean temperature at the sliding interface. In any case, the designer should analyze the influence of ϑ_{fl} on the mean frictional temperature.

The system of equations (14a) is reduced to a differential equation for ω, which, for an intermittent duty, takes the form

$$\dot{\omega} + \gamma_{fr} \left\{ K_2 + \frac{K_2}{1 + \left\{ \dfrac{\beta_1}{\alpha} (1 - \omega^2 - 2\theta_m + 2\ddot{\theta}_V) - \Sigma' \beta_1 \omega \dot{\omega} - \dfrac{\beta_2 \omega \dot{\omega}}{\gamma_{fr} \, (\sqrt{\bar{\omega}} + \mu)} \right.}}{} \right. \rightarrow$$

$$\rightarrow \frac{}{\left[m_1 + \dfrac{m_2}{1 + \left[\dfrac{\alpha}{2} (1 - \omega^2) - 2 \, (\theta'_m + 2\theta_V) - \Sigma' \alpha \omega \dot{\omega} \right]^2} \right]^2} \left. \right\} = 0 \tag{25.15}$$

For a single-application duty, in this equation $\theta_V = 0$. Here

$$\sum {}' = \frac{1}{3\mathrm{Fo}_i} - \frac{2}{\mathrm{Fo}_i \pi^2} \sum_{n=1}^{\infty} \frac{1}{n^2} \, e^{-(\pi n)^2 \mathrm{Fo}_i \tau}$$

This equation is used to find ω, and all the other quantities of the system are expressed through ω and $\dot{\omega}$.

Table 25.8 presents formulas used to determine individual parameters of the frictional thermodynamics system. The equations are solved by a digital computer. The structure of the program for the computing is schematically shown in Fig. 25.14.

Solution of a given system of equations makes possible a comprehensive evaluation of the friction device by the information available at the development stage. Data resulting from such a solution are shown in Figs. 25.15 and 25.16.

The system of frictional thermodynamics equations can also be used for optimizing the design of friction devices by varying the basic parameters.

9*

Table 25.8

Calculation formulas of frictional thermodynamics

For-mula	Title	Calculation formula
(16)	Distribution of temperature in depth	$\vartheta_i\,(\xi_i\tau)=\dfrac{\alpha_{hfi}\psi_{Vi}W_{fr}b_i}{\lambda_i t_{fr}A_{ai}}\left[\xi_i\left(1-\dfrac{\xi_i}{2}\right)\tau_N+\dfrac{1}{3}\,\tau_N\right.$ $\left.+\mathrm{Fo}_i\tau_W-\dfrac{2\tau_N}{\pi^2}\Sigma'\right]$ at $i=1,2$
(17)	Mean temperature of rubbing surface	$\vartheta_i^*\,(0,\,\tau)=\dfrac{\alpha_{hfi}\psi_{Vi}W_{fr}b_i}{\lambda_i t_{fr}A_{ai}}\left(\dfrac{1}{3}\,\tau_N+\mathrm{Fo}_i\tau_W-\dfrac{2\tau_N}{\pi^2}\Sigma\right)$
(18)	Mean bulk temperature	$\vartheta_{Vim}=\dfrac{2}{3}\,\dfrac{\alpha_{hfi}W_{fr}}{G_{ief}c_i}$
(19)	Effective thermal conductivity	$\lambda_{ief}=\dfrac{1}{\dfrac{\delta_{11}}{\lambda_{11}}+\dfrac{\delta_{12}}{\lambda_{12}}+\ldots+\dfrac{\delta_{ik}}{\lambda_{ik}}}$, $\delta_{ik}=\dfrac{b_{ik}A_{ahi}}{b_iA_{ai}}$
(20)	Effective thermal capacity	$c_{ief}=\dfrac{\displaystyle\sum_{k=1}^{n}G_{ik}c}{\displaystyle\sum_{k}G_{ik}}$
(21)	Effective density	$\rho_{ief}=\dfrac{\displaystyle\sum_{k}m_{ik}}{\displaystyle\sum_{k}V_{ik}}$
(22)	Effective thermal diffusivity	$a_{ief}=\dfrac{\lambda_{ief}}{c_{ief}\rho_{ief}}$
(23)	Maximum temperature of rubbing surface (single application, intermittent duty)	$\vartheta_{\max}=\vartheta^*+\vartheta_{fl},\quad \vartheta_{\max}=\vartheta''_{Vhf}+\vartheta^*+\vartheta_{fl}$
(24)	Real area of contact (plastic microcontact)	$A_r=\dfrac{p_aA_{ah}}{HB_2}$
(25)	Distribution of temperature in rod-type model of friction couple with allowance for heat transfer into ambient medium	$\vartheta_{1,\,2}\,(z)=\dfrac{fNv}{A_a\,(\lambda_1K_1+\lambda_2K_2)}\,\mathrm{e}^{\pm K_{1,\,2}\,z}$ where $K_{1,2}=\dfrac{1}{b_{ef\,i,\,2}}=\sqrt{\dfrac{\sigma_{cool\,1,\,2}\,u}{\lambda_{1,\,2}A_a}}$, u is the perimeter; $\sigma_{cool\,1,\,2}$ is the heat transfer coefficient for the first and second elements of the friction couple; with $z=0$ $\vartheta^*=\dfrac{fNv}{A_a\,(\lambda_1K_1+\lambda_2K_2)}$

Calculation of the maximum temperature and the thermal dynamics of friction in braking.

(1) Determining the effective depth of heat penetration b_{ief} [by formula (25.4a)].

(2) Computing the Fourier number (Fo) for a given thickness of the friction element (if $b_{ef} > b_i$, $\text{Fo}_i = a_i t_{fr}/b_i^2$; if $b_{1ef} \leqslant b_i$, $\text{Fo}_i = 0.333$).
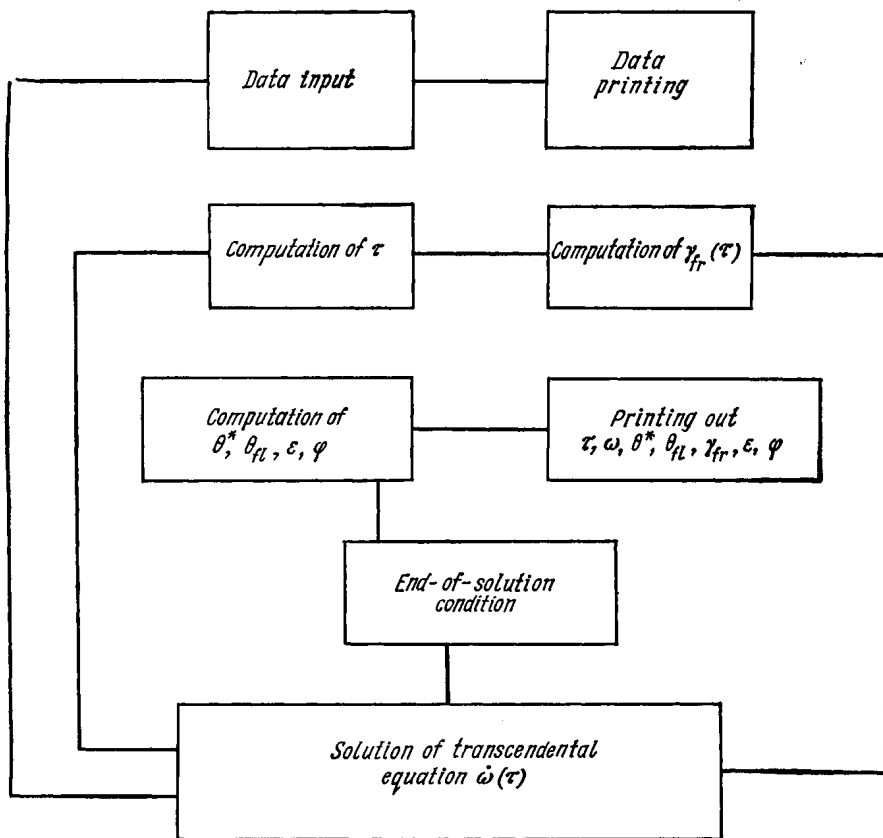
Fig. 25.14. Program for solving a system of frictional thermodynamics equations

(3) Determining the effective volumes ψ_{vi} of the material of friction elements.

(4) Computing the coefficients of heat flow distribution (see Table 25.5).

(5) Computing the mean value ϑ_{vim} of the bulk temperature [by formula (25.18)].

(6) Replacing the initial thermophysical characteristics corresponding to room temperature with the values corresponding to ϑ_{vim}.

133

(7) Updating the values of b_{ief}, Fo_i, ψ_{vi}, α_{hf} and K from the new thermophysical characteristics.

Fig. 25.15. Coefficient of heat flow distribution as a function of Fo

Fig. 25.16. Solutions of frictional thermodynamics equations
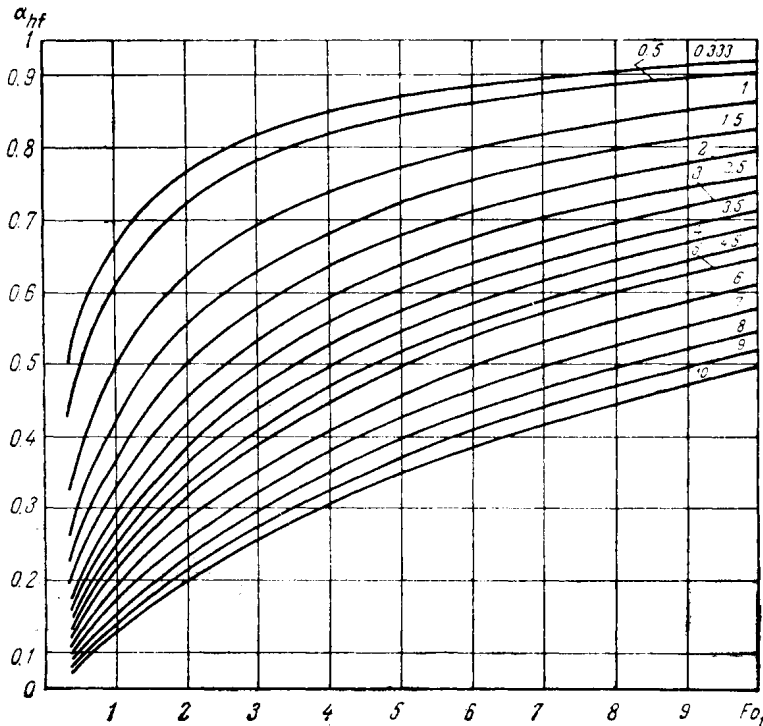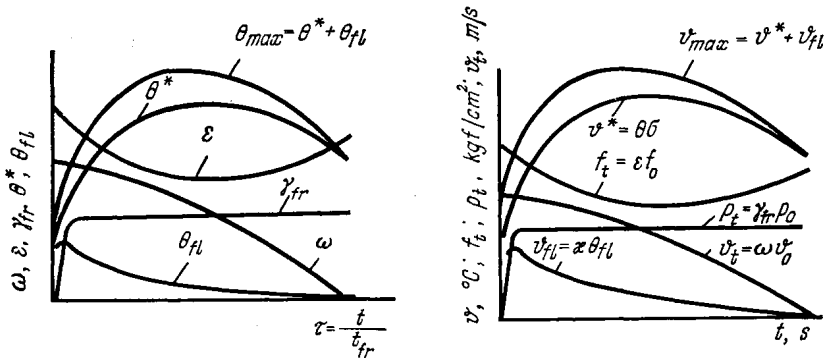
(8) Computing the maximum temperature ϑ_{max} at the sliding interface and its components ϑ''_{vim}, ϑ^*, ϑ_{fl} by respective formulas (25.23), (25.6), (25.17) and (25.13).

The dimensionless parameters σ, χ, μ, β_1, β_2, α are determined by formulas (25.14) and (25.14a). If $\sigma_1 > \sigma_2$, calculation is made for the first friction element; if $\sigma_1 < \sigma_2$, for the second.

Calculation is started with finding $t_{fr} = \dfrac{2W_{fr}}{f_0 p_a A c v_0}$, and then up to point (8) its sequence is the same as for calculating ϑ_{max}.

(9) Computing the working characteristics of the brake by a digital computer.

When radically new problems arise, e.g. prediction of not only frictional but also wearing characteristics, the system can be supplemented by pertinent equations.

The choice of a type of friction device is governed by size specifications and contact load, contact rigidity, and temperature ratings. For disc-type designs with a single rubbing surface and $K_{ov} \approx 1$, the torque $M_{fr} = 2\pi \int\limits_{R_1}^{R_2} fNr^2\, dr$, where R_1 and R_2 are the internal and external friction radii. In devices where contact is effected on the cylindrical surface (band brakes, block brakes, etc.), M_{fr} is determined with regard to K_{ov} by some other formulas.

In designing disc-type friction devices, the friction moment M_{fr} is normally taken to be proportional to the friction coefficient f, load N, and the mean radius of friction R_{mean}. This simplified approach can be justified where $R_1/R_2 > 0.7$ and K_{ov} is close to unity. However, the assumption that the resultant resistance force of the brake lining is applied at a distance R_m from the rotation centre makes it impossible to design properly the lining fastening and to prevent jamming of the friction members.

Therefore, in other situations (where $\rho_\psi = R_1/R_2 \leqslant 0.7$ and $K_{ov} < 1$) it is advisable instead of R_{mean} to use R_{ef} found by solution of the general problem of mechanics:

$$R_{ef} = R_{mean}T/\xi_R$$

Values of the coefficients G and ξ_R are given in Table 25.9.

Table 25.9

Coefficients for calculation of R_{ef}

ρ_φ	Γ	$\varphi°$	ξ_R	ρ_φ	Γ	$\varphi°$	ξ_R
0	1.330	10	0.999	0.6	1.098	50	0.968
0.1	1.223	20	0.995	0.7	1.062	60	0.953
0.2	1.148	30	0.989	0.8	1.037	70	0.936
0.3	1.021	80	0.915	0.9	1.001	140	0.707
0.4	1.010	90	0.891	1.0	1.000	180	0.636
0.5	1.004	120	0.797				

Designations: $\rho_\varphi = R_1/R_2$, φ is the central angle of a friction lining.

Table 25.10

Specifications of commercial test machines

Machine, manufacturer	Number of test methods utilized	Working range						Measuring error	Operating conditions
		N, kgf	n, rev/min	v, m/s	J, kgf m/s²	ϑ, °C	t_{fr}		
УМТ-1 (ZIP, Ivanovo)	4	10-400	⩽ 3 000	—	—	30-1 000	⩽ 24 h	±2.5%	Steady
ИМ-58 (EMZ, Orgstankinprom, Dmitrov)	1-2	10-300	⩽ 9 000	⩽ 20	0.15	30-1 200	0.2-100 s or up to 10 h	±2.5%	Unsteady and steady
СМЦ-2 (ZIP, Ivanovo)	3	20-200	300, 500, 1 500	—	—	⩽ 1 000	⩽ 24 h	±2.5%	Steady
Inertial machines (built to special orders)	1-2	3 000	⩽ 3 000	⩽ 100	13	30-1 200	0.5-100 s	±3%	Unsteady

A rational test cycle. Tests with a view to obtaining a frictional thermal stability characteristic, which is the standard characteristic of a friction couple, make the first stage of a rational laboratory testing cycle. The tests are conducted on testing machines (see Table 25.10). At this stage, the friction/wear thermal characteristic can be roughly estimated without regard to the design features of the device. A specific design arrangement is taken into account at the second stage of the cycle through the use of a scale factor. The maximum savings in testing time are achieved by the use of small-scale models which are affinely or geometrically similar to the full-size design. Here, the scale factors for each parameter (speed, load, size, etc.) are calculated by physical modelling theory methods.

The scale factor calculation based on the theory developed by the IMASh includes the following operations: (1) working out a graphical or structural model of the process to be studied; (2) selecting the basic parameters; (3) determining the similarity criteria and setting up the similarity equation in simplex form; (4) selecting additional boundary conditions with regard to the required ratio between the model and full-scale parameters; (5) solving (manually or by a digital computer) the similarity equation represented as a system of linear equations; (6) analyzing the solution and checking the scale factor values by experiments.

Various methods for calculating the scale factor are given in Fig. 25.17.

Method A is used for hydrodynamic and boundary friction, methods B and C for external friction. For problems with similar conditions the formulas obtained by the A, B, and C methods are similar.

The similarity equation can be solved for the simplex of any parameter assumed as known. Usually, the relationship is known between the masses of the model and the full-size unit, or that between their dimensions, or that between their speeds. Most publications, and also Table 25.11, give solution for a complex of geometrical dimensions of the model and the full-size unit:

$$C_g = \frac{K'_{g1} K'_{g2}}{K_{g1} K_{g2}} = \frac{A'_{a1} A'_{a2}}{A_{a1} A_{a2}} \frac{S_1 S_2}{S'_1 S'_2} \qquad (25.16)$$

where A_{a1} and A_{a2} are the nominal rubbing areas of the first and the second friction element (the prime refers to the model), $S = \dfrac{A_\sigma}{V}$ is the ratio between the heat-radiating or free (out-of-contact) nominal area of the friction element and its volume.

If the friction element does not fully heat for the time of application, the calculation should take into account only the part of the volume or free surface that is limited by the effective depth of heating [formula (4a)]. The calculation of test conditions using the scale factor according to the formulas of Table 25.11 makes it possible to predict the coefficient of friction with an error of under 10 percent, and the rate of wear, under 20 percent.
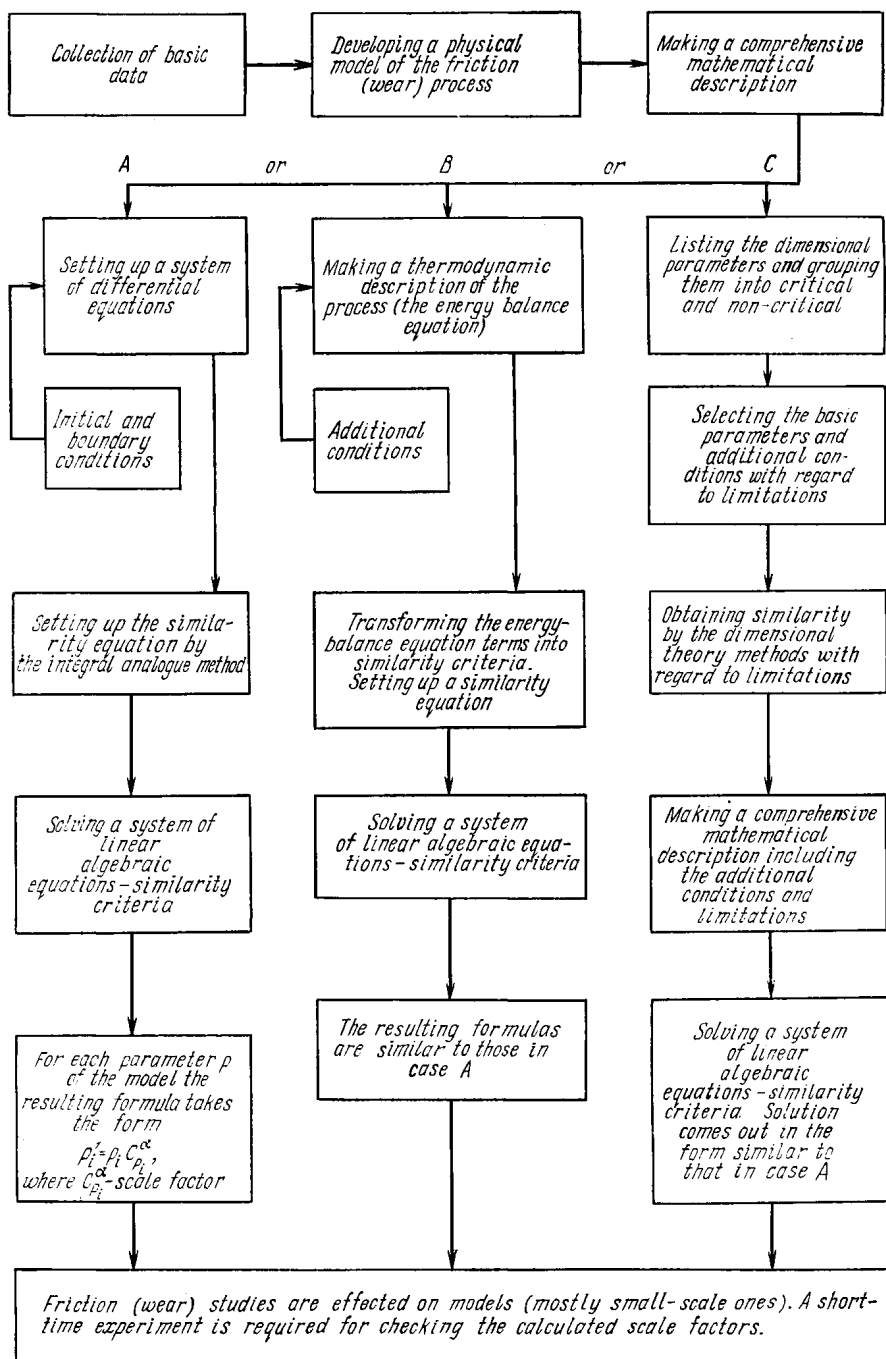
Collection of basic data → Developing a physical model of the friction (wear) process → Making a comprehensive mathematical description

A or B or C

A

Setting up a system of differential equations

Initial and boundary conditions

Setting up the similarity equation by the integral analogue method

Solving a system of linear algebraic equations – similarity criteria

For each parameter p of the model the resulting formula takes the form

$$p_i' = p_i C_{p_i}^\alpha,$$

where $C_{p_i}^\alpha$ – scale factor

B

Making a thermodynamic description of the process (the energy balance equation)

Additional conditions

Transforming the energy-balance equation terms into similarity criteria. Setting up a similarity equation

Solving a system of linear algebraic equations – similarity criteria

The resulting formulas are similar to those in case A

C

Listing the dimensional parameters and grouping them into critical and non-critical

Selecting the basic parameters and additional conditions with regard to limitations

Obtaining similarity by the dimensional theory methods with regard to limitations

Making a comprehensive mathematical description including the additional conditions and limitations

Solving a system of linear algebraic equations – similarity criteria. Solution comes out in the form similar to that in case A

Friction (wear) studies are effected on models (mostly small-scale ones). A short-time experiment is required for checking the calculated scale factors.

Fig. 25.17. Scale factor calculation methods

Table 25.11

Formulas for scale factor calculation

Scale factor for test regime parameters	Scale factor for other parameters	Application
$$v' = vC_g^{1/12}$$ $$N' = NC_g^{1/4}$$ $$W'_{fr} = W_{fr}C_g^{5/12}$$ $$t' = tC_g^{1/12}$$ (27)	Model and full-size unit have equal temperature gradients. To ensure equal temperatures, the heat transfer conditions must be met $$\sigma' = \sigma_{ht}C_g^{5/12}$$	Simulation of (1) cracking at extreme temperatures and (2) friction (wear) without scale factors. The use for light- and heavy-duty friction units is not recommended
$$v' = v$$ $$N' = NC^{1/3}$$ $$W'_{fr} = W_{fr}C_g^{1/2}$$ $$t' = tC_g^{1/6}$$ (28)	Model and full-size unit have equal temperature and specific power values. Scale factor for wear rate $$I' = IC_g^{1/6}$$	For intermittent-duty heavily loaded friction devices
$$v' = vC_g^{1/6}$$ $$N' = NC_g^{1/6}$$ $$W'_{fr} = W_{fr}C_g^{1/3}$$ $$t' = t$$ (29)	Model and full-size unit have the same materials. Scale factor for wear rate $$I' = IC_g^{1/6}$$	Friction (wear) testing of intermittent-duty brake and clutch small-scale models under light and medium loads

Because the friction unit is influenced by the machine where it is installed (the contact rigidity, vibrations of the other units, etc.), it is advisable to test the friction couple at the final stage within the real assembly or within the machine itself. These tests should be checking rather than investigating in character, but the use of instrumentation for indicating the friction moment or force, the surface and bulk temperature, and the normal load is indispensable.

25.4. EXAMPLE OF DESIGN

Problem formulation and basic data. Calculate and test the friction and wear characteristics of a brake. Given: the work of braking $W_{fr} = 5.8 \times 10^4$ kgf m; the speed of braking to a full stop changes linearly from an initial magnitude of 26.1 m/s to zero. The number of applications per hour is not more than 30. Cooling is effected by natural convection. No strict dimensional limitations are placed on the design. The time of braking is 3 s, with the braking torque $M_{fr} = 370$ kgf m.

The main design stages are as follows.

Choice of the brake type. Let us consider a wheel shoe brake with two shoes placed inside the brake drum. The rubbing surface diameter is 0.5 m, the drive is hydraulic, the load on the rubbing surfaces reaches its nominal value in $t = 0.5$ s.

The geometrical characteristics of the brake (Fig. 25.18) depending on the time of sliding are given in Table 26.12.

Determine the relationship $K_{g1}K_{g2} = K_{g1}K_{g2}(t)$, which is necessary for further calculations. The sliding speed in the friction zone is $v = 26.1$ m/s.

Table 25.12

Design characteristics of a brake arranged in accordance with the diagram of Fig. 25.18

t, s	$b_1 \times 10^2$	$b_2 \times 10^3$	$A_{\sigma 1}$	$A_{\sigma 2}$	$V_1 \times 10^3$	$V_2 \times 10^4$	S_1	S_2	$K_{g1} \times K_{g2} \times$ $\times 10^6$
	m		m²		m³		m⁻¹		
1	0.60	1.1	0.32		1.5	1.9	210	970	0.24
2	0.85	1.5	0.35		2.4	2.8	144	685	0.49
5	1.34	2.4	0.40	0.19	4.1	5.4	99	444	1.09
10	1.89	3.4	0.43		6.3	6.2	69	321	2.18

The shoe width is found by the formula

$$b_{sh} = \frac{A_{aef}}{K_{ov} 2\pi R} = \frac{0.164}{0.65 \times 2 \times \pi \times 0.25} = 0.16 \text{ m}$$

where R is the radius of friction (half the adopted rubbing surface diameter, see above); A_{aef} is the effective area of friction:

$$A_{aef} = \frac{M_{fr}}{f p_a R} = \frac{370}{0.3 \times 3 \times 10^4 \times 0.25} = 0.164 \text{ m}^2$$

where p_a is the specific load assigned in accordance with Table 25.3.

Setting the friction couple ratings (Table 25.12). One of the friction couple elements is made of metal for rapid heat removal from the friction zone; the other element is usually of a composite material (see Tables 25.6 and 25.7). Let us consider two kinds of friction couples markedly different in physical properties: an asbestos composition on a metal and a sintered metal ceramic composition on a metal. The first combination provides a higher friction coefficient (about 0.30 to 0.35) than the second (about 0.22 to 0.25), but it develops overheating of the metal member in heavy-duty brakes. The coefficients of heat flow distribution [see Table 25.5, formula (3)] are 0.97 for an asbestos composition with a complex binder on a cast iron, and 0.58 for a metal-ceramic composition on grade ЧНМХ cast iron. Therefore, the second combination has more favourable operating conditions. However, metal-ceramic compositions are not used for shoe brakes because their friction coefficient is not as stable as that of asbestos compositions, and proper contact between the rigid shoes and the drum cannot be achieved. For metal-ceramic compositions, the optimal application is disc-type brakes.

Fig. 25.18. Shoe brake diagram

The choice of a friction couple. The field of application (Table 25.3) of a friction couple is determined according to thermal conditions estimated by the procedure described on p. 132.

Consider a thermal regime calculation for a shoe brake having the friction couple of grade 1-43-60A asbestos composition on grade СЧ24-44 cast iron. The initial data is as follows:

$W_{fr} = 5.8 \times 10^4$ kgf m; $A_{ac} = A_{a2} = 0.17$ m²; $p_a = 3 \times 10^4$ kgf/m²; $HB_2 = 23 \times 10^6$ kgf/m²; $v_0 = 26.1$ m/s; $A_{cool} = 0.7$ m²; $\sigma' = 3.5$ kgf m/(m²s°C); $c_1 = 55$ kgf m/(kg °C); $\lambda_1 = 5.1$ kgf cm/(m s °C); $a_1 = 13.4 \times 10^{-6}$ m²/s;

$\lambda_2 = 0.054$ kgf m/(m s °C); $a_2 = 0.305 \times 10^{-6}$ m²/s; $c_2 = 85$ kgf m/(kg °C); $D = 0.5$ m; $b_1 = 0.024$ m; $b_2 = 0.018$ m; $t_{fr} = 3$ s; $t_{cool} = 90$ s; $K = 7.00 \times \times 10^{-4}$ 1/s; $\vartheta_0 = 20$°C.

For rough estimation τ_N and braking speed can be assumed to change linearly, so that $\tau_N = 2 (1 - \tau)$; $v_t = v_0 (1 - \tau)$; $\tau_W = 2\tau - \tau^2$. Proceeding in the established sequence (pp. 123 and 132) for the shoe as a more thermally stressed element (index 2), with $\vartheta_0 = 20$°C, we find

$$b_{2ef} = 1.73 \sqrt{0.305 \times 3 \times 10^{-6}} = 1.66 \times 10^{-3} \text{ m};$$

$$b_{2ef} < b_i = 18 \times 10^{-3} \text{ m}$$

In further calculation, we use this value of b_{2ef}, with $Fo_2 = 0.333$. Then, similarly, $b_{1ef} = 12.7 \times 10^{-3}$ m; $Fo = 0.333$, $\alpha_{hf2} \approx 0.08$ and $\alpha_{m1} \approx 0.92$.

Find $Kt_{cool} = 70 \times 10^{-4} \times 90 = 6.3 \times 10^{-2}$.

Then, using formula (18) we determine

$$\vartheta''_{Vim} = \frac{\alpha_{hf} W_{fr}}{G_1 c} \left(\frac{e^{-ht_{cool}}}{1 - e^{-ht_{cool}}} \right)$$

$$= \frac{0.92 \times 5.8 \times 10^4}{58 \times 60} \left(\frac{e^{-0.063}}{1 - e^{-0.063}} \right) \approx 240° \text{ C}$$

This temperature ϑ''_{Vim} is found for the drum, because its thermal capacity and heat removal ability determine the accumulation of heat.

It is possible to estimate variation of temperature ϑ^* with time, but we are interested in the maximum contact temperature for a tentative selection of the friction-couple materials. With given τ_N and τ_W the temperature ϑ^* reaches its maximum at $\tau = 0.4$. The expression in parentheses in formula (17) will come to about 0.55. Substituting the known quantities into this formula, we find the maximum value of the rubbing surface temperature, which is $\vartheta^* = 155$°C.

By using the expressions of d_r and A_2 for plastic microcontact, we find from formula (13) that at $\tau \approx 0.4$ ϑ_{fl} will be equal to 19°C; $\vartheta_{max} = \vartheta_0 + \vartheta''_V + \vartheta^* + \vartheta_{fl} = 20 + 240 + 150 + 19 = 434$°C.

Therefore, the 1-43-60A friction plastic composition can be used in this brake, since it is capable of short-time operation at up to 450°C (Table 25.3).

Prediction of the brake thermofrictional characteristics at the design stage by the frictional thermodynamics methods. In order to investigate operation of the brake by means of a system of frictional thermodynamics equations, we need some supplementary data.

These data are as follows[1]:

$$K_1 = 6.27, \quad K_2 = -6, \quad K_3 = 5.2 \times 10^{-4}, \quad \vartheta_m = 650$$

$$f_0 = 0.79, \quad m_1 = 0.17, \quad m_2 = 2.2, \quad m_3 = 4.3 \times 10^{-3}$$

$$\vartheta'_m = -300$$

Changes of the surface temperature (curve 1) and the braking torque (curve 2) with time as obtained by calculations (the solid line) are shown in Fig. 25.19. The dotted lines depict the results of the subsequent tests of the brake.

At the design stage the friction and wear characteristics of the selected friction couple are predicted from test results obtained in testing small-scale models.

---

[1] In these calculations we leave out variation of physical properties of the materials with temperature, because the bulk temperature is relatively low (240°C) and produces no significant changes in the properties of the cast iron, and with the 1-43-60A material the physical properties hardly ever change with temperature.

For the brake in question, 30 applications per hour may cause cracking in the metal member. Furthermore, for wear-life prediction it is necessary to estimate the rate of wear with a fair degree of accuracy.
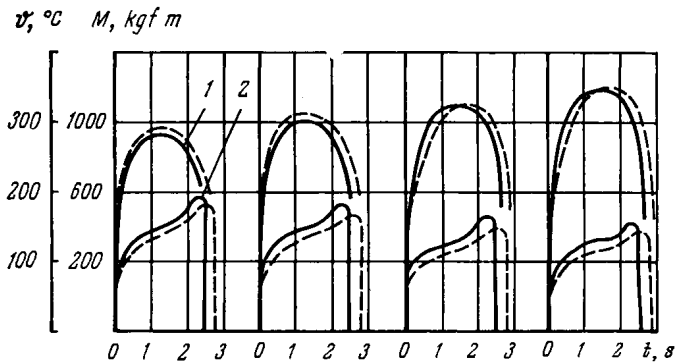

Fig. 25.19. Variation of rubbing surface temperature (1) and braking torque (2) in successive brake applications

The friction and wear characteristics of the brake are determined by testing with regard to the scale factor. According to Table 25.11 [see (27)], $v' = vC_g^{1/2}$ or $C_v = C_g^{1/12}$, $N' = NC_g^{1/4}$, $C_N = C_g^{1/4}$, $C_t = C_g^{1/12}$ and $C_W = C_g^{5/12}$. The tests should be accelerated, since $t \neq t'$ and $t' = tC_g^{1/12}$.

The procedure of finding C_t, C_v, C_p and C_W is as follows.

The first approximation. Calculate C_t, assuming that the braking time is equal for the model and the full-size device.

The model is embodied by specimens specified by the PTM 6-60 Standard (the face type, the outside diameter is 28 mm, the inside diameter 20 mm, and the height 15 mm). The design characteristics of the specimens are given in Table 25.13. These characteristics are subject to changes with the depth of heat diffusion (time of braking).

Table 25.13

Design characteristics of brake model

t, s	$b_1' \times 10^2$	$b_2' \times 10^2$	$A_{\sigma 1}' \times 10^3$	$A_{\sigma 2}' \times 10^4$	$V_1' \times 10^6$	$V_2' \times 10^7$	S_1'	S_2'	$K_{g1,2}' \times 10^{14}$
	m		m²		m³		m⁻¹		
1	0.60	1.1	1.20	3.49	1.81	2.30	667	1 520	6.47
2	0.85	1.5	1.58	4.05	2.55	3.28	621	1 234	8.53
5	1.34	2.4	2.32	5.01	4.04	5.16	575	970	1.73
10	1.89	3.4	2.56	6.36	4.52	7.29	567	874	13.20

$$C_{t_{fr}} = \frac{t'}{t} = \left(\frac{K_{g1,2}'}{K_{g1,2}} \right)^{1/12} = \left(\frac{6.47 \times 10^{-14}}{2.36 \times 10^{-7}} \right)^{1/12} = 0.283$$

Actually, however, the model braking time $t' = 1$ s corresponds to the full-scale braking time $t = \dfrac{t'}{C_{t_{fr}}} = \dfrac{1}{0.283} = 3.53$ s, whereas the full-scale brak-

ing time $t_{fr} = 3$ s corresponds to the model braking time $t_{fr} = 0.85$ s.

From the graph constructed for $K_{g1,2} = K_{g1,2}(t)$, we find $(K_{g1,2})_I$ which corresponds to $t_{fr} = 3.53$ s, $(K_{g1,2})_I = 7.6 \times 10^{-7}$.

The second approximation. Calculate C_t with $t' = 1$ s, $K'_{g1,2} = 6.47 \times 10^{-14}$, $t = 3.53$ s, $K_{g1,2} = 7.6 \times 10^{-7}$:

$$C_{t_{II}} = \left(\frac{6.47 \times 10^{-14}}{7.6 \times 10^{-7}} \right)^{1/12} = 0.257, \quad \text{and} \quad t_{II} = \frac{t'}{C_{t_{II}}} = \frac{1}{0.257} = 3.89$$

From the graph for $K_{g1,2} = K_{g1,2}(t)$ we find $K_{g1,2}$ corresponding to $t_{fr} = 3.89$ s : $K_{g1,2} = 8.65 \times 10^{-7}$.

The third approximation.

$$C_{t_{III}} = \left(\frac{6.47 \times 10^{-14}}{8.65 \times 10^{-7}} \right)^{1/12} = 0.254, \quad C_{g1,2} = 7.48 \times 10^{-8}$$

$$C_v = C_t = 0.254, \quad C_W = 0.001\,07, \quad C_N = 0.016\,6$$

The discrepancy between the first and the third approximation for C_t is

$$\frac{0.283 - 0.254}{0.254} \, 100 \approx 12\%$$

Models are tested on friction machines, types ИМ-58 or МИФИ (Table 25.10). The testing conditions are determined as a product of a given parameter and the scale factor.

For instance, the braking time is $t' = 0.254t = 0.254 \times 3 = 0.76$ s; the initial braking speed $v' = 0.254v = 0.254 \times 26.1 = 6.65$ m/s; the load on
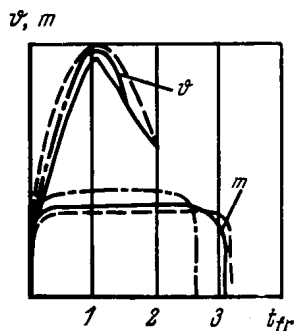

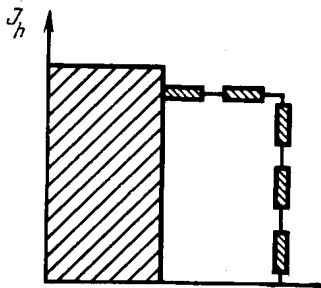Fig. 25.20. Variation of temperature and friction moment with time

Fig. 25.21. Wear rate for the 1-43-60A friction plastic material rubbing against cast iron

the friction couple $N' = 0.016\,6\,N = 0.016\,6 \times 500 = 83$ kgf; the work per brake application $W' = 0.001\,07\,W = 0.001\,07 \times 5.8 \times 10^4 = 62$ kgf m. The interval between applications is also cut down in accordance with $t' = 0.254t$.

The reference characteristic for comparison of the model and full-scale tests is taken to be the time of braking. In evaluating the modelling test error, friction losses in the bearings must be taken into account.

In testing on ИМ-58 friction machines or inertial machines, recording is done of the speed, load, friction force (torque), time, and temperature at no less than three points near the rubbing surfaces.

Figure 25.20 illustrates the calculated temperature and friction force variations with time (the dash-and-dotted lines), and those found by testing the models (the solid line) and the full-size brake (the dash line). Fig. 25.21 shows the rate

of wear of the friction materials in the actual brake and that predicted from the model test results (the dash line).

The problems discussed in this chapter have been treated in greater detail in the publications given in the list of references.

REFERENCES

1. Александров М. П. Тормоза подъемно-транспортных машин. М., «Машиностроение», 1976, 384 с.
2. Германчук Ф. К. Долговечность и эффективность тормозных устройств. М., «Машиностроение», 1973, 176 с.
3. Зверев И. И., Коконин С. С. Проектирование авиационных колес и тормозных систем. М., «Машиностроение», 1973, 224 с.
4. Износостойкость. М., «Наука», 1975, 192 с. Авт.: Э. Д. Браун, А. Г. Гинзбург, А. В. Чичинадзе и др.
5. Исследование структуры фрикционных материалов при трении. М., «Наука», 1972, 132 с. Авт.: З. В. Игнатьева, И. В. Крагельский, А. В. Чичинадзе.
6. Крагельский И. В., Добычин М. Н., Комбалов В. С. Основы расчетов на трение и износ. М., «Машиностроение», 1977, 526 с.
7. Научные принципы и новые методы испытаний материалов для узлов трения. М., «Наука», 1968, 208 с. Авт.: Э. Д. Браун, Л. М. Пыжевич, Г. М. Щеренков и др.
8. Оптимальное использование фрикционных материалов в узлах трения машин. М., «Наука», 1973, 140 с. Авт.: А. Г. Гинзбург, Е. В. Зиновьев, В. П. Мигунов и др.
9. Расчет и испытание фрикционных пар. М., «Машиностроение», 1974, 152 с. Авт.: З. В. Игнатьева, С. С. Коконин, М. В. Малютин и др.
10. Расчет и моделирование режима работы тормозных и фрикционных устройств. М., «Наука», 1974, 104 с. Авт.: Е. Е. Бевз, А. М. Ромашко, В. Ф. Титаренко и др.
11. Словарь-справочник по трению, износу и смазке деталей машин. Киев, «Наукова думка», 1978. Авт.: Е. Л. Шведков, Д. Я. Ровинский, В. Д. Зозуля, Э. Д. Браун.
12. Тепловая динамика трения. М., «Наука», 1970, 172 с. Авт.: В. М. Горюнов, А. К. Погосян, А. В. Чичинадзе и др.
13. Трение и износ фрикционных пар. М., «Наука», 1977, 136 с. Авт.: Е. В. Зиновьев, В. Н. Парфенов, В. Н. Федосеев и др.
14. Тепловая динамика и моделирование внешнего трения. М., «Наука», 1975, 192 с. Авт.: А. К. Дедков, А. Д. Левитанус, В. Д. Лимончиков и др.
15. Трение, износ и методы испытаний асборфрикционных материалов. [Сборник трудов]. Вып. 1. М., Изд. В/О «Нефтехим», 1974, 148 с. (ВНИИАТИ). Авт.: Л. Р. Горелов, А. И. Коряева, В. А. Можаев и др.
16. Чичинадзе А. В. Расчет и исследование внешнего трения при торможении. М., «Наука», 1967, 232 с.
17. Федорченко И. М., Крячек В. М., Панаиоти И. И. Современные фрикционные материалы. Киев, «Наукова думка», 1975, 334 с.
18. Федорченко И. М., Ровинский Д. Я., Шведков Е. Л. Исследование материалов для тормозных и передаточных устройств. Киев, «Наукова думка», 1976, 200 с.

STATIONARY JOINTS

26.1. FRICTIONAL INTERACTION
IN STATIONARY JOINTS

Stationary joints include clamps, flange packing elements, tube fittings and connections, interference-fit joints, threaded fastenings, wedge-, pin-, and key-type assemblies, etc.

The performance of stationary joints is largely determined by the static-frictional force at the joint face, and in precision mechanisms, also by the magnitude of normal and tangential contact displacements. The joint faces where some sliding of the mating parts occurs are subject mainly to fretting corrosion. Wear in seals and force-fitted joints can be caused by plastic deformation of the mating parts; this deformation can result in deterioration of the functional properties, for instance, in a loss of tightness. At elevated temperatures, the performance of stationary joints can be impaired by dimensional changes due to thermal expansion of the components and by the action of frictional forces distributed over the surface.

The value of f can be predicted at the design stage from the following data, which are either specified or found experimentally (see Chapter 2):

—parameters that characterize the strength of molecular interaction in shear (τ_0 and β);

—mechanical properties of materials (E and HB) under the given operating conditions, such as the working temperature, acting vibrations, etc.; other essential data include: normal specific load; surface topography (roughness parameters Ra and Rz), lay and waviness necessary for flat contacting surfaces.

Since external friction has a dual, molecular and mechanical nature, the coefficient of friction is determined by the following three-term formula:

$$f = \frac{\tau_0}{p_r} + \beta + k\alpha_h \sqrt{\frac{h}{r}}$$

where k is a coefficient allowing for the shape of asperities and their distribution in height.

The calculation of static-friction force and contact displacements is given in Chapters 1 and 2.

The formulas obtained for contact of a rough surface with a smooth surface also hold true for contact of two rough surfaces. In this latter case, the effective values of roughness parameters should be used [15], namely*

$$\Delta_{1,2} = \frac{R_{\max_1}^{\nu_1/(\nu_1+\nu_2)} R_{\max_2}^{\nu_1/(\nu_1+\nu_2)}}{r_{1,2}(Kb_1b_2)^{1/(\nu_1+\nu_2)}}$$

where K is a numerical factor (Fig. 26.1); for $\nu_1 = \nu_2 = 2$, $K = 0.16$; $r_{1,2}$ is the effective curvature radius.

With $\nu_1 = \nu_2 = 2$

$$\Delta_{1,2} = \frac{1.6\,(R_{\max_1}R_{\max_2})^{0.5}}{r_{1,2}(b_1b_2)^{0.25}}$$

Where the surfaces differ by more than two roughness classes, the roughness of the smoother contacting surface may be neglected [19].

Simplified formulas for calculating the coefficient of static friction are presented in Table 26.1.

The calculation applies to boundary friction and dry friction and is restricted by the magnitude of relative penetration of the surfaces at which the material ceases to flow round the sliding asperity and plastic displacement changes to micro-cutting. This occurs when

$$\frac{h}{r} \geqslant \frac{1}{2}\left(1 - \frac{2\tau}{\sigma_t}\right)$$

The above relationship determines the threshold of external friction.

Fig. 26.1. Effect of bearing-area curves on coefficient K for contact of two rough surfaces
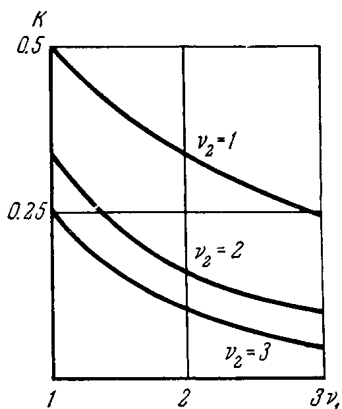
Another extensively used type of frictional calculation applies to contact of surfaces with a large apparent contact area and low rigidity, which can be regarded as elastically supported beams. Examples are taper gibs in machine-tool guide ways or wedge-type clamps for inserted blades in cutting tools. Here the Wincler hypothesis may be used according to which the magnitudes of approach varying with pressure are independent of each other at adjacent sections, that is, the contact approach in each elementary area can be calculated by the mean pressure in this area.

The mechanical properties of the materials, surface topography and normal specific pressure determine together the stress conditions in the real areas of contact, specifically, they determine the type of contact — elastic or plastic, and its normal and tangential stiffness.

---

* Subscripts 1 and 2 refer to either of the contacting surfaces.

Table 26.1

Simplified formulas for calculation of coefficient of static friction

Configuration of surfaces in contact	Type of contact		Note
	elastic	plastic	
1. Curvilinear rough surfaces (higher-order kinematic pairs, shaft-sleeve joints, etc.)	$f \approx \dfrac{2\tau_0}{E^{0.8}\Delta^{0.4}p_c^{0.2}} + \beta$	$f \approx f_m + 0.5\Delta^{0.5}\left(\dfrac{p_c}{HB}\right)^{0.25}$	Contour pressure is calculated by formulas from theory of elasticity for solids of given configuration
2. Small-area planes without waviness (flange-type sealing joints, joint faces in miniature apparatus, etc.) Heavily loaded joints (press fits and threaded assemblies, clamping devices, etc.)			$p_c = p_a$
3. Rough and wavy surfaces, mainly flat ones (machine-tool guide ways, disc brakes and clutches, etc.)	$f \approx \dfrac{2.5\tau_0}{E\Delta^{0.4}\left(\dfrac{R_B}{r_B}\right)^{0.1}} + \beta$	$f \approx f_m + \\ + 0.3\Delta^{0.5}\left(\dfrac{R_B}{r_B}\right)^{0.1}\left(\dfrac{E}{HB}\right)^{0.2}$	f is independent of pressure

It is important to note that an increase in load at the contact causes growth in the number of contact spots rather than any perceptible change in pressure at a separate spot. For this reason, the pursuit of a lower contact pressure through reduction in normal load gives no desired result. Transition from one type of contact to the other is largely due to the change in the shape of asperities, that is, the change in surface geometry.

With elastic deformations in the real contact area, the coefficient of friction grows with better surface finishes (smaller roughness). During plastic contact (at high specific loads), the lower surface roughness leads to reduction in the mechanical component of the coefficient of friction. Waviness manifests itself on flat surfaces whose dimensions exceed a sampling length according to GOST 2789-73, [1]; it mitigates the influence of the specific normal load on the coefficient of friction, that is, the coefficient of friction follows, to a first approximation, the Amontons law (does not depend on load).

Contacting solids shaped with a curvilinear generatrix (for instance, spherical or cylindrical bearings) and small-size planes have the contour area of contact commensurable with the apparent area, and the effect of waviness is insignificant [20]; for this reason, the normal specific load here substantially affects f.

Friction surfaces may be lubricated or dry.

Unlubricated plastic contact requires consideration of all three components of the coefficient of friction; for elastic contact, the first two components (that is, the molecular component of the coefficient of friction) are sufficient.

During the sliding of lubricated surfaces in elastic contact, the coefficient β is predominant and the other components may be neglected (roughly, $\beta = 0.9$ to 0.11). The only exception is elastomers. For plastic contact, two terms should be considered, namely, the coefficient β and the mechanical component of the coefficient of friction.

In the general case, the coefficient of friction as dependent on pressure passes through a minimum. The magnitude of real pressure is determined by the following factors:

—configuration of the tribological unit (a shaft-sleeve, a plane-plane, a cylinder-ring, etc.);

—nature of the materials of the contacting bodies, which affects the magnitude of molecular interaction at the contact (this interaction is characterized by τ_0 and β depending on the presence and type of lubricant and the cleanliness of the surfaces) and which also affects the mechanical properties of materials (elastic modulus and hardness);

—surface roughness and waviness; and

—specific normal load.

Knowledge of the influence of each of the factors in quantitative terms opens the possibility of controlling the magnitude of the coefficient of friction within the following limits:

—the value of the complex parameter Δ for the most frequent surface processing methods varies by three orders of magnitude, which can lead to the coefficient of friction changing threefold;

—the coefficient of friction is more sensitive to the variation of surface roughness than to that of the mechanical properties (elastic modulus and hardness); control of the mechanical properties is hardly feasible;

—the coefficient of friction can be influenced by changing the configuration of the joint, particularly for surfaces with low values of Ra.

To improve the accuracy of a product, the stiffness and dimensional stability of its components are essential. Making the components heavier proves insufficient because large undesirable displacements occurring in the joints have a marked adverse effect on accuracy. Experimental relationships between the approach and the normal load are parabolic in all cases (Fig. 26.2); the exponent for load is

close to 1/2. For parts with identical surface lay the contact stiffness rises up to 20 percent. Surfaces with identical roughness parameters markedly differ in contact stiffness depending on the surface processing method. The presence of lubricant between the contacting surfaces statically loaded with a normal force increases the contact stiffness by about 20 to 30 percent. Superposition of vibrations

Fig. 26.2. Variation of approach with normal pressure $(p_a = p_c)$ for contact of smooth lapped surface of material Д16 (0.04 to 0.08 μm Ra) with steel specimens machined by

1—shaping (0.63 to 1.25 μm Ra); 2——grinding (0.63-1.25 μm Ra); 3—shaping (1.25-2.5 μm Ra); 4—grinding (1.25 to 2.5 μm Ra); 5—shaping (10 to 20 μm Rz); 6—inverse pair (smooth steel surface and rough surface of material Д16)
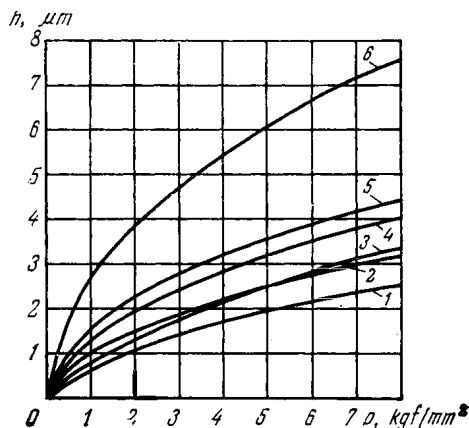
has a considerable effect for lubricated surfaces only. Repeated loading contributes to improvement in the contact stiffness of the joint.

To achieve better reliability and accuracy of precision instruments and mechanisms, it is vital to consider the variation of contact displacements with time. In some instances these displacements are due to rheological processes, which occur even at normal temperatures because of high stresses in the real areas of contact. The creep of materials leads to increased interpenetration of surface asperities and growth in the real contact area. The result of these phenomena is the "stop effect", that is, increase in the static coefficient of friction depending on the durability of the stationary contact. The rate of creep in the real areas of contact decreases with the time the parts are in contact; thus, the process is attenuable.

Closer approach of the contacting surfaces in time leads to increase in f_1 due to growth in the real area of contact and the respective reduction in the mean normal pressure; f_2 also increases due to deeper interpenetration of the asperities.

The formula for calculating the coefficient of friction has the form

$$f = \frac{\tau_0}{HB}\, \xi^2 + \beta + 0.5\Delta^{\frac{1}{2}}\left(\frac{p_c}{HB}\right)^{\frac{1}{4}}\xi \qquad (26.1)$$

where $\xi = h_1/h_0$ is a coefficient allowing for the rheological properties of the contact (here h_0 is approach of the surfaces at the initial

149

Table 26.2

Coefficients of static friction (dry)

Sliding pair	HB	Processing method and surface roughness parameters, μm	Δ	τ_0, kgf/mm²	β	f_1	f with $t \to 0$ $p_c=1$ kgf/mm²	After holding under load	
								t, h	f
Steel 35 ВАД	440 110	G, 0.63-1.25 (Ra) L, 0.04-0.08 (Ra)	1	9.9	0.07	0.16	0.30	90	0.34
Steel 35 ВАД	440 110	G, 0.16-0.32 (Ra) L, 0.04-0.08 (Ra)	0.045	9.9	0.07	0.16	0.22	90	0.27
Steel 35 Steel 35	440 440	G, 0.8-0.16 (Ra) L, 0.04-0.08 (Ra)	0.035	44	0.08	0.18	0.20	22	0.24
Steel 35 ВТ1	440 120	L, 0.04-0.08 (Ra) L, 0.02-0.04 (Ra)	0.002	18	0.08	0.24	0.24	25.5	0.27
ВТ1 ВАД	120 110	G, 0.16-0.32 (Ra) L, 0.02-0.04 (Ra)	0.2	3.6	0.07	0.1	0.16	105	0.19
Steel 45 Copper	130 79	G, 10-20 (Rz) L, 0.08-0.32 (Ra)	1.24	1.5	0.08	0.11	0.15	12	0.16
Steel 45 Aluminium	130 35	G, 10-20 (Rz) L, 0.08-0.32 (Ra)	1.24	—	—	0.12	0.16	12	0.18
Steel 45 Bronze БрАЖМц 10-3-1.5	130 90	G, 10-20 (Rz) L, 0.08-0.32 (Ra)	1.24	2	0.1	0.12	0.14	12	0.16

Designations of processing method: G – grinding; L – lapping.

moment of time, which is calculated through the bulk hardness HB of the softer material; h_t is approach of the surfaces after being held under load).

Thus, the results of tests for durable hardness [2] can be used to predict the variation of the coefficient of friction with time and its dependence on the normal load, the parameters of surface topography, and the contact molecular interactions. The value of the coefficient of static friction for various pairs of mating materials are given in Tables 26.2 and 26.3.

Table 26.3

Effect of durability of stationary contact on coefficient of static friction for lubricated sliding pair of polished hardened steel — duraluminium (after M. C. Hunter)

Time	Graphite lubricant	Grease	Industrial oil	Laminated graphite	Time	Graphite lubricant	Grease	Industrial oil	Laminated graphite
60 s	0.128	0.188	0.176	0.072	60 days	0.145	0.210 0.215	0.210	0.087 0.079
30 days	0.146	0.199	0.195	0.079	90 days	0.158	0.193	0.205	0.103

To obtain more stable coefficients of friction for surfaces in plastic contact held under load over a long time it is essential:

—to process the surface to a high surface finish;

—to apply the lowest possible normal loads sufficient for elastic deformation of material;

—to set up such contact conditions as will ensure lower stresses due to molecular interaction of the contacting surfaces; these conditions are fulfilled by the choice of suitable low-adhesive materials, by the proper cleaning of the joint surfaces with subsequently holding them in air for up to 2 days, by coating, and by introducing lubricants.

The conditions securing elastic deformation of surface irregularities can be created by repeated normal loading ("training") of the contact with forces higher than or equal to the operating forces. One suitable means of stabilizing the coefficient of friction is running-in by repeatedly passing the mating surfaces along one and the same path.

Example 1. Find the coefficient of reliability for clamping a flat cutting blade in the body of a wood working milling cutter in the lightly loaded region between the clamping screws with stresses with the allowance for yield of the clamping elements. The geometric dimensions of the clamping device are given in Fig. 26.3. The cutter body is made from steel 45, HB 293. The flat blades 3 mm thick and 40 mm wide are made from steel 8X4B3MФ2, HRC 55 to 58. The surfaces of the wedgelike slot in the body are machined to 1.25 to 2.5 μm Ra. The blade surface bearing up against the slot wall is finished to 1.25 to 2.5 μm Ra, and the surface supported by the wedge is finished to 0.63 to 1.25 μm Ra. The

blade is clamped in the slot through the wedge by concentrated forces $N =$
$= 591$ kgf exerted by clamping screws. Along with decrease in concentrated
loads, it is necessary to consider the amounts of yield for the blade-to-wedge
joint, the blade-to-slot joint and the screw joint. The rotational frequency of
the cutter spindle is 6 000 rpm.

As the cutter is rotated, the wedge mass produces a centrifugal force of
442 kgf, which tends to shift the wedge and press the blade against the rear
wall of the slot. Let us assume that the specific load generated by the centrifugal
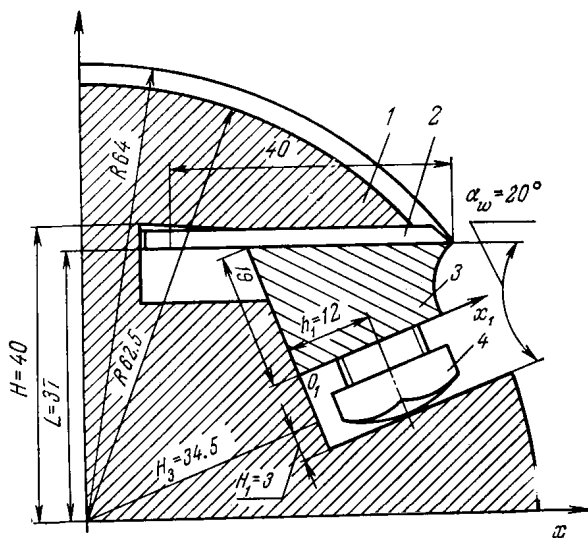
Fig. 26.3. Clamping of cutter blade
—ridge; 2—blade; 3—wedge; 4—clamping screw

force is constant over the length and width of the wedge. We shall consider the
wedge to be an elastically supported beam of a finite length loaded with con-
centrated forces. The wedge deflects as it shifts towards the cutter periphery,
and the clamping force decreases.

The distribution of pressure over the blade-wedge interface is found experi-
mentally or by calculation. The beam length $L = 150$ cm, width $B = 2.4$ cm;
the moment of inertia $J = 0.58$ cm^2; the coefficient of contact deflection $k =$
$= 0.2 \times 10^{-4}$ cm^3/kgf. The calculation is made by the formula $p = \dfrac{\lambda}{2B} N \eta''' (\lambda x)$,

where $\lambda = \sqrt[4]{\dfrac{B}{4kEJ}} = 0.4$ 1/cm is a flexibility factor, x is the distance from
the coordinate origin along the beam length.

The blade bears up against the ridge formed by the back wall of the slot
and the outer periphery of the body; this ridge can be regarded as a cantilever
of variable thickness, whose flexibility affects the diagram of the cross-sectional
distribution of pressure. The differential equation describing the deflection
of the cantilever has the form

$$\Delta^2 \Delta^2 \omega + \frac{1}{D} \frac{\partial^2 D}{\partial y^2} \left(\frac{\partial^2 \omega}{\partial y^2} + \mu \frac{\partial^2 \omega}{\partial x^2} \right)$$
$$+ \frac{2}{D} \frac{\partial D}{\partial y} \left(\frac{\partial^3 \omega}{\partial y^3} + \frac{\partial^3 \omega}{\partial x^2 \, \partial y} \right) = \frac{q}{D} \qquad (26.2)$$

where q is the intensity of load, $\omega\,(x,\,y)$ is the function of the cantilever surface deflection and D is rigidity

$$D = \frac{Eh^2}{12\,(1-\mu^2)}$$

The distribution of pressure across the joint face (Table 26.4) was found [13] through solving the equation (24.2) by the finite-difference method on the БЭСМ-6 computer.

<div align="right">Table 26.4</div>

Distribution of pressure at blade-wedge interface

x, mm	λx, cm	p_c, kgf/mm²	Δp, kgf/mm²	x, mm	λx, cm	p_c, kgf/mm²	Δp, kgf/mm²
0	0	0.124	0.094 5	45	±1.8	0.515*1	0.102*2
15	±0.6	0.188*1	0.094*2	60	±2.4	0.433*1	0.113*2
30	±1.2	0.369*1	0.095 7*2	75	±3.0	0.265	0.123

*1 Along interface
*2 Across interface

The design pressure-distribution diagram is shown in Fig. 26.4.
To a first approximation, we assume that the pressures will be equal across the width of the interface.
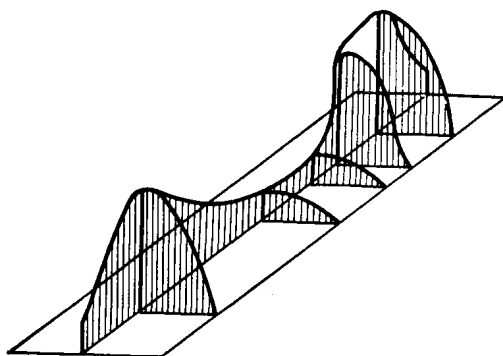
Fig. 26.4. Distribution of pressure at wedge-blade interface

Now we determine the pressure (kgf/mm²) in the lightly loaded region between two clamping screws

$$p = \psi p_{cl} = 0.121 \tag{26.3}$$

where ψ is a correction factor; with $y = 4.8$ mm and $x = 0$, $\psi = 0.977$ (found by calculation on the computer).
The increase in the normal load on the blade due to the centrifugal force acting on the wedge $\Delta N_n = 244.6$ kgf.

The distribution of the pressure increase caused by the action of the centrifugal force on the wedge is given in Table 26.4.

In the lightly loaded region ($x = 0$, $y = 4.8$ mm), we find the total pressure due to clamping forces and the centrifugal force acting on the wedge; $p = 0.215$ kgf/mm^2.

The blade is held by friction forces which are generally given by

$$T = \int\int_A p(x, y) f(x, y)\, dx\, dy \qquad (26.4)$$

where $p(x, y)$ and $f(x, y)$ are the normal pressure and the coefficient of friction at the point of the interface with coordinates x and y.

Figure 26.5 shows the relationship between the coefficient of friction and pressure (see Table 26.1) for the specified frictional conditions ($\tau_0 = 0.14$ kgf/mm^2; $\beta = 0.08$; the blade's planes are ground; for 1.25 to 2.5 μm Ra, $\Delta = 0.02$, and for 0.63 to 1.25 μm Ra, $\Delta = 0.06$). With $p = 0.215$ kgf/mm^2, the coefficient of friction at the wedge-blade interface is $f = 0.103$, and at the blade-body interface, $f = 0.125$. The respective frictional forces T in the between-screws region with an area of $15 \times 4.8 = 72$ mm^2 are equal to 1.59 kgf at the wedge-blade interface and 1.94 kgf at the blade-body interface.

Now we find the centrifugal force acting on the blade ($m = 92$ g) on one clamping screw

$$Q = m\rho\omega^2 = 70.1 \text{ kgf}$$

Fig. 26.5. Coefficient of friction vs pressure
1—ridge-blade interface; 2—wedge-blade interface

Taking into account that this force acts on half the blade with a $35 \times 65 \times 2\,275$ mm^2 area, we determine the displacement force acting on a 72 mm^2 area: $F_c = 2.22$ kgf.

The coefficient of reliability of clamping the blade in the between-screws region will be

$$K_r = \frac{T - F_c}{F_c} = \frac{1.59 + 1.94 - 2.22}{3.38} = 0.59$$

Hence, the blade is clamped insufficiently in the between-screws region. The reliability of its clamping is secured only in the region where the screws are disposed.

Friction forces cannot be effectively enhanced in the between-screws areas through increase in the clamping pressure; the use of rougher surfaces is essential. For instance, change from 0.16-0.32 μm Ra to 1.25-2.5 μm Ra gives the same increase in friction force as a 1.5 times stronger clamping force does.

The centrifugal forces exerted on the wedge level off the distribution of pressure at the wedge-blade interface, so that the pressure under the clamping screws lessens and in the between-screws area grows.

26.2. DISPLACEMENT-RESISTANT JOINTS

Displacement-resistant joints put together with high-strength bolts find ever increasing application in building structures. The performance of such joints is based on the friction arising between the contacting parts as they are pressed together with bolts.

The schematic diagram in Fig. 26.6 shows a shift-resistant connection of sheets with the aid of straps clamped together with bolts. The amount of displacement in the middle region of the joint preceding the total shift of the straps relative to the sheet determines the permissible load limit P which can be sustained by the joint. Subjecting the fasteners (bolts or rivets) to shear is unallowable.

Shift-resistant connections are calculated approximately by the mean values of the coefficient of static friction on the assumption that the normal pressure is distributed uniformly among the contacting surfaces at

Fig. 26.6. Diagram of shift-resistant joint and distribution of forces between the sheet being joined (P_{sh}) and straps (P_{st})

1—sheet; 2—straps

the locations of the bolts. For a joint clamped by a single bolt

$$T = fN\psi$$

where ψ is a coefficient allowing for the operating conditions of the bolted joint ($\psi = 0.78$ to 0.9).

Approximate values of the coefficient of friction for some materials are listed in Table 26.5.

In sand blasting the surfaces for higher coefficient of friction, cleaner sand (that is, sand with a lower content of impurities) must be used. According to Proektstalkonstruktsiya R & D Institute [28], the coefficient of friction as dependent on the content of SiO_2 in sand will be

SiO_2, %	88	93.8	98
f	0.45	0.52	0.61

The shifting forces are distributed non-uniformly between the sheet being connected and the straps (Fig. 26.6). The extreme-position bolts are loaded most. The limiting conditions do not provide for equal loading of the components in the extreme rows of bolts. For this reason, it is good practice to adopt an additional limiting condition for achieving the required contact friction forces in the region of the extreme bolt rows. Thereby rational bolt arrangements and surface processing methods can be chosen, and the departure of
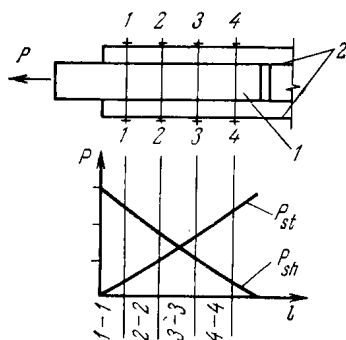
155

Table 26.5

Coefficients of friction in shift-resistant joints [28]

Treatment	Presence of scale on working surfaces	Steels for test specimens			
		Ст3кп	Ст3сп	10ХСНД	14Г2Т
Hand metal-wire brush	Yes	0.21	0.23	—	0.36
	No	0.34	0.35	0.36	0.46
Power metal-wire brush	Yes	0.25	0.23	—	0.32
	No	0.37	0.38	0.37	0.46
Sand blasting with 98% SiO$_2$ sand	No	0.051	0.053	0.58	0.55
Multi-jet flame torch	Yes	0.31	0.25	—	0.25
	No	0.41	0.43	0.47	0.47
Emery cloth	No	0.52	0.51	0.36	0.4

bolt tension from the specified values can be established to achieve a higher load capacity.

For accurate calculation of shift-resistant joints, the designer must consider the actual distribution of normal stresses near the bolts. From the known distribution of normal stresses it is feasible to calculate the coefficient of friction at any contact point and, accordingly, the distribution of frictional forces over the surfaces of the mating sheets and straps. Here, allowance should be made for the effect of such factors as surface roughness, mechanical properties of the materials, load, and the parameters that characterize molecular interactions in the real contact areas depending on the surface processing method.

Example 2. Find the limiting condition for a four-bolt shift-resistant joint with a double-row M-22 bolt arrangement along the line of action of a shearing force [9]. The distance L between the bolts is 75 mm ($L \approx 3.5d_0$).

From measurements made in shift-resistant joints and riveted joints, the maximum amount of displacement in the middle zone of the joint is taken to be 0.005 mm. The friction force is calculated by the formula

$$T = \sum_{i=1}^{n} \tau_i \Delta A_r = \sum_{i=1}^{n} f\sigma_{iz}\Delta A_c$$

here σ_{iz} is the contour pressure determined by superposition of two solutions: 1—the contour pressure arising from the actual bolt tightening force [11], and 2—the contour pressure from the extension of the component being connected [26]; to put it another way, this is a problem of two-dimensional deformation, in which two cases are considered: (a) a restricted width of the strap, and (b) the influence of a next hole.

The distribution of the nominal pressure over the contact area is shown in Fig. 26.7. The average value of pressure is taken to be effective across the sections between the curves, and the needed area is measured with a planimeter.

The coefficient of friction is calculated for plastic contact at an elementary small-size spot (see Table 26.1); the data adopted for the calculation are: $f_m = 0.14$; the surface roughness parameters found from surface profile graphs: $R_{\max} = 37$ μm; $b = 25$; $r = 311$ μm, and $v = 3.2$.
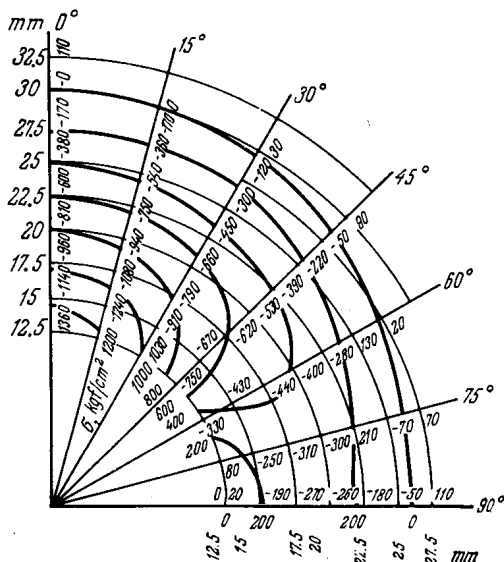
Fig. 26.7. Distribution of normal stresses around hole in contact area

The design value of the friction force is assumed to be its largest value among the values determined for each bolt arrangement times a coefficient equal to 1.35.

The friction force will be a function of two parameters p_t and p_w (p_t is an acting specific force exerted by the clamping bolt at the boundary of the joint being tightened, p_w is the force related to the weakened section of the component at the extreme row of bolts).

Since the friction force T defining the limiting condition is a constant, we can obtain the values of either of the parameters p_w (p_t) by specifying various values of the other parameter. A relationship between p_w and p_t is presented graphically in Fig. 26.8.

With the values of p_w and p_t being found experimentally we can determine the force limits by interpolation (Fig. 26.9):

$$P_l = 38 + (40 - 38) \frac{90}{140} = 39.28 \text{ tf}$$

The described calculation has revealed the following character of performance of shift-resistant joints:

(1) A non-uniform distribution of forces between bolts located along the line of action of the load has a considerable effect on both load-carrying capacity and deformation; for instance, double-row joints have on average a 30 percent higher load-carrying capacity than joints with bolts disposed along the line of action of the load, and their deformation is smaller by a factor of 1.5 to 2.0.

157

Hence, the development of multi-bolt shift-resistant joints should not be directed towards reduction in the number of rows through increase in the number of bolts in each row.
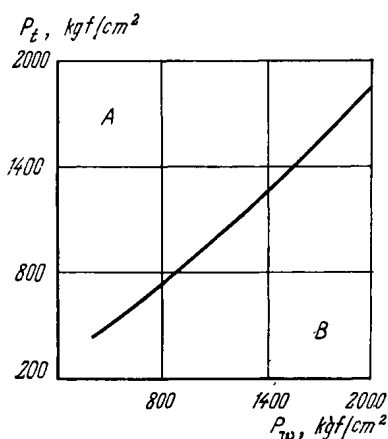

Fig. 26.8. Relationship between bolt tightening force and p_w under limiting conditions ($T = 13$ tons)

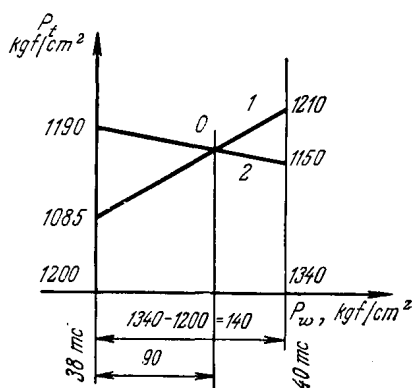A—region of small contact displacements; B—region of large displacements

Fig. 26.9. Finding limiting forces in contact area

1—by p_t-p_w diagram; 2—by table of experimental data

(2) A joint with the bolts spaced at 2.5 d_0 along and across the action of load (65 × 65 mm) proves to be the most effective bolt arrangement. Here the weakening of the component being connected does not exceed 10 percent.

26.3. INTERFERENCE-FIT ASSEMBLIES

The strength of interference-fit assemblies is determined by frictional interaction of the surfaces in the region of preliminary displacement. The maximum loads that can be carried by this type of joints are limited by the magnitude of the incomplete static friction force.

Interference-fit assemblies are mainly calculated for shear strength by the coefficients of friction. Some joints in precision mechanisms, however, need to be calculated for elastic tangential displacements [24], because accumulated irreversible plastic displacements result in a loss of positioning accuracy. The use of keys cannot fully eliminate this defect.

Because of deformations of the mating parts proper, normal and tangential stresses are distributed non-uniformly, and deformation arises along the length of the assembly. The occurrence of local sliding is possible as well as elastic and plastic contact deformations, which is conducive to fretting corrosion of the materials.

The plastic contact regions determine the shock-absorbing capacity of the joint, particularly during the first application of load.

The effect of vibrations and repeated impact loading manifests itself in shifts of the components in the joint. Continual accumulation of plastic displacements leads to a gross shift, which amounts to hundredths of a millimeter and more. Afterwards the process of accumulation of micro-displacements repeats. The maximum amount of displacement before the gross shift corresponds to the amount of preliminary displacement, which can be found approximately by calculation (see Chapter 2).

Normal and tangential pressures in a press-fitted assembly can be calculated by the Lamet formula for elastic deformations [6, 17].

In force fitting, the surface irregularities are deformed plastically, which leads to the decrease in the mechanical component of the friction force.

The flattening of the irregularities is offset through an increase in the specified amount of interference by

$$u = 2 \left(K_{sh} Rz_{sh} + K_h Rz_h \right)$$

where K_{sh} and K_h are the coefficients allowing for the flattening of irregularities in the shaft and the hole, Rz_{sh} and Rz_h are the mean arithmetic values of irregularities of the shaft and hole surfaces.

The coefficients K_{sh} and K_h depend on the physico-mechanical properties of the materials, on the assembly method, and on the surface roughness.

Table 26.6

Coefficients allowing for crushing of asperities [5]

Material		Assembly	Disas-sembly	Machining method	Coeffi-cients	Value of K for interference, μm		
sleeve	shaft					20	40	60
Titanium OT4	Titanium OT4	Heating outer member	Split sleeve	Turning	K_{sh}, K_h	0.10	0.17	0.22
Steel 45	Bronze БрОцС 4-4-2.5				K_{sh} K_h	0.15 0.14	0.19 0.18	0.25 0.20
				Grinding	K_{sh} K_h	0.17 0.14	0.22 0.19	0.28 0.26
					K_{sh} K_h	0.40 0.34	0.58 0.45	0.65 0.55
Titanium OT4	Titanium	By pressure (with glyce-rine lubrica-tion)	By pres-sure	Turning	K_{sh}, K_h	0.30	0.40	0.50
					K_{sh}, K_h	0.25	0.38	0.50
Steel 45	Steel 45	By pressure (without lub-rication)			K_{sh} K_h	0.33 0.20	0.48 0.30	0.63 0.40
	Bronze БрОцС 4-4-2.5							

The values of K_{sh} and K_h for some press-fitted joints are given in Table 26.6 [5].

Approximate calculations may be made with the use of the relationship $u \approx 1.2\,(Rz_{sh} + Rz_h)$. The total interference in the fit

$$\delta = \delta_d + u$$

where δ_d is the design interference without regard to surface roughness.

The coefficient of friction for interference-fitted cylindrical parts symmetric about their axes is calculated by the formula

$$f = \frac{P}{p\pi DL}$$

where P is a pressing-in or a pressing-out force, p is pressure on the apparent area of contact, D and L are the nominal diameter and length of the mating surfaces, respectively.

Some values of the coefficient of static friction obtained experimentally are presented in Table 26.7. Under identical testing conditions, expansion fits (that is, interference fits produced by cooling

Table 26.7

Mean values of coefficients of friction in disassembly of press fits [8]

Diameter, mm	Length, mm	Mean amount of interference, mm	Material of		Contact pressure, kgf/cm²	Coefficient of friction in			
			sleeve	shaft		press fitting, with industrial oil	press fitting, dry	shrinkage fitting, dry	expansion fitting, dry
140	80	0.07–0.08	Steel 30, HB 174	Steel 30, HB 174	—	0.15	—	0.34	0.37
100		0.09–0.11			—	0.15	—	0.32	0.28
80	100	0.035–0.045	Steel 40, HB 192	Cast iron СЧ28-48, HB 212	224	0.14	—	0.28	0.21
40	50	0.027–0.033	Steel 40, HB 192	Bronze БрАЖ9-4 HB 138	329	0.11	—	—	0.27
50	60	0.025–0.035	Steel 50	Steel 50	383	0.18	—	—	0.35
			Same, coated, μm:						
			zinc, $h = 15$		388	—	0.53	—	0.69
			cadmium, $h = 15$		389	—	0.43	—	0.50
			copper, $h = 20$		388	—	0.48	—	0.61
			nickel, $h = 10$		391	—	0.73	—	0.51
			chromium, $h = 10$		384	—	0.82	—	0.45

Notes: 1. Mating surfaces machined to 0.63 to 1.25 μm Ra.
2. Mating surfaces ground. Disassembly in 48 h after assembly, displacement rate 2 mm/s.
3. Sleeve holes bored and subsequently reamed, shaft finish turned. Disassembly in 3 months after assembly; displacement rate 1.2 mm/s.

the inner component) have a 2.0 to 2.5 times the strength of forced fits and 1.10 to 1.15 times the strength of shrinkage fits (interference fits produced by heating the outer component).

Obtaining interference fits by cooling the inner component, which is a promising assembly method, is described in detail in [23].

An effective way of strengthening interference fits is electroplating. Electrodeposited coatings improve the resistance to the action of aggressive environments, and some coatings, for instance, zinc plating, increase the load-carrying capacity under cyclic loads.

During the pressing-in or pressing-out stroke, the coefficient of friction of these materials is, on the average, from 0.5 to 0.7 the start-up value. Nickel- and chromium-plated parts are an exception: they have roughly equal coefficients of friction at rest and in motion, and, after being taken apart, have deep scores. These problems are discussed in more detail in [8, 16].

Cathodic coatings, such as chromium plating, nickel plating, or copper plating, improve the load capacity of interference-fitted joints exposed to simultaneous action of variable loads and corrosive environments.

Induction hardening and roller burnishing increase the real area of contact, and so do soft coatings (for instance, indium plating, zinc plating, cadmium plating, and tin plating), because of their low yield point; in some cases this leads to rise in the coefficient of friction.

The use of lubricants in press-fitting results in more stable values of the coefficient of friction. To remove excessive amounts of lubricant and so to increase the coefficient of friction, longitudinal marks should be traced in the hole of the outer part [25]. In that work, the results are given of experiments which revealed the strength of a conical press fit with some types of lubricants.

Better resistance of surfaces to displacement is achieved by increasing the mechanical component of the coefficient of friction through the use of harder materials having coarser surface roughness with smaller peak curvature radii. The coarser roughness, however, impairs fatigue strength and reduces the real area of contact.

The strength of press fits can be substantially increased by cleaning the mating surfaces of dirt (oil and fat films, dust, etc.), which has a low resistance to displacement. Solvents can only remove adsorbed fatty films partially. A more effective means to this end is cleaning with glow discharge in a gas. Here the thickness of the oxide film emerging on the mating surfaces can also be controlled. The surface cleaning techniques are disclosed in [3]. Studies of a shrinkage fit with an interference ranging from 25 to 250 μm, conducted on specimens made from steel 45 (HRC 45 to 50), having a mating diameter of 90 mm and surface-roughness parameters of 0.16 to 0.32 μm Ra (on the shaft) and 0.63 to 1.25 μm Ra (in the sleeve) have shown that the glow-discharge treatment can increase the strength 2.5 to 2.8 times against conventional shrinkage fits.

The strength of force fits in vacuum without heating and glow-discharge cleaning is practically the same as in the atmosphere [3]. Preliminary heating up to 450°C in vacuum for one hour leads to a 3 to 3.5 times increase in strength of the fit.

Interference-fitted parts have increased fatigue strength, which is largely due to residual compressive stresses arising in their surface layers. The effectiveness of the strengthening of steel surfaces is discussed in [12].

Assembly of thin-walled sleeves by interference fits causes a change in the hole diameter; this change is vital for ensuring the functional properties of precision sliding bearings, guide sleeves, etc. The work [10] discloses a method of calculation of such joints on the basis of the theory of axially symmetric cylindrical shells. It also gives a comparative analysis of the effect of assembly methods on surface shape deviations in joints formed with sleeves from bronze БрОЦС5-5-5, pressed into a casing from steel 45 (the nominal diameter of test specimens was 68 mm, and the amount of interference, 12 to 50 μm). It was established experimentally that departure from the true longitudinal profile of press-fitted sleeves projecting beyond the housing is 1.2 times that of similar expansion-fitted sleeves.

In the course of pressing-in, stick-slip motion is frequently observed, which is due to self-sustained frictional relaxation oscillations. These oscillations emerge under the influence of static and kinetic frictional phenomena and could be predicted if the relationship were known between the coefficient of friction and the durability of short-time stationary contact. This problem is still to be studied [29]. To a first approximation, linear differential equations relating deformation to stress are used to characterize the rheological properties of a contact. For instance, one of the simplest solutions for the coefficient of friction has the form [14]

$$f = f_0 - (f_\infty - f_0) e^{-ut}$$

where t is time, f_0 is the coefficient of static friction with $t \to 0$, f_∞ is the coefficient of static friction with $t \to \infty$, and u is a rheological constant.

Any pair of materials requires experimental determination of the constants f_0, f_∞, and u.

26.4. SCREWED

ASSEMBLIES

Stable tightening of screwed joints is a means towards improving their service life.

Friction in screw thread is the main factor governing the tightening force. Insufficient tightening leads either to deterioration in functional properties of the joint (tightness, rigidity, etc.) or to

loosening under the action of vibrations and variable loads. Excessive tightening results in breakages or jamming in the thread.

Screw fasteners—bolts, screws, studs, and nuts—are mainly produced from carbon and alloyed steels (except Bessemer steels), whose mechanical properties are specified by GOST 1759-70*. The general data on fastener materials are given in [7].

Thermosetting plastics are promising as materials for nuts, particularly those intended for use in variable-load conditions [22].

Screwed assemblies designed for severe-condition applications, namely at high temperatures or in aggressive environments, are made from special steels and non-ferrous alloys. Nuts produced from bronze and pearlitic cast iron provide stable service without jamming at temperatures up to 500°C.

It should be noted that at high temperatures studs made from heat-resistant materials make for a reduction in creep of the assembly by a factor of 5 as compared with studs made from conventional steels, and a similar substitution in nuts reduces the creep by 20 percent [22].

Protection of fasteners from scoring and stabilization of the coefficient of friction are achieved by applying coats according to GOST 1759-70*. The type of coating and its thickness for a specific material are recommended by GOST 14623-69.

The allowable limits of operating temperatures for some coatings and lubricants are given in Table 26.8.

Table 26.8

Allowable temperature limit ϑ_{max} for thread-fastener coatings and lubricants [27]

Coating or lubricant	ϑ_{max} °C
Electrodeposited platings:	
Cd	321
Zn	419
Bi	269
Pb	327
Cu	600
Ag	700
Brass plating (by rubbing in)	450
Electroless nickel coating	900
Lubricants:	
MoS$_2$	250
Fatty	400
Chalky*1	600
ЖС*2	600

*1 Mixture of chalk and transformer oil.
*2 Mixture of 2 parts of cylinder oil 52 and 3 parts of lead carbonate.
Notes: 1. At high temperatures, bolts electroplated with soft metals break owing to reduction in strength caused by adsorption (Rebinder's effect).
2. Use of electroless nickel coatings is limited by prohibitive cost (3 times as high as electroplating costs).

The axial tightening force Q and the wrench torque are related by the expression

$$M = Q \left(f_{th} \frac{d}{2} + f_{br} R_{br} \right)$$

where f_{th} is the effective coefficient of friction in the thread, f_{br} is the effective coefficient of friction on the bearing surface, d is the mean diameter, and R_{br} is the radius of friction of the bearing surface.

For calculation of the frictional moment, it is necessary to know the coefficient of friction. The stability of tightening is practically a matter of stable coefficient of friction since the provision of the specified moment with a torque measuring wrench or a power-operated hand tool presents no difficulty.

The calculation is made with the effective coefficient of friction which allows for the half-included angle α of thread:

$$f_{th} = \frac{f}{\cos \alpha/2}$$

The effect of the helix angle may be ignored for practical purposes.

The mean value of the coefficient of friction in the thread may only be used for approximate calculation of the tightening moment because f depends on load which is distributed non-uniformly among separate threads.

The mean pressure on the active flanks of the thread is determined by the formula

$$p = \frac{Q}{\frac{\pi}{4} (d^2 - d_1^2) n_{th}}$$

where d and d_1 are the outside diameter of bolt thread and the inside diameter of nut thread, respectively, n_{th} is the number of threads.

In finding pressure on each thread, the distribution of load among all the threads should be taken into consideration [7].

Tube fittings make use of screwed connections with plastic union nuts. The values of the effective coefficient of friction for such nuts, which were obtained on M48 $\times$ 22 specimens with a surface roughness of 0.8 to 0.16 μm Rz in unlubricated conditions at $+22°C$, are indicated in [18].

For metric threads, the effective values of the coefficient of friction with various coatings and lubricants are presented in Table 26.9, and the mean values for some materials are given in [4, 18].

Under boundary-friction conditions the coefficient of friction is stable and is, as a rule, equal to 0.11 for most lubricants. Considerable variations of the coefficient of friction in lubricated joints are due to disruption of the lubricant film and formation of dry-

Table 26.9

Coefficients of friction in screw thread for various coatings and lubricants [21]

Screw and nut coatings		Dry	Lubricated		
			Oil И-8A	Solid oil	Oil И-8A with additive 20% MoS$_2$
No coating	f_{th}	$0.40^{+0.12}_{-0.08}$	$0.21^{+0.13}_{-0.02}$	$0.19^{+0.02}_{-0.03}$	$0.13^{+0.02}_{-0.02}$
	f_{br}	$0.20^{+0.04}_{-0.06}$	$0.12^{+0.02}_{-0.02}$	$0.13^{+0.01}_{-0.02}$	$0.09^{+0.01}_{-0.02}$
Black oxide coating	f_{th}	$0.64^{+0.20}_{-0.14}$	$0.45^{+0.06}_{-0.05}$	$0.44^{+0.05}_{-0.07}$	$0.18^{+0.03}_{-0.03}$
	f_{br}	$0.34^{+0.09}_{-0.14}$	$0.26^{+0.03}_{-0.07}$	$0.26^{+0.03}_{-0.07}$	$0.09^{+0.02}_{-0.02}$
Zinc coating	f_{th}	$0.40^{+0.08}_{-0.16}$	$0.19^{+0.01}_{-0.04}$	$0.17^{+0.02}_{-0.03}$	$0.17^{+0.02}_{-0.03}$
	f_{br}	$0.09^{+0.01}_{-0.02}$	$0.10^{+0.20}_{-0.01}$	$0.09^{+0.02}_{-0.01}$	$0.08^{+0.01}_{-0.02}$
Phosphate coating	f_{th}	$0.20^{+0.03}_{-0.05}$	$0.18^{+0.02}_{-0.03}$	$0.17^{+0.02}_{-0.02}$	$0.16^{+0.01}_{-0.02}$
	f_{br}	$0.10^{+0.02}_{-0.01}$	$0.11^{+0.02}_{-0.01}$	$0.11^{+0.02}_{-0.02}$	$0.09^{+0.01}_{-0.02}$
Cadmium coating	f_{th}	$0.29^{+0.03}_{-0.05}$	$0.21^{+0.04}_{-0.06}$	$0.18^{+0.04}_{-0.03}$	$0.14^{+0.01}_{-0.03}$
	f_{br}	$0.17^{+0.07}_{-0.05}$	$0.11^{+0.04}_{-0.06}$	$0.11^{+0.02}_{-0.06}$	$0.06^{+0.01}_{-0.02}$

friction areas. The rubbing of seizure-prone materials, for instance, titanium alloys, involves in such conditions very high values of the coefficient of friction [7].

The temperature resistance of lubricant films plays an important part because the film load capacity decreases with rising temperature.

In operation, the tightening force on the bolt tends to diminish for the following reasons:

—stresses become relaxed predominantly in the bolt, and, to a lesser extent, in the nut, particularly at elevated temperatures;

—the amount of approach changes in all contact areas, that is, in intermediate joint faces (between the bolt head, the nut, and the respective bearing surfaces on the fastened components) and in the thread itself.

The relaxation of stresses is much lower in the bolt body than in the intermediate joint faces* and thread, especially in the first threads.

The rheological effect in threaded assemblies can be minimized by improving the quality of screw fasteners; specifically, higher-grade, heat-treated or strain-hardened steels machined to better surface finish should be substituted for low-carbon steels Grades 10 and 15.

Periodic tightening of screw-fasteners in service is essential if increase in clearances and wear of assemblies are to be prevented.

Variable loads cause periodic radial deformations of the nut and bolt and, thereby, can result in the loosened fastening. Vibrations can also make the nuts work loose because in this case the value of the coefficient of friction drops sharply (down to 80 percent) and is difficult to control. For this reason, the locking of nuts exposed to vibration is mandatory. Methods and means for preventing nuts from loosening are discussed in detail in [7].

The torquing speed has a marked effect on the coefficient of friction. Reduced torquing speeds and increased axial loads can give rise to frictional relaxation fluctuations during tightening. Therefore the dynamic action of power-operated nutrunners needs to be taken into account (Table 26.10).

Table 26.10

Data on relative non-uniformity of tightening effected by various power-operated nutrunners (after Tchen-Bao-Din)

Type of nutrunner	Tightening one threaded joint (5 measurements)	Tightening a number of threaded joints (50-100 measurements)
With motor stopped upon tightening	$\pm 0.08-0.11$	± 0.25
With overload clutch:		
claw-type	± 0.16	—
friction-type	$\pm 0.01-0.10$	$\pm 0.16-0.19$
With impact-type torque converter	± 0.18	$\pm 0.40*$

* With allowance for variation of clearance between nutrunner socket and nut (25 measurements).

Example 3. A flanged fitting of parts made from steel 10X11H20T3P is tightened with bolts M10 × 1.5 by a force of 500 kgf. Nuts are produced from titanium BT1. Determine the required tightening torque.

The *basic data* are as follows:

The dimensions of the thread: $d_0 = 10$ mm, $d = 8$ mm, $s = 1.5$ mm, $\alpha = 60°$, $t_1 = 1$ mm, and $D_1 = 17$ mm.

Mechanical properties of steel 10X11H20T3P: $E = 2 \times 10^4$ kgf/mm²; HV 330. The steel has a high resistance to relaxation and high hardness as com-

* The relaxation of stresses in the real areas of contact.

pared with titanium BT1, and so is regarded as absolutely rigid for the calcula-
tion purposes. Titanium BT1 has HB 120.

For the titanium-steel pair: $\tau_0 = 18$ kgf/mm^2, $\beta = 0.08$.

The flange is machined by turning; its surface roughness is 0.63 to 1.25 μm
Ra, $r = 90$ μm, $v = 1.8$, $b = 1.8$, $R_{max} = 9.4$ μm, and $\Delta = 0.075$.

For the bolt, the surface roughness is 0.32 to 0.63 μm Ra (cylindrical grind-
ing), $r = 15$ μm, $v = 1.95$, $b = 0.9$, $R_{max} = 4.7$ μm, and $\Delta = 0.33$.

For the nut, the surface roughness is 0.08 to 0.16 μm Ra.

Solution. We calculate the normal pressure on each thread by the specified
percentage distribution of load among the threads. The results of the calculation
are listed in Table 26.11. The calculation is made for the first six most loaded
threads.

Table 26.11

Results of calculation of friction moment in screw thread

Parameters	Number of thread						Remain-ing
	1	2	3	4	5	6	
Load on one thread, %	33	23	16	12	8	6	2
W_i, kgf	165	115	80	60	40	30	10
p_i, kgf/mm^2	5.84	4.07	2.83	2.12	1.41	1.06	—
f_i	0.37	0.35	0.34	0.33	0.32	0.32	0.23
$f_{eff.\,i}$	0.43	0.41	0.40	0.38	0.37	0.37	0.27
M_i, kgf mm	319	210	143	102	66	50	12

The coefficient of friction for each of the threads

$$f = \frac{\tau_0}{HB} + \beta + 0.5\Delta^{1/2}\left(\frac{p_{ci}}{HB}\right)^{1/4}$$

where $\Delta = 0.33$ is the surface roughness parameter (the value of Δ for the harder
component, the bolt, is taken for the calculation), HB is the hardness of the
softer material (BT1).

The effective coefficient of friction

$$f_{th} = \frac{f}{\cos \alpha/2}$$

The frictional torque on each of the threads

$$M_{thi} = f_{thi} Q_i \frac{d_0 + d}{4}$$

the total frictional torque

$$M_{th} = \sum_{i=1}^{n} M_{thi} = 902 \text{ kgf mm}$$

The normal pressure between the flange and the nut

$$p = \frac{Q}{\frac{\pi}{4}(D^2 - d^2)} = 3.35 \text{ kgf/mm}^2$$

The coefficient of friction $f_{br} = 0.29$.

The frictional torque between the nut face and the flange

$$M_{br} = Q f_{br} \frac{D + d_0}{4} = 970 \text{ kgf mm}$$

The tightening torque

$$M = M_{th} + M_{br} = 1\,872 \text{ kgf mm}$$

REFERENCES

1. Алисин В. В., Комбалов В. С. Учет волнистости поверхностей при расчете площадей касания.—«Надежность и контроль качества», 1975, № 8, с. 38—48.
2. Алисин В. В., Михин Н. М. Прибор для испытания на длительную твердость.—«Заводская лаборатория», 1973, № 7, с. 879—880.
3. Андреев Г. Я., Тихонов В. Ф., Арпентьев Б. М. Прочность тепловых посадок с воздействием тлеющего разряда.—«Известия вузов. Машиностроение», 1976, № 3, с. 41—44.
4. Антифрикционные свойства смазок для резьбовых соединений из нержавеющих сталей.—«Вестник машиностроения», 1974, № 1, с. 29—31. Авт.: В. И. Змиевский, Е. П. Замилацкий, В. С. Привезенцева, Н. Н. Голего, Ю. И. Русинович, Г. Г. Кузнецов.
5. Бежелукова Е. Ф., Курносов Н. Е., Моисеев В. Б. Изменение высоты неровностей при сборке соединений с натягом.—«Вестник машиностроения», 1976, № 4, с. 73—75.
6. Берникер Е. И. Посадки с натягом в машиностроении. Справочное пособие. М.— Л., «Машиностроение», 1966, 167 с.
7. Биргер И. А., Иосилевич Г. Б. Резьбовые соединения. М., «Машиностроение», 1973, 256 с.
8. Бобровников Г. А. Прочность посадок, осуществляемых с применением холода. Изд. 2-е. М., «Машиностроение», 1971, 95 с.
9. Гек А. М., Чернашкин В. Г. Определение предельного состояния сдвигоустойчивых соединений. Влияние размещения болтов и толщин накладок в соединении на наступление предельного состояния.—«Строительство и архитектура», 1974, разд. Б, вып. 9, 5 с.
10. Дальский А. М., Серенко В. А. Изменение размеров отверстий тонкостенных втулок при сборке с натягом.—«Вестник машиностроения», 1976, № 4, с. 71—73.
11. Данилов В. К. О напряжениях и деформациях в деталях затянутого болтового соединения.—«Вестник машиностроения», 1958, № 7, с. 41.
12. Кобрин М. М. Прочность прессовых соединений при повторно-переменной нагрузке. М., Машгиз, 1954, 203 с.
13. Ковнеристов Г. Б., Крыженков Ю. А. Теоретико-экспериментальное исследование контакта по консольной плите.— В сб.: Сопротивление материалов и теория сооружений. Вып. XXVI. Киев, «Строитель», 1975, с. 82—87.
14. Крагельский И. В. Трение и износ. М., «Машиностроение», 1968, 480 с.
15. Крагельский И. В., Алисин В. В. Расчетный метод оценки трения и износа — эффективный путь повышения надежности и долговечности машин. М., «Знание», 1976, 55 с.
16. Лукашевич Г. И. Прочность прессовых соединений с гальваническими покрытиями. Киев, Гостехиздат УССР, 1961, 61 с.
17. Машиностроение. Энциклопедический справочник. т. 2, Под ред. М. А. Саверина. М., Машгиз, 1948, с. 163—176.
18. Менч В. В., Стрижак В. И. Исследование трения в пластмассовом резьбовом соединении.—«Труды Таллинского политехн. ин-та», 1971, сер. А, № 306, с. 113—118.

19. Михин Н. М., Алисин В. В. Метод определения показателей кривой опорной поверхности по зависимости сближения от нагрузки при пластическом контакте.—«Известия вузов. Машиностроение», 1972, № 8, с. 15—19.
20. Михин Н. М., Алисин В. В. Исследование зависимости коэффициентов трения покоя от нагрузки.—«Известия вузов. Машиностроение», 1974, № 2, с. 65—69.
21. Нормирование затяжки резьбовых соединений по величине крутящего момента. Методические указания. М., ВНИИМАШ, 1973, с. 7.
22. Повышение надежности и долговечности резьбовых соединений (подборка статей).—«Вестник машиностроения», 1968, № 10, с. 38—54.
23. Рекомендации по применению охлаждения деталей перед запрессовкой. М., Оргстанкинпром. 1972, 46 с.
24. Решетов Д. Н., Кирсанова В. Н. Касательная контактная податливость деталей.—«Машиноведение», 1970, № 2, с. 88—101.
25. Рохлин А. Г. Влияние смазки на прочность конической прессовой посадки.—«Труды Ленинградского кораблестроительного института». Вып. X. Судостроение и судовое машиностроение. Л., Ленинград. корабл. ин-та, 1962, с. 97—107.
26. Савин Г. Н. Распределение напряжений около отверстий. Киев, «Наукова думка», 1968, 887 с.
27. Финкильштейн Г. М. Устранение заедания резьбовых соединений, работающих при температурах до 700° С.—«Вестник машиностроения», 1964, № 2, с. 19—23.
28. Чесноков А. С., Княжев А. Р. Сдвигоустойчивые соединения на высокопрочных болтах. М., Стройиздат, 1974, 120 с.
29. Iones I. R. A study of stick-slip under Press Conditioning Lubrication Engineering. 1967, vol. 23, No. 10, p. 408-414.

FRICTION AND WEAR
OF VEHICLE WHEELS

27.1. TERMS AND DEFINITIONS

The adhesion coefficient, ψ, is the ratio of the static friction force to the normal component of external forces acting on the body surface or the ratio of the maximum reaction T_{max} in the contact area to the normal reaction N acting on the wheel [5]:

$$\psi = \frac{T_{max}}{N} = \frac{M_\psi}{r_d N}$$

where M is the moment of adhesive friction of the wheel on the road; r_d is the dynamic radius (distance from the wheel axis to the horizontal plane passing through the resultant of the tangential reactions in the contact area).

The adhesion coefficient of a pneumatic tyre on a bearing surface depends on the material and condition of the rubbing surfaces, on the vehicle's speed of motion, on the wheel sliding speed, on the type of wheel drive, and on the wheel-suspension characteristics.

With regard to the external forces acting on the wheel, distinction is made between the longitudinal and the lateral adhesion coefficient.

The longitudinal forces cause either pure or partial sliding of wheels. The resistance to the lateral forces acting in a perpendicular direction to the wheel plane allows the vehicle to withstand centrifugal forces arising at bent road sections.

Specific adhesion coefficients may be introduced for rolling without slipping or sliding, for longitudinal slipping or skidding, and for lateral sliding of the wheel.

27.2. ADHESIVE FRICTION
OF PNEUMATIC TYRE ON ROAD

To calculate the adhesion coefficient, it is essential to know the static force of friction of the tyre on the road and the load exerted on the tyre. As shown in Chapter 2, the static frictional force depends in this case on the roughness and waviness of the roadway and its state (type of covering, dirtiness, moisture, etc.), on the physico-

mechanical properties of tread material (for instance, elastic modulus or the coefficient of the rubber's hysteresis losses), and on tread pattern and tyre design.

The tread pattern is vital to the performance of the automobile tyre. Its main purpose is to remove moisture from the real area of contact between the tread surface and the road and thus to increase
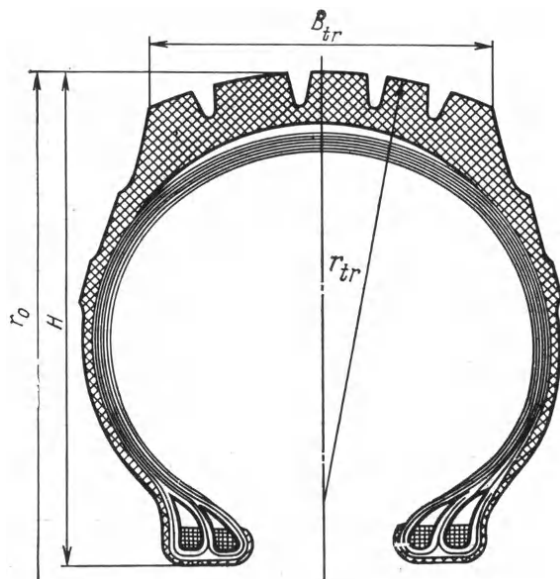
Fig. 27.1. A radial sectional view of tyre
H—depth of tread profile; B_{tr} — width of tread; r_{tr} — cross-sectional view of tread; r_0 — tyre radius

the molecular component of the force of adhesion of the wheel to the road.

All these factors affect the real pressure in the areas of micro-contacts, which is a function of the contour pressure.

The magnitude of stresses and the character of their distribution over the contact area of the tyre rolling on a solid surface are influenced by the tyre design, the tread pattern, the vertical load, the torsional or braking moment, the lateral force acting on the wheel, and the tyre inflation pressure.

The main dimensions of an automobile tyre are shown in Fig. 27.1.

27.3. CALCULATION
OF ADHESION COEFFICIENT
FOR PNEUMATIC TYRES

Analysis of the interaction between the tyre and the road shows that the adhesion of the tyre largely depends on the type of road covering, the design of the tyre and the inflation pressure, the

material and pattern of the tread, and the speed of the vehicle motion
The values of the adhesion coefficient as related to the type and
condition of road covering are given in Table 27.1 [17].

**Values of adhesion coefficient for tyres depending on type and state
of road covering**

Road covering		Adhesion coefficient		
type	condition	high-infla-tion-pressure tyres	low-infla-tion-pressure tyres	off-highway tyres
Asphalt	Dry	0.50-0.70	0.70-0.80	0.70-0.80
	Wet	0.35-0.45	0.45-0.55	0.50-0.60
Cobble-stone	Muddy	0.25-0.45	0.25-0.40	0.25-0.45
	Dry	0.40-0.50	0.50-0.55	0.60-0.70
Crushed rock	Dry	0.50-0.60	0.60-0.70	0.60-0.70
	Wet	0.30-0.40	0.40-0.50	0.40-0.55
End-grain wood blocks	Dry	0.50-0.70	0.60-0.70	0.60-0.70
	Wet	0.30-0.40	0.40-0.50	0.50-0.60
Dirt road	Dry	0.40-0.50	0.50-0.60	0.50-0.60
	Rain-wet	0.20-0.40	0.30-0.45	0.35-0.50
	Sloppy	0.15-0.25	0.15-0.25	0.20-0.30
Virgin soil: sand	Dry	0.20-0.30	0.22-0.40	0.20-0.30
	Wet	0.35-0.40	0.40-0.50	0.40-0.50
loam	Dry	0.40-0.50	0.45-0.55	0.40-0.50
	Wetted to plastic state	0.20-0.40	0.25-0.40	0.30-0.45
	Wetted to sloppy state	0.15-0.20	0.15-0.25	0.15-0.25
snow	Soft	0.20-0.30	0.20-0.40	0.20-0.40
	Compacted	0.15-0.20	0.20-0.25	0.30-0.50
Icy road and smooth ice	Air temperature below 0°C	0.08-0.15	0.10-0.20	0.05-0.10

A diagram of forces and moments acting on the elastic driving
wheel being in motion at a speed v is shown in Fig. 27.2, and a similar
diagram for the wheel in the process of braking is shown in Fig. 27.3.

The designations are: G_{wh} is the radial load, P_{wh} is the traction force applied to the wheel axle; X is the horizontal reaction in the road plane; Z is the vertical reaction; M_t is the torsional moment; a is the lever-arm of the force; r_d is the dynamic radius of the wheel. The tyre is also loaded by the inflation pressure.

The action of the applied forces and moments results in deformation of the tyre.

The peripheral compression of the tread in the driving wheel occurs at the section A-1-2-3-IV, and the restoration occurs at the section 4-5-6. With the wheel being braked, the tyre is compressed
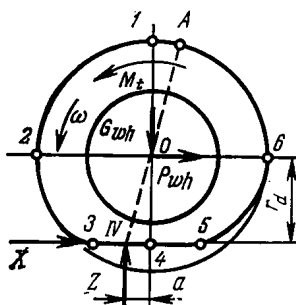
Fig. 27.2. Forces acting on driving wheel
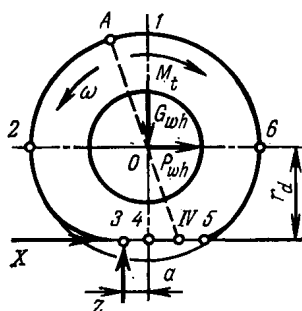
Fig. 27.3. Forces acting on braked wheel

at the section A-2-3-IV. Transition from the expanded to compressed tread portions takes place at the rear part of the contact area, 4-5. The actual load causes deflection of the tyre and formation of the contact area between the tyre and the road, that is, the contour area of contact (section 3-5 in Figs. 27.2 and 27.3). The magnitude of deflection $h = r_0 - r_d$, where r_0—wheel radius corresponding to the tread radius in the wheel free from external load.

With small magnitudes of h, the contour area of contact has the form of an ellipse [14], and with large magnitudes, it is close to a rectangle.

The magnitude of deflection is determined from the equation [2]

$$h^2 - \alpha_2 \frac{hG_{wh}}{p_w + p_0} - \alpha_1 G_{wh} = 0 \qquad (27.1)$$

where p_w is the inflation pressure; p_0 is the stiffness of the tyre casing; α_1 is the constant (with tyres for lorries $\alpha_1 \approx 0.0022$ cm²/kgf, and for cars, $\alpha_1 = 0.0037$ cm²/kgf); $\alpha_2 = \dfrac{1}{2\pi \sqrt{r_0 r_{tr}}}$; here r_{tr} is the transverse curvature radius of tread.

The adhesion force depends on the normal stresses arising in the contour area of contact.

Experiments [14, 17] have shown that these stresses are distributed non-uniformly (Fig. 27.4).

In a longitudinal section *a-a*, the diagram of distribution of normal stresses has a trapezoidal outline for car tyres and low-pressure lorry tyres. For high-pressure tyres, a parabolic law of normal-pressure variation takes place at some distance from the longitudinal symmetry axis.

In a cross-section *b-b*, the normal stresses have two points of maximum. Here, the diagram of stresses is symmetric about the contact-area centre. In the *e-e* plane disposed at some distance from the *b-b* section, the variation of normal stresses is characterized by a single maximum.

The non-uniformity of normal pressure distribution in the contact area across the tread is caused by dissimilar radial stiffness of the tyre in various longitudinal sections and by the effect of tread pattern.

Fig. 27.4. Distribution of pressure at contact of tyre with road

In stationary contact of the tyre with a hard road covering, the normal contact pressure (contour pressure) will be

$$p_c = \frac{1}{k'} \left[p_w \left(1 - 2 \frac{r'}{B_{tr}} \cos m\alpha \cos \beta \right) + q_{df} \right]$$

where k' is the coefficient of density of the tread pattern (Table 27.2); r' is the radius of the deformed casing ply; B_{tr} is the tread width; α is the angle of ply's deviation (Fig. 27.5a); $m > 1$ is the coefficient allowing for flexibility of rubber at the tread shoulders; β is the angle of ply's inclination to the radius (Fig. 27.5b); q_{df} is the contact pressures resulting from the tyre casing deflection.

As the automobile moves, the stress diagram in a longitudinal section changes, taking a trapezoidal form, with the upper base somewhat inclined to the lower base. The normal stresses are somewhat higher at the inlet than at the outlet of the contact (Fig. 27.6), the difference growing with the speed of motion. This character of variation of the stresses is due to hysteresis losses during deformation of the tyre in the contact area. This variation is especially notable at speeds over 100 km/h because of the action of dynamic forces. Thus, the normal stresses in the area of contact of the tyre

174

Table 27.2

Tread patterns for tyres of cars and lorries
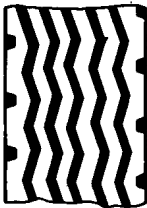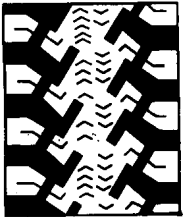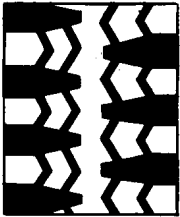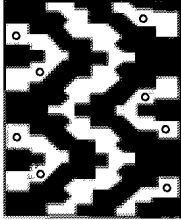
Car	Lorry	Coefficient of density of tread pattern, %	Application
Highway pattern		65-80	For roads with improved covering. Provides good adhesion and balance in longitudinal and transverse directions
Universal pattern		55-60	For hard-covering roads
Off-highway pattern		40-50	For off-highway use*

175

Table 27.2 (continued)

Car	Lorry	Coefficient of density of tread pattern, %	Application
Winter pattern		55-60	For slippery and icy roads

* Use on hard-covering roads shortens service life and impairs car balance.

with the road are distributed non-uniformly, and the character of their variation is rather complex. The torsional and braking moments applied to the wheel cause the diagram of the normal contact stresses
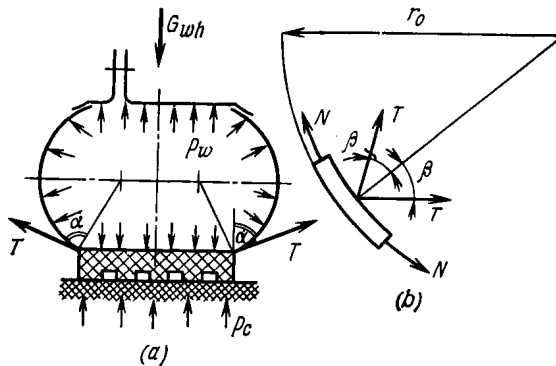
Fig. 27.5. Tyre cross section under the action of normal load G_{wh} (a); equilibrium of peripheral element of tyre model under the action of inflation pressure p_w; N—peripheral forces; T—ply tension forces (b)

vary. According to data in [17], however, this variation is insignificant. For this reason, the adhesion coefficient is normally estimated by the mean contact stresses. These stresses depend on the design of the tyre and its inflation pressure. They can be higher than, equal to, or lower than the inflation pressure p_w [17].

Distinction is made between the mean normal contact stresses (mean pressures) $p_m = \dfrac{G_n}{F_0}$, where F_0 = total contact area under the load G_n, and the real mean contact pressures (contour pressure)

$$p_c = \frac{G_n}{A_c}$$

where A_c is the contour area of contact of the tyre with the road with allowance for the tread pattern. The outline of this area is
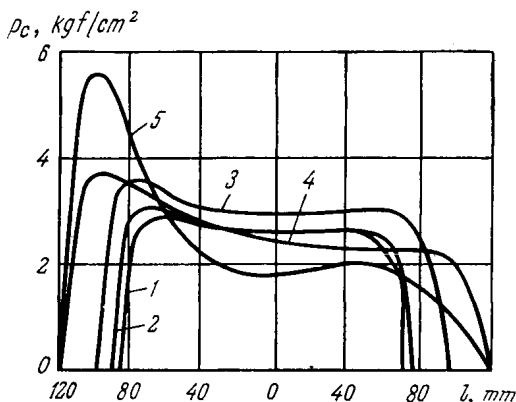
Fig. 27.6. Distribution of pressure at contact of Mod. 7.50-16 tyre. Curves *1*, *2*, *3*, *4* and *5* stand for pressures in the direction of motion at speeds of 25, 50, 100, 150, and 180 km/h [17]

close to a rectangle with a width equal to the tread width B_t and a length

$$l = 2 \sqrt{2Rh - h^2} \approx 2\sqrt{2r_0 h}$$

times the coefficient k' of density of the tread pattern. From the equation (27.1) it follows that

$$h \approx \frac{\alpha_2 G_{wh}}{2p_w} + \sqrt{\left(\frac{\alpha_2 G_{wh}}{2p_w}\right)^2 - \alpha_1 G_{wh}}$$

Hence, the contour area of contact and the mean contour pressure will be

$$A_c = k'B_{tr}l = 2k'B_{tr}\left\{ r_0 \left[\frac{\alpha_2 G_{wh} + (\alpha_2^2 G_{wh}^2 - 4\alpha_1 p_w^2 G_{wh})^{1/2}}{p_w}\right]\right\}^{1/2} \qquad (27.2)$$

$$p_c = \frac{p_w^{1/2} G_{wh}^{1/2}}{2k'B_{tr}r_0^{1/2}\alpha_2^{1/2}\left[1 + \left(1 - \dfrac{4\alpha_1 p_w^2}{\alpha_2^2 G_{wh}}\right)^{1/2}\right]^{1/2}} \qquad (27.3)$$

Thus, both mean contour pressures and contour area of contact will be determined by the load acting on the wheel, by the tyre design characteristics (wheel radius, tread width and curvature radius, tread pattern, coefficient α_1), and by the inflation pressure p_w. As follows from [17], the mean contour pressures with the tyres of lorries can be lower at rated loads than the inflation pressure. The ratio of the mean contour pressure to the inflation pressure will then depend on the magnitude of the latter and the load on the wheel.
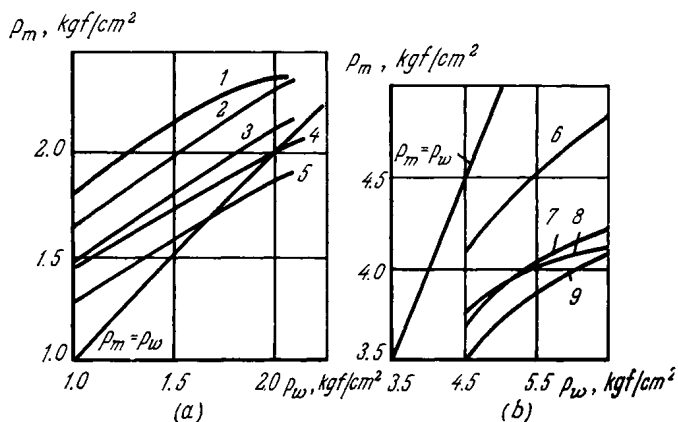
Fig. 27.7. Relationship between mean contact pressure and inflation pressure p_w
(a) low-pressure tyre; (b) high-pressure tyre; 1—5.60-15; M59-A; 2—175-15; Я-26ОР; 3—155-15; M-122P; 4—6.70-15; И-194; 5—155-15; M-83РС; 6—260-20; И-231; 7—260-20; И-203; 8—260-20; И-202; 8—260-20; И-230

A reduced inflation pressure and increased load will result in a growth of the mean contour pressure in excess of the inflation pressure. The relationship between the mean contact pressure (that is, the pressure calculated without account of the tread pattern) and the pressure at a normal load on the wheel is shown in Fig. 27.7 for different makes of tyres according to [17]. From Fig. 27.7 it follows that the mean pressure is as a rule lower than the inflation pressure; however, the contour pressures will exceed the mean value $1/k'$ times, where $k' < 1$ is the coefficient of density of tread pattern.

The real contact of tyre with road occurs at separate spots within the contour area of contact, which is clearly seen in Fig. 27.8.

The tangential contact stresses have a great effect on wear and should accordingly be taken into account in the tyre wear calculations. By the tangential stresses are meant those acting over the contour area of contact, that is, on the tread outer surface in the contact region. These stresses arise from the deformation of the tyre caused by radial load, from the torsional and braking moments developed by the tyre, from the lateral force and the forces resistant to rolling, and from the forces caused by differing angular speeds of an elementary tread portion in the contact zone and outside it.

Like the normal stresses, the tangential stresses are usually considered in two mutually perpendicular longitudinal and transverse sections of the contact area.

The tangential stresses in a longitudinal section

$$\tau_{ln} = \tau_{df} + \tau_{in} + \tau_{out} \pm \Delta\tau_m$$

These stresses result from the deformation of the tyre (τ_{df}), from the resistance to rolling in the contact area (τ_{in}) and outside it
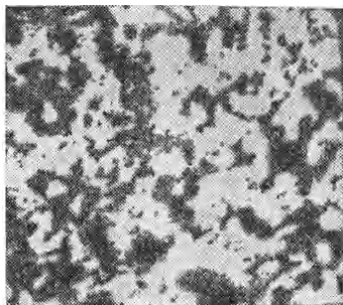
Fig. 27.8. Impression of real area of contact (white spots) between rubber and concrete road covering ($\times 5$)
$E = 30$ kgf/cm²; $p_w = 4$ kgf/cm²; $k' = 55\%$

(τ_{out}), and from the transmitted torsional or braking moment $\Delta\tau_m$, the sign "+" denoting the torsional moment and "—", the braking moment.

At speeds about 80 km/h, the tangential stresses caused by the resistance to rolling, accounting for 2 to 3 percent of the total tangential-stress magnitude, can be neglected in the calculation.

The resultant tangential stresses in a longitudinal section of the contact area due to tyre deformation under radial load (for the stationary wheel see Fig. 27.9c) and due to non-uniform angular speeds of tread elements in the contact area (for the driven wheel) are distributed according to a sinusoidal law (Fig. 27.9b). The magnitudes of tangential stresses τ_{df} and τ_{out} over an arbitrary elementary area in a longitudinal section can be found from the following approximate relationships:

$$\tau_{df} = A \left[\arcsin \left(\cos \frac{\varphi_c}{2} \tan \varphi_i \right) - \varphi_i \right]$$

$$\tau_{out} = 0.5A \left(\frac{\varphi_i}{\varphi_c} \sin \varphi_c - 0.5 \sin \varphi_i \right)$$

where A is the coefficient allowing for the tyre tangential stiffness (kgf/cm²); φ_c is the contact angle of the tyre (Fig. 27.9); φ_i is the current value of the contact angle. The torsional and braking moments originate additional tangential stresses, which are distributed over the contact area in accordance with a triangular function as shown in Fig. 27.9d (1 and 2).

The magnitude of these additional stresses is

$$\Delta\tau_m = \frac{T_M}{A_c} \left(1 - \frac{2\varphi_i}{\varphi_c} \right)$$

where T_M is the pulling or braking force. The magnitude and character of distribution of the resultant tangential stresses in a cross section of the tyre depend on its design, inflation pressure, radial load, and specific forces of adhesion to the road. These stresses cause local sliding of tread elements on the road surface.

The distribution of τ_m in the mean longitudinal contact plane is shown in Fig. 27.10.

From the curves presented in Figs. 27.10a and b, it follows that with rising torsional moment, the longitudinal tangential stresses, particularly in tyres with a diagonal cord structure, rapidly grow in the region located near the tread contact outlet. But in some instances, for diagonal-cord tyres, and especially for the P-type tyres, the tangential stresses reach a maximum both at the inlet and outlet of contact of the tread with the road.

When the tangential stresses exceed the specific force of tyre-road adhesion, the tyre slips. The specific adhesion force depends on the contour pressures and on the coefficient of friction (or the adhesion coefficient) of the tread rubber on the road at a particular contact point. A schematic diagram for slip and adhesion in the contact area for the driving, driven, and braked wheel is given in Fig. 27.11a-c. From Fig. 27.11 it follows that slip occurs in all the instances of wheel rolling. For the driven wheel, the contact sliding is insignificant.

Fig. 27.9. Rolling diagram for driven wheel (a); distribution of longitudinal tangential stresses (b); and distribution of tangential forces over contact area of tyre at rest (c)

The contact area during the rolling of the tyre on the road can generally be divided into a sliding region and an adhesion region. In various points of the sliding region, the direction of sliding can be different. As the magnitude of the force that causes the sliding
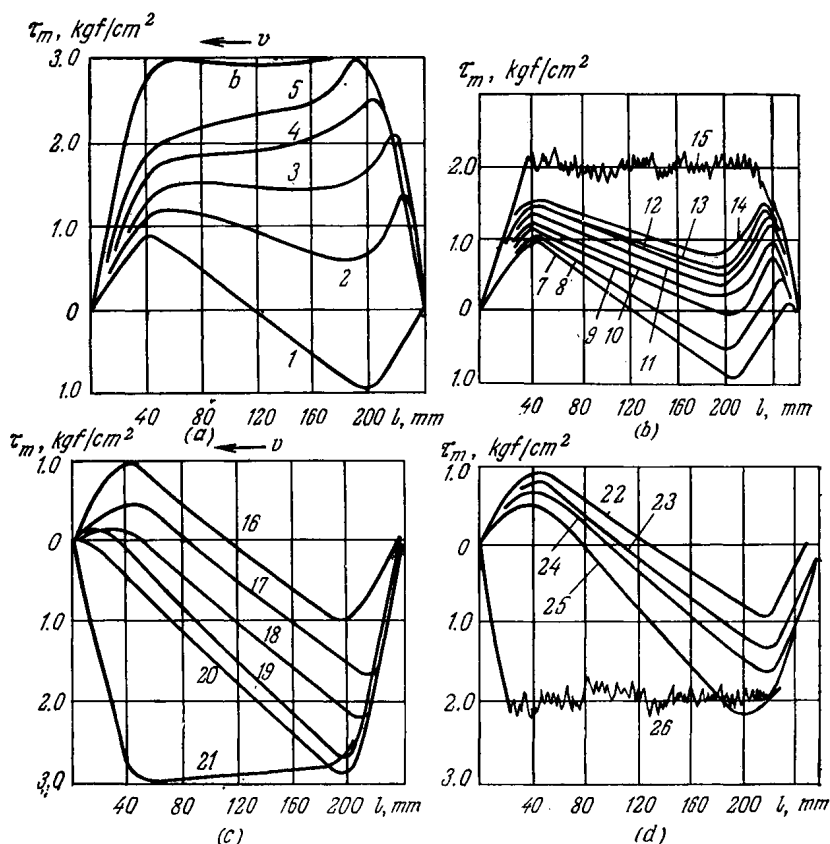
Fig. 27.10. Variation of tangential stresses in the middle of longitudinal section of contact for tyre of the diagonal-ply construction (a, c) and the P-type (b, d) at $G_{wh} = 1\ 500$ kgf, $p_w = 4.5$ kgf/cm^2

(a, b) driven wheel; (c, d) braking wheel; 1—for driven wheel; 2-5 at torques of 140, 225, 295, and 340 kgf/m, respectively; 6—normal pressure distribution; 7—for driven wheel; 8-14—stresses at rising torque; 15—stresses arising in slipping; 16—for driven wheel; 17-20—stresses at torques of 105, 145, 190, and 215 kgf·m; 21—normal pressure distribution; 22—driven wheel; 23-25—stresses at rising torques; 26—skidding stresses [17]
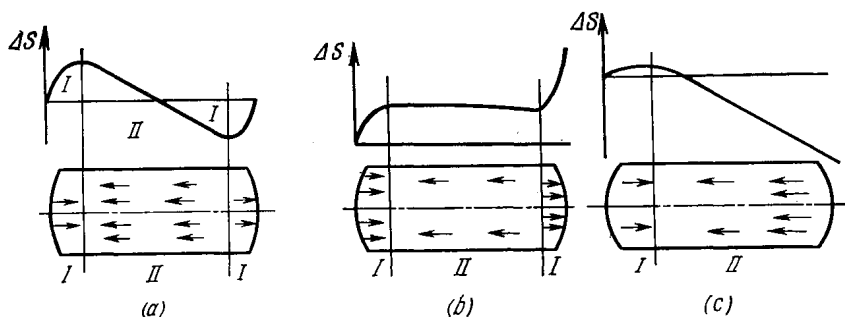
Fig. 27.11. Sliding region and engagement region for (a) driven, (b) driving, and (c) braked wheels along contact spot

grows, the adhesion region decreases, and at the moment the engagement between the tyre and the road is upset, it disappears altogether. With a great magnitude of the force, slip in the direction along which the force acts is prevalent.

The magnitude of sliding varies in different longitudinal sections of the contact area. Fig. 27.12 illustrates the character of variation
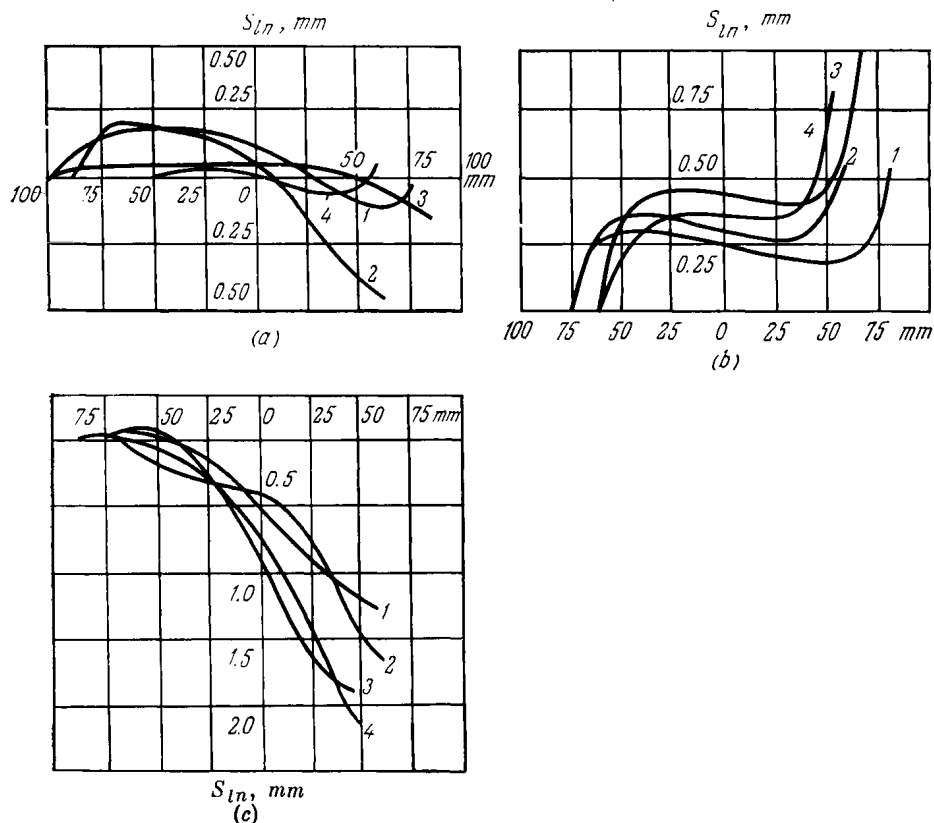
Fig. 27.12. Slipping in various longitudinal sections of contact area between Type 6.00-16 tyre and road surface

1—middle of tread; 2-4—at a distance of 17, 34, and 51 mm from the middle of tread [14]

of slip in different longitudinal sections of the tread contact area for driving, driven, and braked wheels (a, b, and c, respectively), the type of tyre being 6.00-16, the contour pressure, G_c, 460 kgf, and the inflation pressure p_w, 2.2 kgf/cm².

Slip depends on the specific adhesion forces effective in the real areas of contact. These forces and, hence, the adhesion coefficients depend on the road surface topography, which has various profile

182

deviations. The deviations commensurable with the tyre contact area are related to waviness [7], and those of fractions of a milli-metre, to roughness. The tyre-road interaction is governed by the processes occurring in the contact areas. This interaction depends on the distribution of the material in the road surface layer
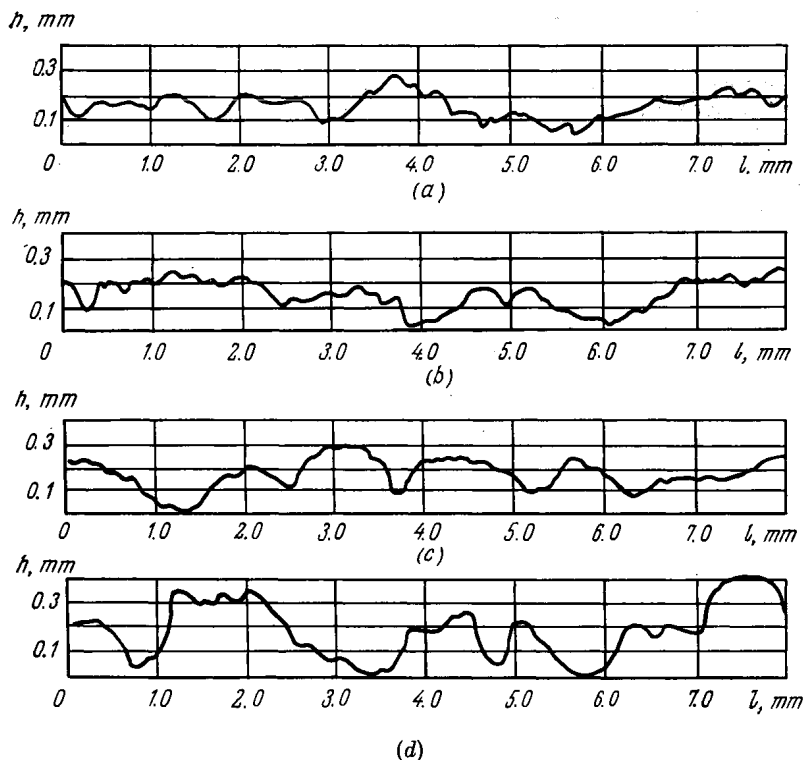
Fig. 27.13. Surface profile graphs for different types of road covering
(a)—concrete after long-term service; (b) newly deposited concrete; (c) concrete after short-term service; (d) asphalt (vertical magnification is twice the horizontal one)

and is characterized by the number of asperities over a unit area, their geometric shape, and their height distribution [4].

Profile graphs of typical road coverings are presented in Fig. 27.13 [12]. Analysis shows that surface asperities are close to spherical segments in shape; they are spaced apart on a certain base and distributed in height. For this reason, a hemispherical model of surface asperities is used for the assessment of their interaction with the rubber tread. Surface roughness parameters for some types of road covering are given in Table 27.3.

The distribution of the material in the road surface layer is represented by a bearing area curve whose initial section is des-cribed by

$$tp = b\varepsilon^{\nu}$$

Table 27.3

Surface geometry characteristics for road coverings

Covering	R_{max}, mm	r, mm	b	v	Δ
Asphalt	0.26	0.12	3.5	3.8	1.560
Newly-deposited concrete	0.31	0.30	2.0	4.4	0.885
Concrete after short-term service	0.43	0.20	5.0	3.9	1.420
Concrete after long-term service	0.24	0.15	3.8	2.7	0.980

At contour pressures determined by the formula

$$p_{c_d} = \frac{8 \cdot 10^{-2} \Delta^{\frac{1}{2}}}{\Theta \, (b^{3/2v+1} v)^{\frac{2v+1}{2(v-1)}}} \qquad (27.4)$$

contact of the road covering with the tread surface becomes densified [9, 11].

In formula (27.4) p_{c_d} is the contour pressure corresponding to the lowest asperity coming into contact within the contour area. This pressure depends on the surface roughness of road covering and the elastic modulus of tread rubber. In the dense-contact area, the bearing-area curve is described by the relationship

$$t_p = b \varepsilon_{cr}^{v} \left(\frac{v \varepsilon}{\varepsilon_{cr}} + 1 - v \right)$$

where ε_{cr} is the approach for the lowest contacting asperity over the contour area of contact.

Taking into consideration that for typical road coverings $b \approx 3.0$, $v \approx 3.0$, $\Delta \approx 1.2$, the elastic modulus of tread rubber $E = 30$ to 40 kgf/cm², and $\mu = 0.5$, we shall have $p_{c_d} = 0.9$ to 1.4 kgf/cm².

Thus, all tyres work in dense contact conditions.

Further increase in contour pressures can lead to coalescense of separate contact spots; this condition is referred to as the densification of the real area of contact, which is described, as a function of approach, by the following expression [1]:

$$t_p = 1 - e^{-c' \frac{p_c}{E}}$$

where c' is the coefficient depending on the surface roughness. According to E. F. Nepomnyashchy, $c' = 6.8$ for rubber working on concrete.

In determining frictional adhesion, we assume that the tread surface is elastic and smooth and the road surface is hard and rough.

Because of dissimilar mechanical properties of the road and tyre materials, the asperities on road covering will penetrate into the tread surface in the real contact areas.

In the general case, adhesion (static friction force) will be equal to the sum of two components. One, the molecular component of the friction force, T_{ml}, is a matter of molecular interactions at the tyre-road interface in the real contact areas. The other, T_{mc}, is determined by the hysteresis losses arising from deformation of the tread surface layer by the penetrating asperities of the road covering. Thus, for a single asperity, $T = T_{ml} + T_{mc}$.

The molecular component of the friction force (see Ch. 2)

$$T_{ml_i} = (\tau_0 + \beta p_r) A_{r_i} = (\tau_0 + \beta p_r) \pi r h_i$$

The frictional parameters τ_0 and β depend on the road surface condition (dirtiness, moisture, etc.).

The mechanical component for a hemispherical asperity is given by

$$T_{mc_i} = \frac{0.25 \alpha_{eff} h_i^2}{\Theta}$$

where α_{eff} is the coefficient of hysteresis losses in a complex stress state; $\alpha_{eff} = 2.5\alpha$ (here α is the coefficient of hysteresis losses in extension-compression).

The two above formulas contain the quantities h_i and p_r, that is, knowledge of deformation characteristics of rubber penetrated by a spherical indenter is essential for determining the friction force arising at a single asperity. According to E. F. Nepomnyashchy, the Hertzian classical solution is applicable to describing the penetration of a spherical indenter into rubber up to $h/r = 1.6$.

The total frictional adhesion of the tread to the road

$$T = \sum_{i=1}^{n_r} T_i \Delta n_r$$

where Δn_r is the number of asperities with an identical penetration magnitude in an arbitrary section.

In calculation of the adhesive force, the mutual effect of individual asperities may be neglected.

According to [9, 10], the static friction force during dense contact will be

$$T = \frac{0.125 \alpha_{eff} A_c \varepsilon_{cr}^{\nu-1} b R_{max} \xi^2}{\pi \nu r \Theta} + \left(\tau_0 + \frac{0.42 \beta R_{max}^{1/2}}{r^{1/2} \nu^{1/2} \Theta} \xi \right)^{1/2} \frac{A_c}{2\nu} \xi \quad (27.5)$$

where $\xi = \nu \varepsilon - (\nu - 1) \varepsilon_{cr}$.

The value of ξ depends on the contour pressure (see Ch. 2):

$$\xi = \frac{3\nu}{b^{1/3\nu} \Delta^{1/3}} (p_c \Theta)^{2/3} \quad (27.6)$$

With regard to relationship (27.6), the specific friction force (adhesion) will be

$$\tau_T = \frac{T}{A_c} \frac{\alpha_{eff}\Delta^{1/3}p_c^{4/3}\Theta^{1/3}}{\pi b^{\frac{3\nu-1}{3\nu}}}$$

$$+ \left[\tau_0 + \frac{0.71\beta\Delta^{1/3}b^{1/3\nu}p_c^{1/3}}{\Theta^{2/3}}\right]\frac{1.45p_c^{2/3}\Theta^{2/3}}{\Delta^{1/3}b^{1/3\nu}} \qquad (27.7)$$

For the most typical types of road covering with $b = 3.0$ and $\nu = 3.0$, and rubber with $\mu = 0.5$, we shall have

$$\tau = \frac{0.13\alpha_{eff}\Delta^{1/3}p_c^{4/3}}{E^{1/3}} + [\tau_0 + \beta\Delta^{1/3}E^{2/3}p_c^{1/3}]\frac{p_c^{2/3}}{E^{2/3}\Delta^{1/3}} \qquad (27.8)$$

From formulas (27.3) and (27.7) it follows that the specific adhesion (specific static friction force) depends not only on the tyre design characteristics (B_t, r_0, α_2, α_1, and k'), inflation pressure (p_w), load on the wheel (G_{wh}), and the mechanical properties of tread rubber (μ, E and α_{eff}), but also on the road surface topography (b, ν, and Δ) and condition, i.e. dirtiness (τ_0 and β).

The adhesion coefficient equal to the coefficient of static friction at $G_{wh} = N$ is given by

$$\Psi = \frac{T}{N} = \frac{\tau}{p_c} = \frac{0.13\alpha_{eff}\Delta^{1/3}p_c^{1/3}}{E^{1/3}} + \frac{\tau_0}{\Delta^{1/2}E^{2/3}p_c^{1/3}} + \beta \qquad (27.9)$$

Substituting p_c as expressed by formula (27.3) we obtain

$$\Psi = \frac{2^{1/3}\tau_0 k'^{1/3}B_{tr}^{1/3}r_0^{1/6}\alpha_2^{1/6}\vartheta^{1/6}}{\Delta^{1/3}E^{2/3}p_w^{1/6}G_{wh}^{1/6}} + \beta + \frac{0.13\alpha_{eff}\Delta^{1/3}p_w^{1/6}G_{wh}^{1/6}}{2^{1/3}E^{1/3}k'^{1/3}B_{tr}^{1/3}r_0^{1/6}\alpha_2^{1/6}\vartheta^{1/6}} \qquad (27.10)$$

where $\vartheta = 1 + \left(1 - \frac{4\alpha_1 p_w^2}{\alpha_2^2 G_{wh}}\right)^{1/2}$; $\vartheta \approx 2$.

Thus, the above relationship takes into account the main characteristics of the road covering, the tyre design parameters, the tread material and the external conditions (load on the wheel).

The first two components of the adhesion coefficient are dependent on molecular interactions between the road and the tyre in the real areas of contact. The third term in formula (27.10) depends on the hysteresis losses due to deformation during the slip of the tread rubber on the road surface asperities.

It can be seen that the adhesion coefficient depends largely on the road surface condition in the contact area (frictional parameters τ_0 and β) and on tread rubber (elastic modulus E and hysteresis losses coefficient α_{eff}), and, to a lesser extent, on the geometric characteristic of the tyre (B_{tr}, r_0, α_2 and α_1), the inflation pressure, the load on the wheel, and the road surface roughness.

Analytical relationships allowing additionally for the effect of the internal friction in rubber, the molecular activation energy, the sliding speed, and the temperature have been proposed [15, 17]

for the calculation of the wheel adhesion coefficient on a dry hard road covering.

Generally, with increasing inflation pressure, load on the wheel, and road surface roughness, the adhesion coefficient passes through a minimum (the molecular component diminishes while the mechanical component grows) [see formula (27.10)].

On dry hard coverings, the mechanical component of the adhesion coefficient is small and may be ignored; however, it must be increased where a stable adhesion coefficient is required. This component is practically unaffected by the road-covering condition (moisture, dirt, etc.); its growth can be achieved by increasing the road surface roughness, inflation pressure and load on the wheel in excess of the values computed by the formulas given below.

By using the concept of an extremum of a function, it can be shown that the adhesion coefficient will be at a minimum under the following conditions:

the road-covering roughness

$$\Delta = 1.34 \times 10^2 \left(\frac{\tau_0}{\alpha_{eff}} \right)^{3/2} k' B_{tr} \left(r_0 \alpha_2 \right)^{1/4} \left(\frac{\vartheta}{E p_w G_{wh}} \right)^{1/2} \quad (27.11)$$

the inflation pressure

$$p_w = 1.18 \times 10^3 \left(\frac{\tau_0}{\alpha_{eff}} \right)^3 \left(\frac{k' B_{tr}}{\Delta} \right)^2 \frac{r_0 \alpha_2 \vartheta}{E G_{wh}} \quad (27.12)$$

the load on the wheel

$$G_{wh} = 1.8 \times 10^3 \left(\frac{\tau_0}{\alpha_{eff}} \right)^3 \left(\frac{k' B_{tr}}{\Delta} \right) \frac{r_0 \alpha_2 \vartheta}{E p_w} \quad (27.13)$$

27.4. WEAR OF TREAD IN MOTOR-VEHICLE TYRES

Wear of the tread is the main cause of replacement of tyres (60 to 90 percent of all tyres in service) in motor vehicles run on improved road coverings.
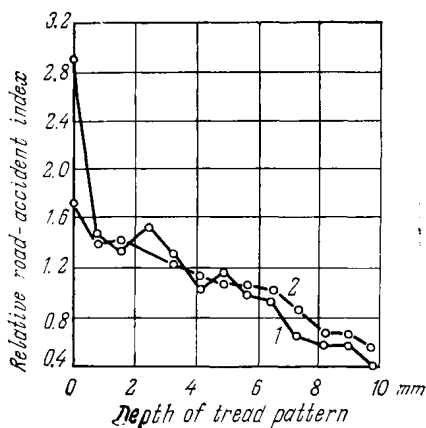
Fig. 27.14. Influence of tread profile depth on relative road-accident index

1—wet asphalt covering; 2—dry asphalt covering [17]

187

It should be emphasized that the number of road accidents caused by tread wear, which involve the loss of balance (adhesion) on wet roadways, reaches from 25 to 40 percent.

The effect of depth of the tread pattern on a relative index of road accidents is shown in Fig. 27.14.

27.4.1. Allowable Wear Ratings

Wear limits for tread pattern, beyond which a tyre is not allowed into service, are practiced in the USSR. According to [16], the wear limit of a tread pattern (that is the remaining depth in the middle of the pattern) in millimetres is:

Lorries 1.0
Buses 2.0
Motor cars   . . . . up to wear indices*

_____

* Protrusions 1.5 + 0.15 mm high in six sections around the bottom of the tread pattern, or, where absent, 1.6 mm of the remaining pattern depth.

Similar ratings on the allowable tread wear are adopted in the USA and other countries.

27.4.2. Wear Mechanism
in Tread Rubber

The main causes of tread wear are friction between the tread-pattern elements and road covering and the fatigue of the rubber surface layer; these phenomena, in turn, depend on the physico-mechanical properties of tyre materials, and mechanical and thermal loads sustained in operation.

The wear of tyres is governed by numerous factors, which can be conditionally reduced to the following ones: the tyre design (physico-mechanical and fatigue properties of the rubber), the state of repair of the motor vehicle (toe-out or toe-in of the wheels), the type* of vehicle and the load on the axle, the manner of driving, the type and condition of road covering, and the tangential forces arising in the tread-road contact.

The indicated factors have effect on the magnitude of displacements of tread elements, and, hence, on their wear.

The friction and wear theory developed in the USSR considers three consecutive stages: the contact interaction of the rubbing pair, the changes in the rubbing surfaces that result from their interaction and the rupture (wear) of the surfaces.

_____

* In the USSR, the inflation pressure ratings are established by special rules [16].

27.4.3. Changes in Rubber Surface Layers during Interaction with Road Covering

The surface layer of the tyre tread is subject to various changes.

Temperature changes caused by the dissipation of energy in external friction and internal friction (hysteresis losses) and also the environmental temperature action diminish the strength of rubber. The oxidation of the surface layer due to the action of temperature and atmospheric oxygen reduces the rupture strength; as this takes place, the rubber becomes structured, and its stiffness increases. The oxidized film, which is less elastic than the underlying layer, wears away more heavily.

Fatigue. Repeated alternating deformations cause the molecular chains to break. The forming radicals can react with impurities and so change the physico-mechanical properties of rubber. The structural defects lead to formation of cracks and tears, which are stress concentrators.

Rupture and tearing. If friction between the tread and the road covering is high and the angle of the road-surface asperities exceeds a certain critical value, the possibility of slipping is reduced. As a result, the tread surface layer becomes "stagnant". With large tangential displacement, the "stagnant layer" may tear because the shear stress τ exceeds the strength of the rubber.

The wear of rubbers is largely caused by fatigue. The separating of wear debris results from elastic displacements of the material due to the repeated deformations of individual road-surface asperities [3, 6, 8, 13]. Mechanical wear produced by a single interaction between the rubber and the road covering [18, 22] can also take place. Abrasive wear occurs at high sliding speeds and elevated temperatures. Where the road asperities are not harsh, wear results from "rolling off", that is, the formation of rubber rolls known as the Schallamach pattern [18, 21, 22]. High sliding speeds $(v \geqslant 200$ km/h) and high temperatures give rise to ablative wear [19].

The rate of wear is determined by a combination of factors or predominance of some factors over others, the factors in question being temperature, normal pressure, slip, the mechanical properties of tread rubbers, and the state of road covering. These factors also govern such important characteristics of the sliding pair as the shear stress τ and the coefficient of friction f, which are related by the formula $\tau = f p_r$.

As has been stated before (see p. 184) all tyres operate under dense contact conditions. The assessment of wear should be made by using the concept of its linear rate

$$I = i_h \frac{p_a}{p_r} \qquad (27.14)$$

The volume of wear debris parting off during a single interaction cycle

$$V_d = \frac{U_v}{n}$$

where U_v is the deformed volume; n is the number of cycles up to the removal of a wear particle.

Let us calculate the wear rate of a tyre tread during restrained rolling on the basis of the theory of fatigue wear; we shall proceed from the wear rates effective in sliding at elastic dense contact.

According to E. F. Nepomnyashchy [13], let us assume the following:

—there is neither slip nor tangential stresses in the contact area during pure rolling;

—the tangential load in the contact area is insignificant as compared with the adhesion limit;

—the surface of the tread elements is elastic and smooth, and

—the road surface is hard and rough.

If the normal and tangential stresses across the contact spot are distributed uniformly, the wear rate in rolling will be related to that in sliding in the following way:

$$I_r = \frac{1}{l} \int\limits_0^{S_m} I \, dS \qquad (27.15)$$

where I_r is the wear rate in rolling; I is the wear rate in sliding; l is the length of contact (with small amounts of slip, it is roughly equal to the rolling distance passed in wheel rotation through the contact angle); S_m is the sliding distance of a wheel-surface point with reference to the incident point on the bearing surface during traverse of the contact area.

For elastic dense contact

$$U_v = \sum_{i=1}^{n_c} U_{v_i} \approx \sum_{i=1}^{n_c} cK\pi r h_i \Delta n_r$$

where c is the coefficient depending on the stress state in the contact region; here $c = 0.25$; $K > 1$ is the coefficient allowing for the actually deformed volume; Δn_r is the number of asperities with an identical penetration.

Calculations show that

$$U_v = \frac{cKbA_cR_{\max}\varepsilon_{cv}^{v+1}}{2(v+1)} \left[v(v-1) - 2(v^2-1)\frac{\varepsilon}{\varepsilon_{cr}} + v(v+1)\frac{\varepsilon^2}{\varepsilon_{cr}^2} \right] \qquad (27.16)$$

Then, the specific linear wear rate

$$i_h = \frac{cKR_{\max}^{1/2}\varepsilon_{cr}}{2(v+1)\,nr^{1/2}\varepsilon^{1/2}} \left[\frac{\varepsilon_{cr}v(v-1) - 2(v^2-1)\varepsilon + v(v+1)\dfrac{\varepsilon^2}{\varepsilon_{cr}}}{v\varepsilon + \varepsilon_{cr} - v\varepsilon_{cr}} \right] \qquad (27.17)$$

With $\varepsilon \leqslant \varepsilon_{cr}$, formula (27.17) is transformed into the previously found formula for i_h in the sparse contact area [6], that is, formula (27.17) is more general, and the known formula

$$i_h = \frac{cKR_{\max}^{1/2}\varepsilon^{1/2}}{2\,(v+1)\,nr^{1/2}} \tag{27.18}$$

is its particular variant.

A simplified formula

$$U_v = U_{v_{i_m}} n_c \tag{27.19}$$

is more convenient for rough estimation.

To find $U_{v_{i_m}}$, it is essential to know the mean magnitude of approach

$$h_m = \frac{A_{r_m}}{\pi r} \tag{27.20}$$

where A_{r_m} is the mean contact area of a single asperity:

$$A_{r_m} = \frac{A_r}{n_c} = \frac{\pi r R_{\max}\varepsilon_{cr}}{v}\left(\frac{v\varepsilon}{\varepsilon_{cr}}+1-v\right) \tag{27.21}$$

Obtaining the expression for h_m from (27.20) and (27.21) and substituting it into (27.19), we shall have:

$$U_v = \frac{cKA_cbR_{\max}\varepsilon_{cr}^{v+1}}{2v}\left(\frac{v\varepsilon}{\varepsilon_{cr}}+1-v\right) \tag{27.22}$$

The specific linear wear rate will be

$$i_h = \frac{mcKR_{\max}^{1/2}\varepsilon_{cr}^{1/2}}{2v^{1/2}r^{1/2}n}\left(\frac{v\varepsilon}{\varepsilon_{cr}}+1-v\right)^{1/2} \tag{27.23}$$

where m is the coefficient depending on v; $m = 1$ at $v = 2$, and $m = 0.8$ at $v = 3$.

Within the range of approach $1 \leqslant \dfrac{\varepsilon}{\varepsilon_{cr}} \leqslant 3$, discrepancy in the results given by formulas (27.17) and (27.23) is small. For this reason, formula (27.23) will be satisfactory for computing i_h up to $\dfrac{\varepsilon}{\varepsilon_{cr}} \leqslant 3$. The integral value of linear wear rate can be found by substituting the value of i_h from formula (27.23) into formula (27.14), and taking into account that

$$\left(\frac{v\varepsilon}{\varepsilon_{cr}}+1-v\right)=\left[\frac{5p_c\Theta v^{1/2}r^{1/2}}{be_{cr}^v R_{\max}^{1/2}}\right]^{2/3};\quad A_c=lB_{tr}$$

$$A_a = 2\pi r_0 B_{tr};\quad b = 3;\quad v = 3\quad\text{and}\quad n = \left(\frac{\sigma_0}{\tau}\right)^t$$

Thus,

$$I = \frac{0.48mcK\Delta^{1/6}p_c^{2/3}\Theta^{2/3}\tau t \, l}{2\pi r_0 \sigma_0^t} \tag{27.24}$$

Assuming $m = 0.8$, $c = 0.25$, and $K \approx 1$, we shall obtain

$$I = \frac{0.1\Delta^{1/6}p_c^{2/3}\Theta^{2/3}\tau t \, l}{2\pi r_0 \sigma_0^t} \tag{27.25}$$

E. F. Nepomnyashchy has shown, that the fatigue properties (exponent t) of the tread rubbers he investigated virtually coincide
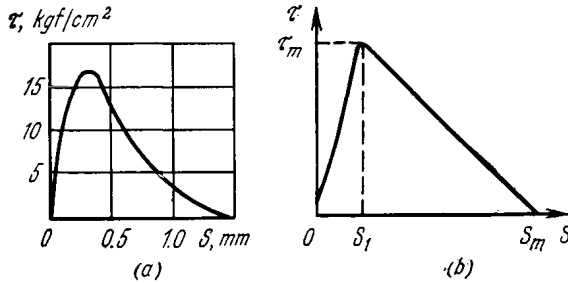
Fig. 27.15. Variation of tangential stresses with slipping of tyre tread on road surface
(a) experimental data; (b) approximated relationship

in the bulk and the contact fatigue conditions; as a result, the exponent t can be found from tests for the bulk fatigue. In rough estimates for the most applicable tread rubbers, the following parameter values may be taken: $t = 3$ to 4; $\sigma_0 = 1500$ to 2000 kgf/cm^2, $\tau = 200$ to 270 kgf/cm^2 (for dry road coverings).

From formula (27.15) it follows that knowledge of the relationships between tangential stresses τ and slip magnitude S is essential for finding the wear of the wheel. According to [13], the tangential stresses vary with slip as is shown in Fig. 27.15. Approximating the experimental curve by straight lines, we can express the relationship between τ and S for section OS_1 as

$$\tau = \tau_m \frac{S}{S_1}$$

for section $S_1 S_m$

$$\tau = \tau_m \frac{S_m - S}{S_m - S_1}$$

Substituting (27.25) into (27.15) and making integration, we shall have

$$I_r = \frac{0.1K\Delta^{1/6}p_c^{2/3}\Theta^{2/3}}{2\pi\sigma_0 r_0} \int_0^{S_m} \tau^t \, dS$$

$$= \frac{0.1K\Delta^{1/6}p_c^{2/3}\Theta^{2/3}\tau_m^t S_m}{2\pi r_0 \sigma_0^t \, (t+1)} \tag{27.26}$$

The formula (27.26) is a general expression for computing the amount of wear when the tangential force acting on the tyre is directed arbitrarily. In particular instances, there are definite relationships between τ_m, S_m and the design parameters of the tyre.

If the tyre is loaded by a lateral force, then, according to [14]

$$\tau_m = \frac{\chi_w p_w \alpha l}{H}$$

and

$$S_m = \psi' \alpha l$$

where χ_m and ψ' are the coefficients that depend on tyre design; α is the slip angle; H is the tread pattern depth.

Substituting into formula (27.26) the values of p_c, τ_m, and S_m, we shall have in this instance

$$I_r = \frac{1 \times 10^{-2} \Delta^{1/6} \Theta^{2/3} \chi_w^t (\alpha l)^{t+1} \psi' Q_{wh}^{1/3} p_w^{t+1/3}}{\sigma_0^t r_0^{4/3} (t+1) k'^{2/3} \beta_{tr}^{2/3} \alpha_2^{1/3} \vartheta^{1/3}}$$

Thus, tread wear substantially depends on the inflation pressure, the tread material, and the tyre design characteristics.

If the wheel is loaded with a torsional moment or a braking moment M, then, according to [13]

$$\tau_m = \frac{2M}{\beta_{tr} l r_0}$$

$$S_m = \psi_x \frac{2M}{k_x l r_0}$$

where ψ_x and k_x are the coefficients determined by the tyre design. Then

$$I_r = \frac{1 \times 10^{-2} \times 2^{t+1} \Delta^{1/6} \Theta^{2/3} M^{t+1} \psi_x}{\sigma_0^t (t+1) k'^{2/3} r_0^{t+7/3} l^{t+1} \beta_{tr}^{t+2/3} \alpha_2^{1/3} \vartheta^{1/3} k_x}$$

In this instance, wear is strongly dependent on the amount of the torsional or braking moment applied and the tyre design parameters.

REFERENCES

1. Бартенев Г. М., Лаврентьев В. В. Трение и износ полимеров. Л., «Химия», 1972, 240 с.
2. Бидерман В. Л. Автомобильные шины. М., Госхимиздат, 1963, 383 с.
3. Бродский Г. И., Резниковский М. М., Сизиков Н. Н. Оценка износостойкости протектора шин по данным лабораторных испытаний резин.— В сб.: Резина — конструкционный материал современного машиностроения. М., «Химия», 1967, с. 118-124.
4. Комбалов В. С. Влияние шероховатости твердых тел на трение и износ. М., «Наука», 1977, 112 с.
5. Крагельский И. В., Виноградова И. Э. Коэффициенты трения. М., Машгиз, 1962, 217 с.

6. Крагельский И. В. Об изнашивании протекторных резин.—«Каучук и резина», 1959, № 11, с. 20-26.
7. Крагельский И. В., Добычин М. Н., Комбалов В. С. Основы расчетов на трение и износ. М., «Машиностроение», 1977, 526 с.
8. Крагельский И. В., Непомнящий Е. Ф. Усталостный механизм износа протектора автомобильных шин.— В сб.: Фрикционный износ резин. М.-Л., «Химия», 1964, с. 9-20.
9. Михин Н. М. Внешнее трение твердых тел. М., «Наука», 1977, 221 с.
10. Михин Н. М., Комбалов В. С. О зависимости коэффициента трения от нагрузки при упругом контакте в зоне насыщенного контакта.— В сб.: Контактное взаимодействие твердых тел и расчет сил трения и износа. М., «Наука», 1971, с. 146-153.
11. Михин Н. М., Крагельский И. В. Изменение площади фактического касания твердых тел при значительном сближении.— ДАН СССР, т. 176, № 6, 1967, с. 1285.
12. Непомнящий Е. Ф. О фактической площади касания протектора шины с шероховатыми поверхностями дорожных покрытий.—«Автомобильная промышленность», 1963, № 10, с. 18-20.
13. Непомнящий Е. Ф. Износ эластичного колеса при качении с проскальзыванием. Роль спектра нагрузок.— В сб.: Резина — конструкционный материал современного машиностроения. М., «Химия», 1967, с. 58-72.
14. Новольский В. И., Непомнящий Е. Ф. О взаимодействии протектора и автомобильной дороги.— В сб.: Фрикционный износ резин. М.-Л., «Химия», 1964, с. 250-261.
15. Петров И. П. Сцепление шины с твердой поверхностью.— Труды НАМИ. Вып. 146. Влияние дисбаланса шин и колес на работу автомобиля. М., 1974, с. 75-85.
16. Правила эксплуатации автомобильных шин. М., «Химия», 1975, 96 с.
17. Работа автомобильной шины. М., «Транспорт», 1976, 238 с. Авт.: В. И. Кнороз, Е. В. Кленников, И. П. Петров, А. С. Шелухин, Ю. М. Юрьев.
18. Резниковский М. М., Бродский Г. И. К вопросу об истирании резины по относительно гладким поверхностям.—«Каучук и резина», 1960, № 7, с. 17-23.
19. Saibel E., Chenglung Tsai. The wear by ablation. Wear, 24 (1973), p. 161-176.
20. Saibel E., Chenglung Tsai. Tyre wear, a review. Mecanique materiaux electricite (tome 1). 1972, p. 65-76.
21. Schallamach A., Friction and abrasion rubber. Wear, vol. 1, N 5, 1958, p. 384-417.
22. Schallamach A. The mechanics of tyre wear. Mecanique materiaux electricite (tome 1), 1972, p. 77-83.

FRICTION AND WEAR
OF METAL-CUTTING AND
METAL-FORMING TOOLS

In metal cutting, the friction and wear conditions for the contacting surfaces of the tool and the workpiece are severe: they slide against each other at high temperatures, speeds, and normal contact loads, which in some instances reach the hardness of the material being cut. The contact is characterized by a small size, sufficiently high "juvenility", nonuniform distribution of stresses and temperatures, and non-identical conditions on the tool surfaces.

Typical of friction in metal forming are high contact stresses, elevated surface temperatures due to both heat transfer and displacement and deformation of the material being formed, high temperature gradients and, hence, thermal stresses in the surface layer, plastic deformation of the surface layer, and the occurrence of oxidation, strengthening, weakening, and structural transformations.

An adequate tool hardness alone is not sufficient for economic operation. The tool must also have a good wear resistance (especially, in finishing operations). For this reason, a tool material should be chosen with regard to both these characteristics, which depend to a great extent on the temperature of tool surfaces.

28.1. TOOL MATERIALS

Materials for metal-cutting tools must meet the following basic requirements: high strength and hardness (not lower than HRC 62 to 64), good wear resistance, heat resistance (up to 1000°C), and thermal shock resistance. The materials for metal-forming tools must have, in addition to above characteristics, high impact strength, thermal fatigue resistance, and erosion resistance. The physicomechanical properties of some tool materials are given in Table 28.1.

Table 28.1

Physico-mechanical properties of tool materials

Tool material	Physical properties				
				Coefficients	
	Density, g/cm³	Thermal resistance, °C	Specific heat, cal/(cm·s·°C)	thermal conductivity, $1 \cdot 10^6$, cal/(cm·s·°C)	thermal expansion $\alpha \cdot 10^{-6}$, 1/°C
High-speed steels (P18)	8.7	400–600	1.4	0.065	11
Tungsten carbides (ВК8)	14.6	850	0.53	0.130	4.5
Tungsten-titanium carbides (Т15К6)	11.4	—	0.65	0.065	6.5
Mineral ceramics (ЦМ332)	3.75	1 200	—	0.055	6.3–9.0
Synthetic diamond	3.48–3.51	600–800	—	—	—
Natural diamond	3.01–3.56	600–800	0.42	0.35	0.9–14.5
Cubic boron nitride	3.5–3.54	1 300–1 500	—	—	—
Synthetic corundum	3.93–4.01	—	—	0.047	7.5
Silicon carbide	3.16–3.99	1 200–1 300	0.31	0.37	6.5
Boron carbide	2.48–2.52	500–700	—	0.038	4.5

Tool material	Mechanical properties					
	Microhard-ness kgf/mm²	HRA	Ultimate strength		Elastic modulus, kgf/mm²	Impact strength, kgf cm/cm²
			in comp-ression	in bend-ing		
			kgf/mm²			
High-speed steels (P18)	—	83	380	370	—	0.89
Tungsten carbides (ВК8)	1 600	88.5	330	140	62 000	—
Tungsten-titanium carbides (Т15К6)	1 700	90.2	415	110	54 000	0.25–0.6
Mineral ceramics (ЦМ332)	—	91–93	500	38	—	0.05–0.12
Synthetic diamond	8 600–10 000	—	300	30	72 000–93 000	—
Natural diamond	10 060	—	200	21–49	90 000	—
Cubic boron nitride	8 000–10 000	—	—	—	—	—
Synthetic corundum	1 200–2 400	—	76	27	—	—
Silicon carbide	2 700–3 500	—	100–200	10–15	36 000	—
Boron carbide	3 700–4 500	—	180	30	29 600	—

28.1.1. Tool Steels

Tool steels include carbon, alloy, and high-speed types of steel.

Carbon tool steels. These exhibit a high hardness, *HRC* from 62 to 64 after heat treatment (hardening), but low thermal resistance (up to 200-250°C). The following grades of carbon tool steels are in use: У7, У7А, У8, У8А, У8Г, У8ГА, У10, У10А, У11, У11А, У12, У12А, У13, and У13А.

Alloy steels. Depending on their applications and properties, alloy tool steels (GOST 5950-73) are divided into two groups: steels for cutting and measuring tools, and steels for forming tools (dies).

The most commonly used steels for cutting tools are Grades 7ХФ, 11Х, ВХ, ХВ5, В1, Ф, 9ХС, ХВГ, 9Х55ВФ and ХВСГ, and for
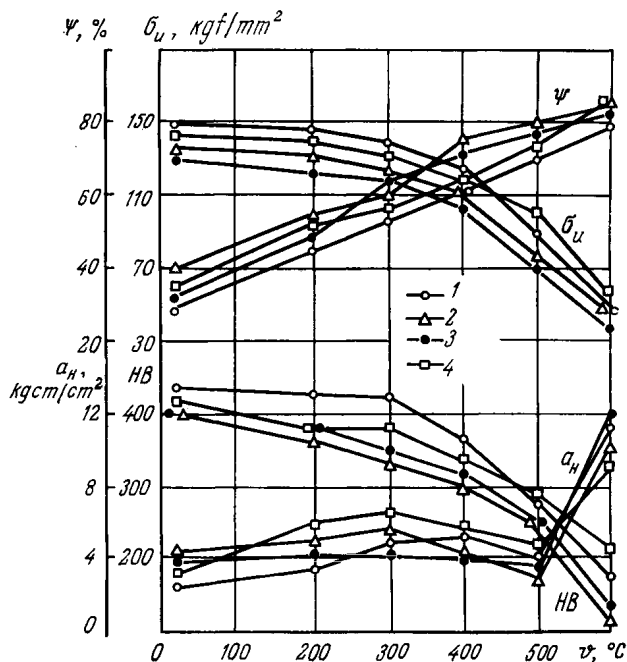
Fig. 28.1. Mechanical properties of die steels at elevated temperatures
1—5ХГСВФ; 2—5ХНМ; 3—5ХВГ; 4—5ХНВ

dies, Grades 5ХНМ, 5ХНВ, 5ХГМ, 5ХНСВ, 3Х2В8Ф, and 45Х3В3МФС.

The mechanical properties of these steels defining their performance at different surface temperatures are illustrated in Figs. 28.1 and 28.2.
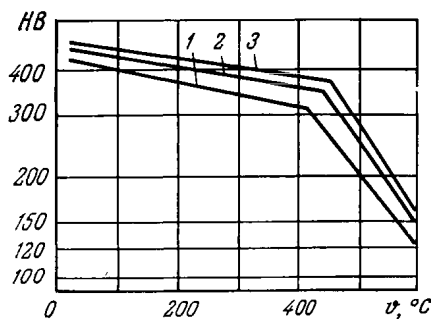
Fig. 26.2. Variation of hardness with temperature for die steels
1—5ХНМ; 2—5ХГСВФ; 3—5ХВГ

The alloy steels have high toughness in the hardened state, deep hardenability, and low tendency to develop deformations and cracks

197

in hardening. Their thermal resistance, however, is low (200 to 250°C).

High-speed tool steels. These acquire high hardness, strength, and wear resistance owing to heat treatment, and keep good cutting properties in operation up to 600-650°C. Along with application of conventional Grades P9, P12, and P18, new grades of high-speed steels (Table 28.2) have come into use; they provide a high stock

Chemical composition (%) of tungsten-molybdenum high-speed steels

Grade of steel	C	Cr	W	Mo	V
P6M3 (ЭП342)	0.85-0.95	3.0-3.6	5.5-6.5	3.0-3.6	2.0-2.5
P9M4 (ЭП344)	0.8-0.9	3.0-3.6	9.5-10.0	3.6-4.1	1.8-2.2
P12M3 (ЭП351)	0.8-0.9	3.0-3.6	11.5-12.5	3.0-3.6	1.8-2.2

removal rate and have a lower content of costly and scarce alloying elements (primarily, tungsten), while retaining good cutting properties.

28.1.2. Cemented Carbides

The Soviet tool industry produces metal-ceramic hard metals, usually referred to as *cemented carbides*, in three groups: tungsten group, titanium-tungsten group, and titanium-tantalum-tungsten group. They are commonly made by sintering the basic material at a high temperature. The hard metals of the first group comprise tungsten carbide and metallic cobalt; they are designated by letters ВК (Russian letters) and a figure indicating the percentage of cobalt.

The second group contains tungsten carbide, titanium carbide, and metallic cobalt. These hard metals are designated by letters ТК and figures. The figure following the letter T indicates the percentage of titanium carbide, and the figure following the letter К—the percentage of cobalt.

The third group comprises tungsten carbide, titanium carbide, tantalum carbide, and metallic cobalt. The figure following the letters TT indicates the percentage of titanium and tantalum carbides, and the figure following the letter K, the percentage of cobalt.

Tables 28.3-28.5 and Figures 28.3-28.9 present data on the mechanical properties of different grades of cemented carbides that determine their performance at various tool surface temperatures; Table 28.6 and Figs. 28.10 and 28.11 show the influence of processing methods on tool fatigue strength.

The grades of cemented carbides used for diemaking are: ВК11, ВК15, ВК20, ВК25, and ВК30.

Table 28.3

Physico-mechanical properties of cemented carbides

Group	Grade	Ultimate strength in bending, kgf/mm^2	Density, g/cm^2	HRA
Tungsten (BK)	BK2	100	15-15.4	90
	BK3 } (KO1)*	110	15-15.4	90
	BK3M	110	15-15.3	91
	BK4 (K30)*	130	14.9-15.1	89.5
	BK4B	140	14.6-15	88
	BK6 (K30)*	135	14.8-15	88.5
	BK6M (K10)*	130	14.8-15	90
	BK6B	140	14.4-14.8	87.5
	BK8 (K40)*	140	14.4-14.8	87
	BK8B	155	14.4-14.8	86
	BK10 (K50)*	150	11.2-14.6	87
	BK15	165	13.9-14.1	86
	BK20	190	13.4-13.7	85
	BK25	200	12.9-13.2	84.5
Titanium-tungsten (TK)	T30K4 (P01)*	90	9.5-9.8	92
	T15K6 (P10)*	110	11-12.7	90
	T14K8 (P20)*	115	11.2-12	89.5
	T5K10 (P30)*	130	12.3-13.2	88.5
	T5K12B (P40)*	150	12.8-13.3	87
Titanium-tanta-lum-tungsten (TTK)	TT7K12 (P40)*	160	13-13.3	87
	TT10K8Б (M20)*	140	13.5-13.8	89

* Given in brackets are designations according to ISO recommendations.

Table 28.4

Coercive force and fatigue strength for some cemented carbides of BK group

Grade of cemented carbide	Coercive force, Э	σ_{-1}, kgf/mm^2
BK4	69-73	105
BK6	64-68	116
BK8	65-69	121

Table 28.5

Effect of cobalt content on percent elongation of BK-group cemented carbides

Co, % (by mass)	δ, %	Co, % (by mass)	δ, %
100	7.5	50	0.4
90	4.8	37	0.2
65	0.8	22	0.1

Table 28.6

Effect of surface-treatment methods on fatigue strength of cemented carbides BK8 and T5K10

Processing method	Operating conditions	Surface roughness class by GOST 2789-73	Fatigue limit of alloys, kgf/mm²	
			BK8	T5K10
Grinding with abrasive wheel K325CM1K	$v_{cr} = 15$ m/s; $s_{tr} = 0.03$ mm/double stroke; $s_{ln} = 3$ m/min	8	70	67
Lapping with cast-iron lap charged with kerosene-wetted boron carbide (grain size 5)	$v_{cr} = 2$ m/s	10	92	85
Lapping with diamond wheel ACM-40B	$v_{cr} = 25$ m/s	10	105	93
Electrochemical lapping with graphite-filled abrasive wheel	$U = 66$ V	10	91	85
Chemico-mechanical treatment	$v_{cr} = 2$ m/s	9	82	79
Combination of electrical-discharge and electro-chemical machining	$v_{cr} = 15$ m/s; $U = 18$ V; $I = 3.5$ A	9	51	50
Electrical discharge machining	$I = 0.5$ A; $E = 10$ μV	9	42	42
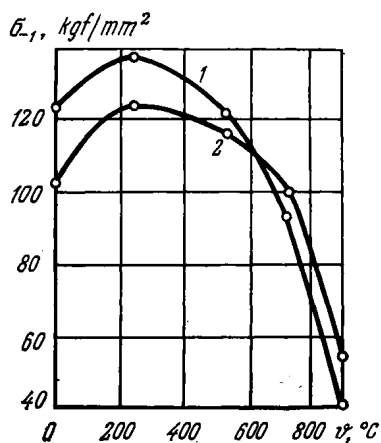
Fig. 28.3. Relationship between fatigue limit σ_1 and test temperature for cemented carbides ВК-4 (2) and ВК-8 (1)
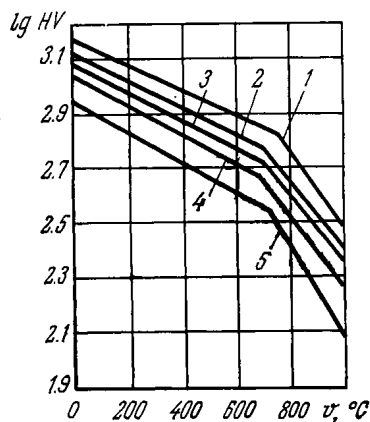
Fig. 28.4. Logarithm of hardness vs temperature for WC-Co-type cemented carbides (4-5 μm grain size)[8].
Co percent by mass: 1—4; 2—6; 3—8; 4—15; 5—20
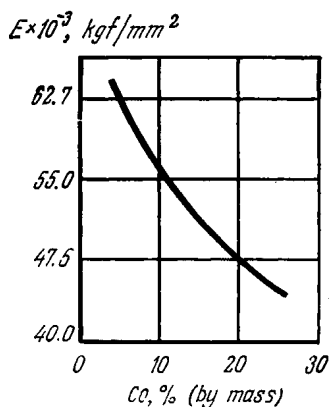
Fig. 28.5. Relationship between elastic modulus of WC-CO cemented carbides and content of cobalt
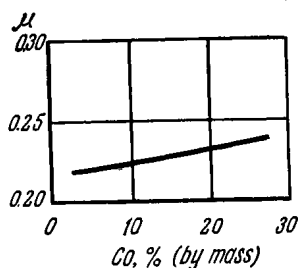
Fig. 28.6. Poisson's ratio vs cobalt content for cemented carbides
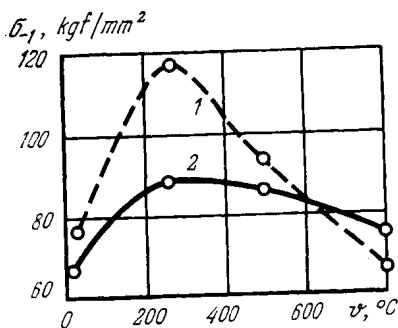
Fig. 28.7. Logarithmic relationship between fatigue limit of cemented carbides T15K6 (*1*), T30K4 (*2*) and test temperature
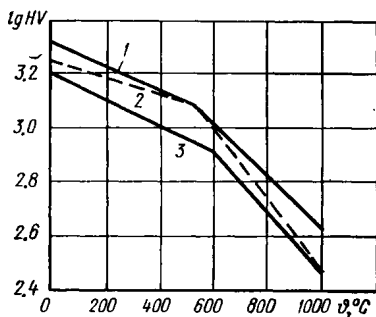
Fig. 28.8. Logarithm of hardness *vs* testing temperature for T15K6 (*1*), T14K8 (*2*), and T5K10 (*3*) alloys [8]
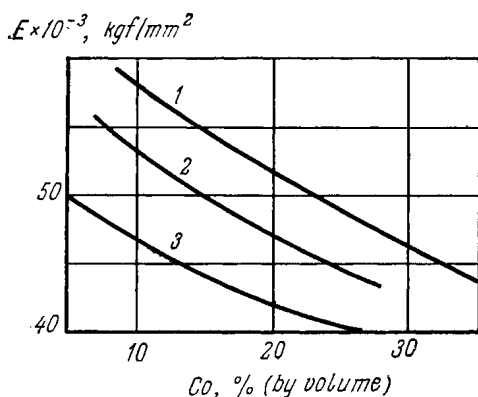
Fig. 28.9. Elastic modulus of cemented carbides WC-TiC-CO *vs* Co content, with different mass content of titanium carbide, percent
1—6; *2*—15; *3*—25
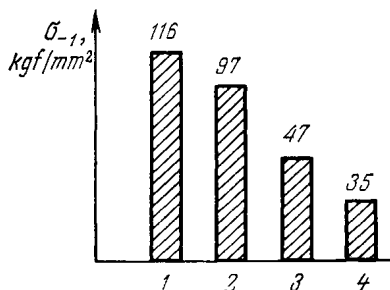
Fig. 28.10. Bar graph relating fatigue limit σ_{-1} of cemented carbide BK6 to surface treatment of test specimens
1—chemico-mechanical treatment and lapping by boron carbide; *2*—chemico-mechanical treatment; *3*—anodic treatment *4*—spark-discharge treatment
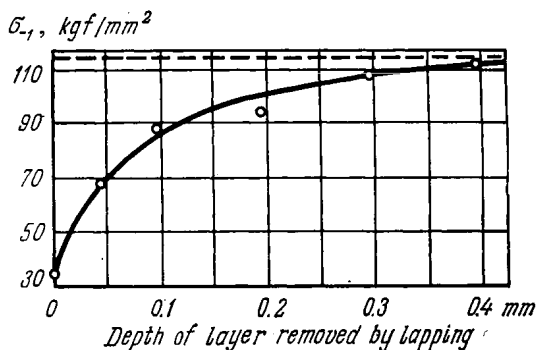
Fig. 28.11. Fatigue limit of cemented carbide BK6 as a⸱   tion of depth of layer lapped by boron carbide (dash line designates fatigue limit after abrading with boron carbide)

28.1.3. Mineral Ceramics

The mineral ceramic alloy, Grade ЦМ 332, which is essentially aluminium oxide Al_2O_3, is used for cutting tools.

28.1.4. Natural Diamond and Synthetic Superhard Materials

Diamond (A) is a pure carbon mineral; it is the hardest of all known natural substances (see Table 28.1).

Cubic boron nitride (КНБ) is a new hard material, a chemical compound of boron and nitrogen. Its physico-mechanical properties are almost identical with those of diamond (see Table 28.1), but the temperature resistance is higher.

Polycrystalline cubic boron nitride (ПКНБ), known under the trade name of *Elbor*, has a density of 3.45 g/cm³, Moh's scale degree 10, and heat resistance of 1500°C.

28.2. WEAR IN METAL-CUTTING TOOLS

Plastic deformation of the metal being worked by cutting occurs simultaneously in the chip-forming areas and in the areas of contact of the material with the face and flank of the tool. Depending on the particular operating conditions, stresses and deformations in these areas are more or less interrelated. These interrelations govern the character of the phenomena accompanying the cutting process: heat evolution and conduction, diffusion, adhesion, work hardening, phase changes, and chemical reactions with the environment.

28.2.1. Contact Processes on Tool Cutting Surfaces

Tool face. The characteristics of the contact of chips with the tool face are as follows:

(1) chemical cleanliness of the contacting surfaces varies; they can be very clean, practically free of films of chemical compounds and adsorbents, but they can also be coated by films of such thickness that direct metal-to-metal contact is practically impossible;

(2) contact loads (stresses) are distributed non-uniformly; near the cutting edge the normal contact stresses are very high, but they drop to zero at the point where the chip breaks away from the tool face;

(3) the contact temperature varies over a wide range, from room temperature to the melting point of the work metal.

Owing to the mentioned characteristics, the chip can slide over the tool face under a variety of conditions, from the boundary friction without substantial secondary plastic deformations in the contacting

chip layer (Fig. 28.12a) to a complete seizure of the contacting surfaces with a severe deformation in the chip layer (Fig. 28.12b).

The contact conditions mostly encountered in practice are complex, that is, seizure occurs in the part of the contact area adjoining the cutting edge, and the part adjoining the chip breakaway boundary is subject to elastic deformation. In such conditions, a stagnant

Fig. 28.12. Main types of deformation of chip contact layer

(a) without plastic contact deformation; (b) with continuous plastic contact deformation attended by formation of stagnant zone; (c) plastic contact deformation attended by destruction of contact layer and formation of built-up edge
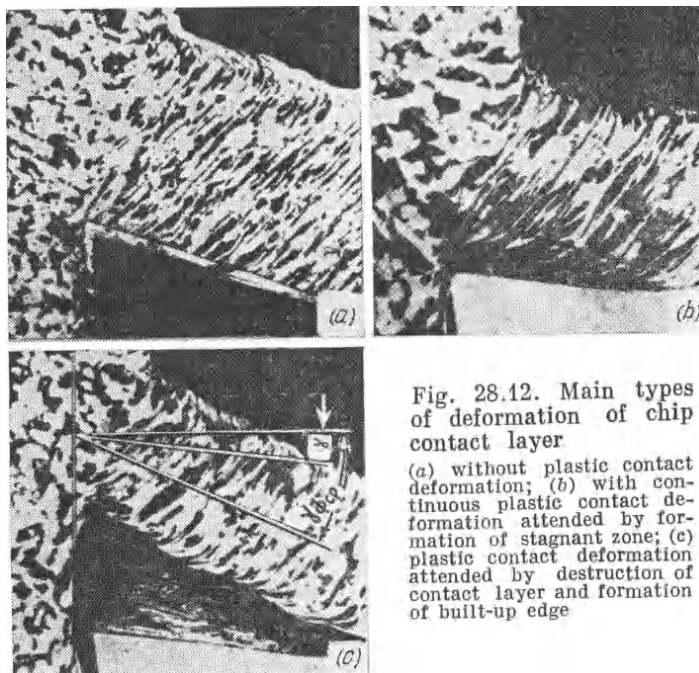
zone emerges on the tool face and a clearly identifiable longitudinal texture arises in the contacting layer of the chip. Each of the parts takes approximately one-half of the total contact area.

The contact stresses are spread non-uniformly along the width of the contact. Analysis of experimental data [9] has given the following expression for determining the normal contact stresses

$$\sigma_N = \sigma_M \left(\frac{x}{c} \right)^n$$

where σ_M is the normal contact stress near the cutting edge; x is the distance of a given point of the tool face from the point where the chip breaks away; n is the exponent characterizing the non-uniformity of stress distribution.

The distribution of tangential contact stresses is more uniform; their magnitude grows in a direction away from the point of chip breakaway, then it lessens sharply at the centre of the contact area

and changes insignificantly within the stagnant zone. The latter phenomenon can be explained by the fact that the magnitude τ_F of the tangential stress is restricted by a limit, that is, the shear strength of the chip material (with regard to strengthening and weakening processes) at the plastic contact region

$$\tau_F \approx \tau_{S_1}$$

where τ_{S_1} is the shear limit of the chip material.

The maximum normal stresses σ_M and tangential stresses τ_{S_1}, are related linearly to the mechanical properties of the work material
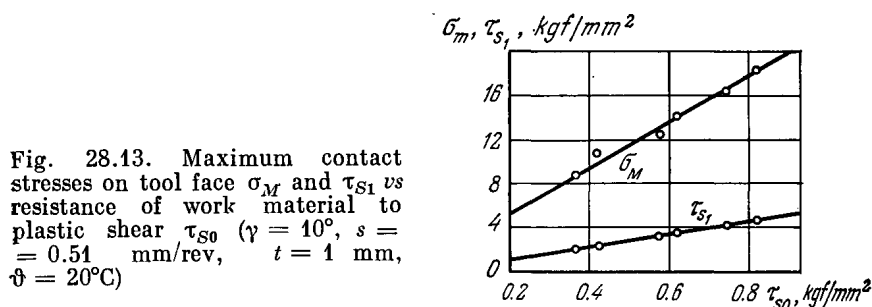
Fig. 28.13. Maximum contact stresses on tool face σ_M and τ_{S1} vs resistance of work material to plastic shear τ_{S0} ($\gamma = 10°$, $s = 0.51$ mm/rev, $t = 1$ mm, $\vartheta = 20°C$)

(Fig. 28.13). Here, the values of σ_M and τ_{S_1} are given as dependent on the shear strength τ_{so} of the material at a relative shear equal to 2.5.

Over an area of elastic contact between the tool and the structural metals having a considerable elastic modulus, the coefficient of friction, f, is determined largely by the molecular component f_1 [3], that is

$$f \approx f_1$$

The molecular component f_1 of the coefficient of friction depends on the contact conditions [11]. When $p_r = \sigma_N$

$$f_1 = \frac{\tau_0}{\sigma_N} + \beta$$

here, τ_0 is the tangential stresses in the absence of normal stresses; β is the coefficient allowing for the action of normal stresses.

The values of τ_0 and β depend on the contact temperature (Figs. 28.14 and 28.15), whose variation across the width of the contact between the chip and the tool is rather complex (Fig. 28.16) [10].

Typical diagrams of distribution of the contact stresses and the coefficient of friction (found as the ratio of tangential stresses to normal stresses) are given in Fig. 28.17.

The mean coefficient of friction, f_m, on the tool face largely characterises the mean tangential-to-normal stress ratio in the deformed contact layer of chip, because the main part of the contact load is
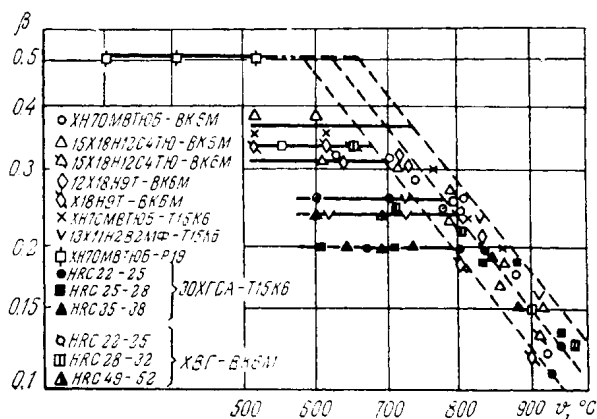
Fig. 28.14. Effect of contact temperature and contacting materials on coefficient β
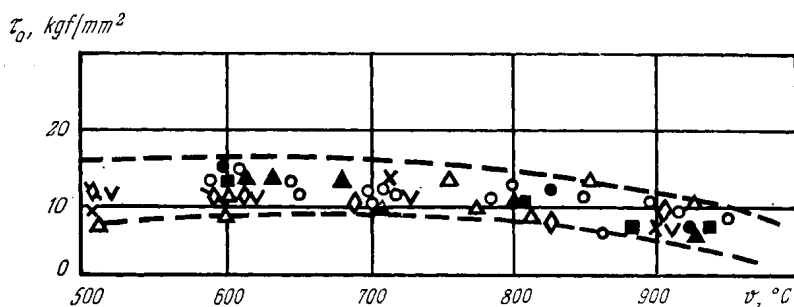
Fig. 28.15. Effect of contact temperature and contacting materials on magnitude of τ_0 (the same designations as in Fig. 28.14)
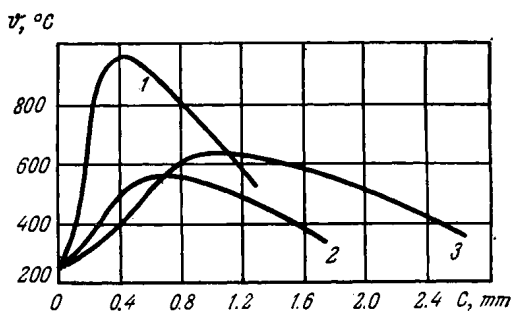
Fig. 28.16. Variation of temperature across contact of chip with tool: s = = 0.3 mm/rev, $t = 2$ mm, $\varphi = 45°$, $v = 60$ m/min
1—BK8 on steel 12X18H9T; 2—T15K6 on steel 25; 3—BK8 on steel 25

concentrated in the plastically deformed area. For this reason, f_m depends to a considerable extent on the mean normal contact pressure (Fig. 28.18).
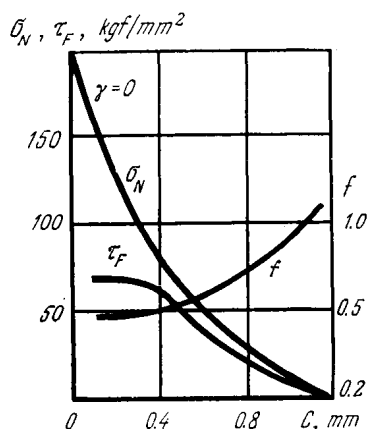
Fig. 28.17. Distribution of contact stresses and coefficient of friction over the face of tool T15K6 during cutting steel 08Х18Н9Т
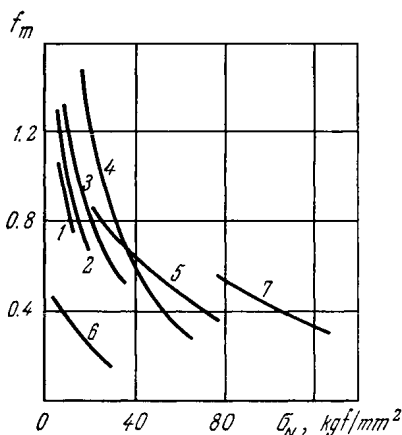
Fig. 28.18. Mean coefficient of friction f_m vs contact stress in cutting various materials

1—copper B, $\gamma = 10°$; 2—copper A, $\gamma = 25°$; 3—iron, $\gamma = 10°$; 4—steel 12ХН3, $\gamma = -10°, +20°$; 5—bronze БрБ2 HB 110, 120, $\gamma = 10°$; 6—bronze БрБ2, HB 320, $\gamma = 10°$; 7—cadmium, $\gamma = -30°$ to $+10°$

An indirect influence of f_m on the parameters of the cutting process manifests itself mainly through the chip-forming characteristics [9].
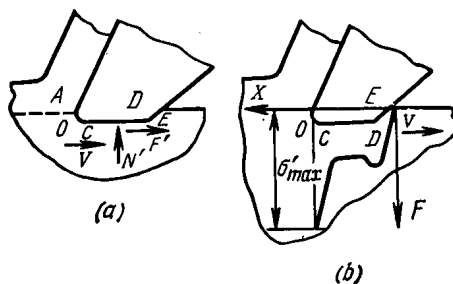
Fig. 26.19. Contact of tool flank with cutting surface (a) and typical distribution of normal stresses over tool flank (b)

Tool flank. Fig. 28.19 shows a contact diagram for the tool flank in an actual instance, with regard to the cutting-edge rounding and a land caused by wear, which emerges immediately after the cutting process is started. The rounding of the cutting edge forms a junction

207

of the face and the flank. At the point O, the material being processed comes off, forming the chip. This point belongs both to the tool face and tool flank. As is noted before, the normal stresses reach a maximum magnitude σ_M at this point. Hence, the maximum normal stress is equal to σ_M on the flank as well.

At the point D, the sharp edge of the wear land is bound to produce a stress concentration similar to that arising under the edges of a rigid, symmetrically loaded die.
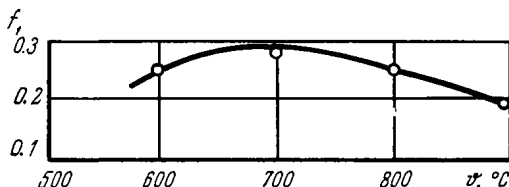
Fig. 28.20. Relationship between molecular component of coefficient of friction and temperature. BK8 on alloy XH77TIOP

The normal load due to the reaction of elastic recovery of the cutting surface acts over the rest of the contact area on the tool flank.

Like the tool face, the whole contact width on the flank can be divided into two sections: the section directly contiguous to the cutting edge (the stagnant zone) and the section at which external friction is effective*. As the wear land on the tool flank grows, the second section increases and becomes predominant. To a first approximation, the coefficient of friction, f', at this section equals the molecular component f_1' [3], that is

$$f' \approx f_1' = \frac{\tau_0}{p_{eff}} + \beta \approx \frac{\tau_0}{HB} + \beta$$

where HB is the hardness of work material at a given temperature, measured with the use of a spherical indenter made from the specified tool material. Since with rising temperature ϑ the value of HB decreases, whereas the value of β begins to decrease from a certain temperature ϑ_t (see Fig. 28.14), the function $f_1' = f(\vartheta)$ has a maximum at a temperature close to ϑ_t (Fig. 28.20).

28.2.2. Wear Characteristics of Cutting Tools

The tool face and flank wear away over their contact areas.

Wear elements. Depending on the cutting conditions, subject to severe wear is either the flank (Fig. 28.21a) or the face (Fig. 28.21b) of the tool. In some instances, flank wear and face wear reach the

---

* A spot of plastic contact may appear around point D (Fig. 28. 19b).

limit values simultaneously (Fig. 28.21c). The cutting-edge radius also changes because of tool wear (Fig. 28.21d).

Tools wear away predominantly on the flank where the chip section is small, particularly in the finish machining of low-ductile materials.
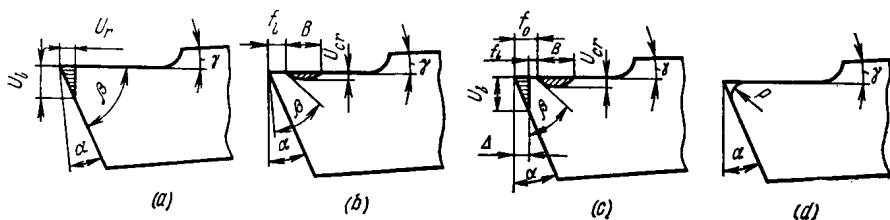
Fig. 28.21. Wear elements of cutting tool
(a) flank wear; (b) face wear; (c) flank and face wear; (d) rounding-off of cutting edge

Face wear is prevalent where the flank is protected against wear by the stagnant zone (the built-up edge) or where the face temperature is substantially higher than the flank temperature. Typical of face wear is a crater emerging on the tool face at some distance from the
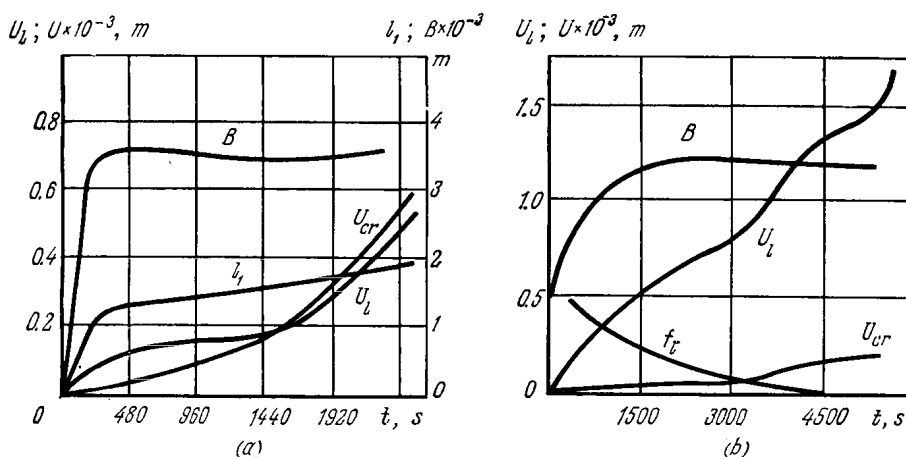
Fig. 28.22. Change of wear elements in time in machining steels (U_{cr}—depth of crater, B—width of crater, l_1—length of crater; U_l—width of wear land on flank, f_l—width of wear land on face)
(a) for high-speed steel tool; (b) for cemented-carbide tool

cutting edge. As wear is in progress, the width and depth of the crater increase, and its curvature radius diminishes.

Flank wear results in a wear land of a constant or a variable length. When the face and flank wear away simultaneously, the width of the face portion between the crater and the cutting edge gradually decreases from both sides and the strength of the cutting edge diminishes.

Typical wear curves. Effect of the cutting time (or travel) on wear of high-speed steel tools and cemented-carbide tools in machining structural steels is shown in Fig. 28.22. Ceramic tools wear predominantly on the flank. In finishing and operations, the accuracy and surface roughness of the workpiece is mostly affected by the radial wear U_r (referred to as dimensional wear) measured in a direction perpendicular to the surface machined (Fig. 28.21a).
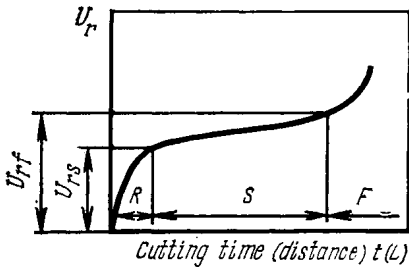
Fig. 28.23. Change of dimensional wear with cutting time (distance)

The rate of dimensional wear in cutting tools varies with time non-uniformly (Fig. 28.23). The first period of operation (R) is characterized by fast wear (running-in) because of micro-chipping, sharpening defects, etc. The third period (F) also features fast wear due to the increase in contact temperature, cutting force, vibrations, etc. The second period (S) corresponds to steady-state wear. Normally time of operation at the running-in section is comparatively short, and the cutting distance is tenths of the total cutting distance.

Tool-dulling criteria. The amount of wear at which a tool must be taken out of operation is called the *dulling criterion*. The time of tool operation between two successive sharpenings characterizes its life period T.

When the face wear predominates, the dulling criterion is expressed by the ratio

$$K_{cr} = \frac{U_{cr}}{\frac{B}{2} + f_b}$$

(the designations are given in Figs. 28.21 and 28.22).

The allowable wear of the tool face has effect on the strength of the cutting end and is determined by the tool material.

With the prevailing flank wear, distinction is made between the optimum and the manufacturing dulling criterion ($U_{d,\ opt}$ and $U_{d,\ mfg}$, respectively). The $U_{d,\ opt}$ criterion provides for a maximum tool life. This criterion is used where no special requirements concerning the workpiece accuracy, surface finish, etc. are imposed on the cutting process. In contrast, the $U_{d,\ mfg}$ criterion makes allowance for workpiece accuracy and surface-finish; therefore, it is applicable mostly to finishing operations. The values $U_{d,\ mfg}$ cannot be taken constant because they change with the cutting conditions. For this reason, the tool life T is difficult to determine where the cutting conditions vary over a wide range, and wear has to be assessed by the following relative characteristics:

(a) wear rate

$$I = \frac{U_r - U_{st}}{(l - l_{st})\,10^6}$$

and (b) relative wear of the surface being machined

$$U_w = \frac{(U_r - U_{st})\,1000}{1\,0\,(l - l_{st})\,s}\,\frac{\mu m}{cm^2}$$

where l is the length of path of the tool in the metal, over which wear has been measured, m; U_r is the shortening of the tool, μm; s is the factor numerically equal to the feed of the tool, mm. The index "st" designates the values effective at the starting moment of measurement.

Characteristics of machinability depend not only on the work-material properties, but also on the physico-mechanical properties of the tool material, the geometry of the tool, the cutting fluid, and other factors. Among those factors, the cutting conditions alone have a direct influence on the machining costs and output. For this reason, the effect of other factors is assessed through the allowable cutting conditions among which the depth of cut, t, and the feed, s, are usually controlled by other additional factors (machining allowance, surface-roughness parameters, etc.). Normally, the cutting speed v alone is an independent variable; therefore, the effect of other cutting conditions on wear should be considered in conjunction with cutting speed. An experimental relationship between the cutting speed and various factors can generally be presented as

$$v = \frac{c_v}{T^m s^{y_v} t^{x_v}}\,k \qquad (28.1)$$

where c_v is a constant for a particular group of work materials; k is the product of the coefficients that allow for the properties of the tool material and its geometry, the properties of cutting fluid, the type of machining, the allowable wear, etc.

The figures given below are approximate ratios of the lower to the upper magnitude of cutting speed that correspond to changes in each of the vital factors:

Work material	. . . . . . 1 : 100	Chip width	. . . . . 1 : 3
Tool material	. . . . . . 1 : 25	Tool geometry	. . . . 1 : 3
Chip thickness	. . . . . . 1 : 5	Cutting fluid	. . . . . 1 : 2

Formula (28.1) is suitable for calculation of various cutting conditions, the cutting speed v_T being found in accordance with the adopted tool life T. With variation of cutting conditions over a wide range, the exponents and coefficients change substantially.

In heavy and precision engineering as well as in automated production, where the main requirement placed on cutting tools is their long dimensional wear life, formula (28.1) must not be used as it
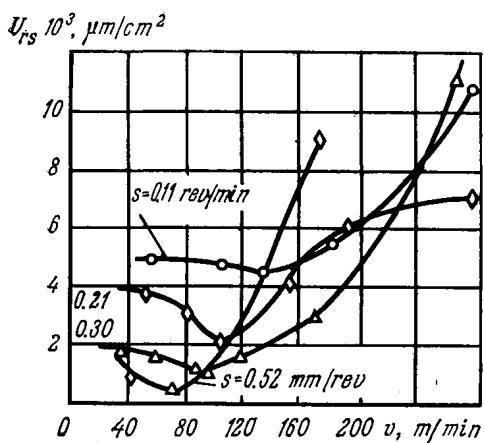
Fig. 28.24. Effect of cutting speed and feed on relative wear of tool T15K6 in turning steel 30XГCA; $t = 1.5$ mm

Fig. 28.25. Effect of cutting speed on relative wear and work surface roughness in turning alloy XH77TЮP with tool BK6M

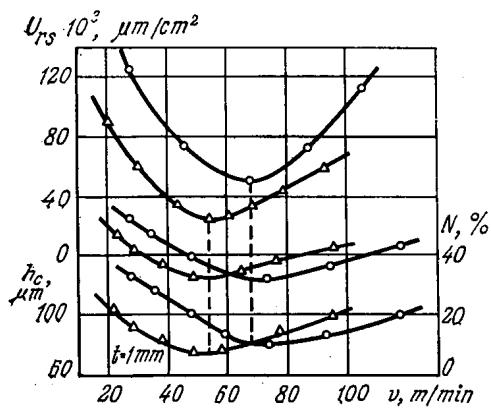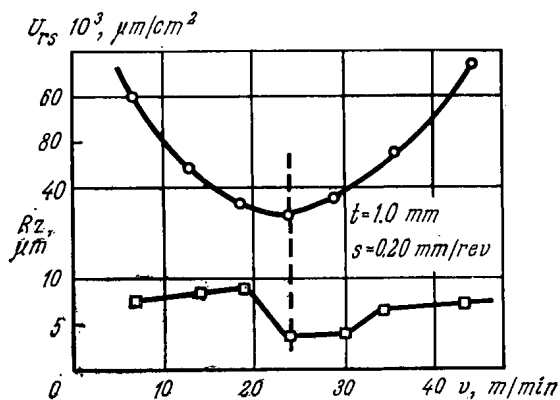Fig. 28.26. Effect of cutting speed and feed on tool wear and work hardness in turning steel 15X18H12C4TЮ with tool BK6

may give cutting speeds unfavourable in regard to tool life. The best results are obtained by specifying an optimum cutting speed v_0 [6] ensuring the lowest dimensional wear rate (Fig. 28.24). Machining
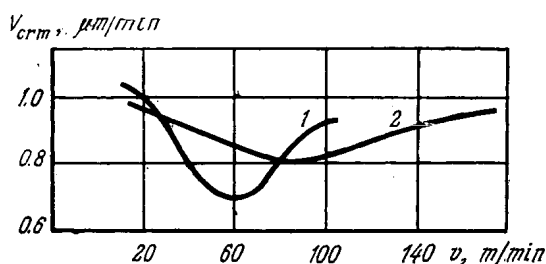
Fig. 28.27. Relationship between dissolution rate of work surface layer for steels 08X18H9T (1) and 15X18H12C4TЮ (2) (electrolyte 51% H_2SO_4, 47% H_3PO_4, and 2% H_2O; current density 0.16 A/cm²)

at optimum cutting speeds gives more than the best accuracy and lowest tool consumption; it produces the smallest surface roughness (Fig. 28.25) and the minimum work hardening (Fig. 28.26), whereby
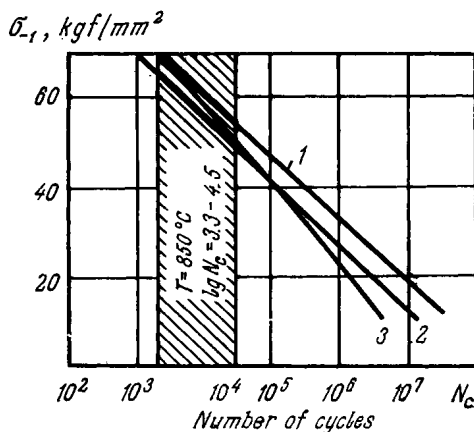
Fig. 28.28. Effect of cutting speed in turning parts from alloy ХН77ТЮР on their fatigue strength in high-temperature service

1—$v = v_0$; 2—$v > v_0$; 3—$v < v_0$

the parts machined acquire the highest resistance to corrosion (Fig. 28.27) and wear, and the highest fatigue resistance in operation at high temperatures (Fig. 28.28).

28.2.3. Effect of the Shear Strength of Intermolecular Bonds on Wear Rate of Cutting Tools

The effect of adhesion (molecular interactions) as an active factor in the wear mechanism of cutting tools can be estimated in quantitative terms by the general laws of fatigue wear at low-cycle fatigue [11]. This conclusion is supported particularly by the fact that for

213

a given tool material and type of machining, and with micro-strength of the tool contact area unaffected by the work material and the
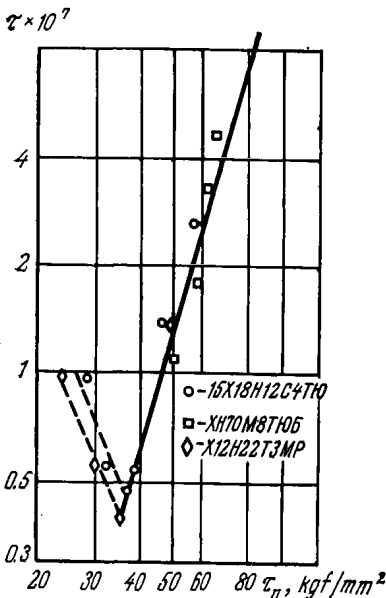
Fig. 26.29. Influence of strength of molecular bonds on wear rate of tool BK6M at different contact temperatures
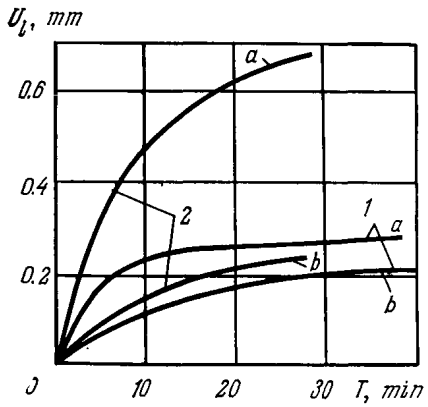
Fig. 28.30. Wear of cemented-carbide tools with nickel-phosphorus coatings (1) and uncoated (2)

(a) near nose; (b) along main flank. Work material-steel 4X14H14B2M

environment, wear rate of the tool is definitely determined by the strength of intermolecular bonds in shear, τ_n (Fig. 28.29):

$$I = A_1 \tau_n^t \qquad (28.2)$$

where A_1 and t are constants typical of a given tool material and type of machining (Table 28.7).

Table 28.7

Values of coefficients A_1 and t in finish turning

Tool material	A_1	t
T15K6	3.4×10^{-13}	3.0
BK6M	1.7×10^{-13}	3.5
P18	1×10^{-11}	2.0

In such conditions, the tool wear rate diminishes with increasing temperature ϑ_c because of reduced τ_n. This process takes place until

214

an optimum temperature ϑ_0, corresponding to the minimum wear rate I, is reached.

At a cutting temperature higher than ϑ_0, the wear rate increases despite further reduction in τ_n, and wear data obtained by machining different materials fail to obey the general relationship. This fact provides evidence of independent effect of the cutting temperature and the properties of work material, which weaken the tool contact area unevenly due to diffusion of various chemical elements [5].

Increasing the tool life. One effective method of increasing tool life is strengthening the tool surfaces by plastic deformation, for instance, by shot peening, diamond burnishing, ball burnishing, or ultrasound.

It has been indicated that single-point tools, made from high-speed steel P18 and P9K5 and strengthened by the ball-burnishing of the face and the flank have the wear life 2.0 to 2.5 times that of unstrengthened tools.

Another, radically different, way of improving tool life consists in setting up conditions that lessen friction and heat generation in the working zone. Such conditions are achieved by applying antifriction coatings to cutting tools. It has been found that multi-component systems including solid lubricants and binders can be used as a coating. Good results have been obtained with electroplated coatings based on compounds of phosphorus and some metals, for instance, nickel (Fig. 28.30). The wear life of tools from high-speed steels P18, P6M3, and P6M5 coated with a phosphorus-nickel compound is increased from 2.5 to 5 times.

The tool life is sufficiently improved through depositing hard coatings of titanium carbides and other materials on tool surfaces by plasma spraying or other methods.

28.3. WEAR IN METAL-FORMING TOOLS

Non-uniform distribution of deformations and stresses is the main factor that governs the operating conditions for metal-forming tools and, hence, their service life*. The magnitude of pressure on the die surface depends on the resistance of the work material to deformation and the speed of the latter; the thermal effect due to fast deformation is also considerable.

Prevailing types of die wear. Wear, or changes in the profile of dies, may be in the form of attrition (removal of wear particles away from the friction area), deformation arising in the course of the stamping process, and cracking due to thermal fatigue. Attrition is governed to a large extent by the work-metal flow rate, the amount

---

* The service life of forging dies is usually determined by the number of forgings produced up to the major repair of the die.

of the flowing metal and the limiting frictional conditions. The wear of the flash recess is in direct proportion to the amount of metal flowing into it (Fig. 28.31).

Deformation, thermal cracking, and attrition are the main, but not unique, factors affecting die profile; other factors, which may also come as prevalent wear forms, are destruction due to fatigue
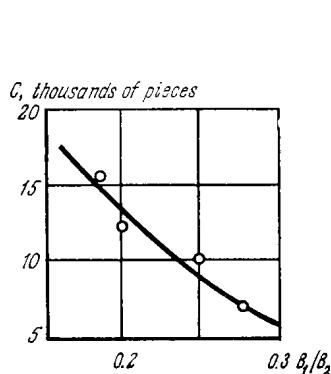

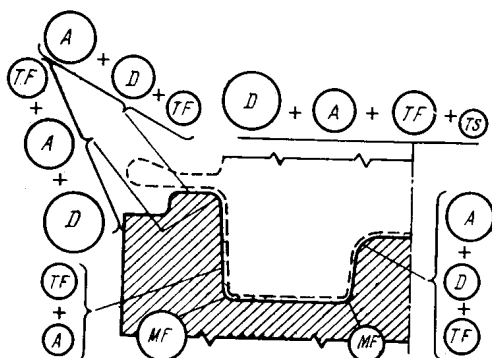Fig. 28.31. Variation of hammer-die service life C with flash-to-forging mass ratio (B_1/B_2)

Fig. 28.32. Types of wear and their combinations in forging dies

TF — thermal fatigue cracking; A—attrition; D — deformation; MF—mechanical fatigue; TS—thermal shock destruction

in places of maximum stress concentration; thermal-shock destruction due to sharp temperature changes; and surface scaling, which is a continually acting cause of wear, determined by temperature and time conditions.

All the above-mentioned factors are interactive (Fig. 28.32). The predominant type of wear can be detected for both individual portions and the whole working surface of the tool. The problem of extending the die service life should be dealt with by stages, as follows:

(1) reveal the predominant type of wear;

(2) single out the most wear-prone sections of the die profile, whose dimensional losses result in failure of the die;

(3) find out the main causes of severe wear (die material or design, operating-temperature conditions, etc.);

(4) specify measures for improving the tool life.

Factor affecting the die service life. Depending on the blank mass, a higher tool life under identical service conditions can be obtained either on hammers, or on presses (Fig. 28.33).

With increasing the die-to-blank mass ratio and also with changing over to gas heating, the service life of dies becomes longer (Figs. 28.34 and 28.35). The life of gear-blank forging dies notably depends on the relative height of the flash recess (Fig. 28.36).
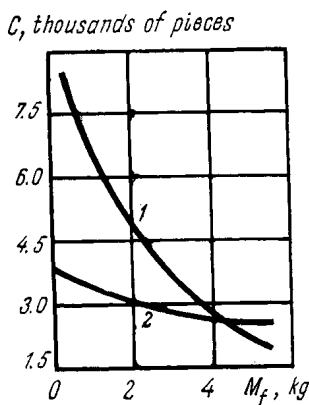
Fig. 28.33. Life of hammer and forging dies (C) as a function of forging's mass (M_f):
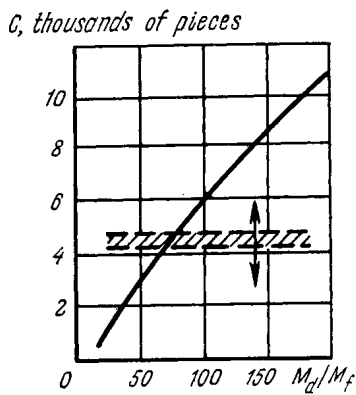
1—on hammers; 2—on forging presses

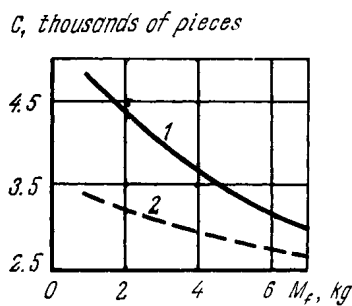Fig. 28.34. Life (C) of hammer dies as a function of die-to-forging mass ratio (M_d/M_f)

Fig. 28.35. Effect of blank heating conditions on die life (C) for forgings of different mass (M_f)
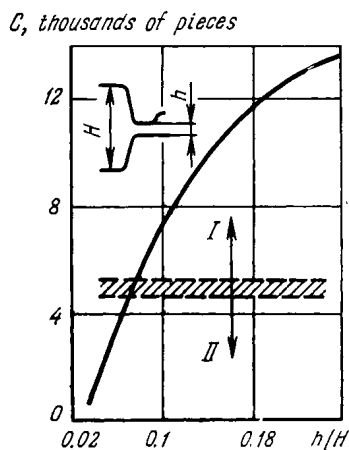
1—gas heating; 2—oil heating

Fig. 28.36. Life (C) of hammer dies as a function of relative height of flash recess (h/H):

I—attrition; II—deformation

Special nomographs (Figs. 28.37 and 28.38) are devised for determining the flash cross-section area and the wear life of the flash-recess surface, depending on the diameter D or length l of the forging.

The nomograph in Fig. 28.39 shows the relationships between the minimum design wall thickness δ_{min} and ГКМ-punch wear life, on the one hand, and the diameter D_{in} and depth H of the recess,
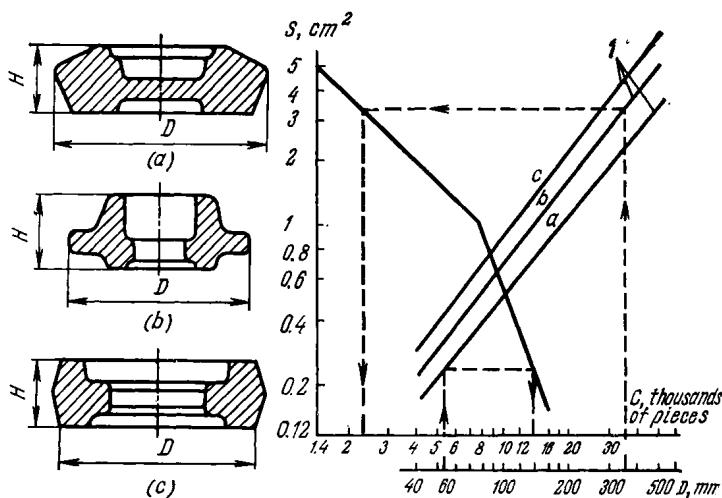
Fig. 28.37. Nomograph for determining flashcross section area S (*1*) and wear life C of die flash recess (*2*) depending on the forging's diameter

(a, b, and c) groups of forgings in terms of complexity

on the other hand. If the punch has, for some reason, a departure from the design wall thickness δ_{min}, then the respective change in life (correction factor P) is determined depending on the δ/δ_{min} ratio, where δ is the actual wall thickness.

Extending the tool life. The application of the lower tolerance limits to the initial, most rapidly changing, dimensions improves, in some instances, the service life of forging tools by 30 to 40 percent.

The external rounding-off radii have a considerable effect on tool life: an increase in the radii from 3 to 6 mm may, in some cases, extend the life by a factor of 2 to 3.

Locating, where possible, the deeper cavity in the upper half of the die ensures identical thermal conditions and identical durability for both die profiles, with the result of increased life of the die set.

On large forgings, changeover from hammers to presses gives an extended tool life even under identical operating conditions.

When forging small parts, the life of МГШП dies can be increased by cleaning the blanks of scale, by changing over to electric heating, by automatic lubrication, by cooling the dies, etc.

An effective way of extending the life and reducing the work content and costs of metal-forming tools is the application of the electrical-discharge and electrochemical methods to producing die cavities. These methods eliminate decarburization of the surface
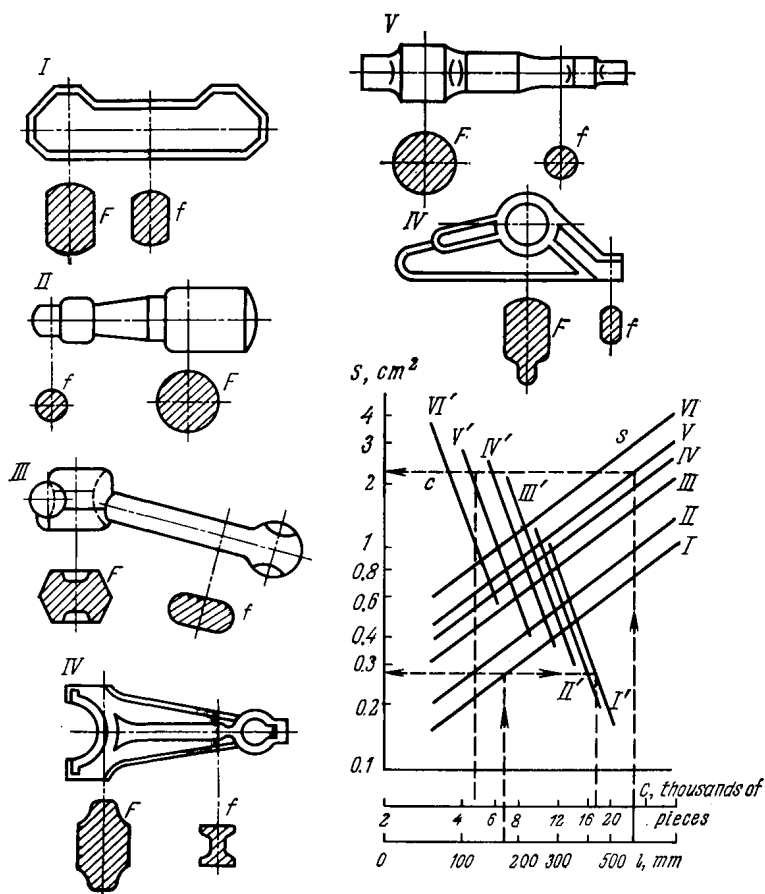

Fig. 28.38. Nomograph for determining flash cross-section area (S) and wear life (C) of die flash recess depending on the forging's length
F/f = 1-1.2 (I); 1.3-2 (II); 2.1-4 (III); 4.1-6 (IV); 6.1-9 (V); over 9.0 (VI)

layer, distortion of the die profile, and thermal cracking, since the heat treatment becomes here a preliminary operation.

Diffusion treatments, which impart a number of specific properties to the surface layers, are also suitable for increasing the service life of hot forging tools. There are reports [1] on successful applications of various diffusion hardening methods, including the tradi-

219

tional (nitriding, carburizing and carbonitriding) and the new ones (chromizing, boronizing, and metalliding).
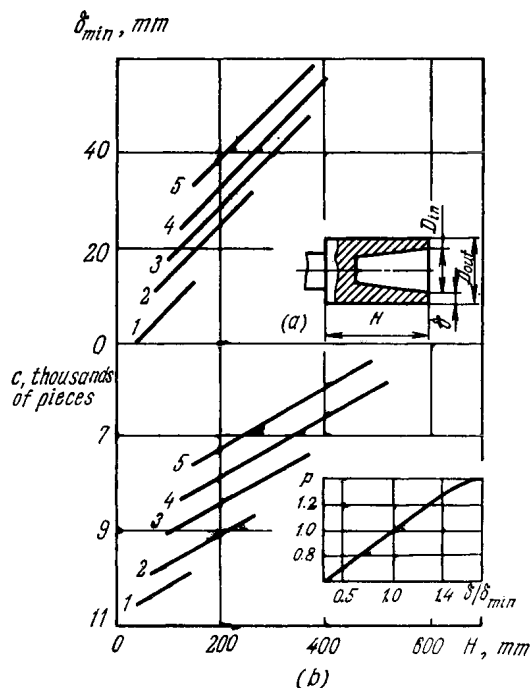

Fig. 28.39. Nomograph for determining punch wall thickness δ (a) and life C (b) at sizes of D_{in}, and influence of wall-thickness deviation δ/δ_{min} on punch life (correction factor P)
1—12 mm; 2—30 mm; 3—50 mm; 4—70 mm; 5—90 mm

28.4. CUTTING FLUIDS AND LUBRICANTS AND THEIR EFFECT ON METAL-CUTTING AND METAL-FORMING PROCESSES

Most machining operations are performed with the use of cutting fluids and lubricants.

The purpose of cutting fluids is to provide lubricating, cooling, and rinsing effect. The lubricating effect is taken to mean the ability of cutting fluids to form on the contacting surfaces of the tool, the chip, and the workpiece itself protective films [2] that reduce the friction forces and the adhesive interaction between the tool and the workpiece. These films make for reduced cutting forces and heat generation; they also improve the work surface finish and the tool life.

220

The cooling effect of cutting fluids consists mainly in the removal of heat from the hot tool and work contact surfaces by convection. The result of cooling is a reduction in cutting temperature and bulk temperature of the tool and the workpiece.

By the rinsing effect of cutting fluids is meant their ability to remove wear debris from the cutting zone. The rinsing effect manifests itself in slower abrasive wear of the tool and better work surface finish.

The chemical composition and main characteristics of the cutting fluids now in use are given in Table 28.8.

The choice of a cutting fluid is determined by the type of machining operation and the properties of the tool and work materials
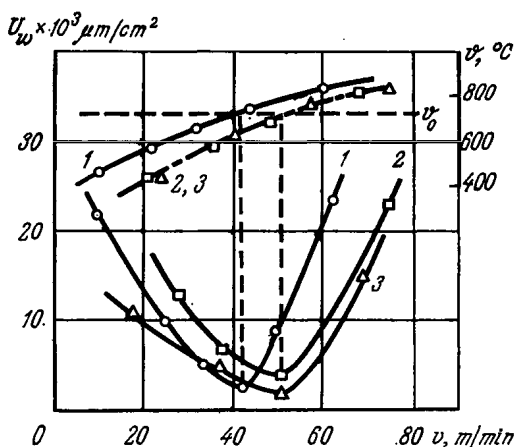
Fig. 28.40. Effect of cutting speed on temperature and wear of tool BK8 in turning of heat-resisting alloy XH77TЮP dry (1) and at flooding with various cutting fluids (2 and 3): 2-5% emulsifying-oil solution Э-2 (GOST 1975-53); 3-5% emulsifying-oil solution based on monoethanolamine oleate ($t = 0.5$ mm; $S = 0.08$ mm/rev)

(Table 28.9). The method of its supplying to the cutting zone has a marked influence on the performance of a cutting fluid (Table 28.10).

The effect provided by a specific cutting fluid depends on the work and tool materials and on the cutting conditions. Heat generation in machining brittle materials (cast irons) is always lower than in machining ductile materials (steels). For this reason, the use of cutting fluids improves the tool life to a smaller extent with cast irons than with steels.

Cemented carbides are more heat resistant than high-speed steels; therefore, the effect of cutting fluids on tool life is less pronounced for cemented carbides, than for high-speed steels.

For each specific tool-workpiece combination, there is a range of speeds and feeds over which the use of cutting fluids gives the best results (Fig. 28.40). From Fig. 28.40 it follows that (1) the applica-

Table 28.8

Composition and characteristics of cutting fluids

Main action	Base	Type of fluid	Additives	Properties and effect
Cooling and flushing	Water	Electrolytic solutions	Corrosion inhibitors (1-5%): soda ash, borax, sodium nitrite, trisodium phosphate, sodium fluoride	High cooling and flushing properties. Increased tool wear and coarser surface roughness
		Surfactant solutions	Apart from corrosion inhibitors, various soaps (2-5%): potash soap, soda soap, soaps of oleic, naphthenic, and other fatty acids	Improved lubricating ability. Longer tool life
		Emulsions	The most common emulsifying oils (1.5-10%): oil И-12А or И-20А, base, with one of the following additives: acid oil (Э-2), acid oil and tallow oil (ЭТ-2), sodium sulphonate (МГЛ-205), molybdenum disulphide (СДМУ)	Retained lubricity at high contact pressures and temperatures
Lubricating	Oil	Vegetable oils (sunflower-seed oil, linseed oil, colza oil, etc.)	No additives	The best lubricants, but costly and insufficiently stable
		Mineral oils И-12А, И-20А		Moderate viscosity. Poor lubricating properties
		Mineral oils with additives	1. Up to 30% of vegetable oils and fats (compounded oils) 2. Oleic acid, oxidized petrolatum, kerosene, carbon tetrachloride 3. Sulphur (sulphurized oil) no less than 1.7%	Low thermal conductivity and heat capacity. High lubricity

Table 28.9

Suggestions on selection of cutting fluids

Type of machining operation	Typical conditions in contact area	Main requirements placed on cutting fluids	Recommended cutting fluid
Rough machining at low cutting speeds (in automatic and semiautomatic operations)	Low heat-release rate	High lubricating properties	Mineral oils, sulphurized oils
Rough machining at high cutting speeds	High heat-release rate	Cooling action	Water-base emulsions
Rough and finish machining of high-strength and heat-resisting steels and alloys	Elevated contact pressures and temperatures	Increased resistance of protective films to normal contact pressures	Emulsions with surfactant additives
Finish and form machining at low and medium cutting speeds: threading, gear cutting, etc.	Low heat-release rate	Lubricating action	Straight and additive oils, sulphurized oils
Finish and form machining at high cutting speeds	High heat-release rate	Reduction of cutting temperature	Emulsions with 5-10% of emulsifying oil
Finish and form machining of cast iron (reaming, tapping, etc.)	Discontinuous chips, abrasive wear of tools	Flushing and lubricating action	Kerosene

Table 28.10

Methods of applying cutting fluids

Applying method	Flow rate, litres/min	Characteristics
Free flow: in turning in drilling in milling in tapping	10-15 8-10 7-20 2-3	Simplicity and high dependability. Intense gushing, high consumption rates. Observation of cutting zone is difficult
Flow directed from tool-flank side at a pressure: low (1-2 kgf/cm²) high (15-20 kgf/cm²)	1-1.5 0.3-0.5	Relatively small consumption of cutting fluid. Improved cooling effect. Careful cleaning of cutting fluid is essential
Atomized cutting fluid	0.5-3.2 g/h (oils); 200-400 g/h (emulsions)	Lowest consumption of cutting fluid. Observation of cutting zone is easy, cooling effect is considerable. Good ventilation is necessary

Table 28.11

Lubricants for cold metal forming

State of aggregation	Type	Base	Properties and performance characteristics
Oils	Fatty and vegetable oils	Fats (esters of glycerine and fatty acids)	Chemically stable. Resistant to high pressures and have excellent lubricity. Expensive
	Mineral oils	Neutral hydrocarbons, naphthenic acids, and sulphides	Non-saponifiable. Inactive, well-resistant to oxidation. Used in forming soft non-ferrous metals
Emulsions	With liquid emulsifiers (soaps)	Water-oil (most frequently, spindle oil)	High cooling ability, viscosity and tackiness. High chemical stability. Foam formation is possible
	With solid emulsifiers (kaolin)		
Solid lubricants	Sodium and calcium soaps	Compounds of salts and fatty (including synthetic) acids	Applicable chiefly to drawing. Moisture in soap is objectionable
	Molybdenum disulphide	MoS$_2$	Withstands high pressures and temperatures. Good for working hard-deformable steels and alloys and also magnesium and its alloys
	Graphite	Carbon	Withstands high pressures and temperatures. Used in mixture with oil
	Salts, liquid glass, phosphates	—	Withstand high temperatures
Greases and oils with fillers	Solid oils	Mineral oils or fats thickened with soaps (up to 10-20%) and other fillers	Convenient to use. Consumption is not high. No fouling of working place. Cooling ability is insufficient
	Oils filled with graphite, molybdenum disulphide, crushed rod sulphur, talc, fine powder of soft metals or organic substances (sawdust, bran, etc.)	Mineral oil, fat, or compounded oil	Better surface quality of product. Excellent lubricity. Used for working ferrous metals, nickel, and its alloys

Table 28.12

Lubricants for hot metal forming

State of aggregation	Type	Operating temperatures, °C	Performance characteristics
Liquid lubricants	Silicone lubricants	400-500	Non-inflammable. Applicable in industry
	Lubricants based on ethers of phosphoric acid	≤ 760	Cheap. Insufficiently studied.
	Fluorocarbon compounds	300-320	High cost. Low vapour pressure
	Halogenated oils	≤ 300	High thermal stability. Low strength of lubricant film. Toxic
Liquids with fillers	Oils filled with molybdenum disulphide, graphite, talc, mica, chalk	≤ 400	Provide liquid and gas lubrication for short-term processes
	Phosphate solution of a 10-15% concentration with 5-15% mica		Gives a good lubricating effect and reduces rolling pressure
Solid mineral lubricants	Graphite	≤ 700	Carburization of product surface may occur at high temperatures. Produces persistent dust, and fouls the working place
	Molybdenum disulphide (pastes)	≤ 630	High thermal resistance and lubricity
	Talc, mica, bentonite	≤ 1 000	Exceptionally high thermal resistance, but low lubricity
	Glasses (enamels)	450-1 200	In use melt and operate as liquids
	Salt melts: chlorides, phosphates	400-800	Suitable for application and removal. Used on piercing presses, in hot die forging, and stamping bars of non-ferrous alloys

tion of a cutting fluid does not change the extremum-type character of the curve representing the relation of the tool wear rate to the cutting speed and the optimum operating temperature; (2) surfactants added to a cutting fluid do not practically alter its effect on the

cutting temperature; and (3) the optimum cutting speed v_0 is 25 percent higher with a cutting fluid than without it. At a speed lower than v_0, the operating temperature (with the use of a cutting fluid) departs from the optimum value ϑ_0 to a greater extent, and the wear rate of the tool grows, thus making the application of the cutting fluid ineffective. In machining at a speed v_0, a cutting fluid with surfactant additives gives a 1.5 to 2 times increase in tool life.

Thus, the correct specification of cutting speeds and feeds in combination with a particular cutting fluid is an important factor.

The use of lubricants in metal forming. Friction in metal forming is detrimental except for some operations where it plays an active part (for instance, in rolling, expanding, some sheet-metal working operations, etc.). An appropriate lubricant sharply reduces the coefficient of friction. A lubricant must form a strong lubricating film; it must well adhere to the contacting surfaces and, at the same time, be easily removable after machining.

The formulations of current lubricating substances for low-temperature metal forming are many and varied [12], and their classification by the state of aggregation is considered to be the most convenient (Table 28.11).

Lubricants for high-temperature metal-forming operations make up a separate group that features high thermal stability (Table 28.12).

REFERENCES

1. Бельский Е. И. Стойкость кузнечных штампов. Минск, «Наука и техника», 1975, 240 с.
2. Вопросы применения СОЖ при резании металлов. Под ред. М. И. Клушина. Иваново, Верхне-Волжское книжное издательство, 1965, 179 с.
3. Крагельский И. В. Трение и износ. М., «Машиностроение», 1968, 480 с.
4. Креймер Г. С. Прочность твердых сплавов. М., «Машиностроение», 1971, 200 с.
5. Лоладзе Т. Н. Износ режущего инструмента. М., Машгиз, 1958, 355 с.
6. Макаров А. Д. Износ и стойкость режущих инструментов. М., «Машиностроение», 1966, 264 с.
7. Подураев В. Н. Резание труднообрабатываемых материалов. М., «Высшая школа», 1974, 590 с.
8. Платов А. Б. Твердые сплавы.— Сб. «Труды ВНИИТС», № 2, Металлургиздат, 1960, 82 с.
9. Развитие науки о резании металлов. Под ред. Н. Н. Зорева, Г. И. Грановского, М. Н. Ларина, Т. Н. Лоладзе и И. П. Третьякова. М., «Машиностроение», 1967, 416 с.
10. Резников А. Н. Теплофизика резания. М., «Машиностроение», 1969, 288 с.
11. Роль сил трения в износе режущих инструментов. Под ред. А. Д. Макарова.— Труды УАИ, вып. 69, Уфа, 1974, 104 с.
12. Чертавских А. К., Белосевич В. К. Трение и технологическая смазка при обработке металлов давлением. М., «Металлургия», 1968, 362 с.

FLEXIBLE DRIVE ELEMENTS

29.1. BELT DRIVES

One of the main reasons for belt drive failure is wear resulting from slippage of the belt on the pulley. A high coefficient of friction reduces the slippage, and that makes for increased life of the belt. The overall amount of slippage is made up of the slippage component due to longitudinal deformations of the belt on the driving pulley
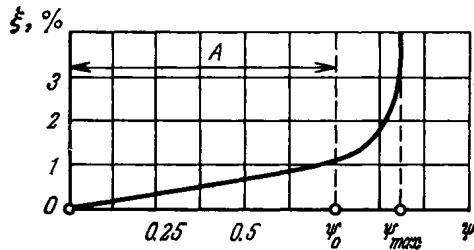

Fig. 29.1. Slippage curve
A—region of elastic slip

and of that due to tangential deformations at the arcs of contact. The slippage is determined as a relative slip $\xi = 1 - \dfrac{v_2}{v_1}$, where v_1 and v_2 are velocities of the tight and slack sides of the belt, the difference in the velocities being due to different tensions of the belt sides. The angle α of belt contact and the absolute value of belt slip grow with the load.

Service qualities and performance of belt drives are assessed with the aid of slippage curves (Fig. 29.1), which depict relation between relative slippage ξ and pulling factor $\psi = \sigma_l/2\sigma_0$, where σ_0 is belt stress due to pre-tension and σ_l is the stress of the belt under load.

A linear relationship between ξ and ψ is observed up to a certain critical value ψ_0, which sets the limit to the rational use of the drive.

Within the region of $\psi_0 < \psi < \psi_{max}$ the belt drive can provide stable operation without slippage, particularly with small-diameter

pulleys. Therefore, in applications where wear is not the principal limiting factor, the belt drive may well be rated for load by the permissible values of the grip factor [11].

Relationship between tensions F_1 and F_2 of the tight and slack sides of the belt, respectively, is expressed by the ratio

$$\frac{F_1}{F_2} = e^{\beta f}$$

where $\beta \approx 0.7\alpha$ is the slip angle.

The pull of the drive is limited mainly by the forces of friction between the belt and the pulley. The coefficient of friction depends on the belt and pulley materials, the condition of the rubbing surfaces (moisture, roughness, etc.), and the belt tension. For each specific case f can be calculated by the method described in Chapter 2.

The life of the belt depends among other things on its resistance to repeated bending.

Belt bending is characterized by the ratio between the design diameter of the pulley and the belt thickness, that is d/δ. With $d/\delta < 20$, peeling of V-belts is observed. The d/δ ratio has a substantial effect on the efficiency η of the drive; a leather belt, for instance, shows $\eta = 0.95$-0.96 at $d/\delta = 70$; $\eta = 0.88$-0.89 at $d/\delta = 40$, and $\eta = 0.83$-0.84 at $d/\delta = 25$. The life of the belt increases with the diameter of the pulley. Another important factor is belt tension, which should be maintained at its optimum value; specifically, for the most commonly used cord-fabric V-belts $\sigma_0 = 9$-12 kgf/cm². Increased pre-tension of the belt raises the pull of the drive but adversely affects its life.

Table 29.1

Physico-mechanical and frictional properties of materials used for pulleys

Material	σ_u, kgf/cm²	$E \cdot 10^{-4}$ kgf/cm²	$f*$
Cast iron СЧ 15-32	—	100	0.32-0.40
Fibre-filled moulding material	300-600	8.5	0.28-0.36
Glass fibre plastic АГ-4В	800	12-15	0.6-0.7
Fabric laminate ПТК	1 000	$(4$-$6.5)10^4$	0.36
Moulding powder К-18-2	200-400	—	0.3-0.32
Polyamid П68	450-500	1.2	0.3
Polycaprolactam (capron)	500-800	0.7-1.05	0.42

* In operation with rubber belt

Pulleys are generally made of cast iron СЧ 12-28 and СЧ 15-32 (Table 29.1) for speeds $v = 25$-30 m/s and СЧ 18-36 for speeds $v = 30$-35 m/s. Plastics also find application for pulleys [7]. The choice of a material should be justified by its wearing characteristics, the most convenient being the linear-wear rate (see Chapter 3),

which is calculated by the formula

$$I = k_1 \varphi p^{-\frac{t_y}{5}+1} E^{\frac{4}{5}t_y-1} \Delta^{\frac{2}{5}t_y} \left(\frac{kf_1}{\sigma_0}\right)^{t_y}$$

where k_1, k, φ are the coefficients (see Chapter 3); p is the normal pressure on the pulley groove sides which is determined by the specified load (tension of the tight side of the belt) and the groove cross-sectional shape.

Table 29.2 presents approximate values of the wear rate of some pulley materials. Wear rate I is used to determine wear U of the

Table 29.2

Wear of drive pulleys in the 1K62 engine lathe with rubber belts depending on pulley material [7]

Material	$I \times 10^9$	Average monthly wear of pulley grooves*, mm
Fibre-filled moulding material ВЛ-2	3.2	0.05
Fibre-filled moulding material heat-treated at 115°C	1.6	0.025
Asborezol (moulding material filled with asbestos fibres)	5	0.07
Fibre glass plastic АГ-4В	1	—
Moulding material filled with:		
cloth laminate waste	2	—
ВЛ-227-63 material + 3% MoS_2	2.2	0.03
Moulding powder К-18-2	3.5	—
Cast iron СЧ 15-32	210	—

* Data obtained in field tests.

groove side over the specified distance of friction. As slip occurs only on the arc of slip rather than the whole arc of contact, the expression for wear calculation takes the following form [11]

$$U = I \frac{2\pi}{f} R_p \psi \left(1 + \frac{\psi^2}{3}\right) nt$$

where R_p is the pulley design radius; n is the number of revolutions per minute.

Wear of pulley grooves produces a change in torque and transmission ratio. These effects can be compensated for by allowances for wear on the groove width.

Laboratory tests of single-groove pulleys with $D_p = 157$ mm at $n = 1\,790$ to $3\,520$ rev/min have shown [12] that among fibre-filled moulding materials the greatest wear resistance is exhibited by grade АГ-4В glass fibre plastic and grade ВЛ-227-65 plastic filled with textile fibres. Calculation of belt drives and choice of the materials are treated in greater detail in reference [10].

29.2. ROPES

In addition to fatigue, wear resistance of wire ropes is influenced by friction between wires in the strands, which results in fretting. Whipping and vibrations intensify this process.

The most effective measures used to increase the wear life of wire ropes are lubrication and protection against abrasive particles. Properly selected lubricants can extend the rope life fivefold.

Ropes are lubricated by brushing, dipping in oil baths or spraying. Lubricants and their properties are described in Chapter 9.

The wear life of a rope is affected by the contact pressure against the sheave surface. The simplest way to prolong rope life is to use sheaves of greater radii made of materials with lower moduli of
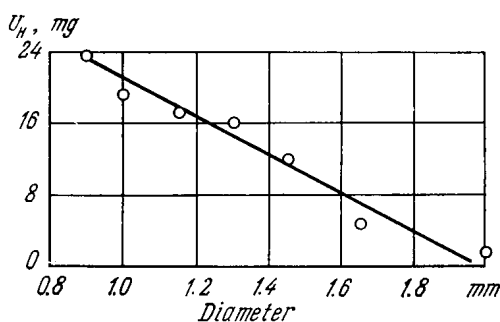
Fig. 29.2. Relation between wear of rope wire specimens and their strain hardening acquired in drawing

elasticity. Friction between the rope and the sheave is reduced by facing the latter with antifriction materials. Steel sheaves are faced with aluminium and cast iron. The facing methods used are given in [8].

Rope wires considerably depend for their wear life on the quality of the surface layer and the extent of the strain hardening developed in drawing. As the wires are drawn to increasingly smaller diameter, the strength and hardness of the material grow but the wear resistance decreases (Fig. 29.2). Hence, the wire material should be checked for frictional qualities as well as for strength.

The extent of rope damage is the most difficult to assess. Roughly, the rope may be removed from service for one of the following reasons: there are from 3 to 5 broken wires for one pitch of a strand; pitch elongation has exceeded 10 percent; the rope diameter has decreased by 10 percent due to wear (the rope diameter should be measured as the largest dimension across the opposite strands).

Ropes of polymeric materials find use as lifting or pulling flexible elements. Table 29.3 gives friction coefficients for a capron rope sliding on a cast iron sheave [9].

Table 29.3

Coefficients of friction of capron rope on cast iron sheave

Friction	Coefficient of friction		Temperature in contact zone, °C
	static	sliding (load moves downward)	
Without lubrication	0.220	0.182	45-50
In oil	0.257	0.190	45-48
In water	0.264	0.271	22-23

At low pressures of the rope on the sheave ($p < 8$ kgf/cm²), wear resistance of polymer ropes is much higher than that of cotton ropes. At higher pressures their wear resistances level off.

At $p = 30$ kgf/cm² dry capron ropes wear 2.5 to 2.7 times longer than when soaked in oil, and 10 to 11 times longer than when soaked in water.

29.3. TRANSMISSION CHAINS

A loss in chain drive performance is largely the result of chain elongation due to wear of the joints. An increase in the chain pitch leads to greater dynamic loads and to failure of individual chain components; the chain may even come off the sprockets.

The maximum permissible increase Δt of the chain pitch is used as a criterion of the chain working condition; chains with pitches increased beyond this limit should be replaced.

For steel roller chains used in general engineering applications the permissible value of Δt is 3 to 4 percent.

Transmission chains used in farming machinery [13] feature a great safety factor, and they have higher limits of Δt (Table 29.4).

The pressure in chain joints should not exceed 360 kgf/cm²; its value depends on the chain speed and lubricating conditions, which are recommended in [3].

Experimental relationships between the wear rate of roller-chain materials and the load are generally described by the expression

$$I_{i} = Kp^m$$

where $m = 1\text{-}3$. For run-in chains $m \approx 1$. The values of $m > 1$ are accounted for by the running-in regime where the initial rubbing surfaces wear off by the amount of the height of surface irregularities. Results of wear tests of open lubricated single-strand roller chains of the ПР-25.4-5000 type are presented in publication [4]. The chains were tested under abrasive action at various working speeds and pressures.

The coefficient of friction with relation to surface roughness, load, and mechanical properties of the materials can be calculated as recommended in Chapter 2. For rough estimation, f can be assumed

Laboratory test data on roller chains

Table 29.4

Chain designation	Specifications				Test conditions		Test results					
	Num-ber of links	Number of sprocket teeth			Load trans-mitted P, kgf	Chain speed, m/s	Operation time				Chain elongation (increase in pitch over nominal size) Δt, %	
		driv-ing	driven	idler			to wear-off dif-fusion layer on pins and bushing		to failure		for chain with worn-off diffu-sion layer on pins and bushings	for chain run to failure
							h	cycles $N_c \cdot 10^{-5}$	h	cycles $N_c \cdot 10^{-5}$		
ПР-12.6-1800-2	240	16	36	16	40	1.98	450	10	540	12	4.7	6.5
ПР-15.875-2300-2	198	25	25	18	100	2.10	180	4.0	415	15	3.8	6.3
ПР-19.05-2500	170	27	27	16	100	2.57	575	1.6	620	18	6.3	6.8
ПР-25.4-5000	106	19	19	14	250	1.28	600	10	720	12	4.7	6.2
ПРД-31.75-2300	88	17	17	8	100	1.34	200	3.4	400	6.8	2.9	3.8
ПРД-38.1-2500	80	8	8	8	100	1.60	550	10	650	12	3.1	4.3
ПРД-38-3000	76	17	17	10	300	3.80	400	19	700	33	3.2	5.0

to be 0.1 for lubricated steel roller chains and 0.25 to 0.3 for chains without lubrication. Values of Δt as a function of operating time may be used for calculation of similar chains only as approximate data, because wear of chain joints depends on many variables.
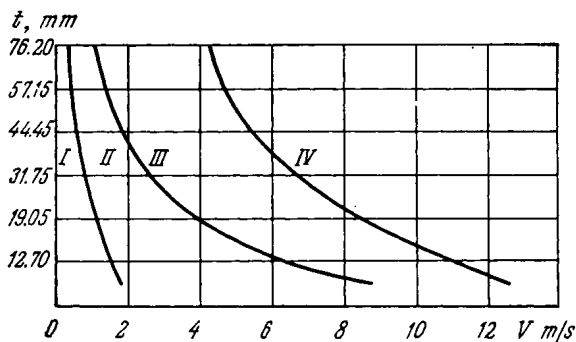
Fig. 29.3. Choice of lubricating method for chain drives [5]
I—periodic; *II*—continuous dripping; *III*—oil pool; *IV*—circulatory

These are loads, dimensions, kinematics, mechanical properties of the materials, lubrication, accuracy of the components, initial clearances in the joints, surface texture, and so on.

The wear life of the transmission chain in hours

$$T = \frac{\Delta t}{60 n I l}$$

where n is the chain rotational frequency, rpm; l is the sliding distance in a joint per revolution of the chain, mm.

To prolong the wear life, the chain should be protected against abrasives and moisture. The oils recommended for chain drives are given in Table 29.5.

The oiling method should be applied [5] with regard to chain pitch t and speed v (Fig. 29.3). With drip lubrication, oil should be delivered to the chain at a rate of 5 to 10 drops per minute at $v < 3$ m/s and no fewer than 20 drops at $3 < v < 7.5$ m/s. At $v > 7.5$ m/s either centrifugal or forced lubrication is required. In lubrication by immersing the bottom slack side of the chain into an oil bath, the level of the oil should not be higher than that of the link plates at the lowermost point of the chain. Where the chain side is at the top, oil is fed by means of a rotary disc into a shute placed under this side. The disc revolves at a peripheral speed of $v \geqslant 3$ m/s.

Circulatory oiling (by means of a lubricator) should provide lubrication of each chain side at a rate of 0.9 l/min.

Nomographs for determining the amount of oil required for transmission-chain lubrication are shown in Fig. 29.4. Data on chain drive troubleshooting and adjustment are given in [14].
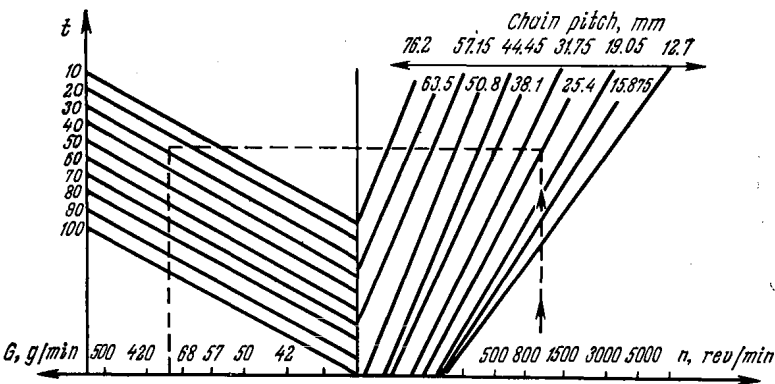
Fig. 29.4. Graphs for determining the amount of lubricant for chain drives [5]

29.4. CONVEYOR CHAINS AND DEVICES WITH BEARING ROLLERS

Conveyors are used to transfer workpieces in batch and mass production, and for handling materials in warehouses, shops, etc. Conveyors widely differ in design (Fig. 29.5), but they usually have

Table 29 5

Oils for chain drives depending on operating conditions (after K. M. Badyshtova)

Chain speed, m/s	Oils used at temperature, °C					
	Up to 40		From 40 to 75		From 180 to 200	
	oiling method					
	hand lubrication	drop lubrication	oil-bath lubrication	stream lubrication	shot lubrication	automatic lubrication
≤ 2.5	Cylinder 11	И-40А	И-40А	—	—	—
From 2.5 to 8.0	—	Cylinder 11	И-100А	—	ИЦп-40	ИЦп-20
From 8 to 10	—	—	Cylinder 11	—	—	—
Over 10	—	—	—	АК-15	—	—

one common principal element which determines their service life, namely, bearings in the form of rollers mounted on steel pins. Characteristically, such a roller slides on its fixed pin. Here, the roller bushing wears uniformly on its rubbing surface, whereas the pin features local wear.

Resistance to the movement of a load on a roller (neglecting the inertial forces) is made up of two components

$$T = T_1 + T_2 = Nf \frac{d}{D} + N \frac{2f_r}{D}$$

where D is the roller diameter; d is the pin diameter; N is the load on roller pin.
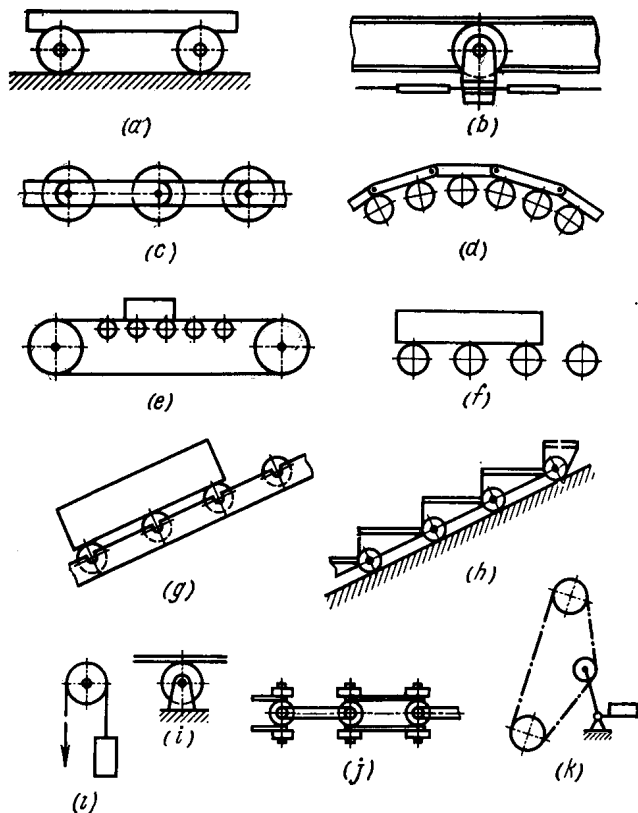
Fig. 29.5. Application of rollers
(a) floor trucks, assembly conveyor trucks, etc.; (b) trolleys in overhead chain conveyors, skip hoists, and dump slips; (c) roller chains; (d) turning mechanisms for pulling chains; (e) belt conveyors; (f) roller conveyors; (g) disc conveyors; (h) travelling stairs; (i) sheaves; ( ) buckle chains; (k) idler sprockets in chain drives; (l) rope sheave

The first component T_1 defines resistance to sliding friction at the contact of the roller with the pin, and the second, T_2, resistance to rolling.

In engineering calculations, use is most commonly made of the coefficient of resistance to movement

$$C = \frac{f\,d + 2f_r}{D}$$

Inclined conveyors are used for movement by gravity, with the inclination angle α being selected from the condition that tg $\alpha \geqslant$ $\geqslant C$.

The gradients of inclination for the most common kinds of load are given in Table 29.6.

Table 29.6

Inclination recommended for roller conveyors

Kind of load	Mass, kg	Gradient, %
Sheet steel, flat-surface castings, filled moulding flasks	30	1-1.5
Rough boards and wooden crates from rough boards	7 100	5 3.5-4
Surfaced boards and crates, wooden beams	25 10-50	2.5 1.5-2.5
Sheet-metal containers	10-30 30-150 150-500	2-3 2-2.5 1.5-2
Cardboard boxes	3.8-8.0 8.0-25.0	5-6 4-6

For stockpile conveyors and for conveyors on which loads have to stop, the gradients should be increased by 10 percent. For disc-type conveyors and light loads (a load per disc of 5 to 7 kgf) the gradient may be increased by 30 percent. The minimum mass S of a load that is necessary for movement by gravity is found from the formula

$$G = G_r n \frac{f_r\, d}{D\left(f \cos \alpha - \frac{f_r\, d}{D}\right)}$$

where G_r is the roller mass; n is the number of rollers.

Example. A roller conveyor with rollers 500 mm long and $\frac{d}{D} = 0.3$ is to be used for moving metal containers 0.2 kg in mass, each resting on three rollers. The conveyor will be installed in an unheated storeroom. Select rollers for this application.

For the given operating conditions $f_r = 0.004$; $f = 0.2$; $\cos \alpha \approx 1$.

Then

$$0.2 > G_r \frac{3 \times 0.4 - 0.3}{(0.2 - 0.04 - 0.3)} \; ; \; G_r < 1.05 \text{ kg}$$

According to the applicable standard these requirements can be satisfied with machined rollers 55 mm in diameter and with a mass of 0.78 kg.

The need to reduce metal consumption in building conveyor systems has resulted in extensive use of plastics rollers. Their advantages over metal rollers are less strict lubrication requirements; reduced wear of rollers, which is especially important for light-structure conveyors; less noise and explosion-proof properties, etc.

The choice of a roller material is governed by its antifriction and mechanical properties under actual service conditions.

Thermosetting plastics (such as cloth laminates and fibre-filled moulding materials), as compared with thermoplasts, are brittle and poorly withstand contact stresses and temperature effects, which results in the crumbling of roller edges, etc. Wood laminates and densified wood plastics are subject to drying up and excessive wear.

As materials for conveyor rollers, polyamides show better service properties: high wear resistance and strength, a low coefficient of friction (Fig. 29.6), and moderate oiling requirements. For instance, in dry friction capron has the life twice that of cloth laminate.

The main factors influencing the coefficient of friction of a capron roller on a steel pin are given in Table 29.7, and roller testing results,

Table 29.7

Variation of the friction coefficient in joints (capron roller-steel pin) of a buckle chain, type Д160

Variable	Sliding speed, m/min				Operating conditions
	1.8	3.5	5.5	6.9	
Load, kgf:					
20	0.13	0.14	0.15	0.17	Clearance of 0.5 mm
40	0.1	0.12	0.12	0.13	
100	0.07	0.1	0.11	0.12	
Surface roughness:					
20-40 μm *Rz*	0.08	0.09	0.10	0.12	Load of 40 kgf
0.63-1.25 μm *Ra*	0.1	0.11	0.12	0.14	
0.08-0.16 μm *Ra*	0.12	0.14	0.16	0.17	
Radial clearance, mm:					
0.05	0.22	0.24	0.27	0.28	Load of 40 kgf
0.1	0.16	0.18	0.20	0.22	
0.5	0.12	0.13	0.14	0.15	
1.0	0.1	0.11	0.12	0.13	0.63-1.25 μm *Ra*

in Table 29.8. The optimal surface roughness of the pin is 0.32-1.25 μm Ra. The amount of radial clearance should be specified at 1.5 percent of the pin joint diameter. Smaller clearances produce an increase

in the moment of friction, whereas greater clearances result in consi-
derable distortions of the roller bore. For polyamide rollers with
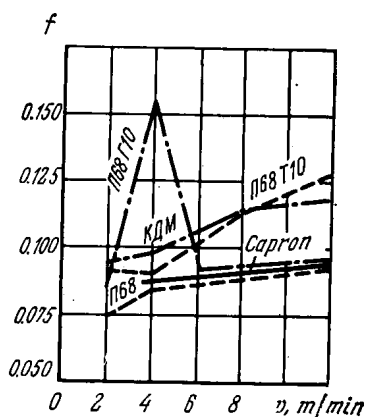
Fig. 29.6. Relation between mean values of friction coefficients and sliding speed for rollers of different materials turning on steel pins in conveyor chains

(a)   (b)
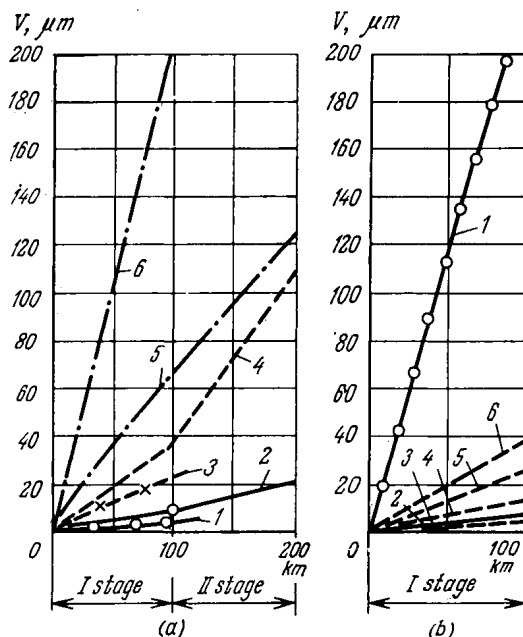
Fig. 29.7. Wear of rollers of different materials
(a) wear in roller hole; (b) wear on roller periphery; 1—metal ceramics; 2—heat treated capron; 3—untreated capron; 4—polyamid П68; 5—КДМ-1.5 material (capron + MoS₂); 6—polyamid П68Т10

a wall over 5 mm thick working without lubrication, $pv = 0.2$ to 0.4 kgf·m/(cm^2·s).

Coefficients of resistance to movement for rollers made of different materials in buckle chains are given in Table 29.8.

238

Table 29.8

Coefficients of resistance to rectilinear motion of type Д160 buckle chain with rollers of different materials

Load on chain link, kg	Capron					Capron filled with molybdenum disulphide		Polyamid П68		Polyamid П68Т10		Metal ceramic	
	primary (un-treated)		primary (heat treated)		secondary								
	U	G	U	G	U	U	G	U	G	U	G	U	G
1.5	0.098	0.096	0.088	0.059	0.126	0.108	0.082	0.11	0.11	0.10	0.082	0.047	0.042
16	0.076	0.073	0.062	0.052	0.406	0.085	0.064	0.074	0.072	0.071	0.063	0.041	0.037
32	0.067	0.064	0.054	0.048	0.095	0.074	0.056	0.063	0.062	0.058	0.055	0.038	0.036
50	0.06	0.058	0.051	0.045	0.088	0.069	0.063	0.057	0.056	0.051	0.05	0.036	0.035
100	0.049	0.048	0.044	0.041	0.08	0.061	0.045	0.048	0.045	0.044	0.044	0.034	0.034
150	0.047	0.047	0.425	0.041	0.078	0.06	0.044	0.047	0.044	0.043	0.043	0.034	0.034

Notes: 1. Roller periphery is machined to 0.63–1.25 μm *Ra*; clearance between roller bushing and pivot pin 0.2–0.3 mm.
2. G — ground roller bushing; U — unground roller bushing.

In service, rollers wear on the periphery and in the bore (Fig. 29.7). The bore surface wears hardest and so sets a limit on
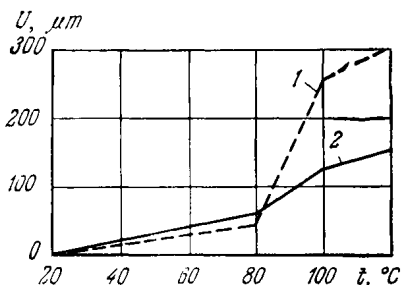
Fig. 29.8. Wear of rollers as a function of ambient temperature
1—wear in roller hole; *2*—wear on roller periphery

the roller wear life. Capron rollers can properly perform at ambient temperatures under 80°C (Fig. 29.8); operation at higher temperatures leads to catastrophic wear.

29.5. CONVEYOR BELTS

The most commonly used belting for conveyor applications is rubberized fabric (about 90 percent of the total) and rubberized ropes. Belts of these materials wear on the working and bottom facings and the base layer, and that is conducive to belt failure. The heaviest wear is found in the middle of the belt; toward the sides it decreases. In addition, the belt edges gradually wear to threads as they rub against the side guiding surfaces. The application of conveyor belts and their average wear life ratings, depending on working conditions, are treated in detail in [1].

The life span of a conveyor belt is predicted from its rated service life or from the amount of load to be moved after which the belt is replaced or repaired. In long conveyors, only worn sections of the belt are replaced.

Actually, the wear life of belts of the same type may vary 1.5 to 3 times. Soviet-made and imported conveyor belts with layers of synthetic fibres are approximately equal in wear life and live 1.5 times longer than belts with cotton fabric layers.

The belt-facing wear rate can be estimated by simplified formulas when handling:

iron ore

$$I = 0.92 p^{1+0.11 t_y} E^{0.89 t_y - 1} \left(\frac{f}{\sigma_0} \right)^{t_y}$$

lime

$$I = 0.7 p^{1+0.11 t_y} E^{0.9 t_y - 1} \left(\frac{f}{\sigma_0} \right)^{t_y}$$

Conveyor-belt wear rates are given in Table 29.9. Calculations make it possible to evaluate the effect of various factors on the wear rate of belt facings.

Table 29.9

Wear of conveyor belts in handling lime

Size of lime lumps, mm	Operating feature	$I \times 10^{-8}$
60	—	0.6-1.14*
0-100	No impacts, low slippage	1-1.33
0-100	Light impact loads, heavy slippage	0.6-1.2
0-300	Heavy impact loads and slippage	Failure

* Estimated wear. Estimation based on $E = 35$ kgf/cm²; $\sigma_0 = 1\,140$ kgf/cm²; $t_y = 2,76$; $p = 0.1$ kgf/cm²; $f = 0.6$-0.7.

REFERENCES

1. Волотковский В. С., Нохрин Е. Г., Герасимова М. Ф. Износ и долговечность конвейерных лент. М., «Недра», 1976, 175 с.
2. Воробьев Н. В., Герасимов В. Я. К вопросу о влиянии удельного давления в шарнирах втулочно-роликовых цепей на их износ.—«Известия вузов. Машиностроение», 1971, № 12, с. 32-35.
3. Глущенко И. П., Азнаурян Р. В., Лысенко В. В. К вопросу определения эффективного действия периодической смазки в шарнирах роликовых цепей.— В сб.: Механические передачи.—«Труды Краснодарского политехнического ин-та». Вып. 56. Краснодар, 1974, с. 36-41.
4. Добровольский В. П. Экспериментальное исследование механизма износа роликовых цепей в условиях абразивного загрязнения.— В сб.: Механические передачи (цепные и зубчатым ремнем). М., НИИМАШ, 1971, с. 89-98.
5. Жуков К. П. Исследование влияния способа смазки на работоспособность приводных роликовых цепей.— В сб.: Механические передачи (цепные и зубчатым ремнем). М., НИИМАШ, 1971, с. 81-89.
6. Ивановский К. Е., Раковщик А. Н., Цоглин А. Н. Роликовые и дисковые конвейеры. М., «Машиностроение», 1973, 216 с.
7. Кестельман В. Н., Короб А. Д. Пластмассовые шкивы и клиноременные передачи. М., «Машиностроение», 1968, 133 с.
8. Коваленко Н. И. Износостойкость проволочных канатов.— В сб.: Повышение износостойкости и срока службы машин. Киев, АН УССР, 1960, с. 159-174.
9. Мамцев Е. Н., Пахнов М. Н. О работе пар трения металлокапроновых шнуров в различных средах.—«Рыбное хозяйство», 1969, № 8, с. 50-52.
10. Пронин Б. А., Ревков Г. А. Бесступенчатые клиноременные и фрикционные передачи (вариаторы). Изд. 2-е перераб. и доп. М., «Машиностроение», 1967, 404 с.
11. Пронин Б. А., Шмелев А. Н. Об определении скольжения в клиноременной передаче.—«Вестник машиностроения», 1973, № 9, с. 15-16.
12. Титова Т. А. Возможности повышения сроков службы пластмассовых клиноременных шкивов.—«Вестник машиностроения», 1971, № 5, с. 39-41.
13. Федоров Ю. И., Метильков С. А., Карасов М. А. О показателях предельного состояния роликовых цепей сельскохозяйственных машин.— В сб.: Механические передачи. Вып. 56. Краснодар, Краснодарский политехн. ин-т, 1974, с. 42-48.
14. Oliverson R. L. Plant Engineering Magazine Troubleshooting Chain Drive Operating Problems. Plant Engineering, vol. 22, X; 1968, p. 61-63.

FRICTION AND WEAR
OF ELECTRIC CONTACTS

30.1. MAIN DEFINITIONS.
PHYSICAL PRINCIPLES OF PROCESSES
IN ELECTRIC CONTACTS

An *electric contact* is a junction of two conductors (usually solids) brought into engagement for transmitting an electric current.

All electric contacts can be classified according to their function, kinematics, and design features (Fig. 30.1).

With two solids touching each other to create an electric contact, the real area of contact that provides the passage of an electric current from one solid to the other is much smaller than the apparent contact area because of the surface irregularities and various surface films.

The *surface microtopography* of the electric contact is characterized by form errors, waviness, and surface roughness (for greater detail see Chapter 1).

Films on the surfaces of electric contacts develop mainly on exposure to the ambient medium. The main kinds of such films are adsorbed (adhesional) oxygen films, tarnish films, commonly oxidic or sulphidic, water film, etc.

When surfaces are brought in contact they initially touch at the highest peaks of surface irregularites. Waviness, a typical feature of machined surfaces, results in contact spots scattered over the contact area.

In addition, each individual contact spot can itself have various regions: those with direct metallic contact, with quasi-metallic contact where the contact elements are separated by a thin adhesional film or a thin (up to 20 Å) tarnish film, and with non-metallic contact where the contact elements are separated by thick tarnish films.

The passage of an electric current through the contact of two conductors with a definite surface roughness involves characteristic phenomena. Electric contact takes effect only at small conductive spots where the current flow lines deflect and contract, giving rise to so-called constriction resistance. The latter is the result of a non-uniform density of the current flow lines in the apparent contact area. As the contact surfaces carry various films whose conductance is lower than that of the main metal, they create an additional resistance. In the general case, these two resistance components R_c and

R_f are supplemented by the resistance due to distortion of the crystal lattices in the deformation zone, but normally this factor does not exceed fractions of a percent of R_c and in most cases may be neglected.
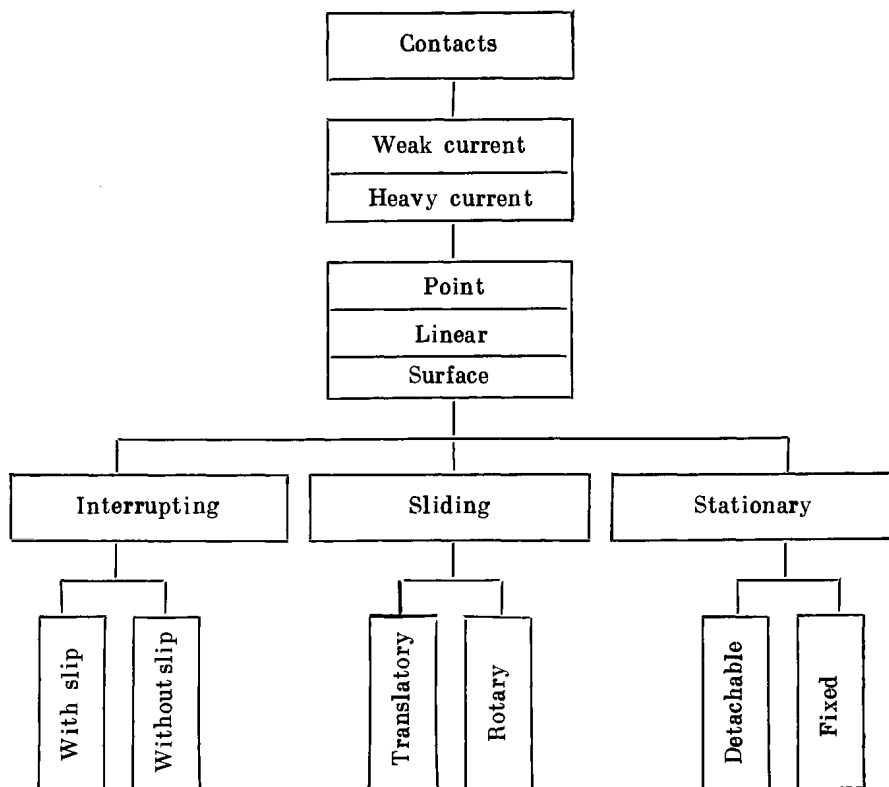
Fig. 30.1. Classification of electric contacts

The contact resistance of elementary metal contact spots is normally much lower than that of surface films and can be expressed as

$$(\Delta R)_i = (R_{c_1})_i + (R_{c_2})_i$$

where $(R_{c_1})_i$ and $(R_{c_2})_i$ are constriction resistances of the first and the second contact member, respectively.

In the absence of direct metal contact, the quasi-metal conductance of thin films is determined by the tunnel effect and thermionic emission. In this case

$$(\Delta R)_i = (R_{c_1})_i + \left(\frac{R_t R_s}{R_t + R_s} \right)_i + (R_{c_2})_i$$

where R_t is the tunnel resistance; R_s is the resistance due to the Schottky emission.

The resistances R_t and R_s are fairly difficult to calculate. Since their share in the resistance of most contacts, particularly sliding ones, is insignificant, their calculation is not considered here; it can be found in special literature, for instance in [13].

Calculating the constriction resistance of a stationary contact. The overall contact resistance is found from the expression

$$\frac{1}{R_{ov}} = \sum_{i=1}^{n} \frac{1}{(\Delta R)_i} = \sum_{i=1}^{n} \frac{1}{(R_{c_1})_i + (R_{c_2})_i}$$

where n is the number of contact spots.

The constriction resistance of an individual contact spot is calculated on the assumption that the contact spot is a circle whose diameter is much smaller than the contact area in which constriction of current flow lines takes place. According to R. Holm [14],

$$R_{c_i} = \frac{\rho_i}{4a}$$

where a is the radius of the contact spot (see Chapter 1).

With the contact spots equal in diameter and the contacts of the same material,

$$\rho_i = \rho; \quad (R_{c_1})_i = (R_{c_2})_i; \quad R = 2\frac{\rho}{4 \sum_i a_i} = \frac{\rho}{2an}$$

where ρ is the specific resistance of the contact materials, ohm·mm²/m; $n = A_r/\pi a^2$.

Generally, the resistance resulting from the density of constricted current flow lines due to proximity of metal contact spots should be added to the constriction resistance R_{c_i}. For practical purposes, however, this factor can be left out of consideration as well as the fact that the contact spot normally proves to be elliptical rather than circular.

A detailed calculation of the contact resistance for various specific cases can be found in [13].

Wear of contacts. Sliding, fixed, and break contacts wear in operation. Finally, after a certain number of switching cycles, wear causes failure of the contact system. Electric contacts are subject to wear of two principal kinds: mechanical (fatigue) wear due to friction and impacts, and electrical (erosive) wear due to the action of electric current on the material. Reliability and wear life of electric contacts vary within a wide range owing to a great variety of operating conditions. Table 30.1 presents statistical data on failure rate λ (the ratio between the number of failures per unit time and the total number of operative cycles for the same time).

It can be seen that a higher failure rate is observed in sliding electric contacts, where the effect of mechanical and electrical wear is the most pronounced.

244

Table 30.1

Failure rate for contacts of different kinds

Kind of contact	Failure rate $\lambda \cdot 10^5$ 1/h
Soldered connections	0.004
Fixed connections	0.005
Plug-and-sockets	0.175
Relays	0.04-0.70
Switches	0.05-0.50
Potentiometers	0.1-7.0
Rheostats	1.13
Connectors	0.4-2.0
Contact breakers	0.25
Contactors	0.5
Electric motors and generators with slip rings	0.3
Electric motors and generators with commutator	Up to 2.9

Mechanical wear in sliding electric contacts occurs in the same forms as in plain sliding pairs, although loads on these contacts are usually small.

Electrical wear in sliding contacts involves the transfer of ions of one contact member to the other and the fritting* of oxide films leading to a rise in the force of molecular adhesion between juvenile metal layers. This rise, in its turn, causes microwelding with tearing in depth, the sparking and formation of electric arc resulting in massive heat generation in the gap between the contact members. The heat causes evaporation or spraying of the metal in the contact gap, which sharply impairs the surface quality and thereby promotes mechanical wear.

30.2. FIXED AND DETACHABLE ELECTRIC CONTACTS

Fixed electric contacts are formed mainly by fastening the contact members by means of screw threads; for these contacts friction and wear are not crucial phenomena.

In detachable contacts, however, mechanical wear plays an important part. Such contacts are used in most electric and electronic applications. The main design type is the plug-and-socket. Specific arrangements are governed by numerous factors, which are described in detail in [1].

The materials used for contacts are usually copper, brass Л63, covar, and bronzes grade БрОФ 6.5-0.15 (tin-phosphor bronze), БрБ2 (berillium bronze), БрОЦ 4-3 (tin bronze), and БрКМц 3-1 (silicon-manganese bronze). Contacts are coated with electrodeposited precious metals: gold, silver, platinum, palladium, rhodium, etc. [17].

---

* Fritting is an electrical break-down occurring as the electrostatic field within the surface film reaches approximately 10^6 V/cm

Calculation of friction and wear characteristics is important in the detachable-contact design, because these determine the force of disconnection and the wear life of such contacts.
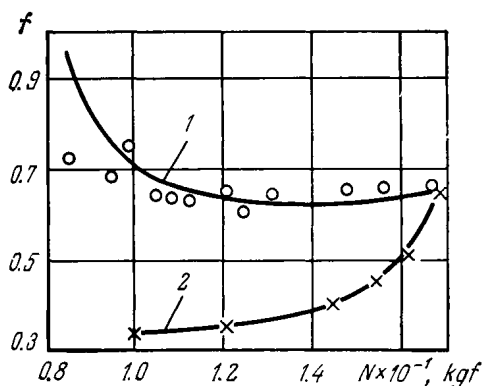
Fig. 30.2. Coefficient of friction as a function of contact force (Type PC connector, speed of disconnection 0.1 m/s)
1—silver plating; 2—gold plating

The force of disconnection is equal to the force of friction. Relationship between the friction coefficient and the contact force is determined by the f_{ml}/f_{mc} ratio and therefore depends on the kind of contact (elastic or plastic), the microgeometry, and the surface
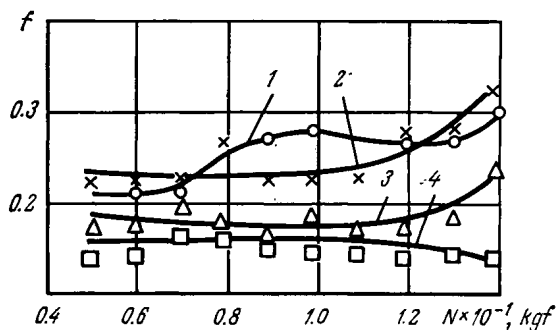
Fig. 30.3. Coefficients of friction as a function of contact force in silver test contacts finished to
1—1.25-2.5 μm Ra; 2—0.32-0.63 μm Ra; 3—0.02-0.04 μm Ra; 4—0.05-0.1 μm Rz and 10-20 μm Rz (disconnection speed 0.1 m/s)

films (see Chapter 2). Examples of such relationships are given in Figs. 30.2 and 30.3. Wear of contacts is determined mainly by molecular and mechanical factors that arise in disconnection, and it can also be calculated for a specific application by the formulas of Chapter 3. The most difficult design problem is to provide for mini-

mum wear and, at the same time, for a minimum stable contact resistance. As the contact force is the most important factor in contacts of this type that determines their working characteristics, the optimal magnitude of the contact force must be calculated for each specific situation. Examples of such calculations are presented in the literature [1].

30.3. SLIDING ELECTRIC CONTACTS

Contacts of this type are subject to a particularly strong action of friction and wear aggravated by electrodynamic processes.

The most common and important sliding electric contacts are those in electrical machines, current collectors in transport vehicles, and weak-current contacts in electronic and electric equipment. The latter can be calculated for friction and wear by methods described in Chapters 2 and 3 without regard to the effects of weak currents and low voltages, and therefore only the first two kinds of sliding contacts are discussed below.

The sliding electric contacts of electrical machines generally come in two varieties: the brush/commutator type, where brushes of different polarities slide on a single sliding path, and the brush/slip-ring type, where brushes of different polarities slide on different rings. Diverse operating conditions for electric machines require that the properties of the materials and the working characteristics of the sliding pairs should be as varied as possible. This is achieved by selecting various materials for brushes.

Commutators are predominantly made of electrolytical copper (grade M1), or copper with small additions of cadmium, silver, magnesium, zirconium or tellurium (for instance, copper with cadmium, grade Кд-2). Slip rings are made of alloys of copper with zinc, lead, aluminium, and, in some high-speed applications, of ferrous metals and alloys.

Brushes are generally made from multi-component compositions of powdered graphite, black soot, copper, and coke. The types and characteristics of brushes are specified by standards. Most sliding contacts in electrical machines operate in air without lubrication. At present, there is a limited class of machines with sliding contacts working in liquid dielectrics, hydrogen, vacuum or vapours of water.

The most important operating characteristics of sliding contacts are the coefficient of friction and the rate of wear. They can be determined in model and full-scale tests.

Methods for simulating friction and wear in sliding electric contacts have yet to be fully developed, and for this reason f and I are determined by laboratory testing of actual sliding contacts at nominal magnitudes of current I_{nom} and pressure p_{nom} and at variable sliding speed v.

Relation between f and v is essential for assessing the stability of operation of electric contacts (Fig. 30.4).

For approximating experimental characteristics $f(v)$, use can be made of the formula $f = C - Dv$, where C and D are constants depending on brush materials.
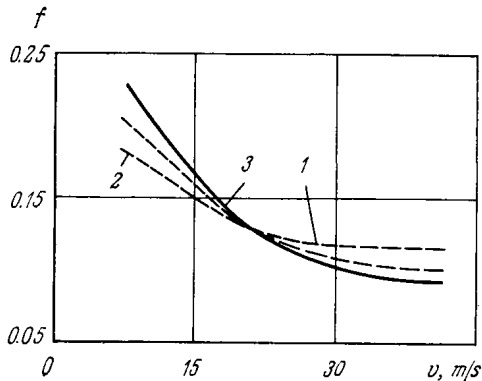
Fig. 30.4. Frictional characteristics of electric brushes
1—metal-graphite brush; 2—graphite brush; 3—brush with electrodeposited graphite

The limitation of this formula is that it holds only for current densities that are close to the nominal value. Values of C and D for some brush materials are presented in Table 30.2.

Table 30.2

Values of slope D and term C in the frictional characteristic equation for electric brush materials [9]

Grade of material	D	C	Grade of material	D	C
Г3	0.005	0.25	М3	0.003	0.20
ЭГ2А	0.003	0.21	М6	0.003	0.19
ЭГ4	0.003	0.20	М20	0.003	0.20
ЭГ8	0.005	0.22	МГ	0.004	0.22
ЭГ14	0.005	0.23	МГ2	0.004	0.23
ЭГ74	0.006	0.26	МГ4	0.004	0.21
611М	0.004	0.21	МГ64	0.004	0.22
М1	0.004	0.23	МГС5	0.004	0.21

Relation between the friction coefficient and the current density, the load, the direction of current flow and the temperature. The coefficient of friction as a function of load (pressure) P and current density D_t on the contact in sliding on brass at $v = 10$ m/s is depicted in Fig. 30.5. The solid lines pertain to brushes with anodic polarity and the dash line, to brushes with cathodic polarity.

The effect of pressure proves substantial over the whole range of variation of D_c for graphite and carbon-graphite materials, and at $D_c > 0$ for carbon materials. With the latter, the curves $f(D_k)$ for different pressures come from nearly a single point. The same is also true for copper-graphite compositions.

The graphs in Fig. 30.5 also carry information on the effect of the direction of current flow on the coefficient of friction f. When
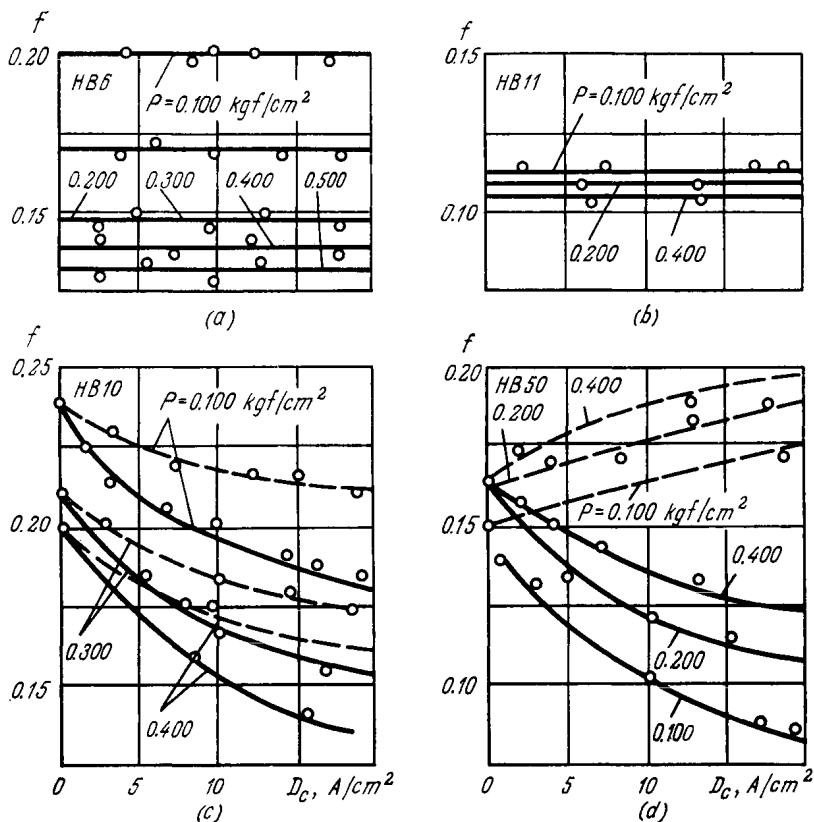
Fig. 30.5. Relation between friction coefficient and current density at different contact pressures for

(a) graphite brush; (b) metal-graphite brush; (c) carbon-graphite brush; (d) carbon brush

the current passes from a brush to the ring (anodic-polarity brush), f always proves to be smaller than it is with the cathodic-polarity brush, and a rise in D_c causes f to drop in all cases. The friction coefficient for the cathodic-polarity brush, being always higher than that for the anodic-polarity brush $(f_c > f_a)$, varies with D_c differently for different materials.

The relation $f_c > f_a$ can be ascribed to different steady-state roughness of the metal ring under brushes of different polarity.

The friction coefficient as a function of temperature $f(\vartheta)$ for electric brushes is influenced by the content of water vapours in the ambient medium. In sliding of graphite brushes on a heated commutator, f exhibits a weak dependence on the temperature up to 100°C, with a vapour content exceeding 13 g/m^3. With a lower vapour content, the $f(\vartheta)$ characteristic takes a V-shape with the minimum in the region of $70 < \vartheta < 90$°C.

The friction coefficient also depends on ambient conditions determined by the chemical composition, mechanical impurities, and thermodynamic parameters.

The influence of pollutants in the ambient air on the frictional behaviour of graphite brushes sliding on a copper commutator is illustrated in Table 30.3. Similar effects are produced by silicon-

Table 30.3

Effect of ambience impurities on frictional characteristics of electric contact [9]

Initial value f	Substance introduced into ambient atmosphere	Resulting value f
0.18	Tobacco smoke	0.31
0.20	Burning insulation smoke	0.60
0.13	Carbon tetrachloride vapours	0.25

containing substances and vapours of chlorine, acids, paints, acetone, alcohol, etc.

Thermodynamic factors, such as the partial pressure of oxygen and water vapour, determine the frictional characteristics of sliding electric contact at high altitudes.

For conventional brushes, a rise in altitude to 12-15 km above sea-level produces a linear increase of f from 0.15 to 0.3. To neutralize this factor, special brushes with fusible alloying components of tin and lead have been developed to facilitate lubrication at high altitudes. For such brushes, f is as follows:

Altitude, km	0	6-18	24
Friction coefficient	0.17	0.12	0.13

Wear of sliding contacts in electric machines.

Resistance to wear determines the reliability, service life and many other operating characteristics of sliding contacts. If a sliding contact operates under normal conditions, wear of the brushes and slip rings (commutator) can be assumed to comprise the mechanical (fatigue) and electrical (erosion) wear components

$$U = U_m + U_{el}$$

The mechanical component is estimated by the respective formulas given in Chapter 3.

The share of U_m in the resultant wear amounts to from 1/3 to 1/2 depending on brush polarity. Mechanical wear of the slip rings or commutator made of the above-mentioned materials is not predominant owing to the more favourable working conditions for these elements.

The electrical wear component depends on a complex of factors (current flow direction, conditions for electrical discharge between the contact members). The amount of material transferred from one
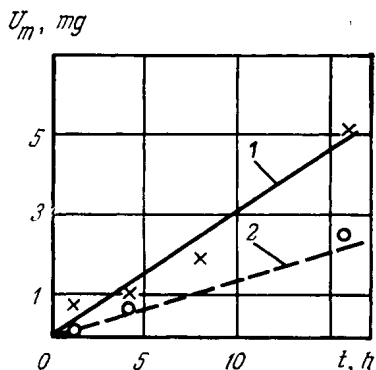
Fig. 30.6. Transfer of material between brush and commutator
1—anodic-polarity brush; 2—cathodic-polarity brush
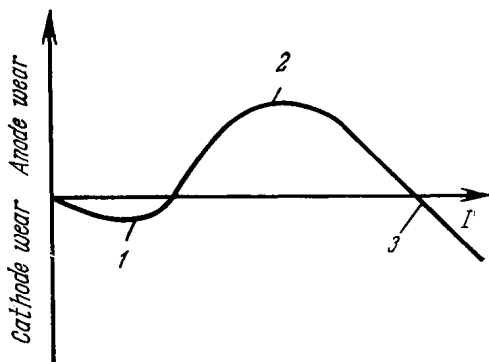
Fig. 30.7. Relation between the type of discharge and electrode wear
1—glow discharge; 2—spark discharge; 3—arc discharge

contact member to the other and, consequently, wear depend on the current-flow direction and intensity. The transfer of material between brushes of different polarity and the slip rings observed in tests by the radioisotope method is graphically illustrated in Fig. 30.6. As is seen, the transfer of material from the anodic-polarity brush is more intensive.

The effect of the kind of discharge that occurs in operation of brushes on their wear can be evaluated using the chart shown in Fig. 30.7. Any kind of spontaneous discharge in gas produces erosion of electrodes. A glow or arc discharge affects predominantly the cathode, and a spark discharge wears mostly the anode. A changeover form one kind of discharge to another is accompanied by the inversion of the electric component of electrode wear.

In addition to the above-mentioned wear components, attention should be paid to the chemical wear factor. There are some grounds for explaining the difference between anode and cathode wear by the effect of oxidation. Thus, for instance, friction of brushes on precious metals in the absence of oxidation exhibits equal wear rates of the anode and cathode (Table 30.4).

The effect of the commutator speed and surface roughness on the wear rate of the brushes, as determined by testing, is described in [9].

Table 30.4

Wear of brushes on slip rings made of precious metals at different current intensities [9]

Ring mate-rial	Current inten-sity, A	Distance of sliding, km	Wear of brushes, 10^{-6} cm³/km	
			anodic	cathodic
Silver	0	4500	0.1	0.1
	5	1100	0.5	0.7
	10	1250	0.5	0.8
	20	400	0.5	0.5
Gold	0	1600	0.1	0.1
	5	1070	0.5	0.5
	10	1020	0.4	0.4
	20	1423	0.4	0.3

Note. Peripheral speed — 4.4 m/s; ring diameter — 70 mm.

The sliding-speed effect on wear is variable depending on the brush material. However, this factor should not be identified with
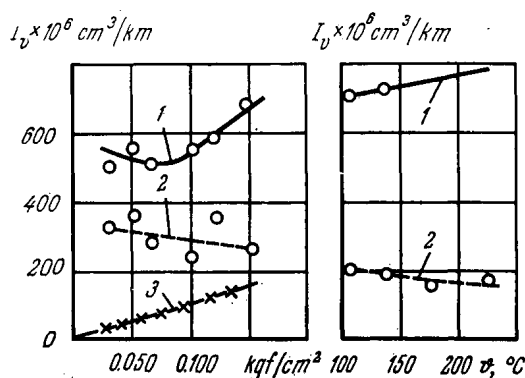
Fig. 30.8. Effect of contact pressure (*a*) and temperature (*b*) on wear rate of brushes (current intensity 60 A)
1—anodic-polarity brushes; *2*—cathodic-polarity brushes; *3*—no current

the commutator rotational frequency. At low sliding speeds, an increase in rotational frequency has been found to promote wear of the brushes.

The runout of commutators due to eccentricity and misalignment of adjacent commutator bars has a substantial influence on the wear rate, particularly in high-speed electric machines. Vibrations caused by external sources have the same effect.

Relation between the pressure exerted on the brush and its wear is somewhat different. For brushes of different polarity, this relation $I_v = f(p)$ proves dissimilar (Fig. 30.8*a*). The minimum on the curve

reflects the share of electrical wear, mechanical wear, and wear from sparking. As the pressure is raised, U_{sp} drops practically to zero, and that accounts for the minimum on the curve. Further increase in p causes the mechanical wear component U_m to grow.

The effect of the ambient medium on wear varies depending on the presence of a thin film formed as the brushes slide on the commutator. The film can be formed by introducing the required
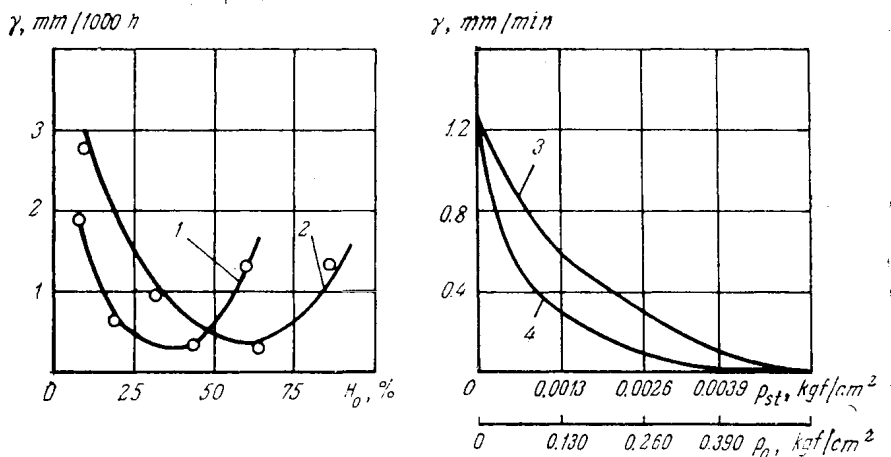
Fig. 30.9. Effect of ambient medium on wear rate

1—air; *2*—hydrogen; *3*—oxygen at partial pressure (p_o); *4*—water steam at partial pressure (p_{st}); H_o—optimal air humidity

agents into the ambient atmosphere, by introducing film-forming substances into the brush material and by using special materials for commutators and slip rings.

The first method is effected by saturating the atmosphere with steam, but not in excess of certain limits. Relationship between wear and the steam content of air and hydrogen is shown in Fig. 30.9 (curves *1* and *2*). The same Figure (curves *3* and *4*) illustrates variation of the brushes' wear rate with the partial pressure of steam and oxygen for operation in air.

The second method involves introducing impregnants and some fusible components, specifically, tin and lead, into the brush material.

In friction, these components melt, penetrate the surface layer of the commutator and, together with graphite, provide the necessary lubricity.

At present, work has begun on the use of metal or alloy brushes that run on a commutator or slip rings in the presence of a lubricant or coolant. This may help to overcome the limitations of carbon-graphite brushes as to circumferential speed, current density, fric-

tional and wearing characteristics, and response to the ambient medium.

The use of impregnants is also very promising, because it drastically reduces wear of the brushes, sometimes by two orders of magnitude. Such agents as molybdenum disulphide, magnesium carbonate, coumarone resin, barium fluoride, fluoroplastic are employed as impregnants.

Metal-polymer brushes developed by an institute of the Belorussian Academy of Sciences also hold promise. The brushes are made from a high-conductance foil, for instance of silver, whose layers are arranged in a stack and moulded to size with a polymer binder, such as polyvinylfurfural with 80 to 90 percent colloidal silver.

The third method is still under development. Here, it might be well to point out the introduction of nickel into the commutator material and the use of graphite and metalceramic compositions as commutator materials.

Relation between the wear rate of brushes and slip-ring materials in a neutral and reducing hydrogen medium is illustrated by the data of Table 30.5.

Table 30.5

Wear of brushes depending on slip ring material [9]

Ring material	Relative wear rate	HB	Ring material	Wear rate, mm/1000 h		HB
				anodic brush	cathodic brush	
In nitrogen			*In hydrogen*			
Silver	1.96	20-25	Cadmium copper	0.86	1.9	95-115
Gold	1.64	19-25	Magnesium copper	0.64	0.9	135
Copper	1.00	120	Chromium copper	0.79	1.3	130-150
Nickel	0.19	111-300	Bronze БрАЖ 9-4	0.71	1.2	—
Bronze	0.00	60-120	Steel	0.86	3.2	180-220

Comparative performance tests in air of brushes on cast copper and metal-ceramic slip rings showed the minimum rate of wear of the brushes when sliding on a copper-base metal ceramic. The wear rate grew in increasing order with the use of copper-cadmium metal ceramics, cast copper, and iron-base metal ceramics.

The wear of commutators and slip rings in electric machines comprises the same components U_m and U_{el} as that of brushes, but, owing to a small mutual overlap coefficient, wear rates of collector rings are usually low with the use of modern brush materials at the spark rating not more than $1^1/_4 - 1\ ^1/_2$ according to GOST 183-74.

The wear of slip rings is not equal because of different polarity. The cathodic-polarity ring generally exhibits a solid layer of carbon material, a smooth sliding surface and low wear. The surface of the anodic-polarity ring is rougher and wears more intensively. For this reason, it is good practice to change periodically, once or twice a year, the direction of the current flow that passes through the contact. After such a changeover, the current load should for several hours be reduced to 40-50 percent of the rated value to allow new brush films on the rings to be formed and to prevent sparking.

Sliding contacts of current collectors in vehicles. Two principal types of heavy-current sliding contacts used in vehicles are a pantograph trolley insert on a contact wire and a current-collector shoe on a contact rail.

The mechanism of friction and wear for both types of collectors is basically similar. The difference is that with the first type one of its elements, the contact wire, is not rigid, and pressure in the contact intricately depends on the shape taken by the wire suspended between its supports.

Besides, the first type of current collector is used in the open without any protection from weather conditions (winds, rain, snow, icing), whereas the second type is mainly used in tunnels, pits and adjoining areas protected from these factors.

The consideration of the contact-wire flexibility and the effect of the climatic factors on it is beyond the scope of this chapter; detailed information on this question can be found in [3, 4, 8, 10].

Electrical (erosive) wear is predominant with sparking and formation of arc that occur during the separation of the sliding contact members in motion or at starting.

In the absence of sparking the action of electric current produces changes in thermofrictional conditions of the contact.

Materials used for current collectors in vehicles are mainly copper and its alloys with cadmium and magnesium (for contact wires), mild open-hearth steel (for contact rails in underground railways), copper, carbon and coke materials and metal-ceramic materials (for pantograph contact inserts), and steel (for contact shoes in underground railways).

Current-collector contacts, excluding the carbon-metallic and special metal-ceramic ones, require lubrication. For this purpose, in the USSR use is made of type СГС-0 and СГС-Д lubricants, which contain coumarone resin and pencil lead.

Friction and wear in the pantograph — contact wire current collector. The principal working characteristic of this couple is wear resistance. The wear of contact wires, which is extremely objectionable, is determined as a decrease in the cross-sectional area by methods described in [8, 10]. Assessment is done by the amount of the mean specific wear of the wire:

$$i = \frac{\lceil \Delta S \rceil}{P \cdot 10^{-4}}$$

255

where ΔS is the decrease of the wire cross-section; P is the number of runs of electric vehicles.

The mean specific wear is estimated for individual anchor spans, sections of the way, and the whole way. Wear of contact inserts is found using the specific inserts' consumption index, that is, the consumption of contact inserts for a million-kilometers run of electric rolling stock:

$$g_{sp} = \frac{G}{R}$$

where g_{sp} is the specific consumption of inserts; G is the total consumption of inserts, thousands of pieces; R is the rolling-stock run, mln km.

The effect of electric current in current collectors of vehicles manifests itself primarily as heating of the inserts and contact wires. In the USSR, the permissible overheating (above the ambient temperature) is stipulated by GOST 12058-72.

The temperatures cited in this Standard are bulk temperatures, and they do not accurately reflect the maximum temperatures in the contact zone, which can be much higher. Increased contact temperature may cause harmful structural changes in the contact-wire material resulting in greater wear and sometimes, in failure. Therefore, it is advisable to calculate the contact temperature using the method presented in [5, 11].

The total contact-surface temperature

$$\vartheta_t = \vartheta + \vartheta_s + \vartheta_{fl}$$

where ϑ is the bulk temperature due to Joule heat; ϑ_s is the surface temperature due to friction and contact resistance; ϑ_{fl} is the flash temperature. The bulk temperature ϑ is determined from the equality of the Joule heat flow and the heat flow to the ambient medium

$$\vartheta = \frac{4I^2\rho}{\pi^2\, d^3\sigma' \cdot 10^2}$$

where I is the current intensity, A; d is the wire diameter, m; σ' is the convectional heat-transfer coefficient, W/(m²·°C). With the quantity σ' expanded,

$$\vartheta = 0.00887 \left[\frac{I^2\rho}{\lambda_f d^3} \left(\frac{dT_0\nu_f}{g} \right)^{0.25} \right]^{0.8}$$

where λ_f = thermal conductivity of air, W/(m·°C);
ν_f = kinematic viscosity coefficient for air m²/s;
T_0 = air temperature, °C;
g = gravity acceleration m/s².

The surface temperature ϑ_s can be found on the assumption that there are two sources of heat in the friction zone — frictional and

256

electrical:

$$\vartheta_s = \frac{0.942 q_0 \alpha_{nf1}}{\lambda_1} \sqrt{\frac{a_1 l_1}{\pi v}}$$

where $q_0 = \frac{1}{A_a}\left[fNv + I^2\left(\frac{\rho\sqrt{HB}}{\sqrt{\pi N}} + \frac{\sigma HB}{N}\right)\right]$ is the heat flow on the contact surface from the frictional and electrical sources; σ is the specific resistance of the contact film; α_{hf1} is the heat flow distribution coefficient, being within 0.75 to 0.90 (usually taken at 0.85); λ_1 and a_1 are the thermal conductivity and thermal diffusivity of the wire, respectively; l_1 is the actual length of the engagement of the contact wire and the collector.

The flash temperature ϑ_{fl} is determined by the method described in [5, 11]:

$$\vartheta_{fl} = \frac{\sqrt{2}+1}{\sqrt{2}}\frac{fNv\,d_m}{A_r\lambda\,[4+(\pi\,Pe)^{1/2}]}$$

where d_m is the mean diameter of the contact spot determined with regard to the actual contact roughness; $Pe = \frac{v d_m}{a}$ is the Péclet's number.

Example 1. Given: a contact couple consisting of wire and pantograph insert of copper $A_a = 0.5\times 10^{-3}$ m^2, $f = 0.3$; $\rho = 1.75\times 10^{-6}$ ohm·cm; $\sigma = 10^{-3}$ ohm·cm^2; $N = 14.7$ kgf; HB 98.1 kgf/mm^2; $I = 500$ A; $v = 50$ m/s; $l_1 = 0.12$ m; $l_2 = 0.00417$ m; $\lambda_1 = \lambda_2 = 381$ W/(m·°C); $a = 0.111\cdot 10^{-3}$ m^2/s; $d_m = 10^{-6}$ m. Then

$$\vartheta = 0.00887\left[\frac{(5\times 10^2)\,1.76\times 10^{-6}\times 10^6}{2.58\times 10}\left(\frac{0.01\times 293\times 227\times 10^{-12}}{9.81}\right)^{0.25}\right]^{0.8} = $$
$$= 128.5°C$$

$$\vartheta_s = \frac{0.942\times 336\times 10^6\times 0.85}{381}\left(\frac{0.111\times 10^{-3}\times 0.12}{3.14\times 50}\right)^{1/2} = 205°C$$

$$\vartheta_{fl} = \frac{1.4+1}{1.4}\frac{0.3\times 98.1\times 50\times 10^{-6}}{381\left[4+\left(\pi\frac{50\times 10^{-6}}{0.111\times 10^{-3}}\right)^{1/2}\right]} = 114°C$$

Adding these components together, we obtain

$$\vartheta_t = 128.5°C + 205°C + 114°C = 447.5°C$$

As is seen, the maximum temperature substantially exceeds the bulk temperature indicated in GOST 12058-72. Consequently, it is this maximum temperature that must be taken into account when assessing the coefficient of friction and the rate of wear of the contact insert and contact wire. This temperature should be simulated in laboratory tests of models and actual contact couples designed for sliding electric contacts.

These requirements have been taken into consideration in a special testing procedure [15, 16].

Empirical values of the permissible current intensity for various contact insert materials at which the bulk temperature does not exceed the limits established by the Standard are given in Table 30.6.

The current intensity during vehicle stops is limited by that causing the overheating of grade MΦ-85 wire.

Table 30.6

Current intensity permissible in practice for contact inserts of different materials

Insert material	Permissible long-time current per collector, A					
	Single-trolley			Double-trolley		
	in motion	at standstill		in motion	at standstill	
		winter	summer		winter	summer
Copper	1 250	520	340	2 200	550	550
Iron-base metal-ceramic material (trolley with four rows of inserts)	1 500	300	200	—	—	—
Type A carbon ($\rho = 27$ ohm $\times$ mm²/m)]	760	80	50	1 335	130	80
Type Б carbon ($\rho = 130$ ohm $\times$ mm²/m)	1 010	100	65	1 770	170	110

The effect of an electric current on the wear of the contact insert-wire couple was assessed in laboratory and field conditions. The laboratory tests have shown that, other things being equal, the wear depends on current intensity to a more-than-unity power.

Field tests of lubricated copper inserts revealed a linear relation between wear and current intensity

$$i_a = 455 \times 10^{-6} I + 56 \times 10^{-4} l + 0.142$$

where i_a is the specific wear on an anchor span, mm²·10^{-4} runs; I is the current intensity, A; l is the distance between the given span and the lubrication point, km.

Relationships between the specific wear and current intensity for different distances from the lubrication point are shown in Fig. 30.10.

The contact pressure has a dual effect on the wear of the contact insert—wire couple. On the one hand, an increase in pressure reduces electrical wear of the wire through lower contact resistance and shorter time of contact separation, and hence, lower sparking. On the other, increased pressure produces heavier mechanical wear.

Relation between contact resistance and pressure for various contact insert materials in operation without lubricants is shown in Fig. 30.11.

The optimum pressure, at which the electrical and mechanical wear components are minimal, has been found empirically as a first approximation only; it lies within limits of 5.5 to 15 kgf for direct current and 4.5 to 11 kgf for alternating current.

As mentioned above, it is difficult to determine the optimal pressure precisely, because the current collector in vehicles operates under

conditions involving the simultaneous action of friction against the contact wire, the aerodynamic resistance of air, and oscillations in the wire-pantograph system.

Qualitative criteria for current collectors are treated in publication [3].

The foregoing considerations also hold true for trams and trolley cars, where the total amperage is under 600 A at voltages of up to
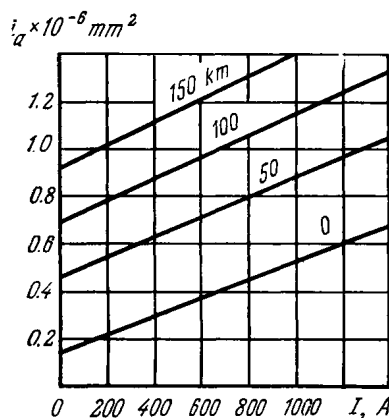
Fig. 30.10. Specific wear as a function of current intensity and distance from oiling point
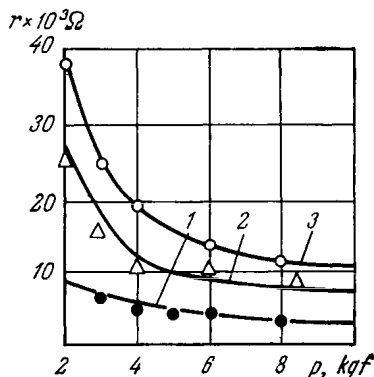
Fig. 30.11. Contact resistance as a function of contact force

1—copper inserts; *2*—metal-ceramic inserts; *3*—carbon inserts

600 V. These operational conditions are not so severe as in railway vehicles; in addition, trams and trolley cars travel at slower speeds but use the contact wires and pantograph inserts made of the same materials as railway vehicles do.

A new metal-ceramic material, grade MKB-1, developed and tested by Soviet research institutes, has proved very promising [13, 16]. The use of this material for contact inserts in trolley car pantographs extended the wear life of the inserts five times and reduced wear of the contact wire. In addition, this material makes it possible to substitute steel contact wires for copper ones and to change over to the so-called steel-aluminium power network, which is much cheaper than the copper one. For rough estimation of the electro-frictional thermal stability parameters for the MKB-1-on-steel 3 sliding pair, the following regression equations have been obtained [15, 16]

$$\vartheta_t = 9.947 + 53.33 p_a + 10.51 D_c + 0.022 v - 80.89 K_{ov} - 4.074 p_{aD}$$

$$f = 0.382 - 0.045 p_a + 0.310^{-3} D_c - 0.510^{-4} v - 0.268 K_{ov} + 0.0026 p_{aD} - 0.007 v K_{ov}$$

$$I = 0.79 \times 10^{-4} + 0.12 \times 10^{-3} p_a - 0.43 \times 10^{-3} D_c + 0.29 \times 10^{-6} v$$

$$- 0.75 \times 10^{-1} K_{ov} + 0.2 \times 10^{-3} p_{aD} - 0.6 \times 10^{-4} D_c K_{ov} \quad (30.1)$$

259

where p_a and p_{aD} are the mechanical and mechano-electric loads, respectively; D_c is the current density; K_{ov} is the mutual overlap coefficient.

The optimal materials for a sliding pair should be selected in the following test sequence, with discarding the less suitable materials [5, 15, 16]:

(1) testing models for friction thermal stability on МТТЭ-type friction machines to determine the extreme values of ϑ_t;

(2) testing models on РСП-type test rigs at actual sliding speeds;

(3) testing the actual sliding pairs in field conditions. For the 1st and 2nd stages it is advisable to use experiment planning matrices.

Operation of the shoe-on-contact rail current collector. Here, the operating conditions are more favourable than those for the contact-wire-on-pantograph-insert couple. The positional relationship between the contact elements is more fixed, the oscillations in the system that lead to separation of the contact elements are absent, and the effect of weather conditions (moisture, freezing, wind) is less pronounced.

With no strict limitations on the mass of the contact rail, it is practical to use as its main material an open-hearth steel with a conductivity lower than that of copper by a factor of 6 to 8. The shoes are made of cast steel.

The pressure between the shoe and the rail ranges from 22 to 28 kgf.

The thermal problem for the shoe-on-rail sliding pair is solved similarly to one for the pantograph-wire pair.

Friction and wear of heavy-current sliding contacts sharply intensify at high and ultra-high speeds ($v \geqslant 50$ m/s), primarily through an extreme thermal action on the contact resulting in melting and destruction of insert and shoe surface layers and considerable thermal cyclic fatigue of contact wires and rails

REFERENCES

1. Белоусов А. К., Савченко В. С. лектрические разъемные контакты в радиоэлектронной аппаратуре. М., «Энергия», 1975, 319 с.
2. Белый В. А., Свириденок А. И., Петроковец М. И. Металлополимерные контактные щетки. Информэлектро. Технология электротехнического производства. т. 6, 1974, с. 82-86.
3. Беляев И. А. Токоприемники электроподвижного состава. М., «Транспорт» 1970, 160 с.
4. Власов И. И., Фрайфельд А. В., Поршнев Б. Г. Проектирование контактной сети электрифицированных железных дорог. М., «Транспорт», 1972, 320 с.
5. Гинзбург А. Г., Маханько А. М., Чичинадзе А. В. Расчет средней температуры скользящего контакта пары контактный провод — токосъемные пластины пантографа.— В сб.: Трение и износ фрикционных материалов. М., «Наука», 1977, с. 20-26.
6. Демкин Н. Б., Дзецкев Н. Н., Коротков М. А. Контактирование шероховатых поверхностей.— В сб.: Сильноточные электрические контакты и электроды. Киев, «Наукова думка», 1972, с. 12-16.

7. Крагельский И. В. Трение и износ. М., «Машиностроение», 1968. 480 с.
8. Купцов Ю. С. Увеличение срока службы контактного провода. М., «Транспорт», 1972. 160 с.
9. Лившиц П. С. Скользящий контакт электрических машин. М., «Энергия», 1974. 271 с.
10. Марквардт К. Г., Власов И. И. Контактная сеть. М., «Транспорт», 1977. 271 с.
11. Маханько А. М. К решению тепловой задачи трения пантографа о контактный провод. 1974, с. 176-186 (Труды МИИТ, вып. 466).
12. Нэллин В. И. Механика скользящего контакта. М., «Транспорт», 1966. 126 с.
13. Смирнов В. И., Митта Ф. Ю. Теория конструкций контактов в электронной аппаратуре. М., «Советское радио», 1974. 173 с.
14. Хольм Р. Электрические контакты. М., ИЛ, 1961. 455 с.
15. Чичинадзе А. В., Маханько А. М. Методика проведения испытаний материалов на трение и износ с прохождением электрического тока через скользящий контакт.— В сб.: Расчет и моделирование режима работы тормозных и фрикционных устройств. М., «Наука», 1974, с. 79-85.
16. Чичинадзе А. В., Маханько А. М., Паштала А. С. Методика определения электрофрикционной теплостойкости материалов.— В сб.: Тепловая динамика и моделирование внешнего трения. М., «Наука», 1975, с. 97-101.
17. Электротехнический справочник. Изд. 4-е, т. 1, кн. 1. Под общей ред. П. Г. Грудинского. М., «Энергия», 1971. 368 с.

A_a =apparent area of contact
A_c =contour area of contact
A_r =real area of contact
N =normal load
T =frictional force
W =work of friction
p_a, p_c, p_r =nominal, contour, and real pressure, respectively
M =moment of external forces
M_T =frictional moment
t =time
ω =angular velocity
v =linear velocity
τ =tangential stress
σ =normal stress
μ =Poisson's ratio
E =modulus of elasticity
σ_y =yield limit
BB, HRC, HV=Brinell, Rockwell, and Vickers hardness, respectively
H =microhardness
α_h =coefficient of hysteresis loss
σ_0 =frictional fatigue parameter
t_y =degree of frictional fatigue curve for elastic contact
n =number of loading cycles causing destruction of the deformed volume of material; number of revolutions
ρ =density
$\Omega = \dfrac{1-\mu^2}{E}$ =elastic constant of material (if both surfaces are deformed, $\Theta_\Sigma = \Theta_1 + \Theta_2$)
d =diameter of contact spot
R_{max} =maximum height of profile irregularities
n_p =reference length of profile
t_p =relative reference length of profile
p =level of profile section
H_b =height of waveform
R_b =curvature radius of wave crests
S_b =spacing (wavelength) of waveforms
Ra =arithmetic mean deviation of the profile
Rz =ten-point height of irregularities
Sm =mean spacing of profile irregularities
Δ_0 =maximum form error
r_{tr} =transverse curvature radius of irregularity
r_{ln} =longitudinal curvature radius of irregularity
$r = \dfrac{r_{tr} r_{ln}}{r_{tr} + r_{ln}}$ =effective curvature radius of irregularity
b, v =parameters of bearing-area curve
ε =relative approach
$\Delta = \dfrac{R_{max}}{v b^{1/v}}$ =complex parameter of surface roughness
f =coefficient of sliding friction (dimensionless); oscillation frequency
f_m =molecular component of coefficient of friction
f_{mc} =mechanical component of coefficient of friction
I =linear wear rate
I_M =wear rate in terms of mass
i_n =specific linear wear
τ_0 =resistance to shear with normal pressure extrapolated to zero
β =coefficient of strengthening of molecular bond (dimensionless)
U =linear wear
U_M =wear in terms of mass
U_V =wear in terms of volume
h =depth of penetration
V_s =volume of intercontact space
h_m =mean clearance
α_τ =tangential contact displacements
γ =time wear rate
θ_s =mean surface temperature
θ =bulk temperature
η =dynamic viscosity
v =kinematic viscosity
N_c =number of loading cycles